Spooled Packaging of Shape Memory Alloy Actuators

by

John A. Redmond

A dissertation submitted in partial fulfillment
of the requirements for the degree of
Doctor of Philosophy
(Mechanical Engineering)
in The University of Michigan
2010

Doctoral Committee:

Associate Professor Diann E. Brei, Co-chair
Assistant Research Scientist Jonathan E. Luntz, Co-chair
Professor Panos Y. Papalambros
Associate Professor John A. Shaw
Alan L. Browne, General Motors Company

The art and the science of spooling

To my parents

Acknowledgments

I am so thankful for the support and encouragement of so many outstanding individuals. Thank you to all of my lab mates, past and present for being there to share ideas, stimulate learning, and breed innovation: Paul Alexander, Joe Clement, Anupam Pathak, Brian Barnes, Julie Abel, Brent Utter, Monica Toma, Jim Otten, Shishira Nagesh, WonHee Kim, Poorna Mane, and Joe Shaktman. Thank you to my friends and colleagues at U of M who have been in my corner, advised me in life and research, and inspired me to achieve: Erin MacDonald, Brian Trease, Jarod Kelly, John Whitehead, Katie Kerfoot, Sarah Calve, and Ross Morrow. I have such a fabulous, fashionable, fun, and loving group of friends who I could not live without: Ayron Michael, Vito Trevino, Courtney Nock, Anne Ryan, Emma Crandall, Jeremy Wheeler, Mariah Cherem, Aric Knuth, Jim Leija, Daniel Menzo, Emily Sickler, Mary Catherine Buchanan, Jess Johnson, Kris Kolky, Jo Horn, Michael Faith, Tony Howard, Adam Boehmer, and John Back. Lillian Back: I can't even begin to express my gratitude to have you as a friend and mentor. You have helped me to see the world in an analytical way that has revealed such intellectual thrill and beauty. Vigi Sklar: Your love and support through this process has allowed me to succeed. Te quiero mucho. Ben and Rachel, I am so lucky to be your brother. Your courage to live and think differently and to recognize the subtle joys in everyday life is truly amazing. This dissertation is dedicated to my parents who have given me the tools to succeed and have encouraged me every step of the way. You have been true partners in learning throughout my life.

I would like to acknowledge General Motors for their commitment to the field of smart materials and their investment in my education and career. My sincere gratitude goes out to my committee members: Panos Papalambros, John Shaw, and Alan Browne. Your successes are humbling, and I am honored by your service. All of you have

challenged me intellectually, and guided my scholarly growth. Special thanks are owed to my co-advisors Jonathan Luntz and Diann Brei. Jon, your curiosity has been inspiring and you have led me to look at all sides of this esoteric problem. Diann, I have learned so much from you over the years here, and I deeply appreciate your dedication to my success. Thank you for challenging me to approach even the most difficult problem with vision.

Table of Contents

List of Figures

List of Tables

ABSTRACT

Spooled-Packaging of Shape Memory Alloy Actuators

by

John A. Redmond

Co-chairs: Diann E. Brei and Jonathan E. Luntz

A vast cross-section of transportation, manufacturing, consumer product, and medical technologies rely heavily on actuation. Accordingly, progress in these industries is often strongly coupled to the advancement of actuation technologies. As the field of actuation continues to evolve, smart materials show significant promise for satisfying the growing needs of industry. In particular, shape memory alloy (SMA) wire actuators present an opportunity for low-cost, high performance actuation, but until now, they have been limited or restricted from use in many otherwise suitable applications by the difficulty in packaging the SMA wires within tight or unusually shaped form constraints. To address this packaging problem, SMA wires can be spool-packaged by wrapping around mandrels to make the actuator more compact or by redirecting around multiple mandrels to customize SMA wire pathways to unusual form factors. The goal of this dissertation is to develop the scientific knowledge base for spooled packaging of low-cost SMA wire actuators that enables high, predictable performance within compact, customizable form factors. In developing the scientific knowledge base, this dissertation defines a systematic general representation of single and multiple mandrel spool-packaged SMA actuators and provides tools for their analysis, understanding, and

synthesis. A quasi-static analytical model distills the underlying mechanics down to the three effects of friction, bending, and binding, which enables prediction of the behavior of generic spool-packaged SMA actuators with specifiable geometric, loading, frictional, and SMA material parameters. An extensive experimental and simulation-based parameter study establishes the necessary understanding of how primary design tradeoffs between performance, packaging, and cost are governed by the underlying mechanics of spooled actuators. A design methodology outlines a systematic approach to synthesizing high performance SMA wire actuators with mitigated material, power, and packaging costs and compact, customizable form factors. By examining the multi-faceted connections between performance, packaging, and cost, this dissertation builds a knowledge base that goes beyond implementing SMA actuators for particular applications. Rather, it provides a well-developed strategy for realizing the advantages of SMA actuation for a broadened range of applications, thereby enabling opportunities for new functionality and capabilities in industry.

Chapter 1. Introduction

Actuation is ubiquitous in everyday life appearing in transportation, manufacturing, medical devices, and consumer product technologies. It is essential for providing mechanical functionality to devices throughout society. Commonly, the advancement of products in any of these fields is enabled or restricted by the state-of-the-art in actuation. By expanding the available means to provide mechanical functionality to devices, innovation and technological advancement can thrive. This chapter provides background to understand the growing need for low-cost, high performance, and form-customizable actuators in industry. Reviewing the state-of-the-art in actuation, smart materials are identified as a major area of growth for addressing industry's actuation needs. In particular, shape memory alloy-based actuators have great potential to enable low-cost, high performance actuation. One of the important factors limiting their impact has been the difficulty to package them compactly or within unusual form constraints. Seeking strategies for overcoming this key obstacle to their success, different packaging techniques for SMA are explored and evaluated based on their ability to enable low-cost, high performance actuation that can be designed compactly or customized to even the most difficult form factors. Spooled-packaged SMA wires, in particular, can be customized to tight, unusually shaped form constraints by wrapping and redirecting the SMA wire around mandrels. As a result, the spooled-packaging approach is an excellent alternative packaging method that allows the performance and cost advantages of SMA wire actuation to be realized within compact, customizable form factors. Spooled-packaging for SMA wire actuators is formally introduced, and the customizable architecture and basic operation are described. For spooling to be a viable packaging strategy, several key research issues need to be resolved regarding performance predictability, understanding the impact of design choices on performance and packaging, applying the spooling technique to an expansive range of configurations, and

synthesizing low-cost spool-packaged actuators with high, predictable performance and compact customizable form factors. The goals and objectives of the dissertation are defined, and a summary of the research approach is provided at the chapter's close.

1.1. Frontiers in actuator research

The growing need for high performance actuators is common throughout industry. Often, improvement of existing products and innovation of new technologies rely on higher performance actuation being packaged within confined, unusually shaped spaces at reasonable cost. In a review of the state-of-the-art in actuation, smart materials are highlighted for their potential to push beyond the current capabilities of conventional actuators. Assessing the ability of traditional and alternative actuator technologies to meet the growing needs, shape memory alloy is identified as a promising candidate to enable low-cost, high performance actuation.

1.1.1. Need for improved actuation

At the forefront of actuator research, dramatic increases in actuator work are being sought. For example, DARPA noted that actuation performance must be increased by orders of magnitude above that of traditional actuators to realize new functionality via the morphing of large aerospace structures (Garcia, 2002). This need led to several programs that focused on creating high energy and power density actuators including the DARPA/AFRL/NASA Smart Wing program (Kudva, 2004), the DARPA Compact Hybrid Actuator Program (CHAP) (Garcia, 2002), and the DARPA/NASA/ONR Smart Aircraft and Marine Propulsion System (SAMPSON) demonstration (Sanders, et al., 2004). In each of the programs, the high work output from energy dense actuators was essential in adding functionality to aircraft structures such as fixed wings, rotor blades, and engine inlets. Due to the critical need to incorporate actuation within aircraft substructures, both high work and form-customized packaging have to be addressed together.

Providing actuator functionality is often made difficult by the need to constrain an actuator to fit within a limited space. The need for actuation within difficult to meet form

constraints is exemplified in morphing aircraft structures with internally packaged actuators (Bein, et al., 2000; Calkins, et al., 2006; Dunne, et al., 1999; Dunne, et al., 2000; Epps & Chopra, 2001; Giurgiutiu, et al., 1997; Liang, et al., 1996; Mabe, et al., 2005; Prahlad & Chopra, 2007; Rey, et al., 2003; Ruggeri, et al., 2002; Singh, et al., 2003; Strelec, et al., 2003), actuators packaged within automobiles closures and the engine compartment (Cifferi, 2005; Brei, et al., 2006; Dynalloy, 2010; Magna Closures, 2010), low-cost latch actuators for consumer appliances (Dynalloy, 2010; Johnson, et al., 2003; ITW Global Appliance Group, 2007; Osvatic, 2009; and Wu & Schetky, 2000), actuators for compact prosthetics and orthotic devices (Pfeiffer, et al., 1999; Wang & Shahinpoor, 1998), and ingestible and implantable biomedical devices (Kim, et al., 2005; Menciassi, et al., 2004; Menciassi, et al., 2005; Utter, et al., 2009). The common thread across these examples is the need to fit actuators within vacant spaces inside the product needing mechanical work. The challenging form constraints in these cases make it difficult to provide the necessary work using traditional approaches.

While actuator packaging and performance affect an actuator's ability to provide mechanical work within an application's device specifications, cost typically affects the device's viability in the market with examples throughout transportation, medical, and consumer product technologies. In addition to the direct monetary costs of an actuator, indirect costs often occur, which may include the cost of energy required to power the actuator or costs related to actuator mass. In mass-critical applications such as spacecraft, aircraft, and cars, the additional energy costs associated with transporting the actuator mass also bear impact on overall cost. The need for controlled costs is illustrated in air travel. For instance, in the late 1990's one of NASA's ten main goals was to reduce the cost of air travel by 25% in ten years and by 50% in twenty years (National Research Council, 1998). With a significant portion of manufacturing costs and weight attributed to actuators and actuated-structures for aircraft, NASA sought cost-reductions by developing alternative actuation that can replace bulky conventional actuators. Moreover, NASA sought the addition of new functionality to aircraft that improves aerodynamic characteristics to reduce fuel consumption (Siochi, et al., 2002). In the automotive industry, cost-control is critical for vehicles to be competitive in the market, and this has led

General Motors to examine how actuation can increase functionality and value of its vehicles at minimal cost, or to reduce the cost and weight of its vehicles through alternative actuation (Browne, et al., 2004; Taub, 2006). The cost factor extends throughout medical and consumer product technologies as well. For instance, high costs are noted to be prohibitive in medical instruments that reduce human tremor (Pathak, 2010). In consumer products, cost is highly regarded to have a pivotal role in purchasing decisions. Cost control is often a result of the ability to provide actuation performance to technologies more cheaply than before or to enable cost saving functionality. However, to realize this vision, the different aspects of industry's actuation needs regarding performance, packaging, and cost must be addressed together.

1.1.2. State-of-the-art in actuation

To understand how current needs for high performance, low-cost, well-packaged actuators can be addressed, the main categories of actuator technologies are considered: conventional actuation, which includes hydraulics, pneumatics and electro-mechanical actuators, and smart materials actuation, which includes piezoelectric ceramics and polymers, shape memory alloys, electroactive polymers, and magneto- and electrostrictives. Evaluating these types of actuators regarding their performance, cost, and packaging illustrates the potential for smart materials to advance the field of actuation.

1.1.2.1. Comparison of actuator technologies

To meet the current challenges for higher performance within less space, actuators with high energy densities are necessary. In comparison to conventional actuators, smart materials often exceed the energy densities by orders of magnitude as demonstrated in Table 1.1 and Figure 1.1. Comparing work output, NiTi shape memory alloy can achieve the highest work densities in the tens of MJm^{-3} range (Figure 1.1a) and specific work in the $kJkg^{-1}$ range (Figure 1.1b) with only hydraulic actuators among the conventional actuators being comparable. While the hydraulic actuators appear to compete with the performance of smart materials, they have major disadvantages of requiring complex,

bulky infrastructure such as piping, valves, working fluid, and compressors. The working fluid is especially problematic requiring continuous filtration to prevent lock-up, and is notorious for leaking (Burdea, 1996). Whereas conventional actuation depends on the conversion of one form of energy (fluidic, electrical, thermal, etc.) into mechanical energy using assemblies of discrete parts, the energy conversion within smart materials actuators occurs at the material level. Thus, smart materials require no moving parts or additional infrastructure that need to be packaged aside from small electrical elements such as wires or electrodes. Additionally, many smart materials are available in different forms, which can aid in the ability to customize packaging. For example, piezoelectric material can be manufactured in plates, tubes, bimorphs, C-blocks, etc. (Chopra, 2002; Niezrecki, et al., 2001) and shape memory alloy can be manufactured in wires, films, springs, tubes, etc. (Chopra, 2002).

Considering cost from both weight and price standpoints, smart materials and conventional actuators have advantages and disadvantages. Among smart materials and conventional actuators, typical mass-based comparisons of energy density indicate hydraulic and pneumatic actuators are favorable over smart materials actuators (for example, Figure 1.1b). However, oftentimes such comparisons (as is the case in the Figure 1.1b) do not factor in additional weight of pumps, tubing, work fluid, etc. that impact an actuator's overall weight. Additionally, hydraulic and pneumatic actuators are in the kilogram range of masses, or beyond, whereas smart materials can weigh grams or less. Smart material actuators do not require the heavy infrastructure and they can be designed with relatively low mass. Therefore, the cost of transporting the smart material actuator within a vehicle (for example, in space shuttles, aircraft, or automobiles) is less, making smart materials more attractive regarding cost. While the cost-factor varies widely for smart materials based on a number of factors including the actuator's technical maturity and current manufacturing capabilities, shape memory alloys are noted for being economically viable for large-scale applications such as for automotive devices (Luntz, et al., 2009; Browne, et al., 2004). As SMA becomes more widely adopted, continued improvement to the material costs is expected.

Table 1.1. Comparison of selected conventional and smart material actuators.

Actuator System	Actuation Stress (MPa)	Actuation Strain (%)	Maximum Work Density (Jm^{-3})	Maximum Specific Work (Jkg^{-1})	Maximum Driving Frequency (Hz)	Maximum Power Density (Wm^{-3})
Conventional Technologies						
Human Muscle [3]	0.1 - 0.4	30 - 70%	$(15 - 200) \times 10^3$	60 - 200	50 - 500	$\approx 500 \times 10^3$
Pneumatics [3]	0.5 - 0.9	10 - 100%	$(50 - 900) \times 10^3$	$(0.5 - 5) \times 10^3$	50 - 300	$\approx 5 \times 10^6$
Hydraulics [3]	20 - 70	10 - 100%	$(2 - 70) \times 10^6$	$(4 - 40) \times 10^3$	50 - 300	$\approx 500 \times 10^6$
Moving Coil Transducer [3]	0.004 - 0.05	1 - 10%	$(0.02 - 5) \times 10^3$	0.05 - 1	$(20 - 50) \times 10^3$	$(0.5 - 2) \times 10^6$
Solenoid [3]	0.04 - 0.1	10 - 40%	$(2 - 40) \times 10^3$	3 - 10	5 - 80	$(10 - 40) \times 10^3$
Thermal Expansion (10K) [3]	20 - 50	0.009 - 0.003%	$(0.9 - 7.5) \times 10^3$	1 - 2	0.4 - 9	$\approx 60 \times 10^3$
Thermal Expansion (100K) [3]	200 - 500	0.09 - 0.03%	$(90 - 750) \times 10^3$	100 - 200	0.4 - 9	$\approx 6 \times 10^6$
Smart Material Technologies						
SMA [3]	100 - 700	0.7 - 7%	$(0.2 - 30) \times 10^6$, $< 7 \times 10^{6‡}$	$(1 - 5) \times 10^3$, $< 1.1 \times 10^{3‡}$	0.02 - 10[3], ~100 (thin film) [4]	$< 700 \times 10^3$
Magnetostrictor [3]	90 - 200	0.06 - 0.2%	$(30 - 200) \times 10^3$	20 - 30	30×10^6	$(100 - 700) \times 10^6$
Low Strain Piezoceramic [3]	1 - 3	0.0005 - 0.003%	3 - 50	0.006 - 0.02	$(0.5 - 30) \times 10^6$	$(0.1 - 1) \times 10^9$
High Strain Piezoceramic [3]	4 - 9	0.005 - 0.02%	100 - 900	0.06 - 0.12	$(0.5 - 20) \times 10^6$	$(90 - 500) \times 10^6$
Piezoelectric Polymer [3]	0.5 - 5	0.02 - 0.1%	$(0.5 - 2.5) \times 10^3$	0.3 - 1	$(0.1 - 10) \times 10^6$	$\approx 300 \times 10^6$
Polymer Gels	0.1 - 0.5 [2]	0.6 - 1% [2]	$(7 - 60) \times 10^3$ [2]	60 [5]	< 1 [1]	$(0.6 - 2) \times 10^9$ [2]
Electrostrictive Polymers	40 [5]	5% [5]	$(100 - 700) \times 10^3$ [2]	600 [5]	$\approx 90 \times 10^{3†}$	$(2 - 9) \times 10^9$ [2]

[1] (Wax & Sands, 2003)
[2] (Pons, 2005)
[3] (Huber, *et al*., 1997)
[4] (Fu, *et al*., 2004)
[5] (Kornbluh, *et al*., 2004)
† Estimated from the work and power densities of reference [2].
‡ Estimated from Dynalloy guidelines (Dynalloy, 2010)

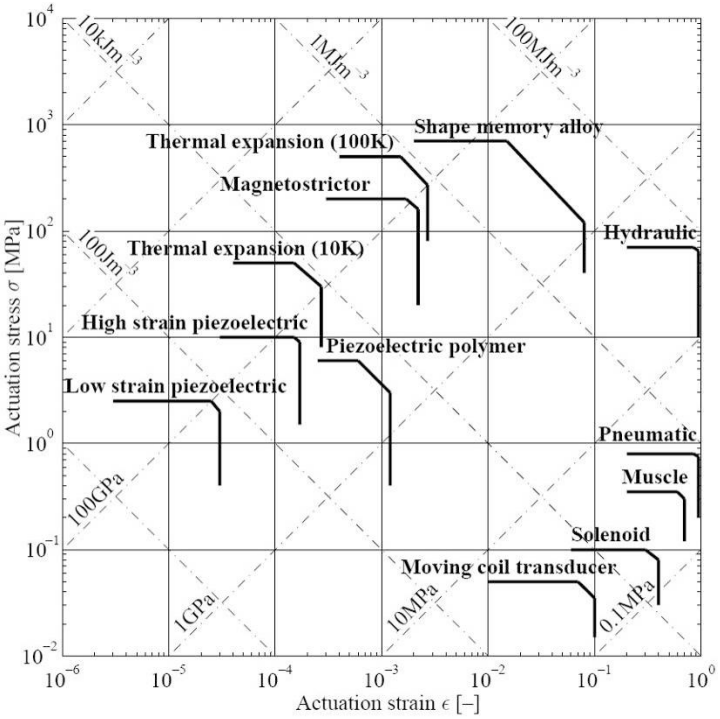

(a) Volumetric comparison of actuator work output

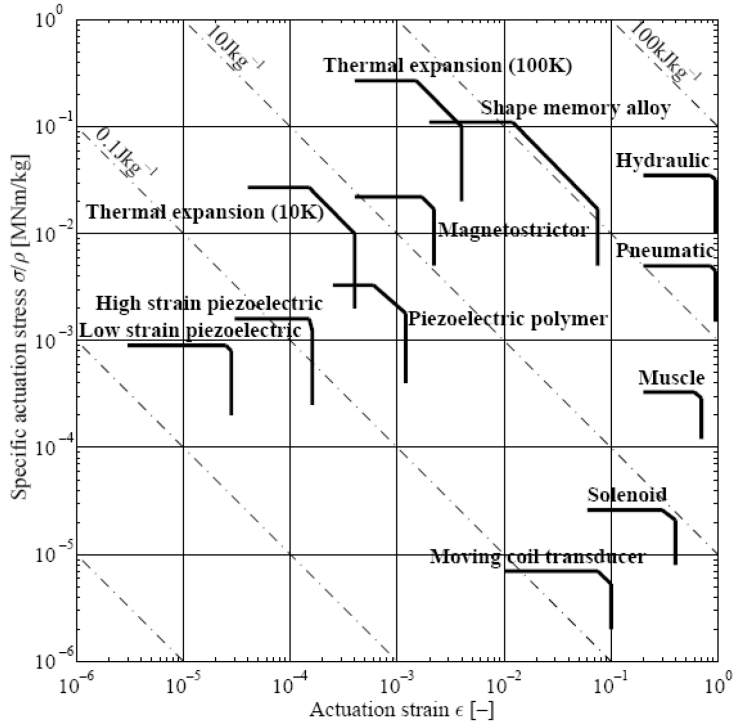

(b) Mass-based comparison of actuator work output

Figure 1.1. Performance charts for linear actuators. (a) Volumetric comparison of actuator work output. In a comparison of actuators of equal size, the graphic shows that shape memory alloy has exceptional energy density properties (measured on axis with slope of -1). (b) Mass-based comparison of actuator work output. Comparing actuators of equal mass, SMA has the highest specific work among the smart materials. Although hydraulic and sometimes pneumatic devices appear to compete well with SMA and other smart materials in some comparisons, it is important to note that these metrics do not account for infrastructure of the fluidic power actuators such as working fluid, valves, compressors, etc. (Charts reproduced from Huber *et al*. 1997).

1.1.2.2. Growth of smart materials actuation

Smart materials are competitive alternatives to conventional actuators due to their high energy density and potential for low-cost, high performance actuation. Yet, one of their primary disadvantages is their lack of technological maturity. During the last two decades, a significant smart materials research effort has sought to improve the state-of-the-art of actuation beyond that of conventional technologies. A variety of sectors have been involved in this effort including the military (e.g., DARPA, AFRL, ARO), government (NSF and NASA), industry (Boeing, Northrup Grumman, Lockheed Martin, McDonnell Douglas, GM, TSI, Raytheon, Dynalloy), medical (3M, Nitinol Medical Technologies, Mitek Surgical Products), and academia (Univ. of Michigan, Univ. of Pennsylvania, Virginia Tech, UCLA, Texas A&M, and Univ. of Maryland among others). Research in these sectors has led to several exciting demonstrations of applications that are either difficult or impossible to achieve with conventional actuation. Examples include the Smart Wing program (Kudva, et al., 2002), the Compact Hybrid Actuator Program (CHAP) (Garcia, 2002), and the Smart Aircraft and Marine Propulsion System (SAMPSON) demonstration (Dunne, et al., 1999; Sanders, et al., 2004). Each of these programs applied smart materials actuation to realize high work output from energy dense materials, which was essential in adding morphing functionality to fixed wings, rotor blades, and engine inlets.

This paradigm shift is also evidenced by industrial investment in smart materials technologies. Automotive interest is indicated by a 600% increase in the number of patents issued for devices based on smart materials (piezoelectric, electroactive polymer, shape memory alloy, shape memory polymer, or magnetorestrictive materials) as illustrated in Figure 1.2 (Brei, et al., 2007). Furthermore, automotive-related patent filings for SMA devices have grown beyond a factor of 10 in the past decade (Johnson, 2006). General Motors is embracing smart materials devices for their potential to reduce cost and add functionality to their vehicles, and has accordingly identified this field to have major importance for the automotive industry (Browne, et al., 2004; Taub, 2006). They have developed several technologies that are beginning to be deployed including hood, door,

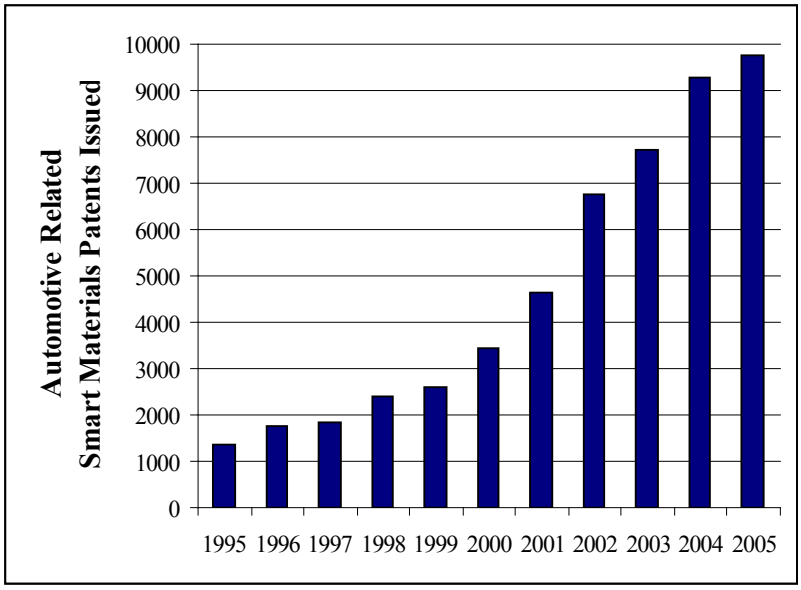

Figure 1.2. Automotive patents for smart materials. The graphic illustrates the number of automotive related smart materials patents issued each year since 1995. The data represents technologies based on piezoelectric, electroactive polymer, shape memory alloy, shape memory polymer, or magnetorestrictive materials and shows a 600% growth in the past 10 years (data provided by Nancy Johnson 2006, figured also appeared in (Brei, et al., 2007)).

and trunk latches, active vehicle surfaces including air dams and engine compartment louvers, and adaptive suspensions. These technologies are intended to reduce costs, enhance performance, add functionality, and improve fuel economy (Taub, 2006).

A wide class of applications at the frontier of today's needs for advanced actuation can benefit from smart materials to enable new functionality that has not been available with conventional technologies. Considering smart materials from a performance, packaging, and cost perspective, shape memory alloys have a number of advantages that make them a practical choice for advancing the paradigm in actuation capabilities.

1.1.3. Advantages of shape memory alloy actuators

Among smart materials, NiTi shape memory alloy (SMA) can deliver moderate to large motions using small amounts of actuator material due to its superior energy density. (While a number of materials exhibit shape memory, this dissertation focuses specifically on the use of NiTi shape memory alloys and uses the terms "NiTi SMA" and "SMA" interchangeably). SMA surpasses most smart materials in terms of maximum actuator stress (near 700 MPa) and maximum actuator strain (up to 8%) (Hesselbach, 2007). Operating near the maximum stresses and strains, however, tends to degrade material

performance and can lead to low-cycle fatigue. Thus, for high-cycle fatigue life (millions of cycles), the manufacturer of Flexinol SMA wire recommends typical operating stresses below 170 MPa and strains below 4-5% (Dynalloy, 2010). Even so, SMA has the best combination of high stress and high strain to give it unparalleled work density near 16 MJm^{-3} (Kumar & Lagoudas, 2008), which is typically more than two orders of magnitude over other smart materials (Huber, et al., 1997). However, using SMA according to the Dynalloy guidelines, about 7 MJm^{-3} energy density is available for higher cyclic use. While hydraulic actuators have similar energy density metrics as SMA (Huber et al., 1997), the hydraulic energy density metric only accounts for the piston portion of the actuator and not for the additional pumps, valves, and fluid lines required. SMA actuators are well suited to gross motion outputs in the millimeters to centimeters range making them suitable actuators for active fasteners (Barnes, et al., 2006; Busch, et al., 1992; Johnson, et al., 2003; Kapgan & Melton, 1990; Redmond, et al., 2007; Wu & Shetky, 2000), active valves (Luntz, et al., 2007; Okhata & Suzuki, 1998; Prince, et al., 1985; Wu & Ewing, 1994; Wu & Schetky, 2000), and morphing structure actuators (Bein, et al., 2000; Calkins, et al., 2006; Dunne, et al., 1999; Dunne, et al., 2000; Epps & Chopra, 2001; Giurgiutiu, et al., 1997; Jardine, et al., 1996; Liang, et al., 1996; Mabe, et al., 2005; Prahlad & Chopra, 2007; Rey, et al., 2003; Ruggeri, et al., 2002; Quackenbush, et al., 2005; Singh, et al., 2003; Strelec, et al., 2003). Most other smart materials such as piezoelectrics and magnetostrictives, by contrast, typically have only microns of motion output making them better suited for low displacement needs such as precision position, noise, and vibration control. Certain electroactive polymers (EAPs), are capable of large shape change (greater than 200% strain for dielectric elastomers under no load), but have much lower actuation stresses (less than 8 MPa) and are a relatively immature technology (Kornbluh, et al., 2004; Pons, 2005).

In addition to having excellent energy density properties, SMA has several advantages that make it a practical actuator including its simplicity, speed, and robustness. SMA actuators are simple due to their solid-state actuation and straightforward operation. Since SMA actuators are solid-state, they are clean, silent, have low part counts, and can be scaled down to very small devices or scaled up to civil

structures (Hesselbach, 2007; Song, et al., 2006). Relying on changes in temperature to actuate, the operation is simple since they can interface with existing electronics and power supplies in a vehicle or device with a very small weight/size contribution due to the electrical circuit (Mavroidis, 2002). High current heating techniques allow for very fast one-way actuation (<5 ms) without causing failure in the actuator (Barnes, et al., 2006). By manufacturing SMA devices in different forms such as wire, tube, rod, ribbon, sheet, foil, spring, or other custom shapes, SMA actuators can have rotational or linear outputs, exert a broad range of loads and deflections, and actuate across a wide range of speeds (Huang, 1998). Due to the rugged, non-corrosive properties of SMA, they can withstand harsh environments and are biocompatible for implanted devices and medical instruments (Morgan, 2004). The high performance and practical advantages of SMA make it a very competitive choice for a broad range of applications.

1.2. Shape memory alloy background

To meet industry's growing need for alternative actuators, it is necessary to push beyond the traditional approaches of hydraulic, pneumatic, and electromagnetic actuation. Shape memory alloy actuation shows great potential to overcome current limitations due to its high energy density, large workable strains, and increasingly affordable cost. Exploring shape memory alloy in greater depth, its development as a technology is detailed in this section. The review of SMA technologies demonstrates that while SMA has achieved a high level of commercial success for superelastic applications, its use as an actuator has yet to reach this same level. To make SMA actuation a practical technology, many of the technical challenges that have hindered the development of SMA actuation are currently being addressed such as improving the speed of actuation, making more robust mechanical connections, and reducing performance degradation over time. Still, packaging difficulties arise in creating high performance actuators with practical form factors since long lengths of SMA wire are often needed to achieve moderate to large deflections.

1.2.1. Pioneering work in shape memory alloy

The first published description of a shape memory property dates back to 1932, when Arne Ölander noted a rubber-like behavior in samples of a gold-cadmium alloy (Ölander, 1932). At the time, he lacked an explanation for this behavior, which is now known as superelasticity. In 1938, the crystallographic phase change responsible for shape-memory was first described by A.B. Greninger and G. Mooradian who noted the temperature sensitive presence of the martensite phase in brass (Greninger, 1938; Greninger & Mooradian, 1938). Also noted in some historical reviews of SMAs (Schetky, 1979; Shaw, 1997; Wayman & Harrison, 1989) are Russian metallurgists G. V. Kurdyumov and Khandros for their observations of the thermal dependence and reversibility of the crystallographic phase transformations in brass. In 1951, L. C. Chang and T. A. Read studied single crystals of AuCd and explained the shape-memory effect and superelasticity in terms of diffusionless phase transformations, discussing the interplay between stress, strain, and temperature of phase transformations (Chang & Read, 1951). During the 1950s, improvements to the understanding of shape memory properties were made with research on materials including InTl (Burkart & Read, 1953), CuZn (Genevray, 1953), and CuAlNi (Chen, 1957). These advances preceded the heightened attention that SMAs received with the discovery of the shape memory effect in equiatomic nickel-titanium alloy.

The breakthrough was spawned by Cold War-era Naval Ordnance Laboratory (NOL) research (Kauffman & Mayo, 1997). William J. Buehler, a Michigan-born NOL metallurgist, was investigating metallic alloys for the nose cone of the re-entry vehicle for U.S. Navy Polaris missiles. He specifically focused on nearly equiatomic Ni-Ti alloys for their superior impact resistance and ductility relative to other alloys he was considering. In 1959, he named the alloy NiTiNOL (Nickel Titanium Naval Ordnance Laboratory). Later that year, to quickly estimate damping in the material, he dropped bars of Nitinol on the lab's concrete floor to observe the acoustic response. He noticed that damping had a remarkable temperature dependency. Whereas room-temperature bars landed with a "thud" one would expect from lead, warmer bars "rang like a bell." Buehler recounts, "This immediately alerted me to the fact that the marked acoustic damping change was

related to a major atomic structural change, related only to minor temperature variation" (Buehler, 1991b). The shape memory of NiTi was discovered at a 1961 laboratory management meeting that Buehler could not attend. He sent an accordion shaped strip of NiTi to the meeting as a demonstration of the excellent fatigue properties of the material. Dr. David S. Muzzey, a pipe smoker in attendance, used his lighter to heat the compressed accordion strip, which stretched out by the change in temperature alone (Buehler, 1991a). This marked the beginning of several decades of research on NiTi's shape memory properties that would follow, which have led to a number of industrial applications that derive their functionality from SMA's characteristic behaviors.

1.2.2. Shape memory alloy characteristics and uses

Shape memory alloys are distinguished by two characteristic behaviors, *superelasticity* and *shape memory effect*, which are the result of reversible, diffusionless phase transformations that are brought on by changes in stress and temperature. On a microstructural level, the shape memory and superelasticity phenomena are both based on changes in SMA crystal structure between the low temperature phase, *martensite*, and the high temperature phase, *austenite*. The key difference is that the shape memory effect (SME) is based on a temperature-induced phase transformation, and the superelasticity property is based on stress-induced phase transformation. Superelastic SMA technologies are relatively mature and they have achieved commercial success. The review of SME technologies, on the other hand, demonstrates that a few technical barriers prevent SME technologies from achieving similar levels of success and impact enjoyed by superelastic devices.

1.2.2.1. Superelasticity

Superelastic behavior is characterized by the ability of shape memory materials to undergo very large strains, up to 8% in NiTi (Kumar & Lagoudas, 2008), when loaded, and can fully recover these strains when the load is removed. The key event that causes this behavior is a stress-induced phase change from austenite to the more compliant

martensite, as opposed to the temperature-induced phase change that will be described for the shape memory effect.

1.2.2.1.1. Superelastic material behavior

To describe typical superelastic behavior, a test based on a specimen of NiTi (50.1% Ni) from Memry Corp. with a 1.07 mm diameter is used as an example based on experiments by Shaw & Kyriakides (1995). Since the thermomechanics of SMA are highly temperature dependent, the experiment was run in a temperature controlled water bath, allowing the superelastic effect to be observed at a constant temperature. The superelastic loading-unloading cycle is shown for the NiTi sample in Figure 1.3 looping sequentially from points ⑤ to ⑩. Prior to loading (point ⑤), the material is austenite in phase and has a cubic B2 lattice structure represented schematically as overlapping square grids of Ni and Ti atoms in bubble "A" of Figure 1.3. As stress is applied to the material, elastic strain is accumulated until stress-induced martensite begins to propagate

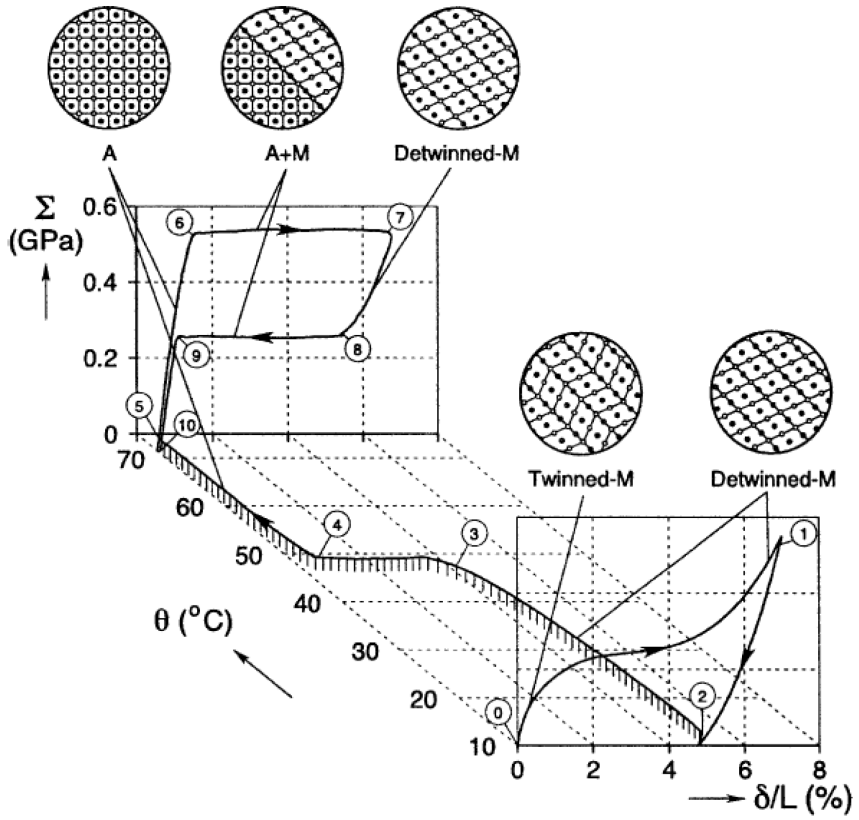

Figure 1.3. Thermomechanical behavior of NiTi wire. This example demonstrates the shape memory effect (points ⓪-④) and pseudoelasticity (points ⑤-⑩) for uniaxially strained NiTi wire. Figure reproduced from Shaw (2002).

(point ⑥) and continues to accumulate until the material is fully detwinned martensite (point ⑦). As the stress is removed, the phase begins to transform back to austenite (point ⑧), with the full reverse transformation nearly complete at point ⑨ and elastic recovery in the austenite phase as the material reverts to the initial configuration (point ⑩).

1.2.2.1.2. Superelastic applications

Superelastic SMA has become widely used across many applications for its remarkable flexibility and ability to recover large strains, and has reached a level of technical maturity that has enabled widespread use across medical, commercial, and civil sectors. Of the $8.1 billion market for smart materials and $27.7 billion market for smart materials-based products[†], 15% of the revenue has been estimated to be for SMA products, the majority of which are for biomedical devices containing superelastic elements (Business Communications Company, 2006 as cited by Hartl & Lagoudas, 2007). Several examples of superelastic products are shown in Figure 1.4. Superelastic NiTi has been successful in biomedical applications and is well suited for implantation due to its corrosion resistance, biocompatibility, kink resistance, flexibility, and ability to provide nearly constant forces over large strain ranges (Morgan, 2004). The earliest biomedical use of superelastic SMA dates back to the initial development and installation of NiTi orthodontic arch wires for braces in the early 1970s (Andreasen & Hilleman, 1971; Andreasen & Morrow, 1978). NiTi arch wires accounted for an estimated 30% market share of arch wires in 1999 (Duerig, et al., 1999); provide even straightening forces over much larger displacements than the conventionally used stainless steel wires; and result in fewer office visits for wire tightening, faster tooth straightening, and increased patient comfort (Duerig, 2002). In addition to use in orthodontics, NiTi has been used in the Mammalok needle wire localizer used to mark tumors in breast tissue (O'Leary, et al., 1990), a thermally deployed vena cava blood clot filter (Simon, et al., 1977), and self-expanding cardiovascular

[†] Figures are for the 2006 market. This year (2010), the market for smart materials was projected to be $12.3 billion and for smart materials-based products to be $52.2 billion (Business Communications Company, 2006 as cited by Hartl & Lagoudas, 2007).

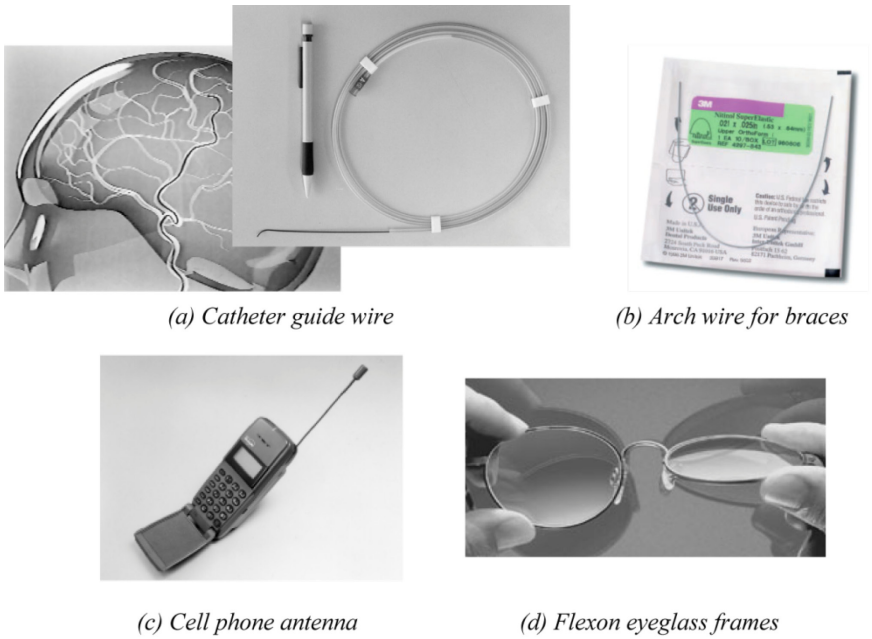

(a) Catheter guide wire *(b) Arch wire for braces*

(c) Cell phone antenna *(d) Flexon eyeglass frames*

Figure 1.4. Examples of products with superelastic SMA. A variety of products utilizing superelastic SMA have successfully come to market including a (a) catheter guide wire (Otsuka & Kakeshita, 2002), (c) cell phone antennas (Otsuka & Kakeshita, 2002), and (d) eye glass frames which use SMA for its ability to recover very large strains without permanent deformation (Flexon, 2006). (b) Superelastic archwires for braces apply even straightening forces to the teeth over a larger range than the traditionally used stainless steel archwire (3M, 2006).

stents, in surgical instruments, and superelastic catheter guide wires (Morgan, 2004), and others. There is a growing market for superelastic SMA-based medical devices (Hartl & Lagoudas, 2007), and the abundance of such applications is testament to superelastic SMA's technological maturity (further reviews of additional biomedical applications for superelastic SMA are available in the literature, including those by Duerig, et al., 1999; Mantovani, 2000; Miyazaki, 1998; Morgan, 2004).

In addition to the medical devices that use superelastic SMA, the material has become a useful structural element for consumer products and in civil structures. Eyeglass frames with superelastic SMA components have successfully been used to reduce eyeglass weight, increase flexibility and comfort, and make the glasses more resistant to damage (Flexon, 2006; Zider & Krumme, 1988, 1990a, 1990b). Other superelastic implementations include cellular phone antennas that are highly flexible and resistant to permanent deformation and brassiere underwires designed to enhance user comfort and are less likely to become bent or kinked when laundered (Otsuka & Ren, 1999). In civil structures, engineers utilize the high hysteresis in superelastic SMA to dissipate energy

and provide ground isolation from seismic loads (Song, et al., 2006). The breadth of applications using superelastic SMA further underscores its technological maturity, demonstrating the use of SMA's unique material properties as a basis for practical and highly functional devices that were not possible with conventional technologies.

1.2.2.2. Shape memory effect

Unfortunately, shape memory effect (SME) technologies have not reached the same level of success as superelastic due to a few technical barriers limiting its widespread use. The *shape memory effect* occurs when a martensitic SMA specimen is loaded and unloaded to induce a residual strain, and then recovers the strain when heated to the austenite phase. Whereas superelasticity is based on the stress-dependent phase transformation between austenite and martensite, the shape memory effect relies on temperature-dependent phase transformation for shape recovery. A large amount of research has gone into the development of SME actuators, but only several niche SME-based products have successfully gone to market. The existing research demonstrates that some issues remain and that more work must be done for SME devices to be more practical, useful replacements or enhancements for conventional actuators.

1.2.2.2.1. Shape memory effect material behavior

To illustrate the typical SME cycle, the stress, strain, and temperature behavior for a NiTi specimen (Shaw & Kyriakides, 1995) is revisited. The SME cycle is illustrated in Figure 1.3 as the stress, strain, and temperature are tracked sequentially through points ⓪ to ⑤, and back to point ⓪. At point ⓪, the material is twinned martensite with the lattice represented schematically as a herringbone pattern of parallelograms in the "twinned-M" bubble of Figure 1.3. The material is subject to zero load and is considered to have zero strain in this state, which is achieved by heating to austenite and cooling to martensite. Loading and unloading the wire (from point ⓪ to ②), the lattice structures are sheared until the material is fully detwinned. The deformation of the sheared lattices accumulates to a residual strain on the macroscopic level. Maintaining a small tensile load and heating the wire above its transition temperature, the material fully transforms to austenite (from

points ② to ⑤). As the detwinned martensite lattice transforms to the cubic austenite lattice, the residual strain is completely recovered. Finally, the wire is cooled to return it to its initial state (point ⓪), and the crystal structure reverts to twinned martensite.

The shape memory effect is fundamental for the functionality of work-producing SMA actuators, which are typically comprised of an SMA element and a biasing element (such as a spring or a weight). Throughout this dissertation, the operation is defined with respect to three main states, which are useful for describing the full range of motion as the wire is thermally cycled between the fully austenite and fully martensite states while under load. In the example shown in Figure 1.5, a straight SMA wire acts against an external load – a deadweight in this case. All motions and wire lengths are referenced to a zero-strain reference, *State 0*, which is reached by heating the SMA wire to austenite with no load and maintained in *State 0* upon cooling assuming a negligible two-way effect in the SMA material. In typical operation, the SMA wire acts against an applied load as it is thermally cycled. Applying load to the *State 0* wire in martensite, the martensite microstructure detwins resulting in large, recoverable strains (up to 8%) for the *State 1* actuator. Heating the SMA wire, the SMA material transforms to the stiffer austenite phase with a cubic microstructure, causing the SMA wire to shorten in length as it transitions to *State 2*. In typical operation, the wire is cycled between *States 1* and *2*, resulting in the actuator's range of motion $\delta\ell$ and a resulting mechanical work output.

To provide an understanding of how the SMA material interacts with a system,

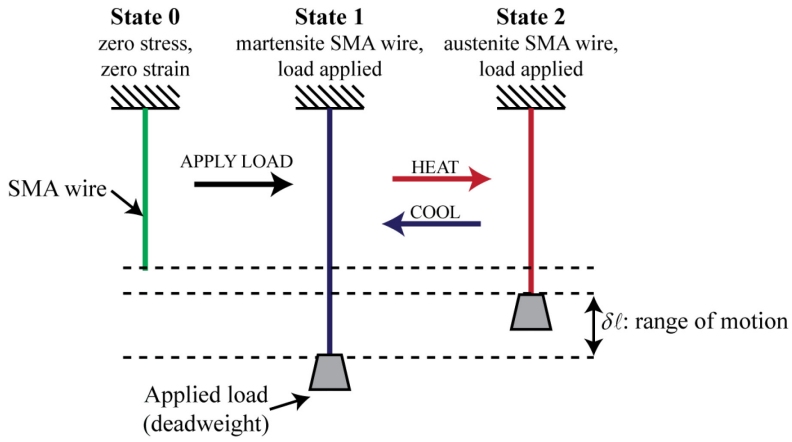

Figure 1.5. Basic SMA actuator diagram. A linear SMA wire actuator is loaded against a bias load, a constant mass load in this case, and cycled between the martensite and austenite phases to achieve useful actuator motion, $\delta\ell$.

substantial research for more than 20 years has focused on developing constitutive models for SMA including early phenomenological models (Tanaka, 1986; Liang & Rogers, 1990; Brinson, 1993; Boyd & Lagoudas, 1994), micromechanical models (Sun & Hwang, 1993; Patoor, et al., 1994; Huang & Brinson, 1998; Vivet & Lexcellent, 1998; Goo & Lexcellent, 1997), coupled thermodynamic and mechanical models (Ivshin & Pence, 1994; Seelecke & Muller, 2004; Shaw, 2002; Shaw & Churchill, 2009), and models predicting the dynamics of phase boundary motion (Abeyartine & Knowles, 1991; Truskinovsky, 1993; Chang, et al., 2006). The models vary in complexity and their ability to predict different aspects of the SMA material behavior. These models provide a glimpse into a broad range of research on SMA material behavior, which is reviewed in greater depth by Otsuka & Ren (2005) and Machado & Lagoudas (2008).

1.2.2.2.2. Shape memory effect applications

For over three decades, the military, industry, and medical fields have invested in shape memory devices and improved the understanding of how SMA works. Unfortunately, the research has not yet crossed the threshold necessary to make low-cost, high performance SMA actuators a norm. In particular, the difficulty in meeting tight or unusually shaped form constraints emerges as a common theme throughout the survey of SMA actuator applications that utilized the shape memory effect.

1.2.2.2.2.1. Couplings

The first successful application of the shape memory effect, which was based on constrained recovery, was the Cryofit pipe coupling from Raychem (Kapgan & Melton, 1990; Kauffman & Mayo, 1997; Mantovani, 2000; Melton, 1998), which dates back to the late 1960s (Mantovani, 2000), was first patented in 1973 (Otte & Fischer, 1973), and is currently sold under the brand name Aerfit (Aerfit, 2009) . The coupling is easily installed between two pipes at low temperatures and contracts around the two as it warmed to typical operating temperatures to form a strong, reliable joint. The couplings were implemented in military aircraft, marine applications, and industrial pipe joining and weld reinforcement (Kapgan & Melton, 1990). Using similar collar-type architecture, SMA actuation has also been used in

Frangibolts, in which the collar is controllably heated to contract around a fastener causing shear failure (Busch, et al., 1992). The devices were successful in demonstrating useful applications for the high work density of SMA, but are expensive due to manufacturing and the need to maintain them at very low temperatures prior to installation, which limits them to niche markets (Melton, 1998). While couplings and collars have yet to be demonstrated for cyclic actuation, they provided an early demonstration of SMA's commercial viability and the ability to provide energy-dense, one-way actuation.

1.2.2.2.2.2. Biomedical devices

Many biomedical SMA applications have involved superelasticity, but few have utilized SMA as an actuator. Examples include SMA wire actuators used to generate rotary motion in prosthetic limbs (Pfeiffer et al., 1999) and in a compact knee/leg muscle exerciser for paraplegics (Wang & Shahinpoor, 1998). SMA wire has also been demonstrated to have ingestible and implantable applications such as a swallowable capsule for gastrointestinal tract monitoring with SMA based locomotion and clamping (Kim, et al., 2005; Menciassi, et al., 2004; Menciassi, et al., 2005) and in an implantable bowel extender that causes therapeutic lengthening of the small intestine for infants afflicted with short bowel syndrome (Utter, et al., 2009). In each of the applications noted, SMA was used in the wire form, which is a common choice since wires are cheaper than other forms and they do not require additional heating elements (whereas collars do). SMA is particularly well suited for biomedical applications because of its low cost, low mass (due to high energy density), and biocompatibility. Commonly, biomedical devices need to be worn, implanted, or ingested, which necessitates very compact packaging of the actuator element. Despite the high energy density of SMA, the extremely limited form factors that are available in biomedical devices restrict the ability of SMA to deliver useful work to the small or unusual spaces where actuators can be placed. The packaging challenge is evident in examples of applications that wrap SMA wire around pulleys/mandrels or use

the material within a ratchet mechanism (Menciassi, et al., 2004; Menciassi, et al., 2005; Utter, 2009).

1.2.2.2.2.3. Valves, latches, and louvers

In the 1980s and 1990s, a group of consumer products using SMA spring actuators arrived on the market. Some of the most notable had temperature sensitive actuation such as an anti-scald showerhead valve (Wu & Ewing, 1994), a vent to prevent overheating of greenhouses (Prince, et al., 1985), and an air conditioner louver (Ohkata & Suzuki, 1998). Other products used electrically heated actuators such as a damper control of an electric oven (Ohkata & Suzuki, 1998), a lid lock for a washing machine (Johnson, et al., 2003), a door lock on a self-cleaning oven (Wu & Schetky, 2000), and a Daimler Benz valve to control flow of transmission fluid (Wu & Schetky, 2000). The temperature dependent devices demonstrated an elegant way to combine sensing and actuation at the material level, which reduced part count and complexity relative to conventional sensor/control/actuator solutions, but these devices were typically was not used in applications where the form constraints were very limited or constrained by unusually shaped spaces. More recently, SMA wire devices are gaining attention for their use in automotive applications for examples including swing-panel latches (Ciferri, 2004; Redmond, et al., 2007), active louvers that control airflow through the front grille (Bucholz, 2007), an active airdam that controls airflow underneath the vehicle (McKnight, et al., 2009), and high-speed valves for safety devices (Luntz, et al., 2007). In automotive applications, the cost and performance of actuators are important. Due to very limited spaces that are available throughout the vehicle to incorporate actuators, the packaging is critical. To expand the potential for SMA to address the growing need for low-cost, high performance actuation, the difficulty in packaging long lengths of SMA wire within more convenient forms needs to be overcome.

1.2.2.2.2.4. Defense and aerospace devices

Several projects focusing on morphing structures and attachment devices, fueled largely by defense and aerospace projects have brought greater technical maturity to SMA actuation while also highlighting the drawbacks of certain SMA forms. One

approach to morphing structures utilizes SMA torsion tubes for active rotor blade tracking by Liang *et al.* (1996), Prahlad and Chopra (2007), and Ruggeri et al. (2002), and in the DARPA/AFRL/NASA Smart Wing program (Jardine, et al., 1996). SMA wires were used in morphing structures as shown in active rotor blade tracking (Epps & Chopra, 2001; Giurgiutiu, et al., 1997; Singh, et al., 2003), in morphing airfoils (Bein, et al., 2000; Strelec, et al., 2003), in a morphing chevron by Boeing (Calkins, et al., 2006; Mabe, et al., 2005), in morphing jet engine inlets on the SAMPSON project (Dunne, et al., 1999; Dunne, et al., 2000; Sanders, et al., 2004), in variable area fan nozzles for jet engines (Rey, et al., 2003), and in deforming a "smart duct" propeller shroud (Quackenbush, et al., 2005). While the high energy density provided potential for producing large forces and displacements using low volumes of actuator material, packaging difficulties often made it difficult to place the high performance actuators within practical form factors. For example, in the SAMPSON Smart Inlet project, an antagonistic SMA actuator was designed and built to deform the cowl of an F-15 engine inlet. To achieve the required 15 cm of deflection, a very long actuator, 3.8 meters in length, was used which made packaging the SMA actuator a challenge (Dunne, et al., 2000; Sanders, et al., 2004). This type of packaging problem is typical for SMA actuators since, without employing mechanical means for trading force for displacement, they often require lengths many times longer than the stroke. Such large form factors can make SMA impractical for many applications if the packaging is not addressed.

1.2.2.2.3. SMA Issues

While a number of SMA actuator applications appear in the literature, many are either still in development or have had only limited success in the market. For SMA actuator technologies to reach a similar level of success as superelastic SMA devices, the technical challenges preventing SMA actuators from being a more practical approach need to be overcome. In particular, SMA actuation has been limited by issues regarding speed, quality, cost, manufacturing, mechanical connections, performance shakedown, and packaging – and in many cases, these issues are beginning to be addressed.

Since SMA is thermally actuated, it is slower than actuators with electric or magnetic field stimuli, but has been shown to contract very quickly (<5 ms, Barnes, et al., 2006) with large current pulses. The main limitation to bandwidth results from the need to cool SMA quickly. Techniques such as cooling the actuator in water have been shown to improve actuator frequency to near 20 Hz (Webb, et al., 1999), while thin-film forms of SMA run at frequencies around 100 Hz (Fu, et al., 2004). Antagonistic SMA actuation has also been shown to improve speed with frequencies up to 10 Hz (Pathak, 2010).

While making mechanical connections is sometimes viewed as a challenge, mechanical crimping has been demonstrated to be a practical method for attachment that can be done compactly. In a recent development, a brazing technique for SMA was introduced that can be used to overcome mechanical attachment issues (Grummon, et al., 2006). Degradation of wire performance as the material is cycled also make consistent operation difficult. However, stabilization of actuator performance is being addressed by developing an enhanced understanding of shakedown and techniques for pre-cycling the SMA under load for more repeatable performance (Erbstoeszer, et al., 2000, Sun, et al., 2006; Churchill & Shaw, 2008).

Many of the hurdles limiting SMA are currently being addressed, but the need to package SMA compactly while maintaining its high energy density remains an active issue. While packaging has been encountered and addressed in specific cases, currently no approaches directly examine packaging strategy and actuator form-integration. Because of the limited ability to package SMA actuators, it is often difficult to provide low-cost, high performance actuation to applications where the form constraints are very limited. Thus, while SMA actuators can occupy very small volumes, the dimensions of the actuators are not necessarily small, but rather bulky and impractical. Additionally, SMA is limited from addressing applications where an irregularly shaped space is available to package an actuator, but the space cannot accommodate an actuator due to its irregular form. Problems that call for more compact or customizable actuator forms highlight a general need for alternative techniques for packaging SMA.

1.3. Shape memory alloy packaging

There are several examples in the literature of technologies that choose SMA for its high work output density (among other properties), but encounter packaging difficulties in transitioning the energy density benefit to a practical actuator form. To design actuators with practical forms, two main types of packaging needs commonly arise: the need for compactness and the need for customizable form factors. Examining how different forms of SMA have been used to address the packaging problem, spooled-packaging is shown to present a distinct opportunity for addressing both types of packaging needs.

1.3.1. Packaging problem

Due to SMA's high energy density, SMA actuators can deliver high performance using small volumes of actuator material. However, linear forms of SMA generally require actuators that are 10 – 50 times longer than the stroke. Thus, despite the distinctively high energy density, low volume, and low-cost characteristics of SMA actuators, the potentially long form factors can limit SMA's use in applications with strict or even moderate form constraints. While the exact definition of a practical actuator form depends on the application, overcoming limitations due to packaging typically necessitates compact or customizable form factors – or both.

1.3.1.1. Compact packaging

From a practical standpoint, the overall dimensions of the envelope surrounding an SMA actuator are often more important that the volume of SMA material used. For instance, a long, narrow SMA actuator is typically very low in volume, but can be too large and unwieldy to be used in a small space. Thus, compact packaging is necessary, for which the overall dimensions of the actuator are reduced, and the actuator has a low aspect ratio. The need for compact packaging is illustrated in biomedical devices where devices need to be implanted, ingested or worn, in aerospace applications where devices need to be packaged within confined spaces such as an airfoil, rotor blade, or jet inlet, or

automotive applications where devices must fit within existing spaces in the engine compartment, swing panels or dashboards. For example, a need to package long wires is noted in an SMA actuated prosthetic device (Pfeiffer, et al., 1999), in a leg muscle exerciser for paraplegics (Wang & Shahinpoor, 1998), and in the design of a swallowable digestive tract monitoring and clamping device (Menciassi, et al., 2005). In Active Velcro, linear SMA wires are used to manipulate an active surface; in this case, the volume of actuator portion of the active surface is very strongly related to the stroke requirements of the actuator (Clement, 2004). Among the examples cited, the amount of motion that SMA provides was limited by the space available, or measures were taken to make the SMA actuator more compact. However, in packaging the SMA material more compactly, tradeoffs typically result including work losses due to inefficient use of the material (using SMA springs, for instance), the need for additional hardware to heat non-wire forms of SMA such as torque tubes, and friction losses that occur for spooled SMA wires. Thus, while compact packaging is often critical for the success of SMA in practical applications, the ability to package compactly is not straightforward.

1.3.1.2. Customized packaging

Engineering applications will often require the actuator be packaged in an existing space such as within the structure of a jet engine inlet, airfoil, rotor blade, car door, car hood, handheld medical instrument, etc. The practicality of an SMA actuator can depend on whether its form can be customized to fit within the vacant spaces of a structure, which may be unusually shaped. In cars, for instance, actuator functionality can increase a vehicle's fuel economy, customer satisfaction, and overall value (Browne, et al., 2004), yet there are very limited spaces where the actuator can be packaged, and the spaces are typically not regular in form. For example, actuated dashboard air louvers have been elusive because of the very limited form constraints. While there is some space available within the dashboard, it is separated from the louvers by narrow channels where wires could pass through, but solenoids or motors could not fit. Additionally, laser printers, duplexers, and copy machines utilize solenoids to controllably direct paper along

different routes, and the solenoid actuation impacts the size, weight, and cost of the machine. SMA actuators could improve on these issues without sacrificing performance, but the space available for actuation is affected by the paper route and the additional components within the printer. Therefore, customizable actuator packaging would be critical in delivering SMA actuation. The need for customizable forms exists throughout aerospace structures where the actuator must fit within strict form constraints, and biomedical devices that are implanted, worn, or ingested. These are just a few examples that illustrate an ongoing problem. To address the growing need for high performance, low-cost actuation in industry, enabling customizable packaging is a critical step to make SMA more practical.

1.3.2. Shape memory alloy packaging forms

While SMA can enable low-cost, high performance actuation in products, its widespread success has been limited by the difficulty of packaging the actuator within limited form constraints. To address the packaging problem, it is necessary to design actuators that are compact, customizable, or both. In the past, packaging has been approached using different forms of SMA including springs, torsion tubes, and spool-packaged wires (examples of each form are shown in Figure 1.6). The use of mechanical levers is another notable strategy for packaging SMA actuators because they can increase the amount of motion by trading off load for stroke. However, since levers are not a means for increasing mechanical work within a confined space, and because they are still viable for use in conjunction with any of the packaging forms, they are considered to be in a different category of approaches than the use of different SMA forms. Furthermore, the use of smaller, leveraged SMA wires also leads to additional issues that become more of an issue as mechanical advantage is increased including: higher part counts, the need for tighter manufacturing and SMA mounting tolerances, the need to account for structural compliances as larger SMA forces are required, etc.

The spring, torsion tubes, and spool-packaged forms are useful for providing larger amounts of work within a given form factor relative to a linear SMA actuator. By

a) SMA springs

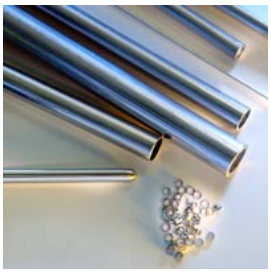

b) SMA torsion tubes

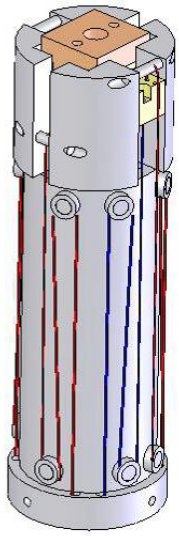

c) Spooled SMA actuator for SMASH handgrip

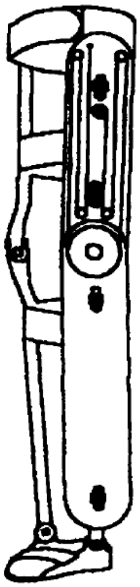

d) Spooled SMA actuator for leg orthosis

Figure 1.6. SMA material forms. Examples of different material forms used for packaging SMA are shown including SMA springs (Middlesex, 2006), SMA torsion tubes (Johnson Matthey, 2006), spooled SMA wire for the SMASH stabilization handgrip (Pathak, et al., 2007), and spooled SMA wire for a actuated leg orthosis (Wang & Shahinpoor, 1998).

comparing these forms based on their performance, cost, and packaging characteristics, it becomes clear that while all the forms improve on the packaging of linear SMA wire, only spooled-packaging can adeptly customize actuators to unusually-shaped form constraints.

1.3.2.1. Springs

Several commercial SMA applications from the 1980s and 1990s used SMA springs to provide large displacements, although they were typically limited to applications with low force requirements (Wu & Ewing, 1994; Prince, et al., 1985; Okhata & Suzuki, 1998; Wu & Shetky, 2000; Otsuka & Kakeshita, 2002). More recent demonstrations have also used SMA springs for consumer products (Johnson, et al., 2003), robotics (Yang & Gu, 2008; Choi, 2006; Yan, et al., 2007), aerospace (Dong, 2008), and medical devices (Dumont & Kuhl, 2005).

Springs are effective in creating large strokes relative to the spring's free length (Ohkata & Suzuki, 1998), but they trade-off much of the force and work output compared to a linear SMA wire actuator. A typical SMA spring can be expected to deliver less than 10% of the force and 20-40% of the work compared to a linear SMA wire actuator of equal material volume and wire diameter[‡]. Since the stresses in a spring vary across the SMA wire's thickness, some regions of the SMA wire may be used ineffectively leading to lower energy density relative to an axially loaded SMA wire where the stress distribution is uniform. Relative to SMA wires, the cost of springs is higher due to additional manufacturing processes required to shape-set the helical form; however, cost is typically not prohibitive. One of the key advantages of SMA springs relative to SMA wires is its compactness. Through the helical packaging, it is possible to provide much larger displacements in small spaces. However, SMA springs are limited in their ability to be customized because they occupy cylindrical form constraints, and cannot be easily tailored to irregularly shaped form constraints.

1.3.2.2. Torsion tubes

SMA torsion tubes can be used to package an actuator in a long narrow space and are capable of generating large rotations. The use of SMA torsion tube actuators gained popularity in the mid-1990s for aerospace needs to twist rotor blades and airfoils for better flight performance (Liang, et al., 1996; Jardine, et al., 1996; Davidson, et al., 1996). Concepts were capable of delivering about 2° rotation with 225 Nm of torque for the DARPA Smart Wing (Jardine, et al., 1996) and 30° rotation with 4.5 Nm of torque for a Boeing rotor blade twister (Clingman & Ruggeri, 2004). A bidirectional actuator based on antagonistic torsion tubes was developed by Kennedy, et al. (2000) and delivered more than ±7.5° and 4.5 N-m. While tubes can deliver significant torque and rotation, the shear loading varies with distance from the torque tube's axis, which can lead to reduced energy densities

[‡] The values for spring force are calculated for typical spring indexes (coil diameter / wire diameter) between 6 and 12 (Shigley & Mischke, 2001) and based on formulas for maximum force and maximum actuator stroke for shape memory alloy actuators (Hesselbach, 2007).

when the tubes are not very thin-walled. Additionally, they are expensive to manufacture, bulky due to additional heating elements, and slow to heat and cool. While they can provide very large moments in narrow spaces, they are limited to applications that require rotational motion and can accommodate long actuators (Singh, et al., 2003; Strelec, et al., 2003).

1.3.2.3. Spooled wire

SMA wires can also be spool-packaged around pulleys and mandrels to make long SMA wires more compact or form-customized by directing wires through irregularly shaped form constraints. Spooled-packaging has been demonstrated in a variety of applications (a few examples are illustrated in Figure 1.7) where SMA wires are desirable, but form constraints make them infeasible to implement without packaging. For example, the technique was used to package long SMA wires in a knee and leg muscle exerciser for paraplegics in which a 4 meter SMA wire wrapped around several pulleys to package the actuator compactly near the leg (Wang & Shahinpoor, 1998). Spooled packaging has also been demonstrated in handgrip stabilization (Pathak, et al., 2007) and in the SAMPSON morphing jet engine inlet (Sanders, et al., 2004). In contrast to torque tubes and springs, spooled actuators use SMA material in tension, which allows a greater work output than shear loaded actuator shapes such as springs and torque tubes (Pons, 2005). SMA wires are the most cost-economical form of SMA due to their simplicity, growing use in industry, and simpler manufacturing. The cost of spool-packaged actuators would be slightly higher than for non-packaged SMA wires due to the additional cost of mandrels and the use of additional material to overcome any performance losses associated with spooled-packaging. Still, since SMA wires are already low in cost and require no additional hardware to heat and cool the wire (Singh, et al., 2003; Strelec, et al., 2003), spool-packaged SMA wires are an economical packaging form.

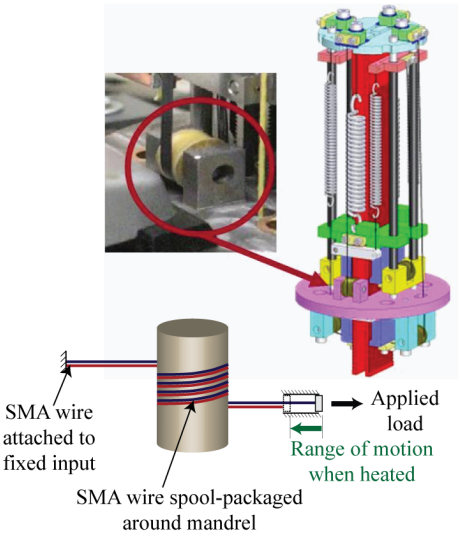

(a) Single mandrel, linear actuator for automotive hood lift (Barnes, et al., 2006)

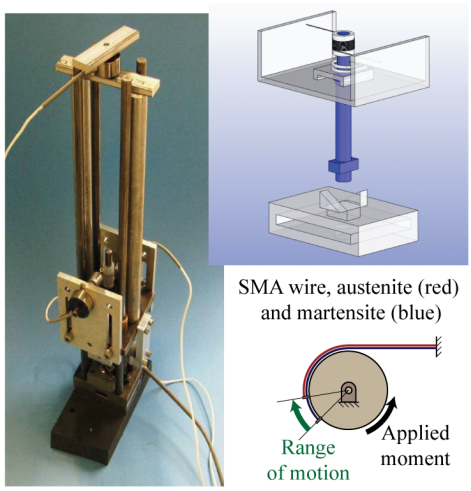

(b) Single spool, rotational actuator for ultrafast, resettable latching (Redmond, et al., 2007)

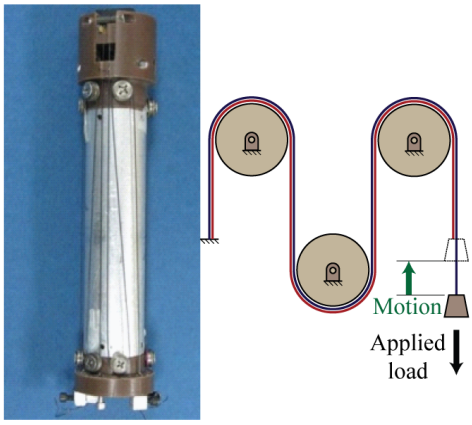

(c) Multiple spool, linear actuator for handgrip stabilization (Pathak, et al., 2007)

Figure 1.7. Spool-packaging categories and example applications.

1.3.2.4. Packaging form comparison

To evaluate the potential for the different forms of SMA to address the needs for high performance, low-cost, and compact, customizable packaging, they are compared qualitatively in Table 1.2. The performance advantage of SMA results from the material's high energy density. Yet, in practical implementation, it is challenging to package the material without making excessive sacrifices to performance. It is advantageous to use SMA in tension rather than shear to maximize the amount of useable work. Among the three forms, only spooled-packaging uses the material in tension. However, losses occur

due to friction and the bending portions are not held in perfect tension. Therefore, while spooled-packaging has a performance advantage, the packaging must account for potential losses and mitigate them when possible. Regarding the actuator's range of motion, springs can provide motions much larger than the coil length, although much of the force and work is sacrificed. While torque tubes provide high authority work, they rarely achieve rotations beyond 90°. Spool-packaged SMA wires have the potential to provide very large motions depending on the amount of space available to package. Considering the different forms from a cost-perspective, SMA wires are advantageous because they are less costly to manufacture and do not require additional hardware to heat and cool.

The spring, torsion tubes, and spool-packaged forms are most distinguished by their ability to address the customization aspect of the performance problem. Springs and torsion tubes have some limited ability to be customized by selecting geometric parameters suited to particular form constraints, but they are limited to cylindrical spaces. Spool-packaged wires on the other hand, are easily adaptable to a wide range of form constraints that are not necessarily regular geometric spaces. For applications where there is room to place an actuator, but the vacant space is a confined and a non-standard shape, only spool-packaged SMA wires can be adapted to the unusual form to produce large motions. Thus, spool-packaged SMA wires have some cost and performance advantages over torsion tubes and springs, but they are truly distinguished by an unparalleled capacity for form customization. Spooled-packaging is a promising candidate for low-cost, high performance SMA actuation, and it is unrivaled in its ability to address the

Table 1.2. Qualitative comparison of SMA actuator forms.

	Performance					**Cost**	**Packaging**	
	Static			*Dynamic*				
Form	**Stroke**	**Load** (force or moment)	**Work density**	**One-way speed**	**Band-width**	**Cost**	**Compact**	**Customiz-able**
Linear wire (benchmark)	Fair	Very good	Excellent	Very good	Fair	Very good	Poor	Poor
Spring	Very good	Poor	Fair	Good	Fair	Fair	Very good	Fair
Torsion tube	Fair	Very good	Fair	Poor	Poor	Poor	Good	Poor
Spool-packaged wire	Very good	Very good	Good	Very good	Fair	Good	Very good	Excellent

packaging problem for compact, customizable form factors. However, the influence of the packaging architecture on actuator performance needs to be understood to enable design of spool-packaged actuators that meet the needs for high performance, low-cost, and compact, customizable form factors.

1.3.3. Spooled-packaging architecture and operation

Spool-packaged SMA wire actuators can vary greatly in size and shape, and they are capable of producing different types of output motions. Yet, all spool-packaged SMA wire actuators comprise four key elements (illustrated in Figure 1.8): 1) a single SMA wire in tension, 2) a fixed input where the SMA wire attaches to a referenced ground, 3) one or more cylindrical mandrels, which are wrapped fully or partially by the SMA wire, and 4) a rotational or linear single degree-of-freedom motion output. More complex actuators with multiple wires can be considered to be multiple spool-packaged SMA wires in parallel or series. For example, the T-latch (Redmond, et al., 2007) uses two spool-packaged SMA wires that work in parallel. Three types of spool-packaged SMA wire actuators are illustrated in Figure 1.7 including variations with single and multiple mandrels, and linear and rotational output motions. The SMA wire is fixed to ground at the "input tail", has alternating linear and wrapped portions depending on the number of mandrels that the SMA wire wraps, and has an "output tail" connected to the motion output.

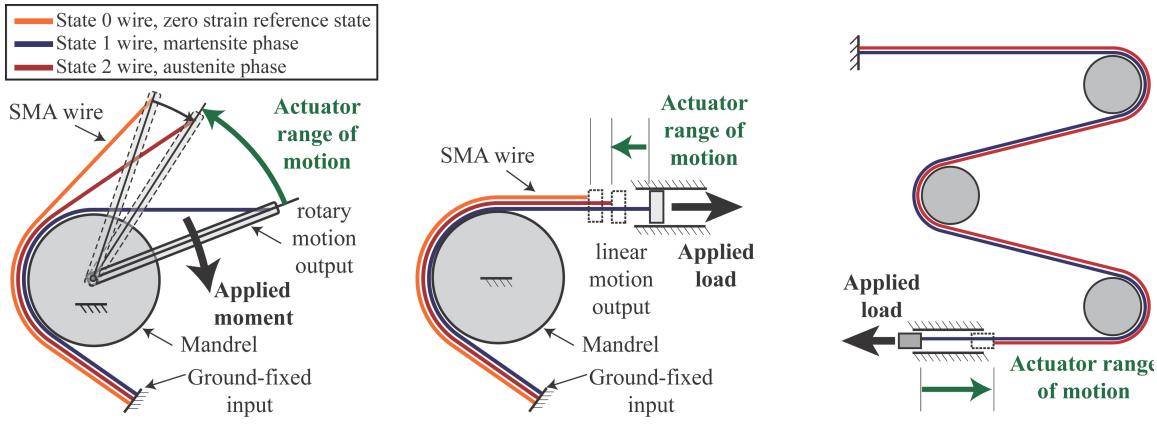

(a) Single spool, rotational actuator *(b) Single spool, linear actuator* *(c) Multiple spool, linear actuator*

Figure 1.8. Basic architecture and operation states for spool-packaged SMA actuators.

The actuator's operation cycle results from the thermal cycling of the SMA wire causing it to contract along its length upon heating to austenite and extend along its length upon cooling to martensite. The net contraction and extension of the wire as it is thermally cycled results in intermediate portions of the SMA wire sliding along the mandrels, which results in linear or rotational motion at the actuator's output.

1.3.4. Spooled-packaging research issues

To overcome the packaging problem, the spooled-packaging strategy can be developed to support the design of SMA actuators for a broad range of problems. While spool-packaged SMA actuators have been demonstrated on a limited scale, several research issues stand in the way of attaining this goal.

To provide a foundation for design, a model is needed that predicts the range of motion for spool-packaged SMA wire actuators with respect to its design parameters including geometry, applied load, friction properties, and SMA constitutive behavior. The key effects on performance need to be predicted including friction and bending, and the limitations on the model need to be understood. For spool-packaged actuators, the performance is typically degraded due to interfacial friction losses between the SMA wire and mandrel. In addition, bending of the wrapped portions of the SMA wire leads to a strain gradient variation across the wire's cross-section that alters, and typically depresses, the strain contribution to overall motion. Previous approaches to predicting the motion of spooled SMA wire actuators have estimated efficiency losses based on empirical observations (Wang & Shahinpoor, 1998), assumed that the wrapped portions do not contribute to the overall motion (Tanaka, 1996), or adapted Capstan or belt-braking models for specific actuator configurations (Howell, 1953; Firbank, 1970; Huang, 2000). Unfortunately, most of these models are derived for only specific configurations and they do not accurately capture large wrap angles, do not account for portions of the wire that gain and lose contact with the mandrel during operation, and do not consider bending strains. To provide the analytical foundation for developing the spooled-packaging, a

versatile model is needed that addresses the effects and limitations due to friction and bending.

To implement the spooled-packaging technique skillfully through each stage of the design process including synthesis, analysis, and revision, a deeper understanding is needed for how spooled actuator performance is influenced by an actuator's packaging and its design. By developing the spool-packaging technique for versatile application using generic architectures and numerous specifiable parameters, more interrelationships among design choices, packaging constraints, and actuator behavior arise. To enable engineers to adeptly analyze and synthesize spool-packaged actuators despite the complexity of the problem, a knowledge base for understanding the relationships between design, packaging, and behavior is necessary.

By packaging around multiple mandrels, an array of topologies and geometries that allows for more flexible and robust form customization is possible. A generalized architecture is needed to specify the expanded range of designs. As in the single mandrel case, multiple mandrel actuators are subject to friction, bending, and binding. Additionally, cumulative effects due to wrapping around multiple mandrels need to be addressed. Thus, for multiple mandrel form customization, the underlying mechanics and the cumulative wrapping effects need to be modeled to provide an analytical basis for design.

For problems with multiple mandrels and different variations in packaging, it becomes even more difficult to select high-quality design without making unnecessary sacrifices to performance and cost. To manage the competing design tradeoffs and meet unusual packaging constraints, a systematic approach to synthesizing spool-packaged actuators is vital. A design methodology for spool-packaged actuators can utilize single and multiple mandrel models as the analytical basis for generating actuator designs with predictable performance, and optimize parameters to best attain performance, packaging, and cost objectives while satisfying application-specific constraints. By resolving these

issues related to the analysis, understanding, and synthesis of spool-packaged SMA actuators, the packaging strategy can be implemented skillfully to applications needs.

1.4. Research goals and objectives

The goal of this dissertation is to develop the scientific knowledge base for spooled packaging of low-cost SMA wire actuation that enables high, predictable performance within compact, customizable form factors. To achieve this goal, there are four main objectives:

1. Derive a quasi-static, analytical model for the mechanics governing a single mandrel spool-packaged SMA actuator that predicts work performance with respect to the specifiable actuator geometry, material properties within the system, and the applied loads while accounting for friction and bending,
2. Build an understanding of how actuator design parameters and packaging constraints influence performance, to facilitate the design of spool-packaged actuators through all the synthesis and analysis stages,
3. Expand the spooled-packaging technique to multiple mandrel actuator topologies by defining a parameterized architecture and developing an expanded model that enables analysis and synthesis of actuators within customizable forms,
4. Develop and demonstrate a model-based design methodology that enables engineers to synthesize spool-packaged SMA actuators with forms and performances that can be customized to specific application requirements.

1.5. Research approach

To fulfill the goals of this thesis and overcome the packaging problem that prevents SMA from being a more practical technology with a wider application space, the main objectives were addressed through four main tasks: deriving a single mandrel model, conducting a parameter study, expanding the model to multiple mandrel configurations, and developing an optimization-based design methodology for spool-packaged actuators.

1.5.1. Task 1: Single mandrel performance model

To meet the first objective, a quasi-static, analytical model for single mandrel spool-packaged actuators was derived in Chapter 2. The model is necessary to support the

analysis and synthesis of spool-packaged SMA actuators, and thus needed to account for the impacts of the packaged architecture on performance with respect to the actuator geometry, friction, SMA constitutive properties, and externally applied loads. A generalized architecture was defined for the versatile specification of single mandrel actuators, allowing the motion to be predictable with respect to a broad range of single mandrel designs. The model considers the effects of friction and bending on the actuator's performance, and assesses the limits of the packaging technique due to the accumulation of friction. Through an experimental study, the model was validated with respect to applied load for rotational and linear actuators. The model's assessment of the effects of bending and binding were also confirmed experimentally.

By addressing the first objective, the model can facilitate the analysis of spool-packaged SMA actuator designs. By making the model versatile, it can accommodate the specification of a large array of design variables and parameters. By accounting for its limitations due to accumulated friction and SMA wire bending, the model can be used predictable and with reasonable losses. Whereas previous modeling attempts were developed on a case-by-case basis for particular applications, a model developed at a high level of rigor can be applicable to a larger scope of applications. By relating the key mechanical effects to an actuator's design and resulting performance, the model can thus serve as an enabling tool for a deeper understanding and analytical synthesis capabilities for spool-packaged SMA actuators designs.

1.5.2. Task 2: Parametric study

While spool-packaged SMA wire actuators can be customized to many applications based on the generic, versatile architecture and the modeled effects of friction, bending, and binding, the multiple specifiable parameters that afford designers flexibility also make for a more complex design problem. To apply the packaging technique skillfully despite the multiple interrelationships within the model, a foundational understanding is needed for how performance depends on key design parameters and different types of packaging constraints. In Chapter 3, the effects of applied load, geometric parameters,

and material parameters were explored based on model-based simulations and select experimental studies. In the study of each parameter, its affect was assessed across a typical range of values, and, in some cases, multiple parameters were explored together to understand their interdependencies and tradeoffs. The impact of packaging on actuator design and performance was examined in three examples cases for which different types of form constraints were considered: a baseline case without particular packaging constraints, a case constraining the actuator footprint within a rectangular envelope, and a case constraining the actuator within a rectangular constraint that contains an internal obstacle. In each case, the range of motion was predicted across a range of mandrel diameters, wrap angles, and, in the latter two cases, the mandrel position within the packaging constraint. Based on the findings of the parameter study, design guidelines were provided and a knowledge base for understanding spooled actuator behaviors was built to aid engineers in selecting parameters well, understanding the behavior of prototypes, and revising existing designs.

The parameter studies conducted in Chapter 3 develop the knowledge base for enhanced abilities to analyze, synthesize, and revise spool-packaged actuator designs. The study on the impact of packaging on performance provides insight into how different types of packaging constraints influence performance and the design choices. Studying the connection between design, packaging, and performance builds the intuitive basis for making meaningful design choices, understanding the behavior of physical prototypes, and skillfully revising designs. By providing the foundational knowledge for using spooled-packaging well, the technique can hasten the design process and support the successful implementation of spooled-packaging for industrial needs.

1.5.3. Task 3: Multiple mandrel packaging technique

In Chapter 4, the single mandrel technique was expanded to the multiple mandrel case to provide for a higher degree of form customization than can single mandrel actuators. A generalized architecture for multiple mandrel actuators was defined along with indexing conventions for describing the topology, geometry, and range of motion.

The multiple mandrel model considers similar mechanical principles as in the single mandrel case, but also accounts for the more complicated geometry and alternating linear and wrapped segments by introducing a cumulative wrap angle term into the model. The cumulative wrap angle was important for modeling how friction affects the behavior of adjacent segments of SMA wire, and allowed the model to be expanded to a much broader range of SMA wire pathways. The full model predicts the actuator's range of motion by accounting for friction and bending with respect to the actuator topology and geometry, the frictional and constitutive material properties within the system, and the externally applied loads. Additionally, the binding limitation due to accumulated friction and the motion of actuators that undergo binding was derived for the multiple mandrel configurations. Finally, an experimental study was performed to validate the expanded packaging technique and model for actuators with different numbers of mandrels and a range of applied loads.

The expanded model allows for the analysis of a much broader range of topologies and geometries, and provides a basis for designing form-customized packaging with predictable performance. Consequently, the multiple mandrel model increases the impact of the techniques and methodologies that result from this research. While more compact packaging of SMA actuators is the first step toward overcoming the packaging problem, the multiple mandrel spooled-packaging techniques and models allow SMA wires to be integrated into empty spaces within existing structures or devices allowing additional actuator functionality to be incorporated into a system without making it larger or adding significant cost or weight.

1.5.4. Task 4: Design methodology

Due to the many tradeoffs between packaging and performance and an increasingly complex problem for the use of multiple mandrel architectures, a systematic approach was needed for designing spool-packaged SMA actuators. In Chapter 5, the single and multiple mandrel models are used as the foundation of a systematic design methodology for customizable performance and form factors, which can be tailored to particular

application specifications. A general framework for designing spool-packaged actuators is provided and applied to three case studies with different performance and packaging requirements. In the first case study, a single mandrel actuator was designed for which there are no particular form constraints, but a more compact form was desired and a minimum amount of motion was required. Gradient-based optimization techniques were applied, and a range of optimal designs with respect to the designer's importance placed the packaging dimensions and SMA wire length was generated and analyzed. In the second case study, a single mandrel actuator is required to fit within an external form constraint without intersecting with an internal obstacle. In this case, a multi-objective optimization was performed that maximizes motion and minimizes SMA wire length for a variety of relative weightings on each objective. A genetic algorithm was used in the optimization to seek the global optimum for a design space that is discontinuous and has many local extrema. Finally, the methodology was demonstrated within the same form factor as in the second case study (external envelope, internal obstacle), but for multiple mandrel designs for which the actuator motion was maximized while minimizing the SMA wire length. Again, a genetic algorithm was applied for the design space, which becomes increasingly complex as more mandrels are used. The resulting designs were used to demonstrate the ability to customize packaging to a difficult form factor and enable greater performance than would be available without packaging the SMA wire.

While the theory alone contributes a new understanding of spooled actuators, the research is bolstered by integrating the modeling knowledge into a cohesive design methodology for synthesizing spool-packaged SMA devices. Whereas SMA actuators are typically difficult to design within tight or irregularly shaped spaces, the design methodology makes strides toward overcoming the packaging problem by providing a more robust capacity to package SMA wires. By delivering the methodology and tools to design spool-packaged SMA devices, the research can be transitioned from theory to a more practical form.

Chapter 2. Single Mandrel Spooling Model

Shape memory alloy actuators have potential to address needs for high performance, low-cost actuation in industry. However, they are often limited by the difficulty in packaging long lengths of wire within limited form constraints. Spooling is a promising alternative packaging strategy for designing SMA wires to fit within tight spaces. While the wrapped configuration can improve the actuator footprint by packaging the wire's long length more compactly, the motion typically is degraded due to interfacial friction losses between the SMA wire and mandrel, and bending losses that result from wrapping SMA wires around tight curvatures. Previous approaches to predicting spooled SMA actuator motion were derived for specific applications, and either estimated efficiency losses based on empirical observations (Wang & Shahinpoor, 1998), assumed that the wrapped portions do not contribute to the overall motion (Tanaka, 1986), or adapted Capstan or belt-braking models for specific actuator configurations (Howell, 1953; Firbank, 1970; Huang, 2000). While previous modeling efforts make reasonable predictions for the specific configurations they address, they neither account for portions of the wire that gain and lose contact with the mandrel during operation, nor consider bending strains. As a result, these approaches do not make accurate predictions for actuators with large wrap angles or tight wrap curvatures (which result in high bending strains). The effect of bending SMA has been explored in the past for non-spooled configurations, typically focusing on superelastic forms including wires, beams, films, plates, and tubes (Auricchio & Sacco, 1999; Berg, 1995a; Berg, 1995b; Lagoudas, et al., 2006; Purohit & Bhattacharya, 2002; Rejzner, et al., 2002). Unfortunately, these current models do not predict for the shape memory effect at the level of computational simplicity required for iterative actuator design as motivated by the scope of this dissertation.

It is noted that accounting for fatigue of spooled SMA actuators is particularly difficult since thermal transformation fatigue, in general, is still an active area of materials research. The thermal transformation fatigue life of SMA wires is dependent on a variety of factors including material composition, temperature processing, loading factors, and the amount of transformation strain (Kumar & Lagoudas, 2008; McNichols, et al., 1981), and has been studied most broadly for cyclic uniaxial loading (Lagoudas & Miller, 1999; Lagoudas, et al., 2000; Eggeler, et al., 2004; Bertacchini, et al., 2008). An early study demonstrated thermal cyclic fatigue lifetimes until structural failure of 10^4-10^5 cycles for helical NiTi wires with transformation strains between 4.4-8.3% (McNichols, et al., 1981). Guidelines by the manufacturer of Flexinol NiTi wires indicate that functional fatigue (also called "shakedown") can be avoided for more than 10^5 cycles by maintaining applied stresses below 170 MPa and maximum strains below 4% (Dynalloy, 2010). For high-cycle fatigue life, alternative guidelines recommend strains below 2.5% (Churchill, 2009). However, fatigue experienced under the coupled bending/tensile loading that occurs in spooled SMA wires increases the complexity of the fatigue problem and remains a research issue. Thus, while the thermal transformation fatigue of SMA is an active area of research and a concern as the mandrel diameter decreases, it is beyond the scope of this dissertation. Even so, there are several categories of applications such as safety, deployment, and active fixture/attachment devices (Wu & Shetky, 2000; Barnes, et al., 2006; Redmond, et al., 2007; Busch, et al., 1992; Lucy, et al., 1996; Melton, 1998) where the presented work is pertinent that require only a low number of cycles (magnitudes of 1 - 10^2 cycles) and can therefore accept reduced fatigue lifetimes attendant with very small mandrels. Likewise, as mandrels are increased to a moderate size, the bending strains are reduced to a level that would not be expected to cause a detrimental decrease to the actuator's lifetime. For example, by selecting a mandrel diameter 100 times larger than the SMA wire diameter, a 1% increase in tensile strain is estimated to occur along the outer edge of the wrapped wire. (While the strain is estimated here, it is predicted with greater rigor in the model that follows).

This chapter presents a predictive model for the quasi-static behavior of single mandrel spool-packaged SMA wire actuators that provides the analytic foundation for spooled actuator design. Despite the complexities related to the SMA constitutive laws, bending of a non-linear material, and portions of the wire gaining and losing contact with the mandrel throughout operation, this chapter distills the behavior of spool-packaged actuators down to three key effects: friction, bending, and a limitation on the packaging technique due to frictional binding. To increase the impact and applicability of the model, a generalized architecture was assumed that encompasses a broad range of designs based on user-specifiable geometric parameters, applied loads, friction properties, and material constitutive laws. Since design optimization is typically an iterative process, steps that can simplify the process of solving the actuator's range of motion are beneficial. Thus, a simple formulation of the constitutive stress-strain behavior is provided in addition to strategies for computing the effect of bending and the range of motion for actuators that undergo frictional binding. The model was validated experimentally for both linear and rotational actuator configurations, while also evaluating its ability to predict accurately in the presence of large bending strains or binding due to accumulated friction. By providing the analytical tools for predicting single mandrel spooled SMA actuator performance, the model makes strides toward being able to design SMA actuators compactly based on an understanding of key losses due to friction and bending, and limitations on the use of spooled-packaging due to accumulated friction. Furthermore, the model develops an initial understanding of the loss mechanisms and key behaviors that occur for multiple mandrel spool-packages actuators, which are important for addressing the customization aspect of the packaging problem.

2.1. Architecture and operation

To provide a wide design space for the analysis and synthesis of spooled SMA wire actuators, a generalized architecture (illustrated in Figure 2.1 with nomenclature defined in Table 2.1) was defined to describe any spooled SMA actuator composed of four basic parts: 1) a single SMA wire in tension, 2) a fixed input where the SMA wire attaches to a

Table 2.1. Nomenclature for spool-packaged SMA actuator model.

Operation state parameters	
χ	Operation state = {0,M,A} for *State 0* zero-strain reference, *State 1* martensite, *State 2* austenite
$\xi^{(M)}$	Martensite phase fraction ($\xi^{(M)}=1$ for martensite, and $\xi^{(M)}=0$ for austenite)
Actuator geometry and topology	
$\ell_{t,in}^{(\chi)}$	Length of input tail
$\ell_{t,out}^{(\chi)}$	Length of output tail
$\ell_{w}^{(\chi)}$	Length of the wrapped SMA wire
$\ell_{tot}^{(\chi)}$	Total length of SMA wire in *State* χ, where $\ell_{tot}^{(0)}$ is also referred to as the total SMA free length
$\delta\ell$	Range of motion, equivalent to $\ell_{tot}^{(M)}-\ell_{tot}^{(A)}$
$\phi^{(\chi)}$	Angular position of output for rotational actuator in State χ referenced to $\phi^{(0)}\equiv 0$
$\delta\phi$	Angular range of motion for rotational actuator between *States 1* and *2*
θ	Angular position mandrel, measured from running on point, counter-clockwise positive
$\theta_{w}^{(\chi)}$	Wrap angle of SMA wire on the mandrel
θ_{B}	Binding angle
D	Mandrel diameter
d_{SMA}	Diameter of SMA wire
$\bar{D}$	Diameter ratio, equivalent to D/d_{SMA}
y	Distance from centroidal axis of SMA wire, direction is normal to mandrel
Loads, stress, strains, and related parameters	
M_{ext}	Externally applied moment to motion output on a rotational motion spool-packaged SMA wire actuator
F_{ext}	Externally applied load to motion output on a linear motion spool-packaged SMA wire actuator
A_{SMA}	Cross-section area of SMA wire
σ,ε	Tensile stress, strain
$f_{SMA}^{(\chi)}$	Constitutive function providing strain in *State* χ as a function of stress
$a,b,c,d,E^{(A)}$	Material parameters defining polynomial approximation for constitutive law
$\sigma_{nom},\varepsilon_{nom}$	Nominal stress and strain due to tensile loading of SMA wire, independent of bending
ε_{ctd}	Strain on centroidal axis of SMA wire
μ	Coefficient of friction between SMA wire and mandrel

referenced ground, 3) a cylindrical mandrel fixed to ground (as opposed to a free-wheeling pulley), and 4) a rotational or linear single degree-of-freedom motion output. The SMA wire is fixed to ground at the input tail, has a wrapped portion in frictional contact with the mandrel, and an output tail connected to the motion output. The SMA wire interacts with the external system at the motion output, which is constrained by either a rotational arm assumed to pivot around the center of the spool (Figure 2.1a) or a linear slider (Figure 2.1b). The motions for the rotational and linear cases are predicted as two cases of the same model, which are distinguished by the constraint at the motion

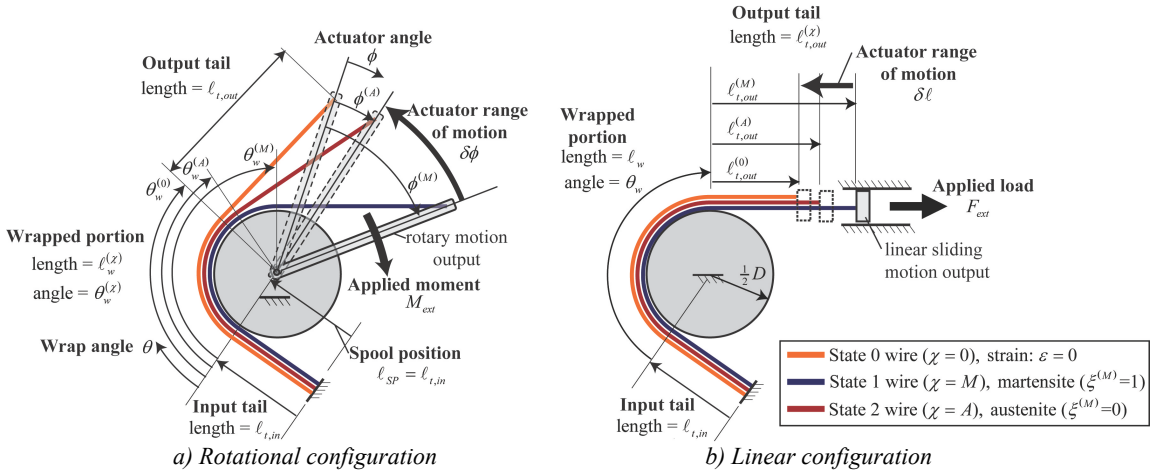

Figure 2.1. General architecture and operation states for a single mandrel spool-packaged SMA wire actuator. The actuator comprises a fixed mandrel, an SMA wire in frictional contact with the mandrel, and a single degree of freedom motion output, which defines whether the actuator's motion is (a) rotational or (b) linear.

output and whether the output tail length or wrapped length is constant. A key difference between the linear and rotational motion cases is whether the wrap angle and output tail length are variables or constant parameters. In the linear case, the wrap angle is constant and the output tail length varies during operation. In the rotational case, the wrap angle varies while the output tail length is constant. The packaging architecture is highly customizable since the wire length, wrap angle, mandrel size, and type of output motion (rotational or linear) can be selected based on the actuator application's needs. Varying the spool position (defined relative to the fixed end of the wire in Figure 2.1) affords further design flexibility.

The cyclic operation of SMA actuators results from temperature-dependent phase transformations allowing large residual strains without permanent, plastic deformations. Below the material's transformation temperature, the more compliant martensite-phase SMA is strained due to the applied load at the motion output. This strain is recovered when the SMA is heated above the transformation temperature as the material reverts to the much stiffer austenite phase. As the material is thermally cycled between these phases, the reversible strain produces the actuator's overall gross motions. To predict the actuator's range of motion, the cyclic operation is defined with respect to three main states, which are related to the material phase and the applied load:

- ***State 0:*** the zero-strain reference state in which no external load is applied to the actuator (state variable $\chi = 0$),
- ***State 1:*** a *martensite* phase SMA wire ($\chi = M$, martensite phase fraction $\xi^{(M)} = 1$) with an applied external load (M_{ext} or F_{ext}), and
- ***State 2:*** for an *austenite* phase SMA wire ($\chi = A$, martensite phase fraction $\xi^{(M)} = 0$) with an applied external load (M_{ext} or F_{ext}).

All motions, geometries, and strains of the actuator are referenced to the zero-strain reference state, *State 0* (diagrammed in orange, Figure 2.1), which is attained by heating the SMA wire to austenite under no load and maintained in *State 0* upon cooling assuming a negligible two-way effect in the SMA material. *State 1* (martensite SMA actuator under an applied load, blue) is achieved by stretching the SMA wire along its length to $\ell_{tot}^{(M)}$, either by applying a load to a martensite *State 0* actuator or by cooling an austenite *State 2* actuator under load. Likewise, the *State 2* (austenite SMA actuator under an applied load, red) is achieved by heating the SMA wire, causing it to contract to $\ell_{tot}^{(A)}$.

The overall change in the SMA wire length results in translational output motion $\delta\ell$ for linear motion actuators and in rotational output motion $\delta\phi$ for rotational motion actuators. For the linear actuator, the output motion is equal to the change in the total SMA wire length, according to the equation

$$\delta\ell = \ell_{tot}^{(M)} - \ell_{tot}^{(A)} \tag{2.1}$$

where $\ell_{tot}^{(M)}$ and $\ell_{tot}^{(A)}$ are the *State 1* and *2* total wire lengths. Since the input and wrapped lengths of the wire do not vary during operation, the change in length is also equal to the difference between the *State 1* and *State 2* output tail lengths, $\ell_{t,out}^{(M)}$ and $\ell_{t,out}^{(A)}$. For the rotational actuator, the angular output motion is geometrically related to the overall change in the wire length according to the equation

$$\delta\phi = \frac{\delta\ell}{D_w/2} = \frac{\ell_{tot}^{(M)} - \ell_{tot}^{(A)}}{D_w/2}, \tag{2.2}$$

where D_w is the wrapped diameter of the spooled SMA wire. The wrapped diameter D_w is measured from the centroidal axis of the SMA wire through the mandrel center to the SMA wire centroid on the opposite side such that

$$D_w = D + d_{SMA} \tag{2.3}$$

where d_{SMA} is the SMA wire diameter. For the rotational case, the input and output tail lengths are constant throughout operation. Thus, the change in length is also equal to the difference between the *State 1* and *State 2* wrapped lengths, $\ell_w^{(M)}$ and $\ell_w^{(A)}$. The change in actuator angle is equal to the difference between the *State 1* and *State 2* wrap angles, $\theta_w^{(M)}$ and $\theta_w^{(A)}$. To predict the actuator's range of motion for both linear and rotational cases, the SMA wire lengths $\ell_{tot}^{(M)}$ and $\ell_{tot}^{(A)}$ are determined independently for each state by means of the analytical model presented in this chapter. The arithmetical difference taken between the two lengths, using Equations 2.1 and 2.2, defines the actuator's range of motion.

2.2. Analytical modeling

The model to predict the quasi-static motion of spool-packaged SMA wire actuators builds on similar mechanics as belt-braking models for passive materials. However, the derivation takes additional steps to model the active material by incorporating phase-dependent SMA constitutive laws, to account for the effects of bending and frictional binding, and to ensure that strain variations along the length of the SMA wire (including those that gain and lose contact with the mandrel) are properly represented. The motion of the spool-packaged SMA actuator results from variations to the SMA wire's strain profile along its length and wire cross-section as the material properties are varied between the martensite and austenite states. Thus, a function for the average (centroid) SMA wire strain as it varies across its length and cross-section is derived, which accounts for the constitutive behavior of the material, shifts in strain resulting from bending the wire around the mandrel, and the variation in strain due to friction. To determine the length of the wire as it varies between *States 1* and *2*, a simple integration of strain along the wire's length is not possible since the distribution of wire around the mandrel in the deformed states, and thus the limits of integration, cannot be known *a priori*. Rather, a compatibility approach is used to couple integration of strain with a built-in criterion that ensures all portions of the wire are accounted for including those that gain and lose contact with the mandrel during operation.

2.2.1. Generalized constitutive law

The model's prediction of the actuator's quasi-static motion relies on a generalized form of the material constitutive law that relates the strain in the SMA wire to the local stress and material phase. Rather than basing the model for spool-packaged actuators on a specific SMA constitutive model (such as models presented by Brinson, 1993; Boyd & Lagoudas, 1994; Shaw & Churchill, 2009), using a generalized form allows for different constitutive laws with varying levels of rigor, simplicity, and ease of use to be applied depending on the application and required accuracy. For this analysis, the strain is assumed to be a function of stress (σ) and martensite phase fraction ($\xi^{(M)}$) according to the general strain function f_{SMA}

$$\varepsilon = f_{SMA}\left\{\sigma, \xi^{(M)}\right\}, \tag{2.4}$$

which is an invertible function that also describes stress as a function of strain and material phase such that

$$\sigma = f_{SMA}^{-1}\left\{\varepsilon, \xi^{(M)}\right\}. \tag{2.5}$$

Stress varies with the position of the wire on the mandrel θ, and is assumed to be constant in the tail portions (Figure 2.1). Assuming that the wire is fully martensite in *State 1* ($\xi^{(M)} = 1$) and fully austenite in *State 2* ($\xi^{(M)} = 0$), the strain is represented by the simplified functions for strain

$$\varepsilon^{(M)} = f_{SMA}\left\{\sigma\{\theta\}, \xi^{(M)} = 1\right\} = f_{SMA}^{(M)}\left\{\sigma\{\theta\}\right\}, \text{ and} \tag{2.6}$$

$$\varepsilon^{(A)} = f_{SMA}\left\{\sigma\{\theta\}, \xi^{(M)} = 0\right\} = f_{SMA}^{(A)}\left\{\sigma\{\theta\}\right\} \tag{2.7}$$

where $f_{SMA}^{(M)}$ and $f_{SMA}^{(A)}$ are the constitutive laws for fully martensite and fully austenite wires.

2.2.2. Friction losses

To derive the function for strain with respect to the position on the wire, the effect of interfacial friction was modeled based on the assumption of static Coulomb friction between the wire and the mandrel. To better support the analysis and design of spool-packaged SMA actuators, the model was simplified based on assumptions of quasi-static

motion and unilateral motion in each state (the entire wire is in a state of extension for *State 1* martensite and a state of contraction from the previous state for *State 2* austenite). As a corollary to the unilateral motion assumption, the entire wire must remains in tension (no compression) throughout operation. Additionally, the applied load is assumed constant. For non-constant applied loads, however, the hysteretic behavior of the SMA would need to be accounted for if the operation cycle included full or partial removal of the applied load.

The applied loads and wrapped geometry for spooled SMA wire actuators result in the tensile, moment, normal, and friction loads diagrammed in Figure 2.2 for a differential element of wire in sliding contact with the mandrel. The motion and loads of the *State 2* austenite actuator are the same as those in the *State 1* martensite actuator, except that the wire contracts rather than extends such that the friction forces are in the opposite direction (counterclockwise friction acting on the wire for *State 1*, clockwise friction for *State 2* for the differential element in Figure 2.2 based on the architecture definition in Figure 2.1).

From the free body diagram (Figure 2.2), the quasi-static force balance in the radial direction (normal to the spool) is

$$\Sigma F_r = dN - \left(2F_{\theta\theta} + dF_{\theta\theta}\right)\sin\left(\tfrac{1}{2}d\theta\right) = 0, \tag{2.8}$$

where N is the normal reaction force between the wire and mandrel, and $F_{\theta\theta}$ is the resultant force in the tensile direction. The quasi-static moment balance is

$$\Sigma M_0 = \left(dF_{\theta\theta} \pm \mu\, dN\right)\frac{D_w}{2} + dM_{\theta y} = 0 \tag{2.9}$$

where μ is the coefficient of friction between the mandrel and the wire, and the positive or negative sign leading the $\mu\, dN$ term depends on whether the actuator is extending (negative for *State 1,* $\chi = M$) or contracting (positive for *State 2*, $\chi = A$). Assuming that the SMA wire has a constant curvature on the wrap portions, the differential moment term $dM_{\theta y}$ can be neglected in the austenite case since the material behaves linear-elastically. The $dM_{\theta y}$ term is also approximated as equal to zero for the martensite case for computational simplicity. However, for tightly wrapped SMA wire (with a low

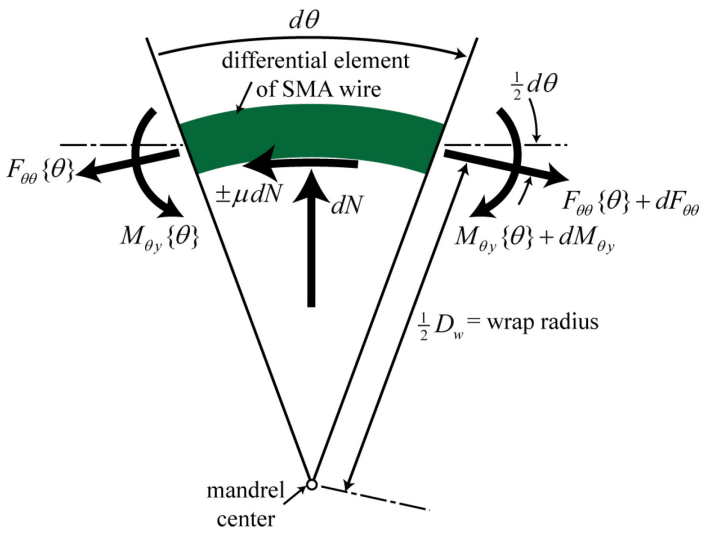

Figure 2.2. Free body diagram of a differential element of SMA wire in sliding contact with the mandrel. In *State 1* (martensite), the wire extends, producing counterclockwise friction (based on the actuator configuration in Figure 2.1. In *State 2* (austenite), the wire contracts, producing clockwise friction.

mandrel to SMA wire diameter ratio), the $dM_{\theta y}$ term becomes more significant and the assumption of a negligible moment differential will begin to break down. While these effects are not accounted for in the model, they occur for actuator geometries with high bending strains that would typically be avoided in actuator design and are deemed reasonable. Combining the equations for the force and moment balances (Equations 2.8 and 2.9), and assuming that the resulting second order term $dF_{\theta\theta}d\theta$ is negligible, the normal reaction forces N cancel to yield the expression

$$\pm\mu d\theta = \frac{dF_{\theta\theta}}{F_{\theta\theta}}. \tag{2.10}$$

Depending on whether a rotational or linear boundary condition is applied to the actuator, the wrap angle $\theta_w^{(\chi)}$ may not be known *a priori*. Thus, the derivation departs from typical belt-braking models by integrating the expression relating the changing tension due to friction (Equation 2.10) from a general point θ on the spool ($0 < \theta < \theta_w^{(\chi)}$) where the unknown wire tension equals $F_{\theta\theta}\{\theta\}$ to the upper limit $\theta_w^{(\chi)}$ at the output where the applied tension is known:

$$\int_{\theta}^{\theta_w^{(\chi)}} \mu d\theta = \int_{F_{\theta\theta}\{\theta\}}^{F_{ext}} \frac{dF_{\theta\theta}}{F_{\theta\theta}}. \tag{2.11}$$

Solving Equation 2.11 for the tensile resultant force $F_{\theta\theta}\{\theta\}$ yields

$$F_{\theta\theta}\left\{\theta\right\} = F_{ext}e^{\pm\mu\left(\theta-\theta_w^{(\chi)}\right)}, \tag{2.12}$$

which relates the resultant force ($F_{\theta\theta}$) to the angular position (θ) given a load applied at the motion output (F_{ext}), coefficient of friction (μ), and *State* χ wrap angle ($\theta_w^{(\chi)}$). For rotational motion actuators applying a moment (M_{ext}) at the motion output, the equivalent applied load in the output tail is

$$F_{ext} = M_{ext} / \ell_{t,out}, \tag{2.13}$$

where the output tail length ($\ell_{t,out}$) is the moment arm to the corresponding load (F_{ext}). Dividing the equation for the resultant force (Equation 2.12) by the cross-sectional area of the SMA wire (A_{SMA}), yields the average stress:

$$\sigma_{\theta\theta}\left\{\theta\right\} = \sigma_{t,out}e^{\pm\mu\left(\theta-\theta_w^{(\chi)}\right)}, \tag{2.14}$$

where $\sigma_{t,out}$ is the tensile stress in the output tail. To relate the resultant force (and average tensile stress) to the centroid strain of the SMA wire, the effect of bending also needs to be considered.

2.2.3. Bending strains

To determine the deformation of the SMA wire in each state, the strain along the wire's length must be known. In limited cases for which the mandrel diameter D is much larger than the wire diameter d, the strain across the wire's cross-section can be assumed uniform. By contrast, spooled actuators with tighter curvatures (for smaller mandrels or thicker SMA wires) create larger bending strains, which have a more significant impact on performance, and therefore cannot be reasonably neglected using the assumption of uniform strain. For non-linear wire under tension, bending can alter the average strain across the cross-section relative to the average strain of a material in tension only. Since such changes in strain affect the overall motion of the actuator, the average cross-section strain in a wrapped segment of SMA wire is derived as a function of the tensile resultant force and the mandrel diameter.

The strains normal to the wire's cross-section originate from two sources: 1) tensile loading in the wire and 2) geometrically induced bending strains. Due to the non-linear

stress-strain relationship for SMA, strains from the tensile and bending sources cannot be superimposed. Instead, a function for tensile strain is defined for which the average cross-section strain is unknown, but can be solved if the tensile resultant force and mandrel diameter are given.

Assuming that plane sections of the SMA wire's cross-section remain plane upon bending the wire, the tensile strain (diagrammed in Figure 2.3) is a linear function of the distance from the centroidal axis (y) according to the function:

$$\varepsilon_{\theta\theta}\{y\} = \varepsilon_{ctd} + \frac{y}{\frac{1}{2}D_w}, \tag{2.15}$$

where $\varepsilon_{\theta\theta}$ is the tensile strain in the SMA wire, ε_{ctd} is the unknown strain at the centroidal axis, and $(\frac{1}{2}D_w)^{-1}$ is the curvature of the wire at the centroidal axis. Because the strain distribution across the wire's cross-seciton is linear, the centroid and average cross-section strains are equivalent. Relating the tensile strain (Equation 2.15) to the average tensile stress based on the generalized constitutive law (Equation 2.4), the tensile stress is

$$\sigma_{\theta\theta}\{\varepsilon_{\theta\theta}\} = f_{SMA}^{-1}\left\{\varepsilon_{ctd} + \frac{y}{\frac{1}{2}D_w}\right\}. \tag{2.16}$$

Integrating the tensile stress (Equation 2.16) over the area of the cross-section (A_{SMA}) yields the resultant tensile force,

$$F_{\theta\theta} = \sigma_{\theta\theta}A_{SMA} = \iint_{A_{SMA}} f_{SMA}^{-1}\left\{\varepsilon_{ctd} + \frac{y}{\frac{1}{2}D_w}, \xi^{(M)}\right\} dA_{SMA}. \tag{2.17}$$

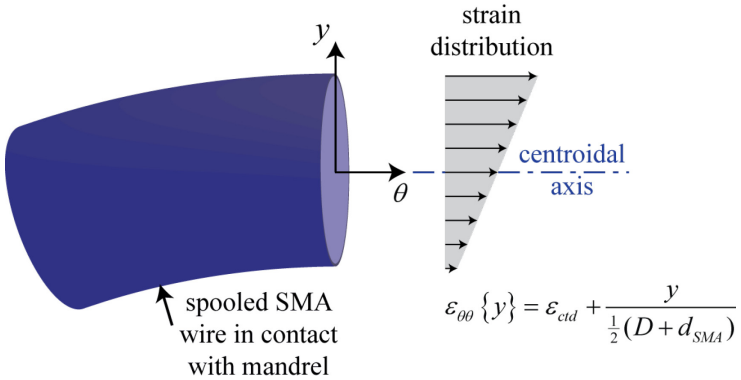

Figure 2.3. Diagram of tensile strain on a cross-section of spooled SMA wire. Strain across the wire's cross-section result from bending and tension. The linear distribution of strain as a function of distance from the centroidal axis, y, results from the assumption that plane sections of the cross-section remain plane upon bending.

Given a resultant force $F_{\theta\theta}$ and wrap diameter D_w, the centroid strain can be solved using Equation 2.17. To relate the variation in strain due to bending to the variation in strain due to friction, the equation for the variation in average stress $\sigma_{\theta\theta}$ (Equation 2.14) is substituted into the equation relating $F_{\theta\theta}$ to the centroid strain (Equation 2.17), yielding:

$$F_{\theta\theta} = \sigma_{t,out}\, A_{SMA} e^{\pm\mu\left(\theta-\theta_w^{(\chi)}\right)} = \iint_{A_{SMA}} f_{SMA}^{-1}\left\{\varepsilon_{ctd} + \frac{y}{\frac{1}{2}D_w}, \xi^{(M)}\right\} dA_{SMA}. \tag{2.18}$$

The expression relates the centroid strain to the output tail stress (resulting from the applied load), actuator geometry, and material properties along the length of the SMA wire. However, since the wrap angle can vary between states and the centroid strain is contained within an unspecified, and potentially complicated constitutive equation, a closed-form solution for the centroid strain cannot be represented from Equation 2.18. For simplicity, the centroid strain and its functional dependencies are represented by

$$\varepsilon_{ctd} = \varepsilon_{ctd}\left\{\theta, D_w\right\}, \tag{2.19}$$

where the ε_{ctd} is the solution to Equation 2.18. Based on the equation relating the resultant force to the centroid strain (Equation 2.17), the effect of bending becomes negligible for large wrap diameters D_w, and has an increasing impact on the centroid strain as the wrap diameter decreases.

By solving for the centroid strain across the entire length of the wire, the *State 1* and *2* total SMA wire lengths ($\ell_{tot}^{(\chi)}$) can be related to the zero-strain *State 0* total wire length ($\ell_{tot}^{(0)}$) by integrating. While strain would generally be integrated along the *State 0* length for a linear SMA wire actuator, the changing stress distribution and regions of wire that gain and lose contact with the mandrel require that the standard approach be modified for determining the actuator's range of motion.

2.2.4. Actuator range of motion

A compatibility condition is defined to ensure that all portions of the wire are accounted for when integrating strain – including those that gain and lose contact with the mandrel during operation. For a linear SMA actuator, the deformation from *State 0* to *State* χ would typically be determined by integrating strain along the *State 0* length. Since

the stress distribution in Equation 2.12 corresponds to the *State χ* wire and not the *State 0*, the task is more complicated. To account for all portions of the wire and apply the stress distribution model properly in determining the deformed *State 1* and *State 2* lengths, a compatibility condition relates the *State 0* reference length to the deformed *State χ* length according to the centroid strain function (Equation 2.19) and the input and output tail strains ($\varepsilon_{t,in}^{(\chi)}$ and $\varepsilon_{t,out}^{(\chi)}$). The derivation begins with the definition of strain for a differential element of wire,

$$\varepsilon = \frac{ds^{(\chi)} - ds^{(0)}}{ds^{(0)}}, \tag{2.20}$$

where $ds^{(0)}$ is the length of a differential element of *State 0* wire (undeformed) and $ds^{(\chi)}$ is the deformed length of the differential element in *State χ*. Solving for $ds^{(0)}$ and integrating across the wire's length, the equation for strain becomes

$$\int_0^{\ell_{tot}^{(0)}} ds^{(0)} = \int_0^{\ell_{tot}^{(\chi)}} \left(1+\varepsilon\right)^{-1} ds^{(\chi)} . \tag{2.21}$$

Expanding the right hand side of the equation into three integrals for the input tail, wrapped length, and output tail portions of the wire, the *State 0* wire length (Equation 2.21) becomes

$$\ell_{tot}^{(0)} = \underbrace{\int_0^{\ell_{t,in}} \left[1+\varepsilon_{t,in}^{(\chi)}\right]^{-1} ds^{(\chi)}}_{\text{input tail}} + \underbrace{\int_0^{\theta_w^{(\chi)} D_w/2} \left[1+\varepsilon_{ctd}^{(\chi)}\left\{\frac{s^{(\chi)}}{D_w}, D_w\right\}\right]^{-1} ds^{(\chi)}}_{\text{wrapped portion}} + \underbrace{\int_0^{\ell_{t,out}^{(\chi)}} \left[1+\varepsilon_{t,out}^{(\chi)}\right]^{-1} ds^{(\chi)}}_{\text{output tail}} . \tag{2.22}$$

Upon applying the boundary conditions for either rotational or linear output motion, and given the geometry, material constitutive law, coefficient of friction, and external applied load, the *State* χ wire length can be determined. The compatibility condition is valid for the rotational and linear motion configurations of the actuator. For linear motion actuators, the wrap angle is constant and the output tail length varies with the change in length defining the actuator's range of motion. Conversely for the linear case, the output tail length is constant and the variable wrap angle defines the actuator motion.

2.3. Solution methodology

The intention of the spool-packaged SMA actuator model is to provide a foundation for the analysis and synthesis of actuator designs. Yet, the behavior of spool-packaged SMA actuators is complicated by a variety of factors relating to the SMA constitutive laws, the effect of bending, and the solving of the compatibility equations used to find the actuator's deformation between states. Since design optimization is typically an iterative process, steps that can simplify the process of solving the actuator's range of motion are beneficial. Thus, a simple formulation of the constitutive stress-strain behavior, strategies for determining the centroid strain of wrapped SMA wire and the range of motion for actuators that undergo frictional binding, and a discussion of the numerical computation of the range of motion are provided.

2.3.1. Constitutive model

The stress-strain behavior of SMA wire can vary widely depending on factors such as composition, manufacturing process, and stress-strain history. In the past 20 years, substantial research has focused on developing constitutive models for SMA including early phenomenological models (Tanaka, 1986; Brinson, 1993; Boyd & Lagoudas, 1994; Liang & Rogers, 1990), micromechanical models (Sun & Hwang, 1993; Patoor, et al., 1994; Huang & Brinson, 1998; Vivet & Lexcellent, 1998; Goo & Lexcellent, 1997), coupled thermodynamic and mechanical models (Shaw & Churchill, 2009; Ivshin & Pence, 1994; Seelecke & Muller, 2004), and models predicting the dynamics of phase boundary motion (Abeyaratne & Knowles, 1991; Truskinovsky, 1993; Chang, et al., 2006). While many of these models are effective predictors of the SMA material behavior with respect to a variety of factors including the partial phase transformation mechanics and the transient time response, a reduced-order model of the constitutive law is used as an example for greater simplicity and clarity of the spooling mechanics. Simple polynomial functions for the fully transformed austenite and martensite states are used because they reasonably approximate the stress-strain behavior based on simple experimental characterization, they reduce model complexity relative to models that are continuous functions of temperature or material phase, and are quickly

evaluated when iteratively solving the actuator's range of motion. For the austenite phase, a linear stress-strain relation was chosen (slope defined as $E^{(A)}$) due to the austenite's linear-elastic behavior below stresses inducing superelastic phase change. To approximate the stress-strain behavior of the martensite plateau, a third-order polynomial stress-strain function was used of the form

$$\sigma^{(M)} = a\varepsilon^3 + b\varepsilon^2 + c\varepsilon + d\,, \tag{2.23}$$

where *a, b, c,* and *d* are constants. The martensite stress-strain function (Equation 2.23) is required to be monotonic and invertible, which is necessary for expressing strain as a unique function of stress when specifying $f_{SMA}^{(M)}$ and $f_{SMA}^{(A)}$ in the simplified strain equations (Equations 2.6 and 2.7). To demonstrate that the linear and polynomial functions approximate the behavior of the physical wire well, experimentally determined stress-strain data for an SMA wire in the austenite and martensite states (Figure 2.4) is used as an example. The least-squares linear and polynomial fits match the data closely (2.4% average error for martensite, 5.9% for austenite), demonstrating that this approximation for SMA's quasi-static stress strain response is appropriate.

2.3.2. Effect of bending

Solving for centroid strain for a linear (non-spooled) SMA wire is a straightforward, algebraic solution of the constitutive law equations (Equations 2.6 and 2.7) for a given

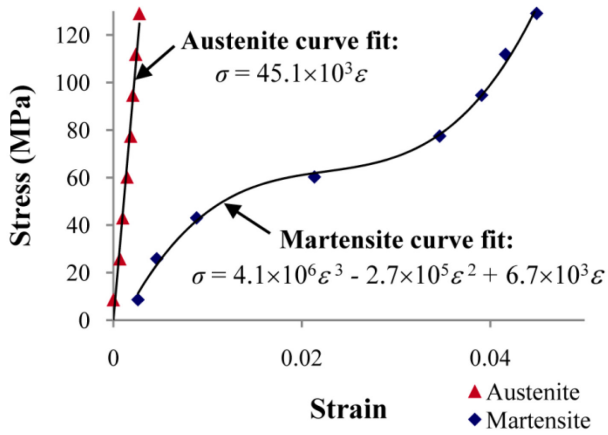

Figure 2.4. Simplified stress-strain model and measured data for shaken down SMA wire. Prior to testing, the SMA wire (15 mil, 70°C Flexinol, Dynalloy, Inc.) was thermally cycled under a constant 45 N load (400 MPa) until its cyclic performance stabilized. The polynomial functions reasonably approximate stress-strain behavior for both states and can be computed rapidly for simulating motion based on the spooling model.

stress. However, solving for the centroid strain of a spooled wire is more complicated because the bent geometry alters the centroid strain depending on the local resultant force ($F_{\theta\theta}\{\theta\}$) and the wrap curvature $(\frac{1}{2}D_w)^{-1}$. The centroid strain can be determined numerically by solving the equation for the equilibrium of tensile force on a spooled wire (Equation 2.18), but the solution would become computationally expensive to compute within an iterative process such as solving the compatibility equations or in a design optimization. To avoid the repetition of solving for the centroid strain due to bending, the solution can be streamlined prior to an iterative process by numerically solving the tensile equilibrium equation (Equation 2.18) for the centroid strain across a grid of points that spans the expected range of average stresses and diameter ratios. In so doing, a mapping is generated from the average stresses and diameter ratios to the resulting centroid strains. The mapping for a sample of SMA wire with an experimentally measured constitutive function (expressed according to the linear and polynomial forms for the austenite and martensite states, Equation 2.23) is represented graphically in Figure 2.5, demonstrating the non-planar, continuous relationship between the average stress ($\sigma_{\theta\theta}$), diameter ratio (D/d_{SMA}), and centroid strain (ε_{ctd}). Given an average local stress and the diameter ratio, the centroid strain adjusted for bending is determined quickly by calling the functional mapping and interpolating the centroid strain. Particular needs for computational accuracy and speed will dictate the coarseness of the grid used for the mapping, the grid distribution (e.g., linear, logarithmic), and the type of interpolation used (e.g., linear, quadratic, spline).

2.3.3. Binding limitation

The assumption of unilateral motion (that the wire is only stretching or only contracting in each state) requires that the friction loads on the wire be in the same direction relative to the mandrel across the entire wrapped region. It is possible for SMA wire wrapped through large angles on the spool to violate the assumption of unilateral motion, and thus an expression was derived to predict whether the unilateral motion assumption is valid. At the input tail ($\theta = 0$), increasing the wrap angle causes the input

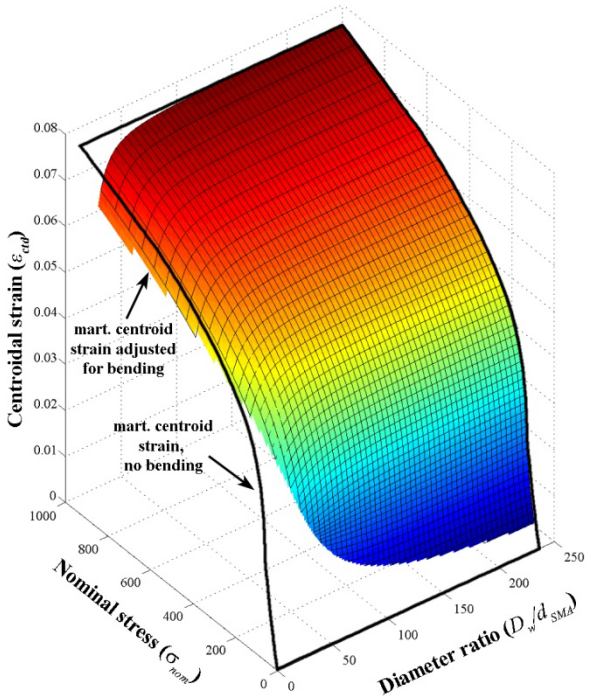

Figure 2.5. Centroid strain adjusted for bending. The surface demonstrates the effect of bending on the martensite strain profile for spooled SMA wire (assuming 0.38 mm wire diameter and the constitutive law in Figure 2.4).

tail strain in the martensite *State 1* actuator to decrease and the strain in the austenite *State 2* actuator to increase. These resulting stress and strain distributions are illustrated in Figure 2.6a, and represent the range of stress and strain along the SMA's wire length based on the previous assumptions of unilateral motion and operation between States 1 and 2 with no removal of applied load. Resulting from the increased wrap angle, the strains at the input tail in each state ($\varepsilon^{(M)}\{\theta=0\}$ and $\varepsilon^{(A)}\{\theta=0\}$) approach one another until they are equal at a critical angle (illustrated at $\varepsilon\{\theta_B\}$ in Figure 2.6b). This critical angle is defined as the *binding angle* θ_B, where $\varepsilon^{(M)}\{\theta=0\} = \varepsilon^{(A)}\{\theta=0\}$, or

$$\theta_B = \theta_w^{(0)} \Leftrightarrow \varepsilon^{(M)}\{\theta=0\} = \varepsilon^{(A)}\{\theta=0\}. \tag{2.24}$$

At the binding angle, the wire neither stretches nor contracts and the assumption of unilateral motion between states is violated. Since no motion occurs, no change in the stress or strain can occur between states for wire between the input tail at $\theta = 0$ and the binding point $\theta = \theta_w - \theta_B$. Thus, wrapping additional SMA wire beyond the binding angle is hypothesized to contribute no further motion to the actuator. For an actuator that binds, the motion prediction can be modified for an equivalent actuator that represents the

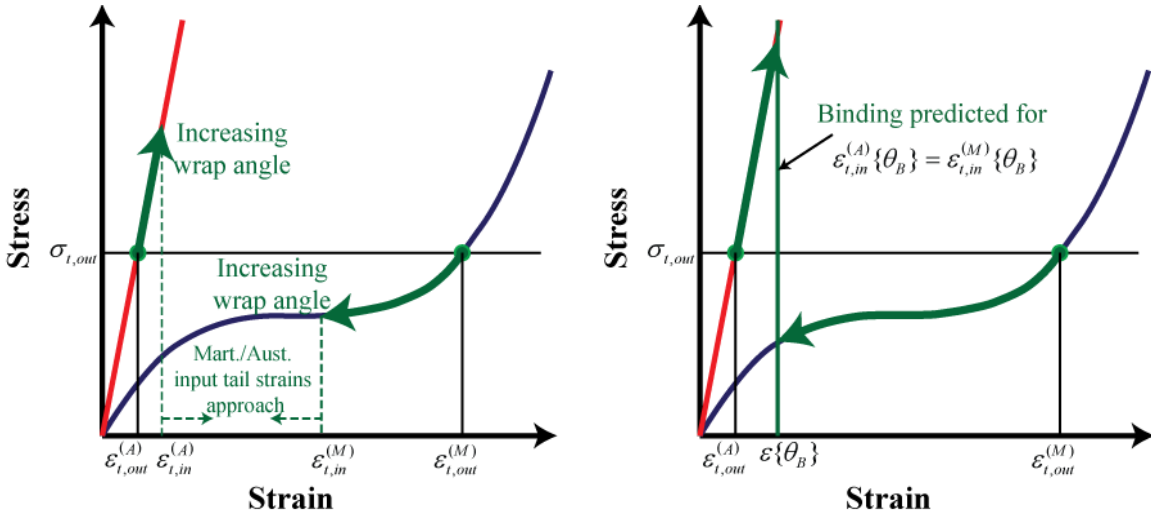

(a) Strain distribution for no binding (b) Strain distribution demonstrating binding

Figure 2.6. Effect of increase wrap angle as it leads to frictional binding. a) As the wrap angle is increased, the strain in the input tail ($\varepsilon_{t,in}$) increases in austenite and decreases in martensite as predicted by the stress-strain relation (Equation 2.14), assuming a monotonic relationship between the two. The ranges of stress and strain are depicted in the figure based on the previous assumptions of unilateral motion and operation between States 1 and 2 with no removal of applied load. b) The binding condition occurs at the angle θ_B where the strains in the input tail are equal in each state, violating the assumption of unilateral motion.

active, non-binding portion of the wire. For the equivalent actuator, the input tail length $\ell_{t,in}$ is set equal to zero since it contributes no motion, the equivalent wrap angle is equal to the binding angle $\theta_w^{(0)} = \theta_B$, and the output tail dimensions are unchanged.

2.3.4. Compatibility equation solving

In the final step to determine the actuator range of motion, the compatibility equations relating the *State 1* and *State 2* SMA wire lengths to the undeformed *State 0* lengths are solved. The solution cannot be expressed in closed-form since the integrand within the compatibility equation contains a transcendental function, the constitutive law utilizes a look-up/interpolation procedure to determine centroid strain, and for the rotational case the unknown wrap angle $\theta_w^{(\chi)}$ appears within the integrand and the limits of integration. A variety of numerical techniques can be used to determine the deformed length of the SMA wire such as bisection, secant, and inverse quadratic interpolation techniques by iteratively searching for the *State* χ wire length that satisfies the compatibility condition.

To provide a basis for the analysis and synthesis of spooled SMA wire actuators, the model effort culminates in compatibility equations relating the actuator length in *States 1*

and *2* to the undeformed *State 0,* and practical guidelines for solving them. Based on the compatibility equations for each state and the techniques described for predicting the actuator range of motion, algorithms can be assembled for predicting the motion of spool-packaged SMA wire actuators across a broad design space.

2.4. Model validation

To verify that the model accurately predicts motion based on the effects of friction, bending, and binding on spool-packaged SMA wire actuators, an experimental study was conducted measuring the range of motion performance of spool-packaged SMA wire actuators with differing geometries and configurations. The results demonstrate the model's validity for physical actuators, and support its use as a foundational tool for synthesizing spool-packaged SMA actuators with predictable performance.

2.4.1. Experimental test apparatus and procedure

Two experimental set-ups were utilized for the linear and rotational tests (Figure 2.7 and Figure 2.8), each with four similar parts: 1) the spooled SMA wire, 2) the fixed attachment point for the SMA input tail, 3) an interchangeable Garolite mandrel, and 4) the motion output – either a linear slider or a rotating arm – depending on the type of motion being tested. In each apparatus, a load cell measures the tension at the fixed input tail of the SMA wire, known weights supply the external load (directly applied weights for the linear configuration and via a pulley for the rotational), and a displacement sensor measures output motion (a laser displacement probe for the linear configuration and a rotary encoder for the rotational).

To reduce variation in SMA thermo-mechanical properties over cycles, the wire was thermally cycled prior to testing by heating and cooling the unspooled wire under a 45 N (400 MPa) load with a 6.0 - 6.5% maximum strain constraint until the motion stabilized according to the shakedown procedure described by Sun et al. (2008). The measured stress-strain behavior was approximated with a linear fit for the austenite phase and a third-order polynomial for the martensite phase (Figure 2.4) based on Equation 2.23. To

further ensure consistent wire performance, curves were re-generated periodically throughout the spooling study. While a mandrel material with a very low friction coefficient can provide the greatest range of motion in practical applications, Garolite was selected due to its good wear and electrical insulation properties and its known, consistent friction properties with respect to temperature. The consistent friction helped to reduce uncertainty with respect to friction and facilitated validation of the model. To estimate the coefficient of friction between the SMA wire and the Garolite mandrel, a known load was applied to an SMA wire wrapped through a known angle with a load cell attached to the opposite end of the wire. By applying a displacement to the wire and measuring the tension in the load cell end of the wire, the Capstan equation (Howell, 1953) could be used to estimate the coefficient of friction. This test was repeated for several applied load (0.25-1.5 kg) and wrap angles (π, $3\pi/2$, and $5\pi/2$) to determine the typical range of friction values being between 0.1 and 0.15.

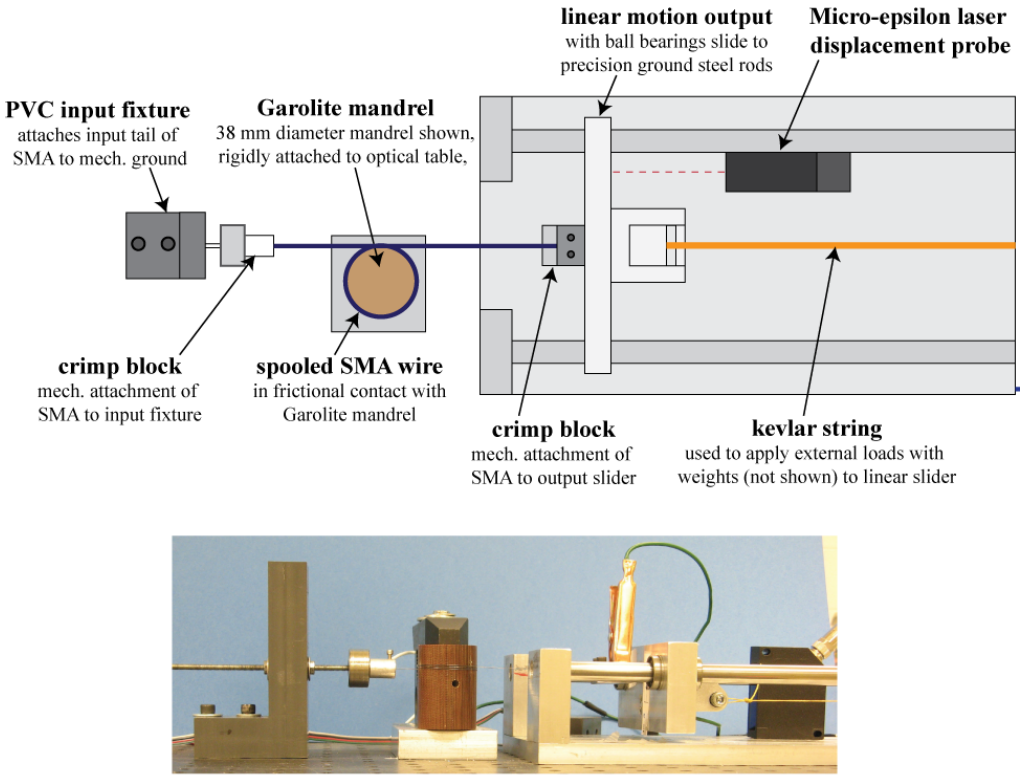

Figure 2.7. Experimental apparatus for linear spooled actuator experiments. The configuration tested uses a spooled SMA wire with 0.38 mm diameter and 1 wrap around a variable mandrel diameter (38 mm shown). The sliding motion output constrains the motion to a linear single degree of freedom, and is also the attachment point for the applied load.

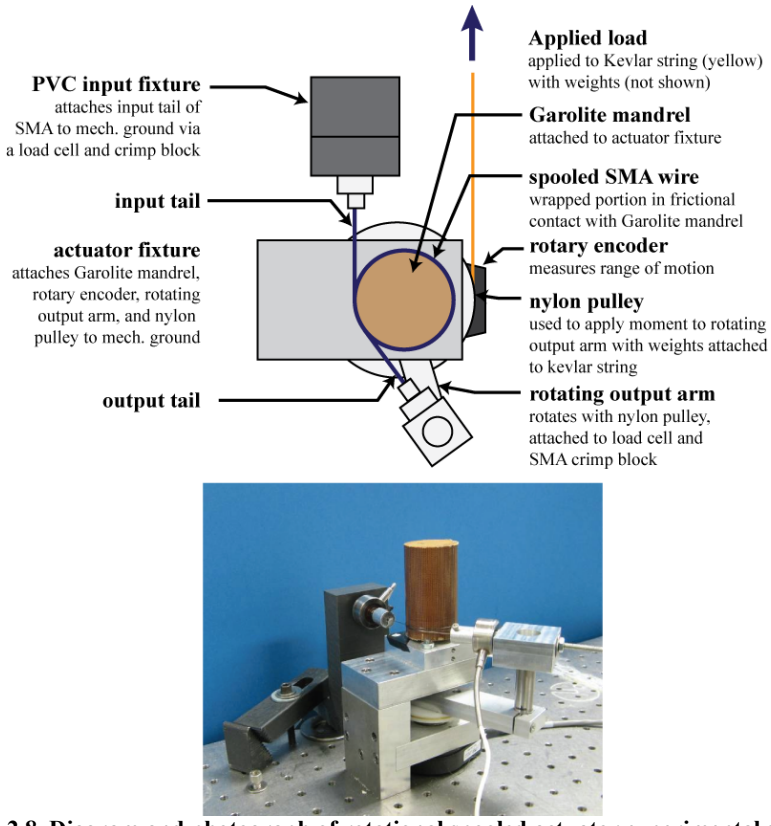

Figure 2.8. Diagram and photograph of rotational spooled actuator experimental setups.

Preparing for a typical test, the SMA wire and mandrel were selected, one end of the wire was clamped to the input structure (which could be positioned to vary the input tail length and/or wrap angle), the wire was wrapped around the spool, and the other end of the wire was clamped to the output slider or rotating arm where the external load was applied. Electrical current was applied to the wire (regulated and monitored by LabView software and a laptop computer equipped with data acquisition hardware) to resistively heat it until a steady state position for austenite was reached (using 1.8 A electrical current). The current was removed and the wire was allowed to cool to ambient temperature reaching its steady state position for martensite (0A for about 3 minutes). Trials were repeated 3 – 5 times to ensure consistency and repeatability. Laboratory temperature was regulated between 19 - 21°C. The experimental study tested three aspects of the spooling model – applied load for linear and rotary actuators, the binding condition, and the effect of bending – testing its accuracy and range and providing insights into the behavior of spooled actuators and the related design issues.

2.4.2. Applied load

To study the effect of applied load for linear and rotational spool-packaged SMA actuators, experiments were conducted by varying the amount of load applied to the output tail (tensile load F_{ext} applied to the linear actuator and moment load M_{ext} applied to the rotational actuator) while measuring its range of motion. In the linear actuator tests, the range of motion was measured for a 450 mm length of wire (measured in *State 0*, $\ell_{tot}^{(0)}$) with a 10 mm input tail and a single wrap. The actuator's linear motion was measured for a range of applied loads up to 13 N; the results are shown in Figure 2.9a. In the rotational actuator experiments, the range of motion was measured for a 200 mm length of wire ($\ell_{tot}^{(0)}$) with input and output tail lengths of 20 mm, a variable wrap angle ($\theta_w^{(0)}$=1.2 wraps), and moment loads up to 570 N-mm applied with deadweights via a pulley.

The experimental results are shown with the theoretical predictions for range of motion as a function of load in Figure 2.9b. For both of the selected actuator configurations, no binding was predicted to occur. In each case, the data matches the model well in shape and magnitude. For the expected range of friction coefficients ($0.1 < \mu < 0.15$), the error of the prediction (at μ = 0.125) relative to the measured data was small with 3.4% average error for the linear configuration and 9% average error for the rotational configuration. The shape of the stroke vs. applied load trends, which each include a point of inflection, results from the characteristic plateau of the martensite

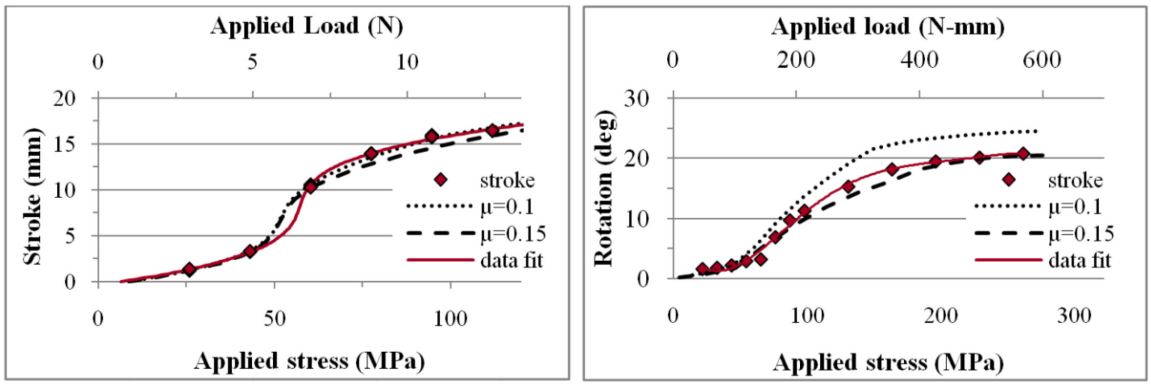

(a) (b)

Figure 2.9. Range of motion response to applied stress. (a) for a linear motion actuator with a single wrap ($\theta_w = 2\pi$), (b) for a rotational motion actuator with a variable wrap angle (initial angle $\theta_w^{(0)} = 2.4\pi$) and 200 mm initial wire length.

stress-strain curve (noting that the displacement variable in Figure 2.9 is on the vertical axis since it is the dependent variable, whereas the strain displacement is on the horizontal axis in Figure 2.4). Since wrapping the SMA wire distributes the stress and strain along the martensite and austenite curves, the shape of the load and displacement curves resulting from the stress-strain ends up being distorted rather than proportional. Additionally, friction has a more pronounced effect in the rotational case than in the linear case, as evidenced by the rotational case having a larger separation between the model curves across the range of friction values. This results from a greater portion of the wire, percentage-wise, being wrapped around the mandrel in the rotational case. Since more wire is under the influence of friction loads in the rotational case, the greater influence from friction is observed.

In general, SMA actuators (both spool-packaged and linear wires) exhibit increasing strokes with increasing applied stress, whereas conventional actuators behave conversely. The increasing strokes for SMA are the result of the increased applied stress that detwins the wire with greater authority. Due to the martensite plateau, the stroke is particularly sensitive to stresses in the range of the plateau. Since the wrapped wire has stresses distributed along the martensite stress-strain curve, however, higher stresses are needed to prevent large portions of the wire from having martensite strains in the range below the plateau where they would produce lower magnitudes of stroke. This has impacts regarding the selection of SMA wire diameter since, for a given applied load, selection of wire diameter impacts the stress. Thinner wires can increases the stress, and thus, the stroke. However, selecting wires that are too thin can overstress the wire and lead to fatigue failure more quickly.

2.4.3. Effect of bending

To validate the model's prediction of the bending effect, a series of experiments was conducted which varied the size of the mandrel relative to the wire diameter. To isolate the effect of bending experimentally, the range of motion was measured for linear actuators with a constant wire diameter, a single wrap of SMA wire around the mandrel,

a 15 N constant applied load (for constant stress in the output tail), mandrel diameters varied between 10-90 mm in random order. All other actuator dimensions (tail lengths and total wire length) were maintained to be proportional to the mandrel diameter. Since all dimensions except the wire diameter are proportional to the mandrel diameter between tests, the range of motion was normalized with respect to the wire diameter, such that $\overline{\delta\ell} = \delta\ell / D_w$ where $\overline{\delta\ell}$ is the normalized range of motion. The set of experimental results provide the normalized range of motion as a function of the mandrel to wire diameter ratio ($\overline{D} = D_w / d$), referred to herein as the "diameter ratio".

The normalized range of motion that was determined experimentally is plotted with respect to the diameter ratio in Figure 2.10. In the figure, experimental data is compared to the spooling model predictions, which accounts for bending and friction effects, and the friction-only model, which provides a baseline for comparison. The data and model demonstrate that the actuator's range of motion is dependent on the diameter ratio with greater motion losses occurring for tighter spooling (smaller values of the diameter ratio). The effective stress-strain profile for the spooled martensite SMA wire is governed by the average tensile stress and centroidal strain along the wire's length, which stiffens as the diameter ratio decreases (Figure 2.5). Since the austenite stress-strain is assumed linear, the model does not predicted a change to the austenite mechanical behavior due to

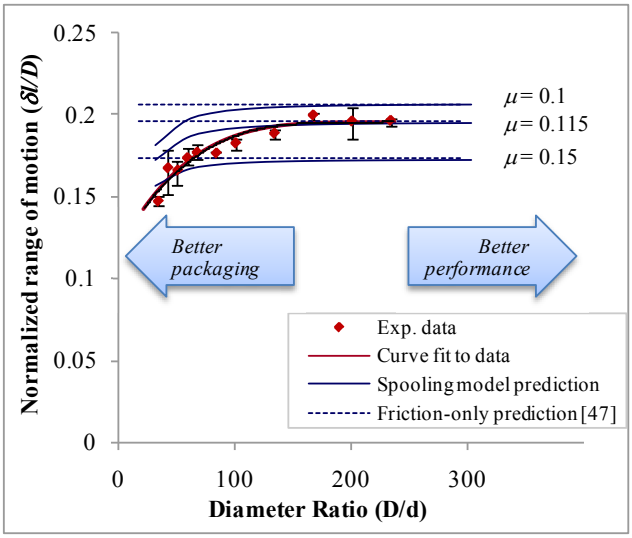

Figure 2.10. Effect of bending on the normalized range of motion. Effect of bending on the normalized range of motion. The experimental data is compared to the friction-only prediction and complete friction-and-bending model for selected values of the expected coefficient of friction.

bending. The reduction in range of motion for smaller diameter ratios results from this stiffening of the martensite stress-strain behavior.

For large diameter ratios ($\overline{D} > 130$), the models are nearly equivalent to each other and both agree with the experimental data within the expected range of friction values ($0.1 < \mu < 0.15$), and most closely at $\mu = 0.115$. Although the precise value of friction was difficult to determine, noticeable wear on the Garolite mandrels and changes in friction were not observed throughout the course of testing. While the deviation between the spooling model and friction-only model becomes significant at diameter ratios below 130, this threshold diameter ratio value is specific to the parameters tested and would be expected to vary for different actuator configurations, in particular with respect to the mandrel material selection and applied load. For the friction value of $\mu = 0.115$, the average error between data and spooling theory is 5.8% across the range of diameter ratios tested, reflecting a slight improvement upon the 8.9% average error for the friction-only model. For larger diameter ratios ($\overline{D} > 130$), the spooling model and friction-only prediction match the data closely with errors less than 3% for the best-fit friction value of $\mu = 0.115$. For tighter curvatures, the spooling model deviates from the data slightly more than for large diameter ratios while the friction-only model deviates significantly more for $\overline{D} < 130$. The spooling model's average error is 8.3% (max. error = 16%), and the friction-only model's average prediction error is 13% (max. error = 25%). Comparing the error between the models and data where they begin to deviate ($\overline{D} < 130$), the friction-only model's errors were 50-150% larger than those of the full spooling model, demonstrating that significant improvement to the prediction is achievable byincluding bending effects.

While the spooling model matches the experimental data well in both form and magnitude, the measured range of motion declines more sharply for decreasing diameter ratios than the spooling model predicts. The sharper decline in motion that was observed experimentally may be attributed to the assumption that the differential bending moment in martensite ($dM_{\theta y}$) is negligible, which is valid for large diameter ratios or very flexible

materials. However, the moment to bend the SMA wire would be expected to further depress the centroid strain, which is consistent with the observed experimental behavior at low diameter ratios. Additionally, portions of the wire that undergo extreme strains due to very tight bending may undergo non-recoverable deformations that would lead to a decline in performance not captured by the constitutive law formulations that would typically be used for the spooling model. For example, a 0.38 mm diameter wire with 130 MPa appled stress (15 N load) would begin to experience net strains exceeding 8% for mandrel diameters smaller than 7.3 mm (D/d < 20). Lastly, any non-linearity in the austenite stress-strain profile could also have led to additional motion losses, especially if stresses caused by tighter curvature approached yielding, where the austenite stress-strain behavior is more compliant.

2.4.4. Effect of binding

To observe binding in physical actuators, tests were performed on a linear motion actuator with constant *State 0* wire lengths ($\ell_{tot}^{(0)}$=450mm) and constant input tail lengths ($\ell_{t,in}$) across the set of experiments, while the wrap angle was varied between 0 and 6.5π radians (0 - 3.25 wraps). The measured range of motion is shown in Figure 2.11a. Initially, the motion decreases non-linearly as more wire is wrapped around the mandrel, but begins to descend linearly once binding takes effect. The linear decline occurs because portions that become wrapped around the mandrel beyond the binding angle

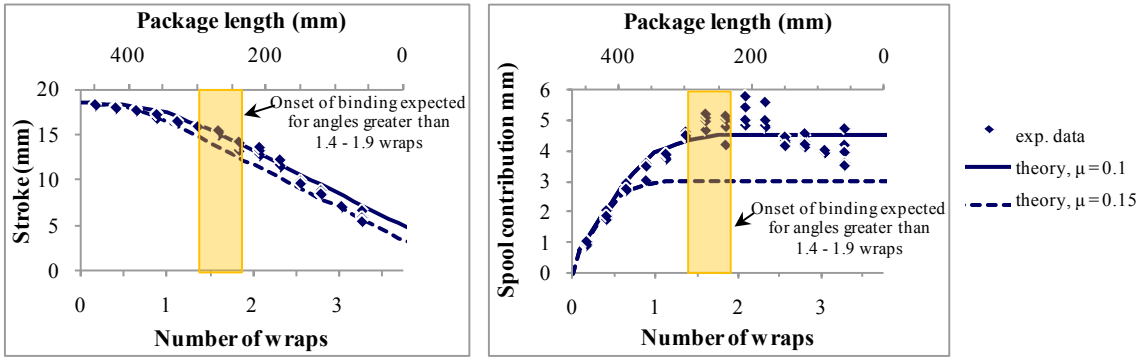

(a) Effect of wrap angle on motion *(b) Spooled contribution to overall motion*

Figure 2.11. Effect of packaging demonstrating the binding effect. (a) The stroke is shown for a spooled actuator with a constant length wire as the amount of wrapping is increased. Once binding occurs the stroke decreases linearly with wrap angle. (b) The contribution of the spooled portion of the SMA wire is shown as wrap angle increases. Once binding occurs, wrapping more wire around the mandrel contributes no additional motion to the actuator's motion.

contribute no motion. Thus, the motion loss becomes proportional to the amount of wire wrapped on the mandrel. Subtracting the theoretical contribution to motion due to the tail portions of the SMA wire, the spooled portion's contribution to the overall motion is plotted in Figure 2.11b. The data correlates well with theory with a 3.4% average error on the overall stroke (least-squares error with respect to friction occurring at $\mu = 0.11$). Since the effect of spooling builds up as more wire is wrapped around the mandrel, the decline in the motion with wrapped length is initially low and becomes steeper in slope until the binding condition is met, at which point the slope becomes constant and the stroke drops off linearly as wrap angle increases. The spooled portion's contribution to stroke agrees with 8.2% average error for the non-binding data points and increases to 9.4% average error overall (least-squares error with respect to friction coefficient $\mu = 0.10$). The initial increases and leveling off of the spooled portion's contribution to stroke is due to the onset of binding, which supports the hypothesis that the binding portions of the wire do not contribute to the overall stroke.

The onset of binding can be regarded as a limitation to performance and the design space for spool-packaged SMA wire actuators. Since portions of the wire wrapped beyond the binding angle make no contribution to motion, packaging wire in excess of the binding angle is an unrecovered expense with regard to SMA material cost and the additional energy needed to heat the longer wire. Furthermore, the input tail provides useful motion to spooled actuators that do not bind, whereas the entire input tail contributes no motion if any of the wrapped portion binds. To avoid packaging of SMA wire that does not contribute motion due to binding, selecting mandrel materials with lower frictional is beneficial when cost and material characteristics allow (for example, electrical insulation and allowable temperature range).

Overall, the validation results demonstrate that the motion performance of spool-packaged SMA wire actuators can be predicted with for a specifiable actuator design, which includes its geometry, material and constitutive properties, and the external applied loads. While the presence of friction and bending strains in the spooled actuator results in

some motion loss, the potential improvements to packaging are notable. In the binding experiments, for example, a 33% reduction in the actuator's package length only suffered a 13% loss in motion. Through spooled-packaging, greater motions are possible within a given form constraint. Furthermore, spooling allows a spooled actuator to occupy a shorter package length than a non-packaged SMA wire that works against the same load and produces the same motion.

2.5. Conclusion

While SMA wire actuators are attractive candidates for lightweight, high performance actuators, difficulty in packaging the long lengths of wire needed for moderate deflections has been one of the factors limiting their widespread use. Spooled-packaging improves the actuator's form factor but also introduces performance losses due to friction and bending. Friction between the SMA wire and the mandrel is the main source of loss in spool-packaged actuators and needed to be modeled for performance to be predictable and losses to be mitigated during the design process. Accumulation of friction can lead to binding between the SMA wire and mandrel, and poses a limitation on the use of spooled-packaging, and thus needed to be incorporated in the model. Since the wrapped configuration introduces a strain gradient across the SMA wire's cross-section due to bending, the motion contribution of wrapped wire depends on bending strains in addition to applied stress. With larger bending strains for more compact, tightly wrapped packaging, the impact of bending also needed to be included in the model. To address the need for an analytical model that can support systematic actuator design methodologies, a quasi-static performance model was derived that: 1) considers the strain profiles across the SMA wire's length due to friction and its cross-section due to bending, 2) accounts for portions of the wire that gain and lose contact with the mandrel during operation, and 3) evaluates limitations of the packaging technique due to frictional binding. Yet, the model was also carefully simplified by taking steps that enhance its ability to be applied to analytical actuator design without making sacrifices to rigor and accuracy. To demonstrate the model's range of motion prediction for physical actuators,

an experimental validation study was performed in which the range of motion was measured and compared with theory. The experiments validated the model for rotational and linear actuators with respect to applied load, account for bending strains, and forecast the onset of binding due to accumulated friction.

In the applied load experiments, the shape and form of the data was predicted well by theory. The model predicts the characteristic load-displacement behavior that results from SMA's martensite and austenite stress-strain behavior, and adjusts for the distribution of strains along the SMA wire's length due to friction. For the applied load experiments, errors were in a reasonable range (3.4% for linear actuators, 9% for rotational), with the experimental data matching the theory well in form and magnitude. The predicted bending effect was verified experimentally with large mandrel diameters (diameter ratios greater that 130) having negligible losses from bending, while for tighter wire curvatures the bending strains began to noticeably degrade performance. By including bending in the model, the experimental error was reduced from 13% to 8.3%. Whereas the friction-only model places no penalty on the performance of very tightly spooled actuators, the full friction and bending spooling model is able to predict the degradation of performance due to bending. This ability to predict performance degradation with higher bending strains is important to guide optimization-based design methodologies away from configurations with very high bending strains despite the more compact packaging. The predicted binding behavior was demonstrated in experiments with a constant SMA wire length and varied wrap angle for which binding occurred between 1.4 – 1.9 wraps and that any SMA wire wrapped beyond the binding angle did not contribute motion to the actuator. Thus, binding configurations should be avoided in physical actuators to prevent unnecessary performance losses. By selecting lower friction mandrel materials the wrap angle can be increased, thus expanding the design space. Even so, the binding condition needs to be evaluated when designing actuators to ensure that the actuators will provide their expected range of motion.

Based on the results of this study, spooled-packaging and the accompanying predictive model can provide a useful foundation for analytical actuator design for synthesizing high performance actuators with compact packaging and minimized losses. Whereas previous modeling attempts had been developed on an *ad hoc* basis for application specific needs, by including the effects of friction, bending, and binding, this model provides a more versatile, accurate predictive tool for analyzing spool-packaged SMA actuators. Building on the model's predictive capabilities, a deeper understanding of the relationships between an actuator's design parameters, packaging constraints, and performance can be developed to enable engineers to make meaningful design choices. In addition, the model is a crucial element for developing optimization-based design methodologies for spool-packaged actuators with high performance, low-cost, and customized form factors. With spooling techniques to overcome packaging challenges, SMA can create expanded opportunities for improving actuator cost, weight, and energy density to bring the numerous advantages of SMA to a broader application space.

Chapter 3. Parameter Study for Spool-Packaged Shape Memory Alloy Actuators

To design spool-packaged SMA actuators with predictable performance, the model is an essential analytical tool. While spool-packaged actuators are highly customizable due to numerous user-specifiable parameters, these multiple dimensions of tailorability make the design problem more complex, and thus more difficult to understand tradeoffs between performance, packaging, and cost as parameters are varied. Thus, a deeper understanding of how the design of spool-packaged actuators influences performance is necessary to enable meaningful design choices, to understand the behaviors of physical realizations of spooled actuators, and to competently navigate design revisions.

This chapter explores how key design parameters and packaging constraints influence the actuator performance to build the knowledge base that can educate the design process, and thus enable better design choices. To investigate how key design parameters influence the tradeoffs between performance and packaging, the interrelated effects of geometry, applied load, material parameters, and different types of packaging are explored using select experimental studies and the simulations that employ the model from Chapter 2 for single mandrel spool-packaged SMA actuators. The observed parameter sensitivities are utilized to develop an understanding of how key mechanics influence actuator behavior, and to construct set of design guidelines regarding each category of parameters studied. The impact of packaging on the actuator design and performance is also examined in three examples cases for which different types of form constraints are considered including: 1) a baseline case in which there are no packaging constraints, 2) a case where the actuator footprint is constrained within a rectangular envelope, and 3) a case constraining the actuator within the same rectangular envelope with an additional internal obstacle where SMA wire cannot be packaged. In each case, actuator displacement is predicted across a range of mandrel diameters, wrap angles, and,

in the latter two cases, the mandrel position within the packaging constraint. By developing a deeper understanding of how actuator design parameters and packaging constraints influence performance, this chapter provides the foundational knowledge-base to support spool-packaged actuator design in the early synthesis stages, the analysis of prototypes, and revision of existing designs. With this background, the spool-packaging approach can be applied skillfully to applications needing high performance, low-cost actuation within practical form factors.

3.1. Geometric parameters

By developing the spooled-packaging technique to encompass a wide range of designs, there is a broadened range of actuator needs that can be satisfied with spooled-packaging. However, the multiple dimensions of geometric customization complicate the task of parameter selection. In this section, the effects of varying key geometric parameters – wrap angle, spool position, and mandrel diameter – are discussed, interrelationships between the different parameters are explored, and guidelines for geometric parameter selection are provided. Many of the parameter studies used a common set of parameters, which are summarized in Table 3.1. These parameters represent a typical SMA wire diameter, an applied load that causes stress within the range recommended by the manufacturer of Flexinol (Dynalloy, 2010), and typical material properties observed in the experimental study (Chapter 2). Exceptions to these parameter choices are noted within each parameter study.

3.1.1. Effect of wrap angle

The wrap angle plays a crucial role in modulating the performance, cost, and

Table 3.1. Typical parameter values used throughout parameter study.

Parameter	Value
SMA wire diameter	$d_{SMA} = 0.381$ mm
Applied load (stress)	$F_{SMA} = 20$ N ($\sigma_{SMA} = 175$ MPa)
Martensite stress-strain function	$\sigma^{(M)} = 4.1\times10^{6}\varepsilon^{3} - 2.7\times10^{5}\varepsilon^{2} + 6.7\times10^{3}\varepsilon$ [MPa]
Austenite stress-strain function	$\sigma^{(A)} = 45.1\times10^{3}\varepsilon$ [MPa]
Friction coefficient	$\mu = 0.1$

packaging of spool-packaged SMA actuators. To gain a deeper understanding of how these qualities are related and affected by wrap angle, the wrap angle was explored in two parameters studies regarding actuators with variable SMA wire lengths and with variable actuator package lengths.

3.1.1.1. Variable SMA wire length

Considering spool-packaged SMA wire actuators with constant package lengths and variable wrap angles, the ability to increase the stroke of an SMA actuator without increasing the package length can be observed. An actuator was examined with a zero length input tail, such that the input end of the SMA wire was fixed to the mandrel (Figure 3.1). Using the single mandrel spooling model (Chapter 2), the parameter set in Table 3.1, and a 25 mm mandrel diameter, the range of motion was predicted for actuators with four different package lengths (L_{pack} = 25, 50, 100, and 200 mm). The model-generated ranges of motion are shown in Figure 3.2a with wrap angles varied between $\theta_w = 0$ (linear, non-spooled case) and up to 25% beyond $\theta_w = \theta_B$, where the maximum motion for the spool-packaged actuator occurs due to frictional binding.

In each case, the lower limit on motion is the stroke of a non-packaged, linear SMA wire equal in length to the package (L_{pack}). The upper limit on motion occurs at the binding angle θ_B. Since the spooled portion's contribution to overall motion is independent of the output tail length, the additional motion that results from spooling is equal for different package lengths. The available package length affects the fraction of SMA wire that can be wrapped around the mandrel, as shown in Figure 3.2b, with the shorter package lengths allowing a larger fraction of the wire to be wrapped at a

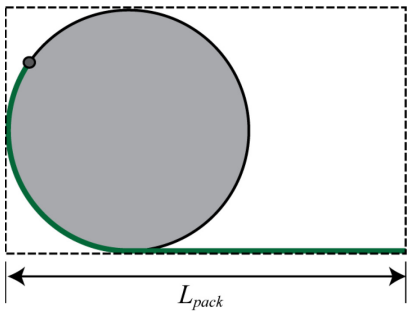

Figure 3.1. Diagram of spool-packaged SMA actuator for wrap angle parameter study. A single mandrel actuator with a zero length output tail was examined.

particular wrap angle.

Whereas a non-spooled wire with the constitutive laws and loads used in this example can provide motion up to 4.6% of its length, the packaged actuators are capable of providing much more motion relative to the length of the package. The metric for effective package strain is defined as the stroke per package length, and is depicted in Figure 3.2c. In this example, the shortest package length (L_{pack} = 25 mm) actuator is capable of delivering strokes up to 19.8% of the package length. The maximum effective package strain available depends on several factors including the mandrel diameter, applied load, and coefficient of friction, which can increase or decrease the effective package strain depending on their selection.

While spooling is capable of increasing an actuator's stroke without increasing its package length and amplifying effective package strains by several times the strains available for linear SMA wires, increasing the wrap angle has some adverse effects that

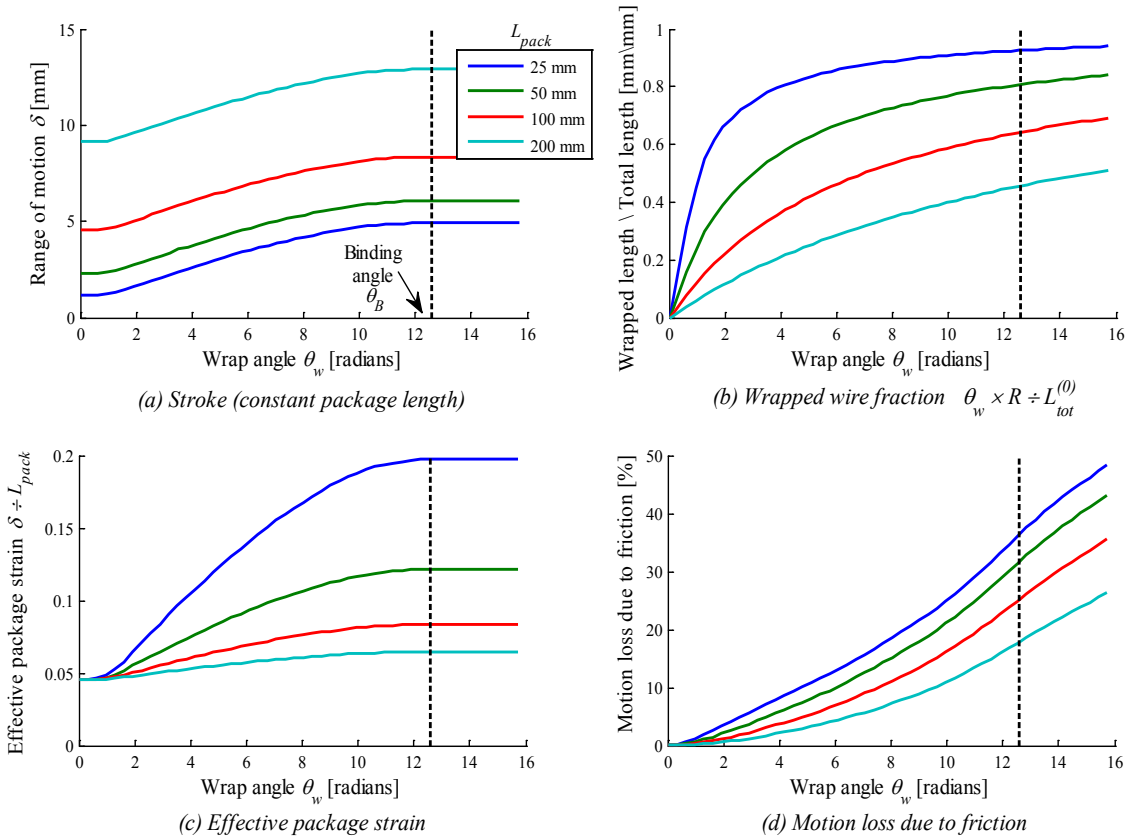

Figure 3.2. Effect of wrap angle for constant package lengths. The results were generated for an actuator with the standard actuator parameters in Table 3.1, a mandrel diameter of 25 mm, and no input tail ($\ell_{t,in}$ = 0 mm).

pose design tradeoffs. For example, packaging longer lengths of wire carries additional material costs and energy costs since longer wires take more energy to heat. In addition, as more wire is wrapped within a constant package length, a greater fraction of the available motion (compared to non-spooled wires of equal length) is dissipated due to friction, as shown in Figure 3.2d. Still, the loss due to friction is within a reasonable range. For the shortest package (25 mm) wrapped up to the binding angle for example, while 35% of the wire's potential motion is lost due to friction, the effective package strain is increased by nearly 400%. Thus, spooling is capable of increasing performance with some costs due to friction losses, but managing such tradeoffs depends on particular application requirements.

3.1.1.2. Constant SMA wire length

The tradeoff between packaging and performance was investigated by calculating the stroke for several different lengths of SMA wire (*State 0* total length, $\ell_{tot}^{(0)}$) across a range of wrap angles. By varying the wrap angle for a given length of wire, the package length (as illustrated in Figure 3.1) was also varied in a corresponding manner. The results generated for this scenario are shown in Figure 3.3. As more wire is wrapped around the mandrel, the predicted range of motion decreases as depicted in the plot of stroke versus wrap angle (Figure 3.3a). The decrease in motion is attributed to the increasing friction losses as more wire is wrapped. This result demonstrates that the package length can be reduced by wrapping more wire around the mandrel, but performance is traded off at an increasing rate. Once the binding condition is reached, the spooled portion can make no additional contribution to the overall actuator motion regardless of how much additional wire is wrapped.

Examining the packaging more directly, the same data is plotted with respect to the package length in Figure 3.3b. In the non-binding range, the motion increases non-linearly and becomes less steep with the increasing package length because the actuator is subjected to reduced friction losses for less wrapping. Reducing the package length for a constant SMA wire length, the slope of the motion versus package length curve becomes

steeper as the binding angle is approached due to the accumulation of friction with wrap angle. Decreasing the package length beyond the binding condition, any additional wire that becomes wrapped around the mandrel is unable to contribute to overall motion. Regardless of the total SMA wire length, the stroke of an actuator under binding conditions follows the same linear function of package length. The function has the same slope as the straight wire case, but the motion is offset vertically by a constant stroke. The slopes are constant because varying the package length in the binding case varies the contribution to motion from the output tail, while the motion contribution from the spooled portion is unaffected. Since a unit of length of output tail wire produces the same stroke as a unit of length of non-packaged wire, varying the package length for either case varies the motion at the same rate. The vertical offset between the straight wire case and the spool-packaged SMA wires undergoing binding reflects the additional motion that is available through spooled-packaging.

The stroke versus package length results are also utilized to determine the effective package strain (δ/L_{pack}) as a function of package length (Figure 3.3c). Compared to the baseline non-packaged case, the improvement to package strain is evident, increasing for smaller package lengths. Additionally, the effective package strain versus package length behavior merges for the binding case indicating that while the best effective package strains are available for the shortest package, there is an upper limit on the amount of wire that can be spooled to provide a benefit to effective package strain. Furthermore, the material and heating costs that results from longer wire lengths can be avoided without degrading performance in this region.

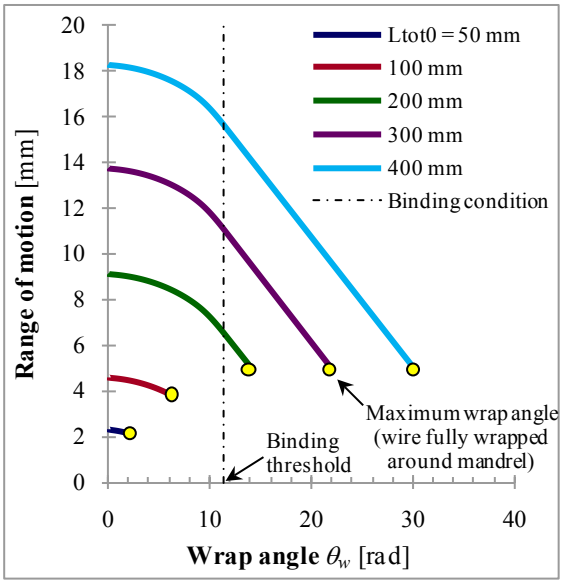

(a) Range of motion vs. wrap angle

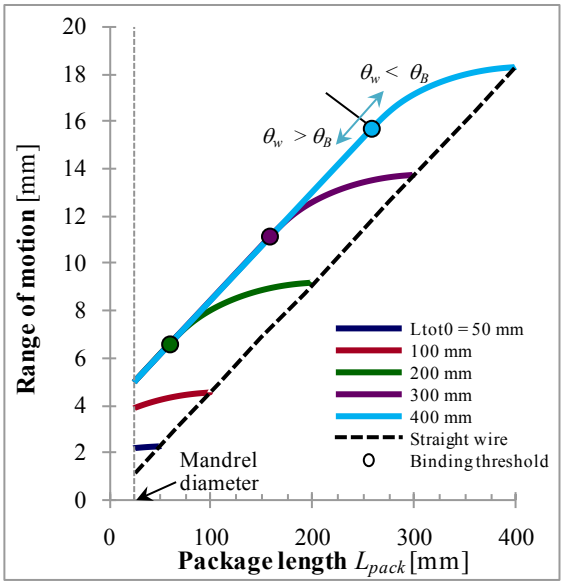

(b) Range of motion vs. package length

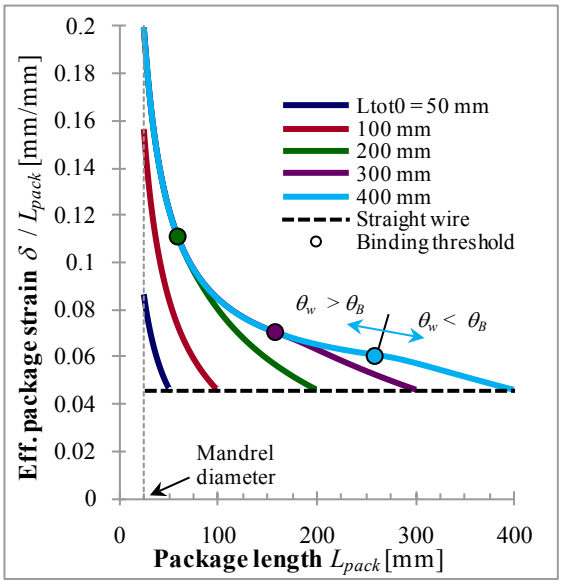

(c) Effective package strain vs. package length

Figure 3.3. Effect of wrap angle for actuators with variable package length. a) The relation between stroke and wrap angle is demonstrated for SMA wires of five different *State 0* wire lengths. b) The same data is plotted, but with respect to package length. Right of the binding threshold for each SMA actuator no binding is predicted, whereas frictional binding occurs to the left of the binding thresholds. c) The effective package strain is shown as a function of package length for each of the five different SMA wire lengths.

3.1.2. Effect of spool position

Varying the position of the spool within a packaging constraint affords further design flexibility. Depending on the constraints for particular applications, the available packaging footprint may only accommodate the mandrel in a limited range of positions, and selection of the spool position may have to account for available space and the performance required. To provide an enhanced understanding of the impact and sensitivity of spool position on the performance, the range of motion was determined from experiments and theory for a constant length wire with variable spool position and three different wrap angles including a non-binding (θ_w = 2π radians), borderline binding (4π radians), and binding case (6π radians) (Figure 3.4). The model predicts that the range of motion is linearly related to the spool position with the highest motions for the shortest input tail lengths, in which the mandrel is positioned most closely to the fixed input end of the SMA wire. Friction acting on the wrapped portion of the wire causes a drop in strain from the output tail to the input tail, which is independent of the spool position. The linear trend results from the input and output tails contributing to the overall motion proportionally to their respective lengths since both the input and output tail lengths are directly related to the position. The reduced strain in the input tail highlights that friction makes a "downstream impact" on the range of motion

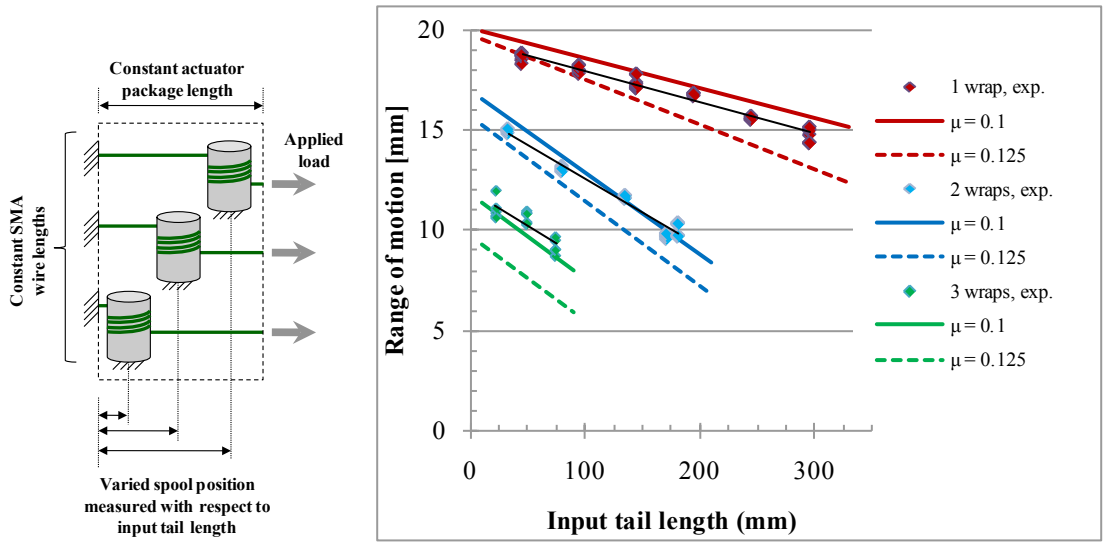

Figure 3.4. Effect of varying spool position. (a) Varied spool positions. (b) Theory lines and experimental data for range of motion as a function of spool position (input tail length).

contribution; friction that acts on a segment of wire also causes the remainder of the wire toward the input end to provide reduced magnitudes of motion. Since the input tail strain is lower that the output tail strain, the stroke is maximized by having the largest output tail possible. Greater sensitivity (steeper downward slope) to the spool position is also noted for larger wrap angles because further reductions in the input tail strain due to wrap angle dependent friction loss are proportional to reductions in stroke.

3.1.3. Effect of mandrel and wire diameter

Spooling provides an enhanced ability to package SMA wires more compactly and to redirect wires around tight corners, but the improved packaging carries additional costs including increased bending strains and related losses as the SMA wire is wrapped around smaller curvatures. To assess the effect of SMA wire bending on the range of motion, the spooling model was used to predict the range of motion for actuators with the SMA wire diameter, applied load, and SMA stress-strain functions specified in Table 3.1 and variable mandrel diameters. All other actuator dimensions (tail lengths and total SMA wire length) were held proportional to the mandrel diameter, and are summarized in Table 3.2. Among the proportional dimensions, the input and output tails are equal in length to the mandrel radius ($\ell_{t,in} = \ell^{(0)}_{t,out} = D/2$) and the total SMA wire length is $\ell^{(0)}_{tot} = D + \pi D$, resulting in about 75% of the wire being wrapped and the remaining length being divided equally between the input and output tails. Since all dimensions except the wire diameter are proportional to the mandrel diameter, the range of motion was normalized with respect to mandrel diameter, such that the normalized range of motion is $\overline{\delta\ell} = \delta\ell / D$. By normalizing, the effect of bending can be isolated since the

Table 3.2. Parameter specifications for mandrel & wire diameter study

Wrap angle	θ_w	= 2π radians
Mandrel diameter	D	= 10 - 90 mm
Diameter ratio	$\overline{D}$	= 26 - 240
Input tail length	$\ell_{t,in}$	= D/2
Output tail length	$\ell^{(0)}_{t,out}$	= D/2
Total SMA wire length	$\ell^{(0)}_{tot}$	= $D + \pi D$

proportionally sized actuators would produce equal normalized motion if bending were not included in the model.

The normalized range of motion is plotted with respect to the diameter ratio in Figure 3.5, shown for three different coefficients of friction spanning a low to moderate range (μ = 0.05, 0.10, 0.15). The normalized range of motion for the "friction-only" prediction is also provided (horizontal dashed lines) to illustrate the impact of neglecting bending strains in the model and to serve as a baseline for comparison. The normalized motion prediction can be divided into two regions according to whether the bending strains influence the range of motion significantly. For this analysis, the threshold between the regions was defined at the diameter ratio where the full spooling model prediction deviates from the friction-only prediction by 5%. For a friction coefficient of $\mu = 0.1$, the full model (including bending and friction effects) deviates from the friction-only model by less than 5% for diameter ratios of $\overline{D} > 60$. For more compact packaging, the deviation increases: up to 10% deviation for diameter ratios of $\overline{D} > 40$, and up to 20% deviation for diameter ratios of $\overline{D} > 25$.

To gain insight into how bending strains affect performance, the strains at different

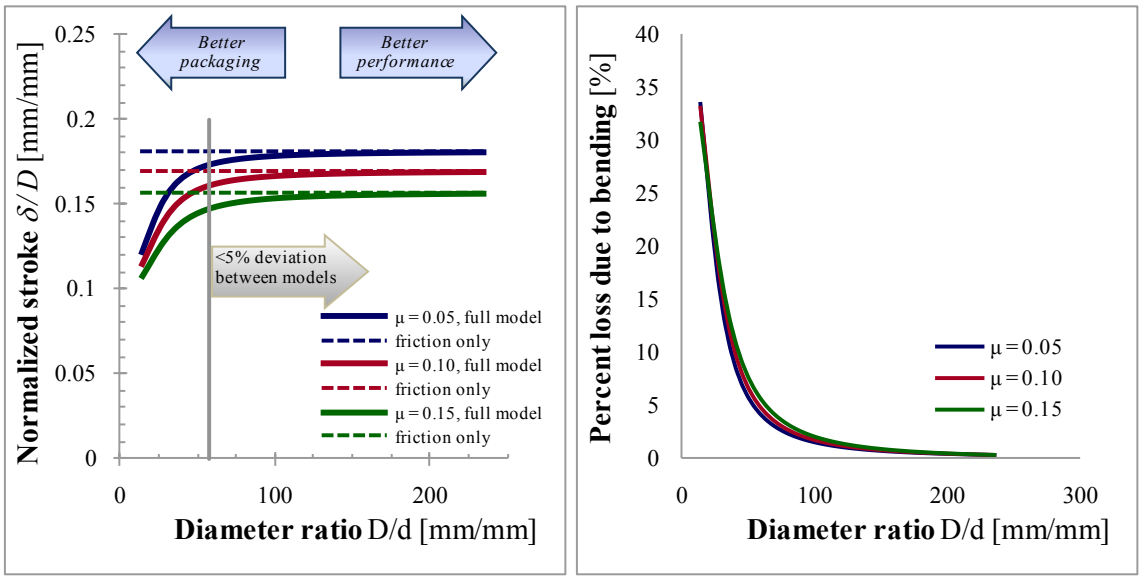

(a) Normalized stroke *(b) Percent motion loss due to bending*

Figure 3.5. Effect of diameter ratio on range of motion performance of spool-packaged SMA wire actuators. (a) The range of motion, normalized with respect to the mandrel diameter, is shown with respect to the diameter ratio, demonstrating the effect of bending on performance. (b) The percent motion loss due to bending, relative to the motion predicted by the friction-only model is shown with respect to diameter ratio.

locations across the SMA wire cross-section were calculated across a range of diameter ratios (D/d = 26 - 240) and applied average stresses ($\sigma_{\theta\theta}$ = 0 - 300 MPa). The centroid strain (ε_{ctd}) was calculated across a grid of applied average stress and diameter ratio combinations using the equation relating average applied stress (and the force resultant) to strains across the SMA wire's cross-section (Equation 2.15). Numerically solving the average applied stress equation for the centroid strain at every combination of $\sigma_{\theta\theta}$ and $\bar{D}$, the centroid strain was generated (Figure 3.6a) omitting infeasible points where compressive stresses occur at the inner surface of the wrapped SMA wire. The spooling model prediction demonstrates that centroid strain has a growing sensitivity to stress as the diameter ratio is reduced (smaller mandrel diameters). The behavior is also compared to the friction-only model for which the effect of bending is neglected. The growing deviation between the centroid strain surfaces for the full model and the friction-only model illustrates that the friction-only model is limited in accuracy for tight wrapping.

The direction and magnitude of the change in centroid strain depend on three key factors: 1) the nominal strain that results from the tensile load on the wire, 2) the diameter ratio, which affects how sharply the stress and strain vary across the wire's cross-section, and 3) the curvature of the martensite stress-strain curve spanned by the stress and strain across the wire's cross-section. For larger stresses, the stress and strain across the wire are mostly distributed above the martensite plateau where the stress-strain curve has a positive curvature ($d^2\sigma / d\varepsilon^2 > 0$) causing the centroid strain to shift upward to satisfy the force equilibrium based on the distribution of stresses in Equation 2.18. For lower nominal strains, the stress-strain curve has a negative curvature ($d^2\sigma / d\varepsilon^2 < 0$), causing the centroid strain to shift down. For more extreme bends in the wire (low diameter ratios), there is a greater stress-strain distribution across the wire that results in higher magnitude shifts of the centroid strains. Typically, actuators are subjected to applied loads that induce stresses above the martensite plateau to achieve useful magnitudes of strain (typically > 2% for NiTi). Thus, actuators generally operate in a region where the centroid strains are depressed due to bending of the wire.

Looking more deeply into distributions of strains across the SMA wire, the strains at the centroid, inner edge, and outer edge are shown Figure 3.6. The minimum strain, shown in Figure 3.6b, decreases at a sharp rate for diameter ratios below 50 due to the tight curvature. The isoline for zero minimum strain ($\varepsilon = 0$ in Figure 3.6b) provides a boundary on the region of the design space where the model is valid since the constitutive law is not defined for compressive stress and negative strains of the wire would cause frictional binding. The maximum strains are shown in Figure 3.6c. The maximum strain needs to be regarded in actuator design because of its impact on fatigue life (Bertacchini, et al., 2008). The maximum strains increase more sharply for small diameter ratios due to the more extreme strain distribution from the small radius of curvature for the wire, and approach the centroid strain in the limit as the diameter ratio increases. These maximum strains are used in the following section to develop design guidelines with respect to fatigue life.

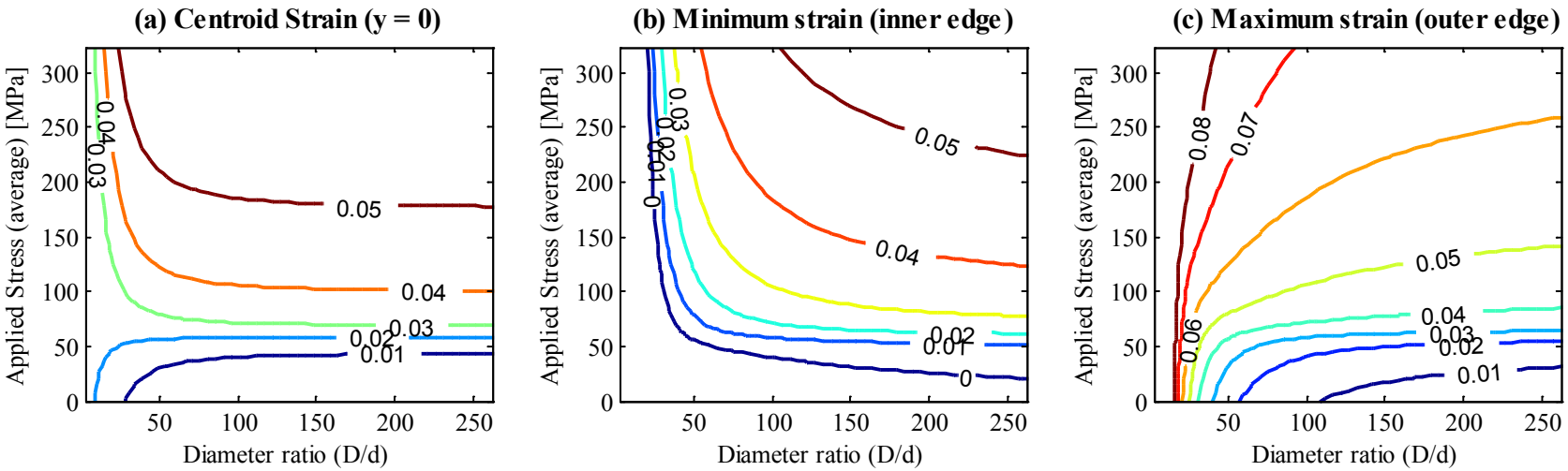

Figure 3.6. Effect of bending on strains across SMA cross-section. Strain in the axial direction is shown with respect to applied stress $\sigma_{\theta\theta}$ and diameter ratio at (a) the centroid, (b) the inner edge where the SMA is in contact with the mandrel and strain is at its minimum, and (c) the outer edge where strain is at its maximum.

3.1.4. Design guidelines for geometric parameters

Expanding on the study of the actuator geometry's influence on behavior, the findings are also considered within a design context for an increased understanding of the practical considerations that go into design of spool-packaged SMA wire actuators. Varying the geometric parameters was often noted to modulate the tradeoff between performance and packaging. Indeed, the tradeoff exists for many parameters, but there are also regions of the design space where packaging was noted to cause excessive losses or have additional impacts on the practicality of actuator design.

Regarding the results on wrap angle, for instance, the use of spooled packaging was shown to enable larger strokes within a given package length and shorter package lengths for a given stroke, but within limits. For an actuator with a given applied load and material properties, the binding angle limits the maximum additional motion that spooling can provide. Considering the effective package strain versus the wire strain, spooling up to the binding angle can increase strains from single percent magnitudes to tens of percents – thus enabling more compact actuation. Wrapping nearly the entire wire with a 175 MPa applied load and friction coefficient $\mu = 0.1$, about two-thirds of the wire's original stroke is available while package strain is quadrupled. For applications using spooling to redirect the SMA wire rather than to package the actuator compactly, the motion losses do not exceed 10%, assuming that for wire redirection less than a full wrap (2π radians) is typical – allowing for the packaging technique to broaden the design space for SMA wire actuators in many scenarios. While wrapping more wire can increase stroke or reduce package length for an actuator, it can only provide these benefits in the non-binding range. Wrapping the wire beyond the binding angle contributes no additional motion to the actuator, and adds additional costs such as energy for heating and material needs, making design of actuators that bind inadvisable.

The range of motion behavior with respect to spool position can be used to guide the selection of design parameters for spool-packaged SMA actuators. When packaging is an issue and the spool cannot be positioned at the input end, the spool position study

demonstrates that it is advantageous to position as closely to the input as possible and that the positioning becomes more critical for larger wrap angles. The study of spool position highlighted the "downstream impact" of friction since the friction applied to a segment of wire degrades the motion contribution for the remainder of the wire between the location of the friction load and the input tail. Furthermore, the observed/modeled behavior demonstrated an increased sensitivity to spool position for greater wrap angles, indicating that spool position becomes a greater consideration for actuator designs that call for larger amounts of packaging.

From the diameter ratio results, the findings suggest regions where additional losses due to bending occur. Using the full spooling model, approximate ranges of designs can be determined where the bending analysis should be used or where acceptable levels of loss occur. Regarding the accuracy of the spooling model in comparison to the friction-only prediction, for diameter ratios $\bar{D} > 100$ there is less than 2% deviation between the two predictions. In general, actuators designed with mandrels two orders of magnitude greater than the wire diameter can neglect the effect of bending in the model. Yet, the need for tighter packaging often requires lower diameter ratios when the constraints of the actuator's package footprint do not allow large mandrels. Since bending was shown to have an increasingly significant effect on the motion for diameter ratios below 100, the full spooling model accounting for friction and bending is recommended for the analysis or synthesis of spooled SMA wire actuator designs. In designing spooled actuators, the amount of motion lost to packaging is a design tradeoff that can be assessed on a case-by-case basis or analytically using an optimization approach. For example, if the losses due to bending are limited below 10%, the model indicates that a diameter ratio greater than 30-50 should be used. However, acceptable levels of loss will often depend on how much of a tradeoff exists with respect to the improvement to packaging, which can often be factored into an analytical design process or design optimization approach. Additionally, whereas friction losses have downstream effects on the performance of the wire, bending strains only affect the motion contribution locally where the wire is wrapped. Thus, for

longer wires with large portions of the length that are not wrapped, the losses due to bending become less significant.

In general, larger diameter mandrels are recommended when possible to reduce bending losses. Still, noting that very large mandrels can increase the area of the footprint, the diameter selection will typically be impacted by particular application specifications. Finally, while an analysis of material fatigue was beyond the scope of this study, smaller diameter ratios are recognized to precipitate functional and structural fatigue more rapidly by inducing higher maximum strains. However, rules of thumb for fatigue can be applied to spooled actuators based on the maximum strains, which occurs at the outer edge of the wrapped SMA wire. The results for maximum SMA strain generated for the study of diameter effects (Figure 3.6) were adapted to guide the selection of the applied stress and diameter ratio parameters according to the expected cyclic lifetime of an actuator (Figure 3.7).

In summary, a wide variety of parameters influence the design in interrelated ways, yet the models provide several key design guidelines that aid in the synthesis of high performance, compact spool-packaged SMA actuators. Wrap angle should be minimized

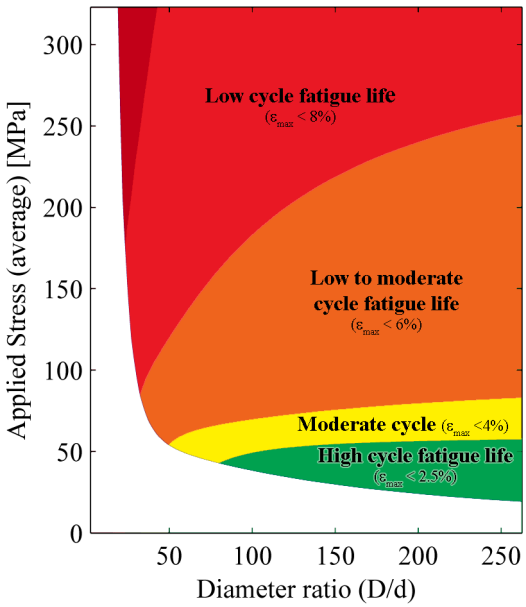

Figure 3.7. Graphical guidelines for selecting applied stress and diameter ratio according to fatigue life. Infeasibile combinations of applied stress and diameter ratio that cause compression in the SMA wire are excluded from the plot (shown in solid white).

within packaging constraints when possible to reduce losses, while noting that more wrapping leads to a more compact actuator. Wrapping beyond the binding angle contributes no additional motion to the system, and is thus not recommended. When possible, the mandrel should be placed as close to the input end of the SMA wire as possible to minimize the input tail length, which contributes less overall motion to the actuator, than the output tail length. To avoid excessive losses and early fatigue due to bending strains, the mandrel diameter should be selected to be as large as the package constraints allow. For mandrel to wire diameter ratio below 60, the binding strains cause the friction-only model to deviate from the full spooling model by more than 5%, at which point the use of the full model is recommended. For mandrel to wire diameter ratios below 50, the maximum strain peaks above 8% for the example actuator provided, which could precipitate premature fatigue for multi-cycle applications. These guidelines are presented as aids to a designer seeking a good, feasible design, but noting that the complexity of the design space and the weight of packaging versus performance objectives can alter the quality of the design for a given application.

3.2. Applied loading parameters

Whereas non-packaged SMA wires have constant stresses and strains across the length of the wire for a given state, spool-packaged actuators have stresses and strains that vary along the length, which makes the relationship between applied load and range of motion more complicated. This relationship between load and motion is explored as the SMA wrap angle is varied and as the bending strains become more prominent due to tighter wrap curvatures. Based on the behavior regarding the applied loading, guidelines are presented for designing actuators with deflections within an ideal range and predictable performance.

3.2.1. Effect of stress

To explore how the motion's functional dependence on applied stress is influenced by the packaging architecture, range of motion versus applied stress profiles were

generated with model-based simulations for variable wrap angles and confirmed with experimental data for a variety of wrap angles including binding and non-binding configurations (Figure 3.8). The motion versus applied stress relationship is further illustrated in surface plots, showing the dependence on wrap angle for both binding and non-binding configurations in Figure 3.9a and the dependence on the mandrel to SMA wire diameter ratio in Figure 3.9b. Throughout the simulations, the applied stresses are the result of quasi-statically applied dead loads.

The form of the motion vs. applied stress curves in Figure 3.8 (and for the motion vs. applied stress behavior for a constant wrap angle in Figure 3.9a) results from the strain difference between the martensite and austenite stress-strain curves at an applied load/stress. The range of motion has a higher sensitivity to stresses in the steep, vertical region of the motion-load curves (about 40 – 60 MPa), which corresponds to whether wire stresses are above or below the martensite stress plateau. However, as more wire is wrapped around the mandrel, the stresses and strains along the SMA wire vary due to friction losses. Considering the distributions of strains from the output tail to the input tail, friction causes strains to decrease for martensite SMA and to increase for austenite SMA. This behavior results from friction working against the motion of the SMA wire relative to the mandrel as it transitions between martensite and austenite. The strain

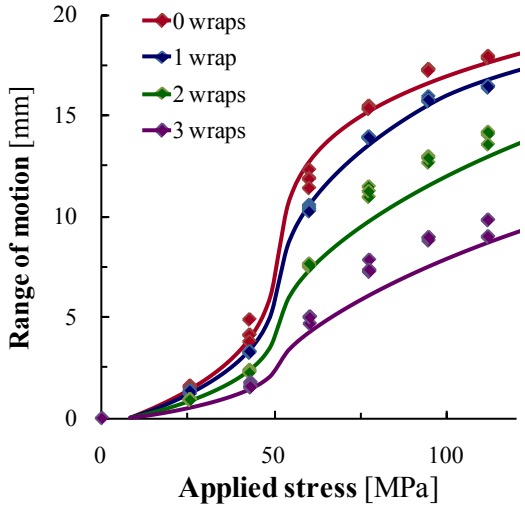

Figure 3.8. Experimental results for variable applied stress. The experimentally determined range of motion is shown with respect to the applied stress along with the theoretical prediction. All tests were performed for a 450 mm wire with a 10 mm input tail, 38 mm mandrel diameter, and the remaining length in the output tail. Data was collected using the experimental set-up and procedure described in Chapter 2.

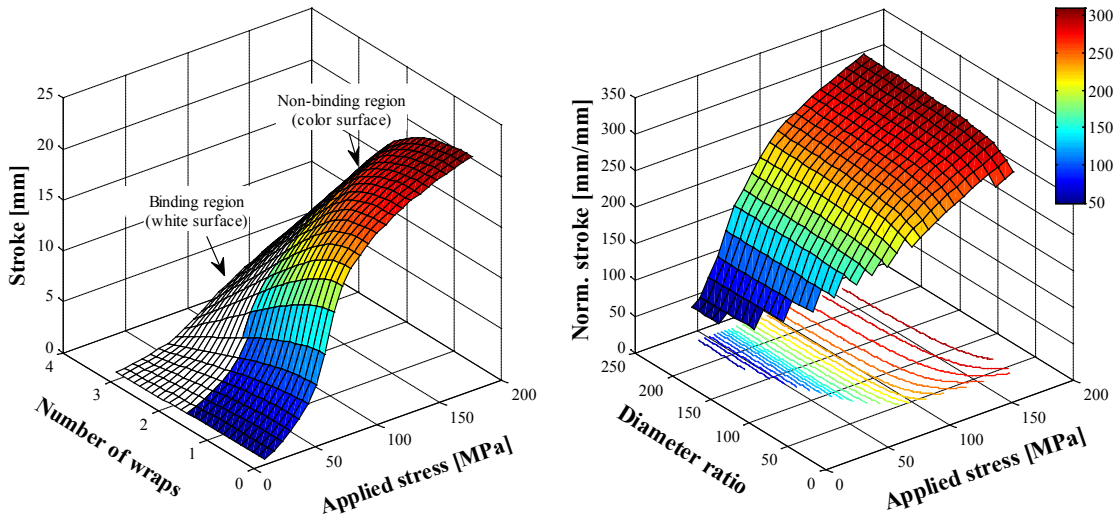

(a) Effect of wrap angle on applied stress behavior *(b) Effect of bending on applied stress behavior*

Figure 3.9. Effect of applied stress for variable actuator packaging. a) The effect of wrap angle and applied stress on the actuator range of motion is shown with non-binding designs in color and binding designs in white. b) Simulated results for normalized range of motion are shown for actuators with proportional dimensions (as described in Table 3.2) for varied applied stress and diameter ratios. Designs with regions of the wire in binding are omitted.

difference between the two states narrows for more friction and more wrapping, which degrades the actuator's overall range of motion. The distribution of strains on the SMA wire is represented by mapping the strain distribution of a wrapped SMA wire under a constant applied load in Figure 3.10, which demonstrates the narrowing of the martensite to austenite strain difference as more SMA wire is wrapped.

To design actuators with large ranges of motion, it is advantageous to apply loads that cause strains to be above the martensite plateau. However, because the strains are distributed, stresses must be selected that cause martensite strains to be sufficiently higher than the plateau so that a significant portion of the wrapped SMA wire also has martensite strains above the plateau. This issue is illustrated by examining the amount of friction loss in the wrapped SMA wire as a function of applied stress (Figure 3.11). Tracing the percent motion loss from the high end of the stress range toward lower stress, the losses increase gradually and become steeper approaching stresses of about 55 MPa from above. The steepening behavior results from more SMA wire having strains below the martensite plateau and contributing less to the overall motion of the actuator. For stresses near 55 MPa there is a peak in the amount of loss because, while the output tail

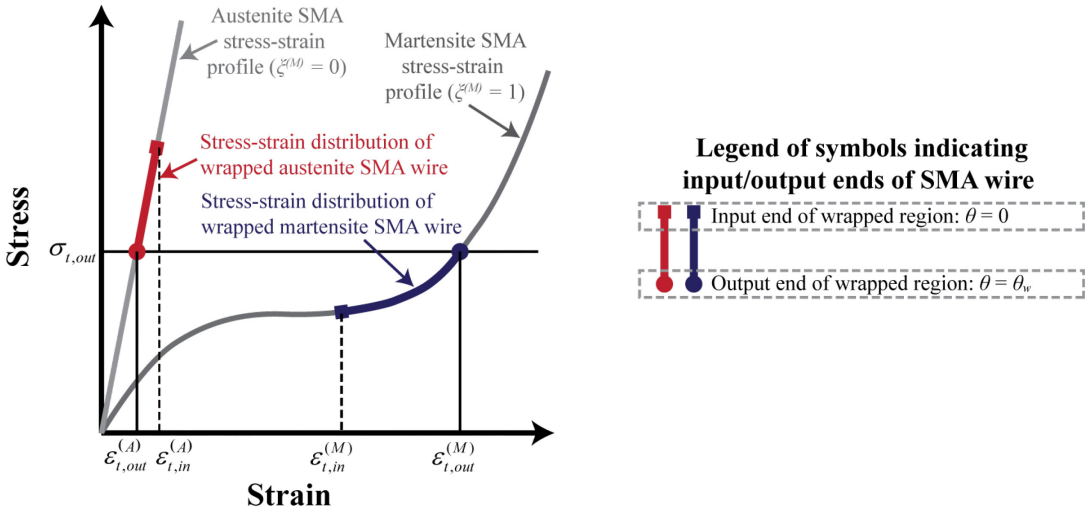

Figure 3.10. Stress and strain distribution along a wrapped SMA wire. As the SMA wire is wrapped, the difference between martensite and austenite strains narrows as the input tail strains approach each other.

strains are above the plateau, the majority of the wire has strains below the plateau. Based on the strain distribution in the SMA wire, it is more important to select an applied load sufficiently above the martensite plateau for spool-packaged SMA actuators than it is for non-packaged SMA wire actuators. For the examples considered in Figure 3.11, increasing the applied stress from 50 MPa to 100 MPa allows 21-25% for the friction losses to be avoided. Consequently, the motions can be increased by a factor of 2.3 – 3.3. However, as was indicated in the parameter study on mandrel diameter, higher loads can also cause SMA wire strains to be excessive leading to low cycle fatigue.

Considering the applied stress behavior with respect to bending (Figure 3.9b), the applied load behavior is not affected significantly by the bending strains for large diameter ratios. The additional strains that occur for tighter packaging at small bending ratios, however, begin to act as a loss on the system, depressing the range of motion vs. applied load curves as the diameter ratio decreases. The tightening diameter ratios shift the centroid strains, typically lower, to satisfy the equation relating the force resultant to the distribution of stresses across the SMA wire's cross-section (Equation 2.18). (This effect was also explored from a geometric point-of-view in the geometric parameters study examining the effect of mandrel diameter (Section 3.1.3).

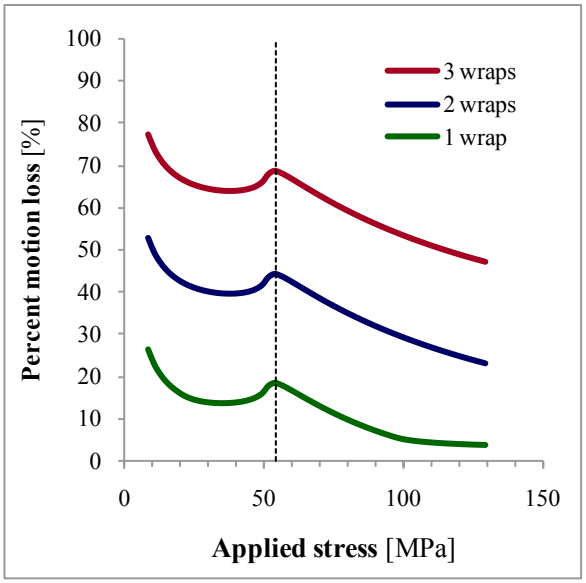

Figure 3.11. Dependence of friction loss on applied stress.

The applied load influences the binding limitation on how much wire can be packaged. The dependence of the binding angle on the applied load is shown in Figure 3.12 for a range of coefficients of friction. Since binding results from accumulation of friction preventing the wire from sliding, the larger binding angles are expected for lower coefficients of friction between the SMA wire and the mandrel. The binding angle is also noted to increase with the applied stress. The increase results from a larger strain difference at the output tails for the increased applied stress, and a consequently larger angle of wire that must be wrapped before the input tail strains become equal (thus satisfying the binding condition). Even so, the binding angle is much more sensitive to the coefficient of friction than applied stress: for a typical coefficient of friction $\mu = 0.1$, varying the applied load across its range (0 - 200 MPa) can cause up to a 20% variation in the binding angle from the mean, while halving the friction increases the binding angle by 200% and doubling the friction decreases the binding angle by 50%.

3.2.2. Design guidelines for applied load

The model-based observations regarding applied load indicate ranges where the applied load can generate the most motion, sensitivity of the motion-load relationship to the wrap angle and the mandrel to wire diameter ratio, and that the maximum amount of spooled-packaging available is influenced by applied load. Based on these observations,

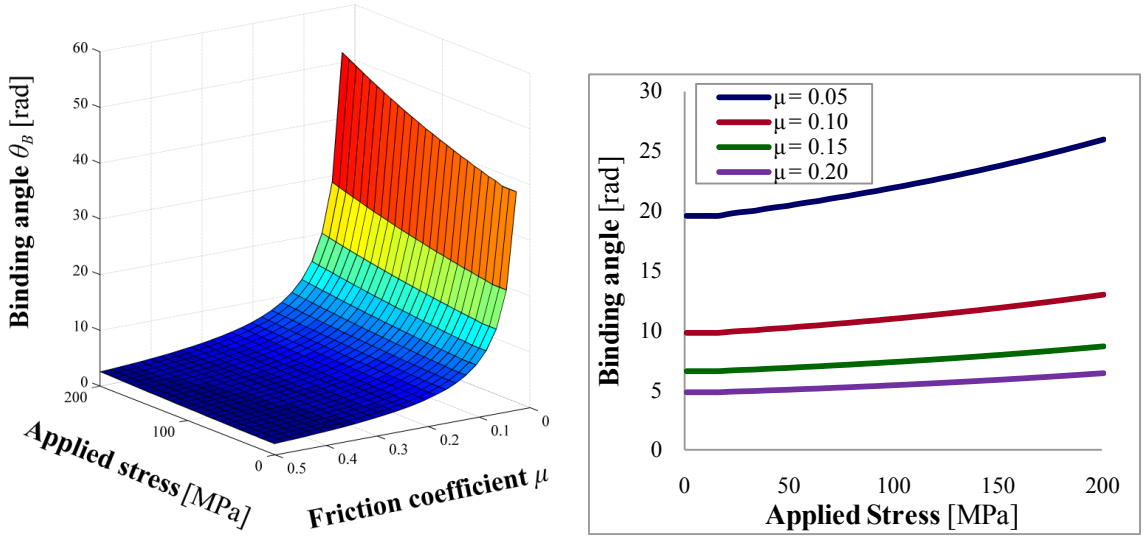

Figure 3.12. Effect of applied stress on the binding angle. The binding angle is calculated for a range of applied stresses from 1-300 MPa (binding cannot be evaluated for zero applied stress) and a range of typical coefficients of friction. Assumptions regarding other aspects of actuator geometry (such as tail lengths and mandrel diameter) were not necessary since the binding angle, as modeled, is functionally independent.

the following guidelines are suggested for selecting design parameters that can impact applied load such as the wire diameter or the number of SMA wires used.

Considering an SMA wire with similar constitutive material properties as in the applied load experiments (Figure 3.8), for example, the SMA wire diameter and number of SMA wires should be selected to yield an output tail stress above 80 MPa to take advantage of the larger strain recovery between states. At stresses beyond the steep vertical region, the range of motion is less sensitive to applied stress, which makes actuator behavior more robust. Furthermore, actuators designed with stresses above the vertical region more effectively exploit the large recoverable strains of SMA wire. Thus, they rely on shorter lengths of SMA wire and less electrical power to heat the wire. However, larger stresses can induce material fatigue more rapidly. The maximum strains that can reduce the fatigue life of spool-packaged actuators are also affected by the mandrel to SMA wire diameter ratio. Ranges of applied loads and diameter ratios that are appropriate for low, moderate, and high cycle actuator use are shown in Figure 3.7, which can be used as a guideline for determining appropriate ranges of actuator stress.

Additionally, the amount of packaging (quantitatively measured by the wrap angle) influences the range of motion with respect to applied stress. While the largest range of motion is available for a non-packaged actuator compared to a spool-packaged actuator of equal SMA wire length, spooled-packaging reduces the overall length of an actuator and can allow it to be customized to a greater range of form factors. For applications where binding limits the amount of wire that can be packaged, increasing applied load increases the binding angle, thus allowing more SMA wire to be packaged within a form factor.

3.3. Material parameters

The material parameters within the spooled SMA actuator system include the SMA-mandrel interfacial coefficient of friction and the parameters defining the SMA material constitutive laws. The material constitutive properties can be affected by a number of factors including alloy composition, actuation history, material processing techniques (including shakedown to condition the wire). In addition, the particular parameters regarding material laws are particular to the constitutive model selected since the different models employ a variety of parameters. Since constitutive law selection is a modeling decision, as opposed to a design decision, the material parameters are not examined within this parametric study. For the example of Flexinol wire, which is available in compositions targeted to 70°C and 90°C transformation temperatures, the choice of transformation temperature affects performance due to differences in constitutive behavior between the two alloy choices. In this study, measured performance characteristics for the 70°C wire were used, but the basic trends and insights discussed throughout this study for applied load, geometry, and friction still apply to 90°C wire, or other similarly behaving SMA materials even if they are not of the Flexinol brand.

In this section, the effect of the friction coefficient is examined with respect to performance and the binding limitation. Sensitivities that relate to the material selection regarding friction are considered, with discussion on how the friction coefficient can impact packaging and performance. Guidelines for selecting mandrel materials are also

presented, accounting for tradeoffs between performance and packaging, and other practical guidelines regarding heating method and consistency of performance.

3.3.1. Effect of friction

While spooled-packaging can improve the compactness and form factor of SMA wire actuators, friction between the SMA wire and the mandrel acts as a loss on the system and is the central, antagonizing factor causing the tradeoff between large motions and compact packaging. If friction were the only factor in the selection of the mandrel's surface material, a very low friction material such as a fluoropolymer (Teflon, for example) would always be recommended. Other factors such as cost, wear, consistency, electrical insulation, and strength are often part of the material selection process. Therefore, selection of materials based on friction alone is not always possible, and understanding the sensitivity of performance to friction can help guide material selection in light of these other factors.

To demonstrate how friction and packaging relate to the performance of spooled actuators, the motion for a range of actuator designs with varying friction coefficients and wrap angles is provided in Figure 3.13. The figure shown is for an example actuator with a 500 mm initial wire length, 25 mm diameter mandrel, and a variable length of the wire wrapped around the mandrel (up to 500 mm occurring at $\theta_w = 20$ rad).

For low wrap angles and low friction coefficients, friction does not make a significant impact on performance, and the packaged SMA wire behaves similarly to a linear wire. Increases to wrap angle or friction coefficient increase friction losses by narrowing the strain difference between the martensite and austenite states (as shown in Figure 3.10), which is responsible for the actuator's overall motion. Increasing the coefficient of friction for a constant wrap angle, there is a rapid decrease in the range of motion, especially for larger wrap angles. The rate of descent of the range of motion with respect to the friction coefficient depends on how much of the wire's stress and strain in the martensite phase is distributed on or below the martensite plateau, where the SMA wire is unable to contribute the same high levels of motion for stresses and strains above

the plateau. The form of the rapid drop off results from the shape of the martensite plateau: and since the motion (corresponding with strain) is the independent variable as shown on the vertical axis, the plateau acts as a vertical drop-off that is highly sensitive to the SMA wire's stress state.

The dependence of the binding angle on both the friction coefficient and applied load was noted in the discussion of applied load (Section 3.2.1, Figure 3.12). While the applied load was shown to affect the binding angle, the friction coefficient had a much greater impact on binding angle. This finding impacts packaging by affecting how much wire can be packaged prior to the binding limitation setting in, in addition to making an impact on the total amount of motion that a packaged actuator is capable of producing. In the binding region of the design space shown (Figure 3.13), the binding condition's functional dependence on both wrap angle and friction coefficient is evident from the three-dimensional path through the angle-friction-stroke space. While satisfying the binding condition depends on wrap angle, however, the binding angle is a function of only friction (for a constant applied load). For a given coefficient of friction, the decrease

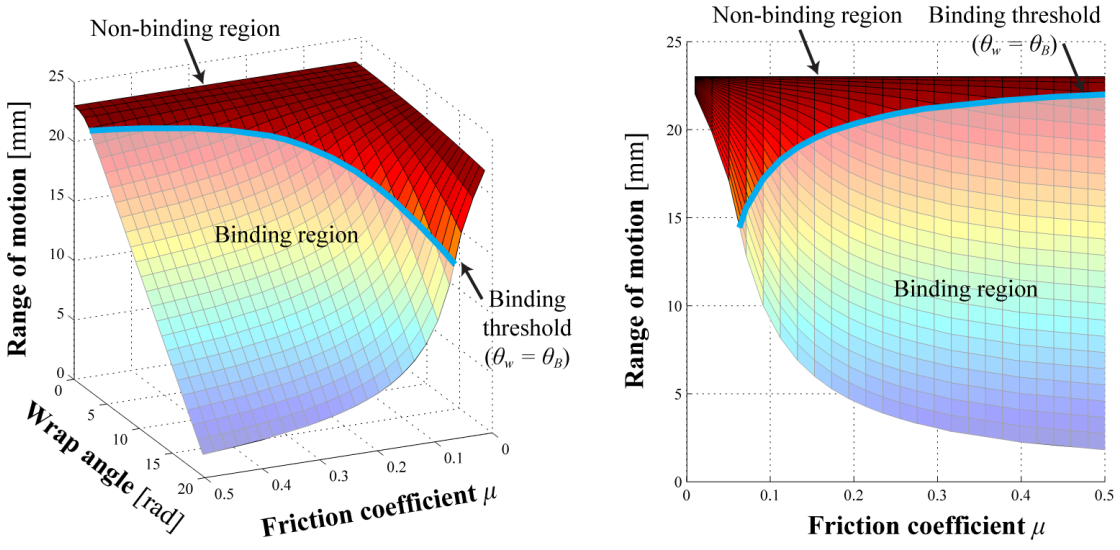

Figure 3.13. Effect of friction on spool-packaged SMA actuators. a) Three-dimensional view of range of motion surface with respect to wrap angle and friction coefficient. b) Two-dimensional view of range of motion with respect to friction coefficient; lateral gridlines in the 2-D figure indicate actuators with constant wrap angle. The range of motion was generated for a spool-packaged SMA wire actuator with a D = 25 mm mandrel diameter, $\ell_{tot}^{(0)} = 500$ mm initial SMA wire length, $F_{app} = 20$ N applied load, and $d_{SMA} = 0.38$ mm SMA wire diameter. The effect of bending was assumed negligible for the simulation. The threshold at which binding occurs was determined numerically, and is shown in the figure.

in motion with increasing wrap angle is linear because all additional wire that becomes wrapped around the mandrel will make no contribution to motion and the wrapped length that does contribute to motion is constant. For a given wrap angle, however, the motion decays non-linearly with increasing friction, even in the binding region. The non-linear decrease in motion with increasing friction results from two factors: 1) decreasing the binding angle as friction increases alters the amount of wrapped wire that contributes to the range of motion, and 2) the strain gap responsible for actuator motion narrows more quickly for the higher friction coefficients. While the range of motion at the binding condition increases with coefficient of friction (as shown by the binding threshold curve in Figure 3.13b), lower friction coefficients are still preferable. The form of the binding threshold, increasing with friction indicates that the onset of binding occurs for smaller wrap angles. For a constant wrap angle, the motion decreases monotonically with increasing friction coefficient.

3.3.2. Design guidelines for material selection

Friction, dissipative by nature, decreases the amount of motion that spooled actuators can provide with larger friction coefficients limiting how much the spool actuator can be packaged. Thus, if friction were the only factor in material selection, the choice of the lowest friction material is straightforward. However, additional factors including material cost, strength, consistency of friction properties, temperature range, and electrical insulating properties also impact material selection. While the coefficient can be evaluated quantitatively, additional qualitative factors are discussed for key categories of materials that can be used for the mandrel in spool-packaged SMA actuators.

Fluoropolymers such as Teflon (PTFE) offer some of the lowest friction coefficients available, typically with friction coefficients between Teflon and a metal specified near $\mu = 0.04$. Thus, Teflon can allow actuators with relatively large wrap angles and low friction losses. Additionally, fluoropolymers are excellent electrical insulators, which is important for resistive heating of the entire SMA wire without current skipping (and thus

not heating) any of the spooled portions. Fluoropolymers are very low yield strength, preventing their use as a structural element of many systems. To overcome the strength issue, a fluoropolymer sheath can be machined to shroud a stronger material such as steel to provide a member with high strength and low friction. Fluoropolymers work well for low loads and rapid heating, but if overheated, the wire may begin to cut into the mandrel, rather than sliding across it, decreasing reliability in some cases and increasing the cost due to maintenance. Additionally, without proper design for unexpected loads, the motion of the wire can potentially cut into the mandrel rather than slide. More expensive fluoropolymers than Teflon are available, including PFA (Perfluoroalkoxy fluorocarbon) or glass-filled PTFE, with better wear, strength, and temperature properties, that may be better suited to specific applications.

Harder and stronger plastics such as Garolite, PEEK, and Delrin have better wear and strength properties than fluoropolymers, but also have higher coefficients of friction. While the coefficient of friction is higher, the strength and wear resistance of the harder plastics is advantageous in comparison to fluoropolymers. Larger loads can be applied to the SMA wire without risking the wire cutting into the mandrel. Furthermore, the friction coefficient is much more consistent than for fluoropolymers, which have friction coefficients that are significantly more temperature dependent. In the experimental validation studies conducted in Chapters 2 and 3, Garolite was favored for testing over lower friction alternatives because of its temperature-consistent coefficient of friction and good wear resistance. Whereas consistency of friction was highly important for model validation purposes, it may not be as critical for certain applications and the choice of lower friction fluoropolymers may be acceptable. A broad range of polymers is available with various strengths, friction properties, and wear characteristics; selection relies on application requirements.

Metals, while a very broad class of many materials, have potential for use in spooled-packaging when the SMA wire is not heated electrically. Since metals are typically highly conductive, heating the wire electrically would allow current to skip

portions of the wire, causing portions of the wire not to be heated. Applications that heat the SMA wire based on conductive or convective heat transfer, however, can benefit from the high conductivity of metals. Diverting a high temperature fluid such as hot water or engine exhaust through a hollow mandrel could provide sufficient heat to enable phase transformation to austenite, and the conductive mandrel would aid in dissipation of heat for faster actuation frequency. In comparison to polymer-based mandrels, metals typically have higher strength properties allowing their use as structural members in addition to providing a medium for packaging the SMA wire actuator. The frictional properties between metals can vary widely, but surface treatments and lubricants intended to reduce friction can aid in their use in spool-packaged SMA actuators.

3.4. Impact of packaging

The spooling model and parametric study provide an understanding of the behavior of spool-packaged actuators based on mechanical principles and develop a more nuanced perspective of parameter dependencies and tradeoffs regarding performance, packaging, and cost. The results so far have provided explanation and analysis intended to support actuator design, but when faced with particular application requirements including stroke criteria and packaging constraints, the parameters can begin to interact in unexpected ways. To understand some of the issues that arise in the design process and how actuator packaging impacts design, the design space is explored for three example cases of spool-packaged actuator requirements and specifications: 1) a base case without explicit packaging constraints in which the compactness of the actuator is an issue, 2) a case in which the actuator is constrained to fit within a rectangular footprint, and 3) a case in which the actuator is constrained within a rectangular footprint with an internal obstacle that the SMA wire cannot intersect. The study demonstrates increasingly complex design spaces and motivates the need for systematic design approaches for spool-packaged actuators in general.

3.4.1. Example 1: Compact packaging

In the first example, the actuator design space is considered for a hypothetical application in which there are no particular packaging constraints, but a more compact actuator is desired to prevent unwieldy packaging dimensions. Defining the packaging dimensions in this example according to the smallest rectangular envelope that encloses the SMA wire (Figure 3.14), the package dimensions vary with the SMA wire length, wrap angle, and mandrel diameter. To quantify compactness, the footprint area ($A_{pack} = L_{pack} \cdot W_{pack}$) is not always a useful metric since multiplication of the package length and package width can lead to actuators having small footprint areas despite having problematic package dimensions. For example, while a non-spooled linear SMA wire has a long package length ($L_{pack} = \ell_{tot}^{(0)}$) making it difficult to use within tight form constraints, it still has a small area due to the very small package width, which is equal to the SMA wire diameter ($W_{pack} = d_{SMA}$). The package perimeter ($P_{pack} = 2(L_{pack} + W_{pack})$), however, represents a more useful measure of compactness since all the package dimensions are considered as a linear sum such that the most compact designs minimize all the package dimensions with equal weighting.

In the example case, actuator designs are generated to provide at least 15 mm of actuator displacement across a range of mandrel diameters (5 - 90 mm) and wrap angles (0 - 13.5 radians, where θ_B = 12.8 radians). The applied stress, SMA wire diameter, SMA stress-strain polynomials, and coefficient of friction are defined in the standard set of parameters (Table 3.1), and additional parameters and the range of variables are summarized in Table 3.3. For a given combination of wrap angle and mandrel diameter, the spooled portion contributes a portion of the required 15 mm of motion, which can be

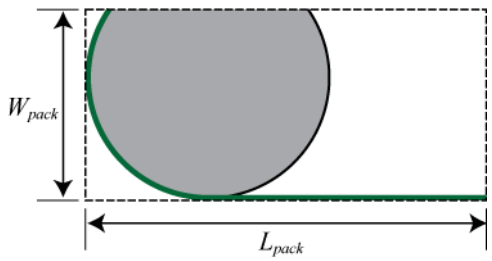

Figure 3.14. Package dimensions for single mandrel SMA actuator with no packaging constraints (Example 1).

Table 3.3. Parameters, variables for Example 1.

Required motion	δ_{spec}	$\geq$ 15 mm
Mandrel diameter	D	= 10 - 90 mm
Wrap angle	θ_w	= 0 - 13.5 rad (θ_B = 12.8 rad)
Input tail length	$\ell_{t,in}$	= 0 mm

calculated using the single mandrel spooling model. The remainder of the motion comes from the output tail portion, which is selected to meet the minimum motion requirement. Thus, for designs with small contributions to motion from the spooled portion, longer output tail lengths are necessary to meet the minimum actuator motion requirement.

The overall length of the resulting designs across the range of wrap angles and mandrel diameters is shown in Figure 3.15a, where longer lengths of SMA wire reflect increased material costs in order to meet the motion constraint. In general, the material costs increase with more packaging, which is achieved through larger mandrel diameters and wrap angles. The increasing material costs are a consequence of the bending and friction losses that accompany the packaging. Comparing the motion of the packaged actuator to the motion of a linear SMA wire with the same free length, the motion losses mount with increased packaging as shown in Figure 3.15b, with up to 40% motion loss before the binding condition sets in. The disadvantages regarding material and performance costs, however, are balanced by the improvements to form factors. In Figure 3.15c, the actuator's package perimeter is shown as a function of wrap angle and mandrel diameter, and the most compact forms result from larger wrap angles and mandrel diameters. While increasing the mandrel diameter increases the package width, the corresponding reduction in package length enables the more compact package perimeter. The increased compactness is further illustrated by the stroke per perimeter (Figure 3.15d), for which larger magnitudes indicate more performance for more compact packaging. The stroke per perimeter is greatest for wrap angles greater than or equal to the binding angle with the largest available mandrel diameter. However, selecting wrap angles greater than the binding angle increases material cost without any additional benefit to performance or packaging.

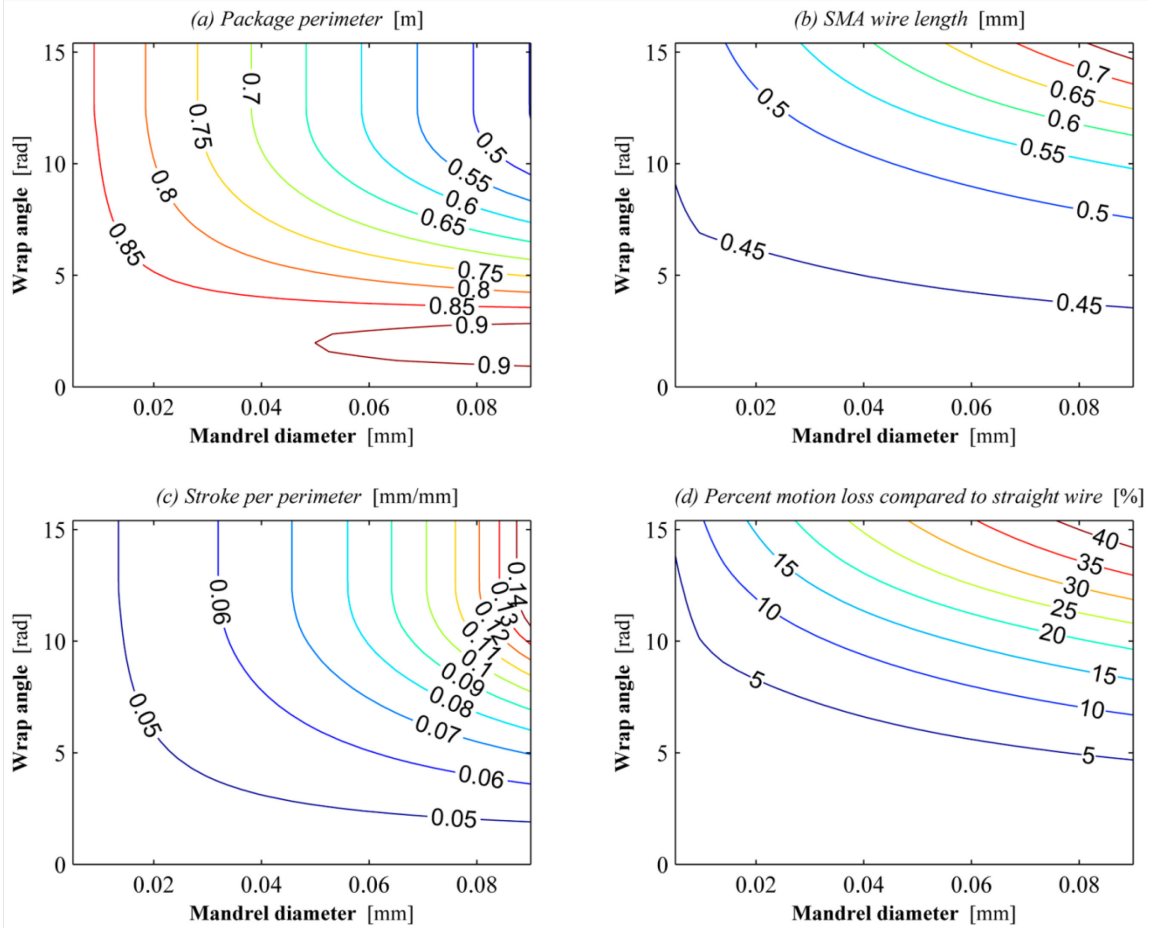

Figure 3.15. Package and performance metrics for SMA spool-packaged actuators with unconstrained packaging and a minimum range of motion requirement.

For single spool actuators without explicit packaging constraints, the packaging metrics and magnitudes of loss due to packaging are continuous, mostly monotonic, and well-behaved. In the example case there are clear tradeoffs between the actuator's compactness and materials costs to meet the fixed performance requirement, and the selection of a design depends on the relative importance of compact form and low material costs for a particular application.

3.4.2. Example 2: Convex packaging constraint

To observe how actuator design and performance is affected by the addition of packaging constraints, an example problem is considered in which the SMA actuator must be fully contained within a specified rectangular envelope. For this example, the package length L_{pack}, package width W_{pack}, and direction and location of output motion are specified as indicated in Figure 3.16. The input end of the wire is required to be

attached to the perimeter of the package envelope. The standard set of parameters is used (Table 3.1). The three design variables are mandrel diameter D, spool position within the package x_{sp} (defined as the horizontal distance between the mandrel center and the left edge of the package constraint: $x_{sp} = L_{pack} - \ell_{t,out}^{(0)}$), and wrap angle θ_w. The remaining geometric parameters ($\ell_{t,in}, \ell_{w,} \ell_{tot}^{(0)}$) are solved from the known geometry and package specifications, and the actuator range of motion was generated using the full spooling model (including friction and bending effects) for three mandrel diameters (D = 10, 30, and 60 mm) across the feasible range of spool positions ($\frac{1}{2} D \le x_{sp} \le (L_{pack} - \frac{1}{2} D)$) and wrap angles ($0 \le \theta_w \le \theta_B$). The resulting range of motion across the design space is shown in Figure 3.17a and the total SMA wire length across the same space is shown in Figure 3.17b. From a performance perspective, stroke maximization is desired, yet there is an additional material and energy cost for longer length SMA. An example multi-objective function that would be typical in optimization of this sort of problem is considered. The function takes this performance/packaging tradeoff into account in which the total SMA wire length $\ell_{tot}^{(0)}$ and the actuator range of motion δ are scaled and summed according to the equation:

$$f\left(\ell_{tot}^{(0)}, \delta\right) = 0.5 \cdot \frac{\ell_{tot}^{(0)}}{150 \text{ mm}} - 0.5 \cdot \frac{\delta}{15 \text{ mm}} \tag{3.1}$$

where the 0.5 coefficients represent equal weighting on each objective. The denominators scale the SMA wire length and range of motion to magnitudes of about 10^0. The example objective function (Equation 3.1) is calculated across the design space using the results from Figure 3.17a and b. The results are shown in Figure 3.17c, for which lower values of the objective are desirable. For each combination of the three example objectives (stroke maximization, SMA length minimization, and minimization of the multi-objective function) and the three mandrel diameters, the optimal value was determined as shown in Table 3.4. While these optimal values were determined by sampling across the two-dimensional cross-sections of the three-dimensional design space, the approach is computationally inefficient for finding optima and standard optimization approaches to similar problems are described in Chapter 5.

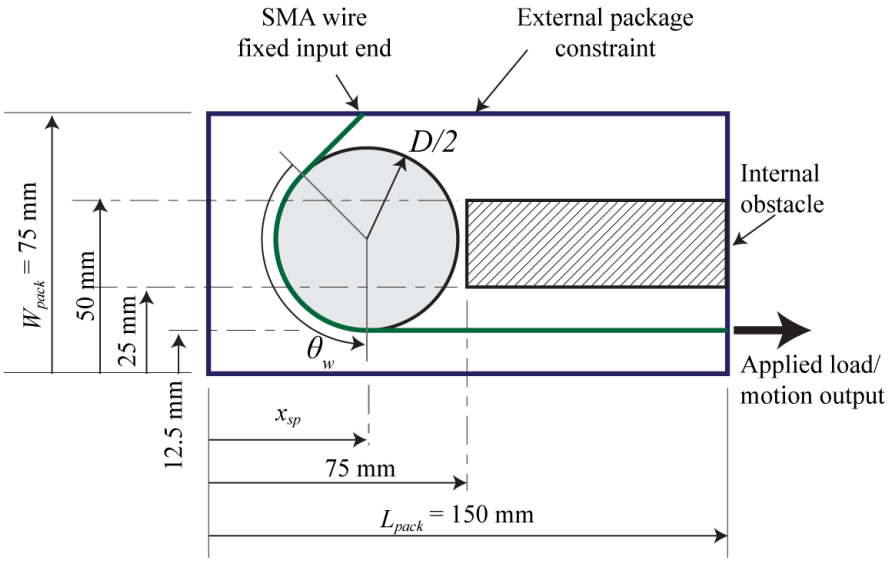

Figure 3.16. Diagram of package envelope and key dimensions for example packaging problems. The packaging problem for a spool-packaged actuator within an external package constraint considers the presence of an external obstical in example 3, while only the external package constraint is considered in example 2.

The range of motion with respect to wrap angle (Figure 3.17a), while typically increasing with wrap angle, also has a periodic characteristic due to geometric similarities among actuators with wrap angles 2π radians apart. Accordingly, there are multiple local maxima and minima within the design space. Reductions to the spool position x_{sp} correspond to increases of the output tail length $\ell_{tot}^{(0)}$, where the SMA wire's strain difference between martensite and austenite states is largest, thus making the largest local contribution to motion. Consequently, reductions in spool position tend to increase the actuator range of motion due to the increased output tail length. While the motion function is continuous across the range of design variables, the range of motion has sharp ridges representing designs in which the input end of the SMA wire is fixed in a corner of the packaging envelope. The ridged contour is a result of the input tail length being governed by the intersection of the wire and two different boundary constraints at the corners of the package envelope.

Noting the designs that produce the globally maximized motions for each mandrel diameter (displayed in Table 3.4), the spool position occurs at the minimum feasible value, $x_{sp} = D/2$, while the wrap angle varies. In each case, the maximum value occurs

near either 0.5 or 1.5 wraps placing the input end of the SMA wire on the right-hand side of the package envelope to maximize the input tail length.

By including SMA wire length in the objective (as in the example objective function, Equation 3.1), an engineer can synthesize actuator designs with high performance and reduced material and energy use. The contour of the total SMA wire length across the feasible design space is shown in Figure 3.17b, which can be viewed as an indirect representation of material and energy costs associated with an actuator's design. Globally, the SMA length can be minimized by decreasing wrap angle and increasing spool position, but the contour is non-linear with periodic behavior as wrap angle is varied. In general, the total SMA length is decreased as the spool position is increased due to the lengthening of the output tail. However, for wrap angles that are multiples of 2π radians ($\theta_w = n \cdot 2\pi$ for $n \in \{0,1,2,...\}$), the SMA wire length is not sensitive to spool position since increases to the spool position in this special case cause an increase to the input tail length that is equal to the decrease in the output tail length. As in the range of motion contours, the ridges on the SMA wire length contour correspond to the input end of the SMA wire positioned at corners of the package envelope.

Considering the stroke maximization and the SMA wire length minimization objectives together according to the example multi-objective formula (Eq. 3.1), Figure 3.17c shows the objective function for which smaller magnitudes of the objective are desirable. The objective function is influenced by the range of motion and SMA wire length factors, producing a non-linearly contoured surface with multiple local minima. In general, the objective function is reduced by decreasing the wrap angle and spool position; however, the global optima cannot be determined by these trends alone due to the multiple local extrema. Sampling across the entire design space for each mandrel diameter, the optimal designs were determined for three example objective functions (stroke maximization, SMA wire length minimization, and minimization of the multi-objective function defined in Eq. 3.1), which are shown in Table 3.4. To illustrate the potential advantages of considering the motion and SMA length, two optimal designs are

considered: 1) the actuator design that yields the greatest stroke (D, x_{sp}, θ_w) = (60 mm, 30 mm, 9.4 rad), and 2) the design yielding the lowest value of the multi-objective function (D, x_{sp}, θ_w) = (60 mm, 30 mm, 3.68 rad). By considering the stroke and length objectives together rather than the stroke objective alone, the stroke is reduced by 17% (from 17.5 mm to 14.6 mm) and the SMA length is reduced by 49%. Thus, the percent improvement to SMA length is greater than the related motion loss. Still, particular application specifications would guide such decisions related to packaging and performance. The case study demonstrates a multi-faceted relationship between performance, packaging, and the design variables for the non-convex form constraint and additional variation to optimality based on the relative importance of the different design objectives. Due to this complexity, systematic design approaches are recommended for customizing spool-packaged actuators with high, tailorable performance and mitigated cost.

Table 3.4. Optimal designs for three example objective functions and three mandrel diameters.

Example 2: external constraint, no obstacle

Mandrel diameter	max stroke (x_c, θ_w)	min length (x_c, θ_w)	min objective value (x_c, θ_w)
D = 10 mm	13.2 mm (5 mm, 2.84 rad)	25.7 mm (145 mm, 3.15 rad)	-0.126 (5 mm, 2.84 rad)
D = 30 mm	13.8 mm (15 mm, 9.19 rad)	77.1 mm (135 mm, 3.15 rad)	-0.131 (15 mm, 2.94 rad)
D = 60 mm	17.5 mm (30 mm, 9.40)	110 mm (120 mm, 1.58 rad)	-0.136 (30 mm, 3.68 rad)

Example 3: external constraint with internal obstacle

Mandrel diameter	max stroke (x_c, θ_w)	min length (x_c, θ_w)	min objective value (x_c, θ_w)
D = 10 mm	12.8 mm (5 mm, 3.15 rad)	25.7 mm (145 mm, 3.15 rad)	-0.121 (5 mm, 2.73 rad)
D = 30 mm	13.8 mm (15 mm, 9.19 rad)	131 mm (89.7 mm, 1.58 rad)	-0.131 (15 mm, 2.94 rad)
D = 60 mm	17.5 mm (30 mm, 9.40)	131 mm (98.9 mm, 1.58 rad)	-0.135 (30 mm, 3.15 rad)

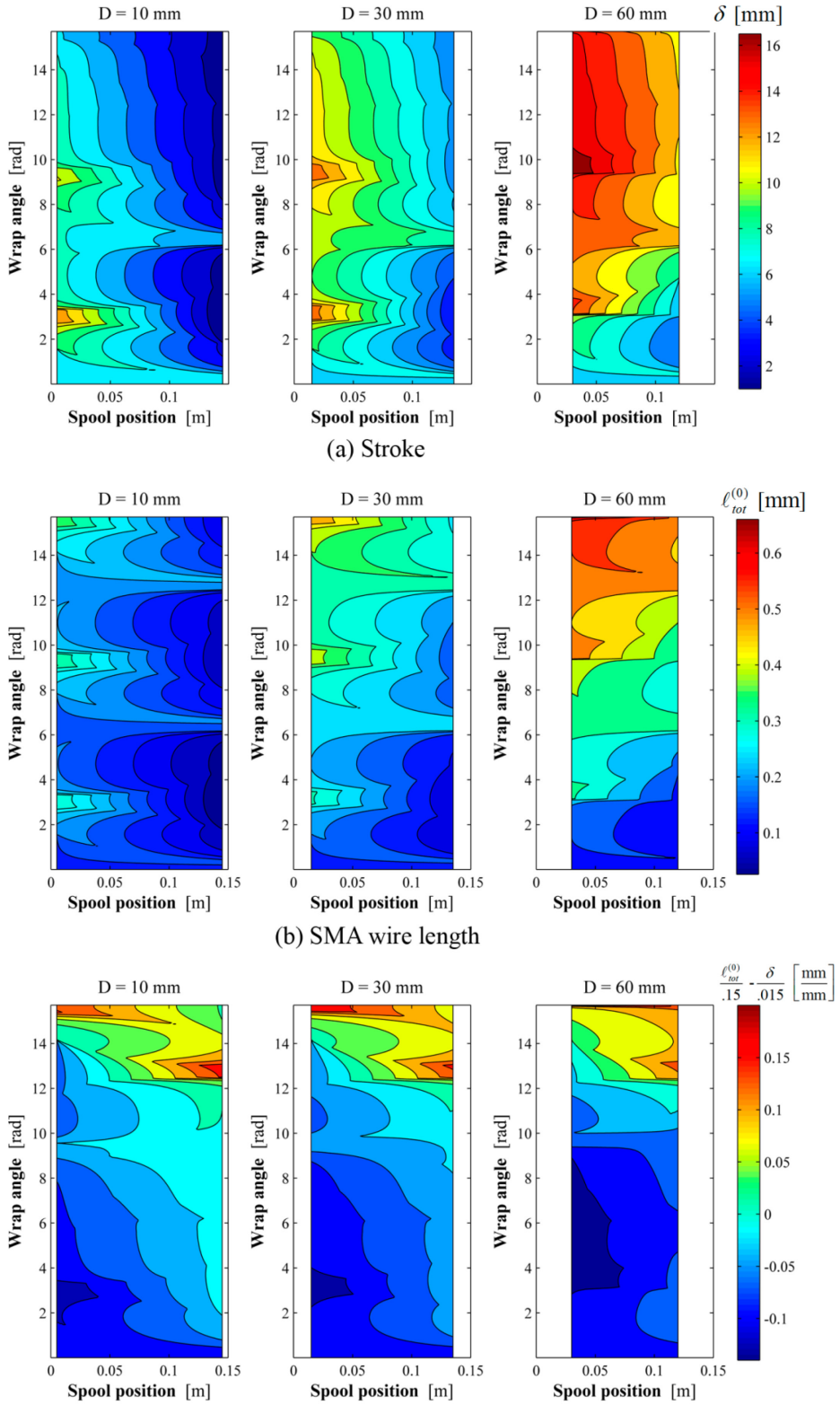

Figure 3.17. Design space visualization for spooled SMA actuators with an external packaging constraint (example 2). The results are shown for three different mandrel diameters across the feasible spool position and wrap angle design space.

3.4.3. Example 3: Non-convex packaging constraint

Adding another layer of complexity to the design of spool-packaged SMA wire actuators, the packaging envelope can also be irregularly shaped or have internal obstacles where the SMA wire cannot be packaged. An example of a rectangular package envelope with an internal exclusion where the SMA wire cannot be packaged is shown in Figure 3.16. The actuator is required to be packaged entirely within a package envelope of the same external dimensions as in Example 2; additionally, the SMA wire may not intersect with the exclusion. In this example, the perimeter of the mandrel is allowed to intersect with the exclusion (for instance, if the mandrel was cut away where it overlaps with the exclusion), although particular applications can also require that neither the mandrel nor the wire intersect with the exclusion.

Generating the range of motion, wire length, and same multi-objective function as in the previous example, the magnitudes and dependencies of motion and length are identical, but the boundaries of the feasible space are different due to the presence of obstacles (Figure 3.18). As a result, large portions of the feasible design space from the previous example are infeasible with the obstacle, and the design space is discontinuous. Since the larger mandrels are more likely to intersect with the obstacle across the range of wrap angles and spool position, the feasible design space for the larger mandrel cases is narrower. Since the mandrel is allowed to intersect the obstacle but the SMA wire is not (as defined in this example), the range of spool positions is greater for half a wrap (less than π radians) because the portion of the mandrel that intersect the obstacle is not wrapped. Due to the complexity of the design space and the additional discontinuities that result when non-convexities are added to the packaging constraint, actuator design metrics are often influenced by multiple interacting parameters, packaging constraints, and performance needs. As a result, analytical design approaches including optimization can be instrumental in selecting quality designs for high performance, low-cost, and form-customized SMA actuators.

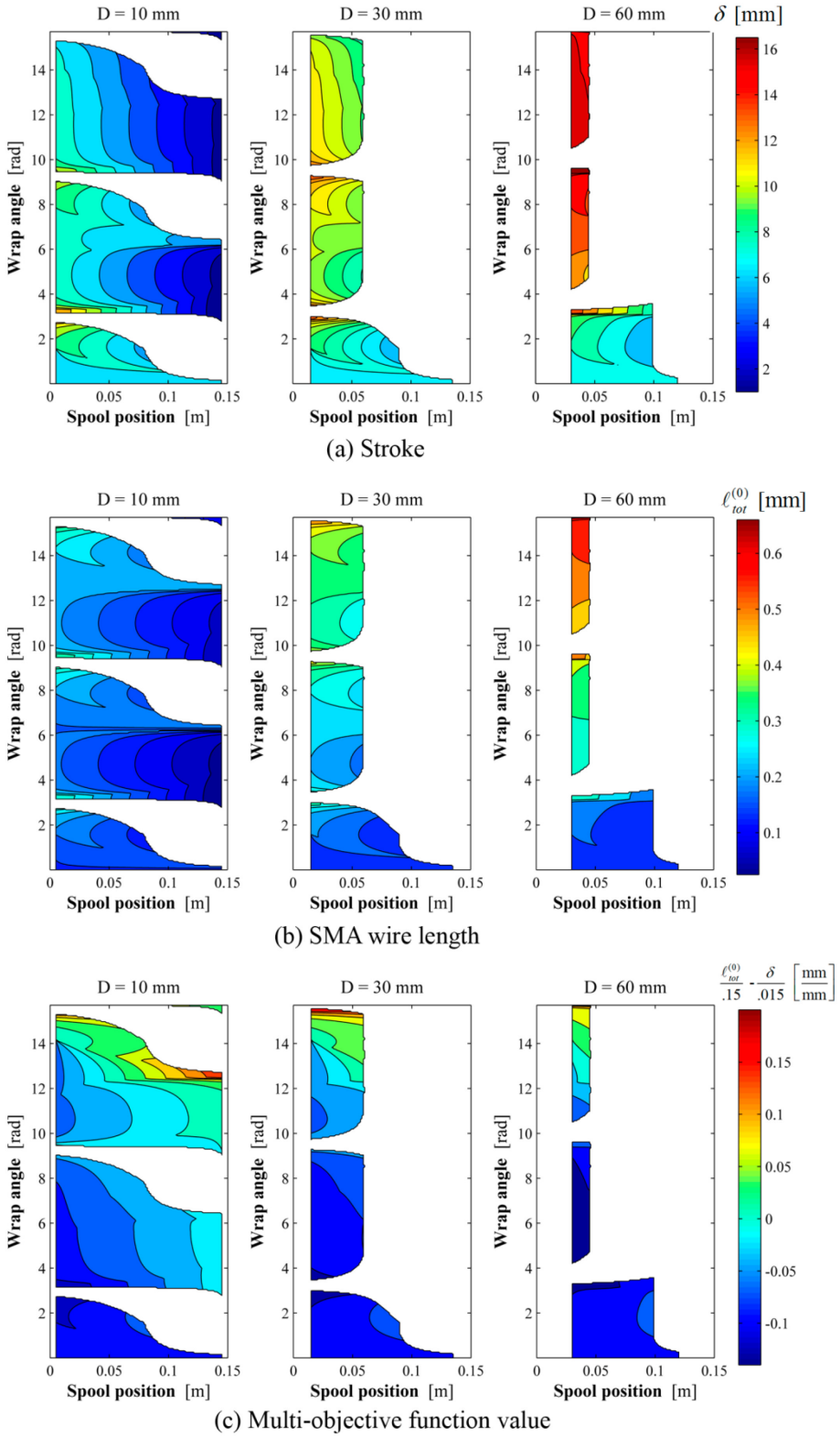

Figure 3.18. Design space visualization for spooled actuators with external form constraint and internal obstacle (Example 3).

3.5. Conclusions

While spool-packaged SMA wire actuators can be customized with great flexibility to suit a wide range of performance, packaging, and cost requirements, the multiple dimensions of tailorability also make the design problem more complex. This chapter addressed these complexities through a series of parameter studies using the single mandrel model derived in Chapter 2 and select experimental studies. The results of the parameter studies provided a more rigorous, scientific knowledge base that can lead engineers to a deeper understanding of how spooled actuators are affected by their design and packaging requirements. With this knowledge and understanding, this chapter provides the background for guiding engineers toward meaningful design decisions, understanding the behaviors of physical prototypes, and skillfully revising existing designs.

The effects of multiple geometric parameters were examined including wrap angle, spool position, and the mandrel to SMA wire diameter ratio. The wrap angle effect was approached for designs with constant package lengths and constant SMA wire lengths. For spooled actuators with constant package lengths, spooling additional wire was able to significantly increase the amount of motion within an available space. For a moderate friction coefficient ($\mu = 0.1$), package strains up to 20% were demonstrated whereas non-packaged SMA wires occupying the same package length could only achieve 4.6% strain. However, the packaging technique cannot be applied without limit due to the accumulation of friction, which leads to the onset of binding. The wrap angle was also considered for SMA actuators with constant lengths of SMA wire, demonstrating the tradeoff between packaging and performance. Significant reductions in package length were demonstrated, but at the expense of motion. In the examples shown, values up to 140 mm in package length reduction were shown representing up to 70% reductions in package length with the tradeoff of 15-30% of the non-packaged SMA wire's motion. The spool position study demonstrated the downstream effects of friction and led to guidelines to place the mandrel closely to the input as possible. While this guideline was

developed for single mandrel actuators, the knowledge of downstream friction effects can be extended to multiple mandrel actuator design where it is also advantageous to select spool topologies that limit downstream friction losses as much as possible. The effect of bending was investigated by examining the performance of actuators with different mandrel to SMA wire diameter ratios. The study demonstrated that bending strains tend to degrade the range of motion in the typical useful range of SMA actuator designs. For large diameter ratios, the losses due to bending are limited, but for diameter ratios below 60, deviations between the full spooling model and the friction-only model become greater than 5%. By examining bending, the maximum strain as it varies with load and diameter ratio was approached. The model-based prediction for maximum strain led to a graphically illustrated regions where applied load and diameter ratios lead to low, moderate, and high cycle actuator lifetimes. The guidance developed for selecting mandrel diameter is important for avoiding premature fatigue failure. The results in the study of geometric parameters demonstrated that spooled-packaging can be used to improve the form factors of actuators with reasonable costs that can be mitigated through educated design choices.

The applied stress in the wire also has important impacts on performance, which is more complicated than for the non-packaged case due to distributions in strain along the wire. An understanding was provided for how distributions in strain along the SMA wire are related to performance for different applied loads, showing the advantages of designing actuators with stresses that cause strains to be higher than the martensite plateau. Actuators with strains barely higher than the martensite plateau are subject to higher losses than actuators with strains significantly higher than the plateau due to the distribution of strains on the martensite curve. Building upon the explanation provided in this chapter for how performance is influenced the distribution of strains along the martensite stress-strain curve, an engineer can better understand why a spool-packaged actuator prototype behaves differently than expected.

The study of friction demonstrated the critical importance of material selection in the design process. The performance is highly dependent on the coefficient of friction. The amount of spooled-packaging that can be employed prior to the onset of binding was also demonstrated to be governed by the friction coefficient. While low-friction is typically desirable for spool-packaged actuators, common practical tradeoffs of using low-friction materials were noted such as higher expense, highly temperature dependent friction properties, and the potential to damage the surface by overheating the SMA wire. A discussion of alternative materials was also provided evaluating their practicality in different scenarios and their effects on performance, cost, and packaging.

The impact of packaging on performance was explored by examining the design space for example actuators with three different types of packaging. In the first case, actuators were explored with variable wrap angles and mandrel diameters for which there were no particular form constraints, but more compact actuation was desirable. Without the presence of packaging constraints, the design space was continuous, mostly monotonic, and well behaved with the design variables. In fact, the design guidelines were consistent with the simulated behavior for which more compact packaging was available by wrapping longer lengths of wire and higher performance was available by wrapping less wire. In the second case, the actuator was required to be enclosed within a specified external envelope. Due to interacting packaging and geometry, the performance with respect to the design variables was not straightforward. Increasing the wrap angle, for example, had a periodic effect on the performance and the design space in general had multiple local minima and maxima. In the third case, the introduction of an internal obstacle made the feasible space discontinuous with respect to the design variables, in addition to having the irregular contour from Case 2.

The parameter studies give insight into how spooled actuator behavior is affect by design choices. For simple packaging problems, the design guidelines can help with parameter selection or adjusting existing designs. However, the addition of packaging constraints to the problem makes for an irregular design space that cannot be easily

manipulated through model adjustments. Thus, a framework for design that helps manage tradeoffs between performance, packaging, and cost is developed and demonstrated in Chapter 5.

Chapter 4. Multiple Mandrel Spooling Model

SMA actuators have potential to meet the growing need for high performance and low cost actuation, but they have been limited by the difficulty in packaging within practical form factors. Single mandrel spool-packaged actuators begin to address these needs by enabling more compact form factors, but there are additional applications that also need the packaging to be more customizable. Often products that can benefit from actuator functionality have empty spaces where an actuator could be placed, but they are small and irregularly shaped making it difficult for conventional actuator technologies to suffice. The literature is replete with examples of applications where an actuator needs to fit within pre-existing form constraints including jet engine inlets (Sanders, et al., 2004) and chevrons (Calkins, et al., 2006), rotor blades (Epps & Chopra, 2001), fixed wings (Kudva, 2004), wind turbine blades (Barlas & van Kuik, 2007), a car's engine compartment, dashboard, handgrips, and swing panels (Brei, et al., 2007; Browne, et al., 2004), and handheld, implantable, or orthotic devices for biomedical applications (Kim, et al., 2005; Pathak, et al., 2009; Utter, et al., 2009; Wang & Shahinpoor, 1998). In each of these examples, packaging the actuator within the limited available spaces was a challenge, and motivated the use of energy dense smart materials actuators. Still, the ability to provide high performance actuation within limited or complicated spaces is not straightforward, and a greater ability to customize actuator form factors to difficult packaging constraints would enable actuation functionality in a broadened range of applications.

To meet the needs for more customizable actuation, the single mandrel actuator architecture can be expanded to multiple mandrels architectures that redirect SMA wires along non-linear pathways. The use of multiple mandrels allows pathways to be specific to the needs and allowances of particular applications. However, to analyze and synthesize multiple mandrel architectures, the single mandrel model needs to be

expanded to the multiple mandrel case. The single mandrel model begins to address the lack of models for spool-packaged SMA behavior by using a more rigorous, analytical approach that can be applied to a broad range of single mandrel actuators. However, for the multiple mandrel case to be developed at the same level of rigor, the cumulative effect of wrapping across multiple mandrels needs to be incorporated into the current understanding of friction, bending, and binding, and the ability to describe a wider range of topologies with variable numbers of mandrels needs to be included.

This chapter provides a framework for specifying a broad range of actuator topologies that enable form customization, and expands upon the mechanics of single mandrel actuators to develop a predictive model for multiple mandrel configurations. The generalized architecture was designed to enable the specification of a large range of spooled actuator topologies with additional specifiable parameters regarding geometry, load, friction, and SMA constitutive properties. The multiple mandrel model is derived based on the friction, bending, and binding effects that were developed in the single mandrel case, but also considers the cumulative effect of wrapping between adjacent segments of SMA wire. To validate the expanded model, an experimental study was conducted on a variety of multiple mandrel actuators including binding and non-binding configurations.

4.1. Generalized architecture

For spool-packaged SMA wire actuators to be customized to an expansive range of potential packaging constraints, a generalized architecture is defined that can account for any pathway composed of a series of linear and arc-shaped segments. The generalized actuator comprises four key components: 1) a single SMA wire in tension, 2) a fixed input where the SMA wire attaches to a referenced ground, 3) n cylindrical mandrels $(n \geq 1)$ fixed to the referenced ground, and 4) a rotational or linear single degree-of-freedom motion output. The basic architecture, nomenclature, and numbering conventions of a general n mandrel SMA wire actuator with a linear output motion are shown in Figure 4.1. The same architecture and numbering applies to the rotational case,

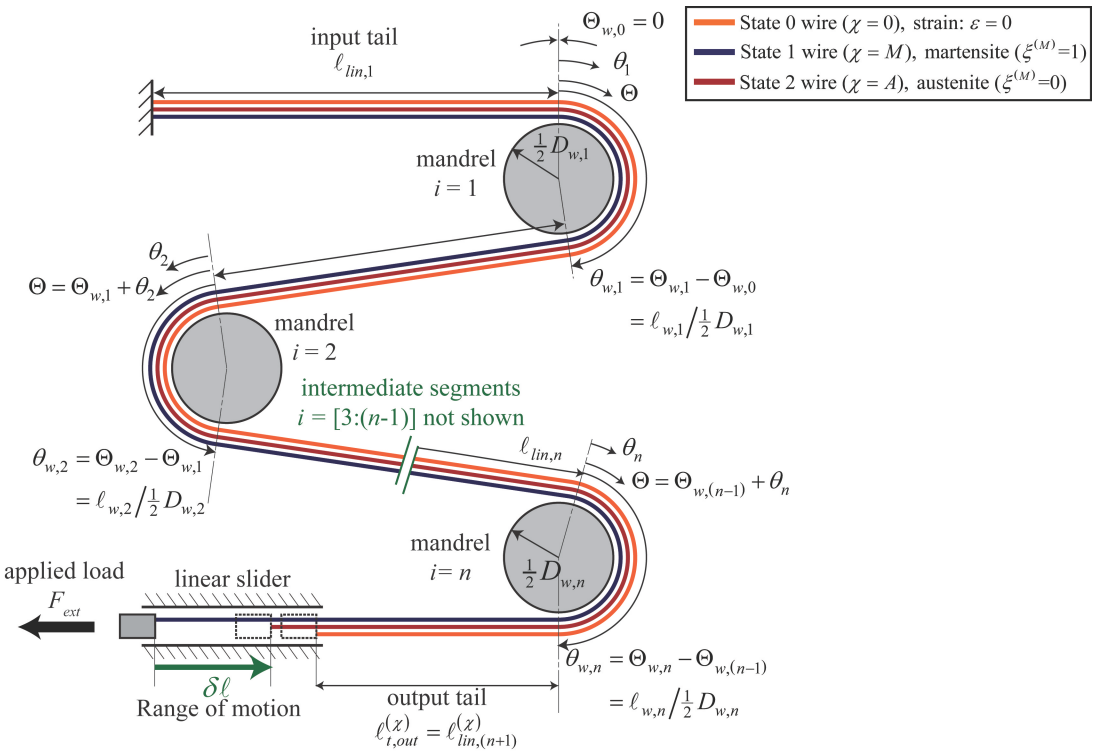

Figure 4.1. Generalized multiple mandrel architecture for spool-packaged SMA wire actuators with linear output motion. The multiple mandrel architecture enables the design and analysis of a wide range of spool-packaged architectures by varying the topology (number and position of mandrels), geometry (SMA wire length, mandrel dimensions, and wrap angles), and type of output motion (linear or rotational).

but with a rotating boundary constraint alternatively placed on the output end of the SMA wire. The actuator's operation cycle is the same as in the single mandrel case in Chapter 2 with a zero-strain reference state (*State 0*), and the fully transformed martensite and austenite states (*States 1* and *2*), which the actuator cycles between in typical operation.

The overall motion depends on the accumulated strain deformation of each wrapped and linear SMA wire segment. To model and describe the mechanics for each segment of SMA wire and to accommodate variable numbers of mandrels, the geometric parameters are defined using an indexing convention for a spool-packaged actuator with n mandrels. The SMA wire is composed of $(2n+1)$ regions with $(n+1)$ linear segments and n wrapped segments. Like the single mandrel case, the linear segment attached to the fixed input (i = 1) is referred to as the "input tail", and the linear segment attached to the movable output (i=n+1) is named the "output tail". Lengths of the first n linear segments are indicated with the variable $\ell_{lin,i}^{(\chi)}$, and the output length is indicated with the variable

$\ell_{t,out}^{(\chi)}$. As in the single mandrel case, superscripts indicate operation state but may be omitted if the variable does not change between states. Thus, for a linear actuator only the output tail $\ell_{t,out}^{(\chi)}$ requires the superscript and for a rotational actuator, only variables regarding the n^{th} wrapped segment ($\theta_{w,n}^{(\chi)}, \Theta_{w,n}^{(\chi)}$, and $\ell_{w,n}^{(\chi)}$) require the superscript.

One of the key differences between the single and multiple mandrel cases is the use of cumulative wrap angle and angular position variables. As was demonstrated in the parameter study of spool position (Section 3.1.2), friction has "downstream effects" since it influences the change in strain between states for regions of the SMA wire where friction does not act. These downstream effects extend to adjacent wrapped and linear regions, and thus need to be accounted for using cumulative variables. The angular position on the i^{th} mandrel is indicated using the variable θ_i and the total wrap angle on the i^{th} mandrel is $\theta_{w,i}$. The *cumulative angular position* Θ of the SMA wire on the j^{th} mandrel $(1 \le j \le n)$ is measured from the running-on point of the first mandrel ($i=1$) such that

$$\Theta = \sum_{i=1}^{j-1} \left(\theta_{w,i} \right) + \theta_j \tag{4.1}$$

For the j^{th} mandrel, the wrap angle is $\theta_{w,j}$ and the *cumulative wrap angle* is

$$\Theta_{w,j} = \sum_{i=1}^{j} \theta_{w,i} \tag{4.2}$$

The total SMA free length $\ell_{tot}^{(0)}$ is defined as a summation of the alternating linear and wrapped segments such that

$$\ell_{tot}^{(0)} = \sum_{i=1}^{n} \left(\ell_{lin,i}^{(0)} + \ell_{w,i}^{(0)} \right) + \ell_{t,out}^{(0)} \tag{4.3}$$

where $\ell_{lin,i}^{(0)}$ is the length of the i^{th} linear segment, $\ell_{w,i}^{(0)}$ is the length of the i^{th} wrapped segment, and $\ell_{out}^{(0)}$ is the length of the output linear segment. Since the wrapped segments are commonly defined according to their angle rather than length, the total free length (Eq. 4.3) can alternatively be defined as

$$\ell_{tot}^{(0)} = \sum_{i=1}^{n} \left(\ell_{lin,i}^{(0)} + \tfrac{1}{2} D_{w,i} \cdot \theta_{w,i}^{(0)} \right) + \ell_{out}^{(0)} \tag{4.4}$$

where $D_{w,i}$ is the mean diameter (sum of mandrel and SMA wire diameters) of the i^{th} wrapped segment and $\theta_{w,i}^{(0)}$ is the wrap angle of contact of the i^{th} wrapped segment.

As with the single mandrel case, the overall change in the SMA wire length as the wire is heated and cooled results in translational output motion $\delta\ell$ for linear motion actuators and in rotational output motion $\delta\phi$ for rotational motion actuators. The output motion results from the change in the total SMA wire length between *States 1* and *2* such that

$$\delta\ell = \ell_{tot}^{(M)} - \ell_{tot}^{(A)} = \ell_{t,out}^{(M)} - \ell_{t,out}^{(A)} \tag{4.4}$$

for linear actuators, and

$$\delta\phi = \frac{\ell_{tot}^{(M)} - \ell_{tot}^{(A)}}{\frac{1}{2}D_{w,n}} = \theta_{w,n}^{(M)} - \theta_{w,n}^{(A)} \tag{4.4}$$

for rotational actuators.

4.2. Analytical model

The derivation of the range of motion for multiple mandrel actuators considers the same key effects of friction, bending, and binding, which were developed and demonstrated for single mandrel spool-packaged actuators. However, the full multiple mandrel model also needs to predict the effect of cumulative wrapping on adjacent mandrels and to formulate the strain variation function for actuators with variable numbers of wrapped and linear segments.

4.2.1. Friction losses

The friction is modeled by considering the same differential element of SMA wire sliding on a mandrel as in the single mandrel case (Figure 2.2), except using the cumulative angular variables. Whereas the single mandrel case had a single region of wrapped SMA wire, the multiple mandrel case has alternating wrapped and linear segments of wire. Since the strain variation only occurs in the wrapped segments, the cumulative wrap angle, rather than the local wrap angle, is used to track variations due to friction. Based on the assumptions of static Coulomb friction and unilateral motion, a

similar derivation as in the single mandrel case leads to the equation for the *State* χ tensile force resultant as a function of the cumulative wrap angle:

$$F_{\theta\theta}^{(\chi)}\{\Theta\} = F_{ext}e^{\pm\mu\left(\Theta-\Theta_{w,n}^{(\chi)}\right)}, \tag{4.5}$$

where $\Theta_{w,n}^{(\chi)}$ is the total cumulative wrap angle of the SMA wire.

4.2.2. Bending strains

The bending strain affects the SMA wire strain locally, altering the centroid strain based on the nominal tensile stress and the wrap diameter. Thus, the average strain in the SMA wire due to tensile stress and geometrically-induced bending relies on the same derivation as in the single mandrel case. Applying the multiple mandrel indices to the single mandrel model, the equation for the tensile force resultant is

$$F_{\theta\theta} = \sigma_{t,out}A_{SMA}e^{\pm\mu\left(\Theta-\Theta_{w,n}^{(\chi)}\right)} = \iint_{A_{SMA}} f_{SMA}^{-1}\{\varepsilon_{ctd} + y/(\tfrac{1}{2}D_{w,i}), \xi^{(M)}\}dA_{SMA}\,. \tag{4.6}$$

The expression relates the centroid strain to the output tail stress (resulting from the applied load), actuator geometry, and material properties along the length of the SMA wire. The equation for resultant force (Equation 4.6) provides the ability to evaluate the average strain of the wire across its entire length, including the intermediate linear portions. To solve for the strain in the i^{th} linear segment, the resultant force equation (Equation 4.6) is solved by setting $\Theta = \Theta_{w,i}$ and neglecting the $y\cdot(\tfrac{1}{2}D_{w,i})^{-1}$ term (since linear segments can be approximated by an infinitely large mandrel diameter. While strain would generally be integrated along the *State 0* length for a linear SMA wire actuator, the changing stress distribution and regions of wire that gain and lose contact with the mandrel require that the standard approach be modified for determining the actuator's range of motion.

4.2.3. Actuator range of motion

In the multiple mandrel case, multiple portions of the SMA wire transition between the wrapped and linear regions throughout operation, and the strain is neither constant along the length nor the cross-section of the wire. As in the single mandrel case, these

computational difficulties are overcome by deriving a compatibility condition that ensures all portions of the wire are accounted for when integrating strain, including those that gain and lose contact with the mandrel during operation. Whereas the compatibility equation in the single mandrel case needs to account for three regions (the input tail, the wrapped length, and the output tail), the multiple mandrel case has to account for a specifiable number of mandrels (n), which results in ($2n$+1) regions. The multiple mandrel compatibility equation uses a similar derivation as the single mandrel equation (Equation 2.22), but employs two additional features: 1) summation terms that allows for the model to be flexible to a specifiable number of mandrels, and 2) cumulative angular variables that track the downstream effects of friction along the length of the wire. The resulting multiple mandrel compatibility equation is

$$\ell_{tot}^{(0)} = \sum_{i=1}^{n+1}\left(\int_0^{\ell_{lin,i}^{(\chi)}}\left[1+f_{SMA}^{(\chi)}\left\{\sigma_{t,out}e^{\pm\mu\left(\Theta_{w,(i-1)}^{(\chi)}-\Theta_{w,n}^{(\chi)}\right)}\right\}\right]^{-1}ds^{(\chi)}\right)+ \sum_{i=1}^{n}\left(\int_{\Theta_{w,(i-1)}^{(\chi)}D_{w,i}/2}^{\Theta_{w,i}^{(\chi)}D_{w,i}/2}\left[1+\varepsilon_{ctd}^{(\chi)}\left\{\frac{s^{(\chi)}}{\frac{1}{2}D_{w,i}},D_{w,i}\right\}\right]^{-1}ds^{(\chi)}\right). \tag{4.7}$$

With constant strains in each of the (n+1) linear portion and continuous strains between the n wrapped portions, the *State 0* wire length equation (Equation 4.7) simplifies to

$$\ell_{tot}^{(0)} = \sum_{i=1}^{n+1}\left(\frac{\ell_{lin,i}^{(\chi)}}{1+f_{SMA}^{(\chi)}\left\{\sigma_{t,out}e^{\pm\mu\left(\Theta_{w,(i-1)}^{(\chi)}-\Theta_{w,n}^{(\chi)}\right)}\right\}}\right)+\sum_{i=1}^{n}\left(\int_{\Theta_{w,(i-1)}^{(\chi)}D_{w,i}/2}^{\Theta_{w,i}^{(\chi)}D_{w,i}/2}\left[1+\varepsilon_{ctd}^{(\chi)}\left\{\frac{s^{(\chi)}}{\frac{1}{2}D_{w,i}},D_{w,i}\right\}\right]^{-1}ds^{(\chi)}\right). \tag{4.8}$$

Upon applying the boundary conditions for either rotational or linear output motion, and given the geometry, material constitutive law, coefficient of friction, and external applied load, only one geometric variable is unknown: the output tail length $\ell_{t,out}^{(\chi)}(=\ell_{lin,n+1}^{(\chi)})$ for linear actuators, or the n^{th} cumulative wrap angle $\Theta_{w,n}^{(\chi)}$ for rotational actuators. Solving the resulting compatibility equation (Equation 4.8) for the unknown variable, the actuator deformation can be solved based on the change in the unknown variable between *States 1* and *2,* such that

$$\delta\phi = \Theta_{w,n}^{(M)} - \Theta_{w,n}^{(A)} \tag{4.9}$$

for rotational actuators, and

$$\delta\ell = \ell^{(M)}_{lin,(n+1)} - \ell^{(A)}_{lin,(n+1)} = \ell^{(M)}_{t,out} - \ell^{(A)}_{t,out} \tag{4.10}$$

for linear actuators.

4.2.4. Binding limitation

As in the single mandrel case, the accumulation of friction can cause the SMA wire to bind to the mandrel when the assumption of unilateral motion is violated. Because of friction's downstream effects, the binding limitation depends on the cumulative wrap angle for multiple mandrel actuators. Replacing the wrap angle within the binding condition for single mandrel actuators (Equation 2.24) with the cumulative wrap angle, the multiple mandrel binding condition is

$$\Theta_B = \Theta^{(0)}_{w,n} \Leftrightarrow \varepsilon^{(M)}\{\Theta = 0\} = \varepsilon^{(A)}\{\Theta = 0\}, \tag{4.11}$$

where Θ_B is the binding angle in terms of cumulative angular position. At the location of binding, the wire neither stretches nor contracts and the assumption of unilateral motion between states is violated. Since no motion occurs, no change in strain can occur between states for wire between the input tail and the binding point ($0 < \Theta < (\Theta^{(0)}_{w,n} - \Theta_B)$).Thus, wrapping additional SMA wire beyond the binding angle is hypothesized to contribute no further motion to the actuator, which was demonstrated to be the case for single mandrel spool-packaged actuators in Chapter 2. The stress between the input end and the binding point is constant for a given state (austenite or martensite), but changes as the SMA wire is thermally cycled since the strain is fixed. For actuators in which binding occurs, the range of motion can be found by analyzing an equivalent actuator in which the wire is rigidly attached to the mandrel at the binding point and all portions between the input and the binding point are discarded.

Because multiple mandrel spool-packaged actuators often have long linear segments (for example, SMA wires packaged in serpentine configurations), the downstream effects of binding can be large depending on the location of the binding point along the SMA wire's length. Additionally, when the binding point is located near the running-on or running-off point of a mandrel, small variations in friction or tension have the potential to

change the location of the binding point from one mandrel to another, which also causes the linear length of SMA wire between the mandrels to become active or inactive. Therefore, the binding limitation can make significant impacts to the motion of an actuator and its sensitivity to variations in parameters.

4.3. Experimental validation

The basic mechanics regarding spool-packaged SMA wire actuators were experimentally confirmed for single mandrel actuators with respect to a number of actuator parameters including the type of output motion (linear or rotational), applied external load, wrap angle, and mandrel to SMA wire diameter ratio in Chapter 2. However, the multiple mandrel model introduces the use of the cumulative wrap angle and the downstream effects of friction are expected to be more pronounced due to the longer lengths of wire that can be packaged before binding occurs. To verify that the multiple mandrel approach to predicting the effects of friction, bending, and binding can sufficiently predict the behavior of multiple mandrel spool-packaged actuators, an experimental study was performed. The experimental study tested two aspects of the spooling model for multiple mandrel configurations: the effect of varying the number of spooled segments of SMA wire and the effect of applied load for two multiple mandrel configurations. Both sets of experiments investigated binding and non-binding actuator configurations.

4.3.1. Experimental setup and procedure

The experimental apparatus (Figure 4.2) is made up of the same four key elements of a basic multiple mandrel spool-packaged SMA wire actuator: 1) a single SMA wire in tension, 2) a fixed input where the SMA wire attaches to ground, 3) one or more fixed cylindrical mandrels, and 4) the motion output where the SMA wire interacts with applied loads from the external system. An aluminum fixture rigidly positions four Garolite cylinders (25.4 mm diameter) on a 50.8 mm square grid. Four PVC input fixtures with aluminum crimp blocks attach the input end of the SMA wire to ground and

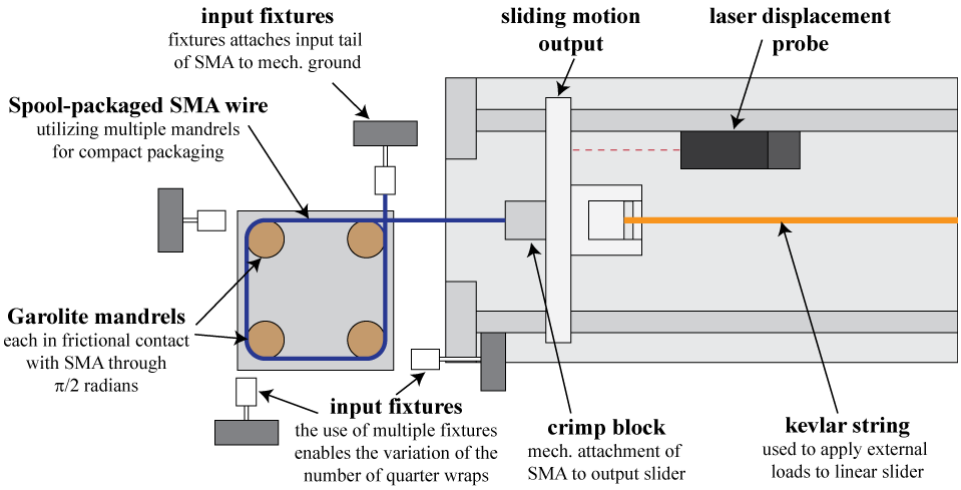

(a) Diagram of experimental apparatus (top view).

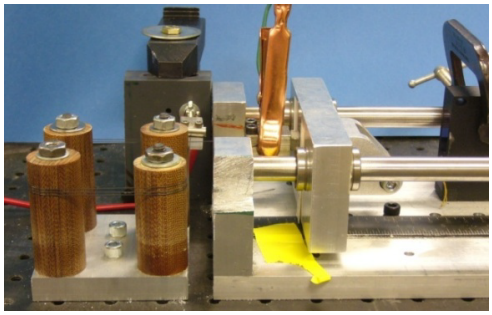

(b) Photograph of experimental apparatus (side view).

Figure 4.2. Diagram and photograph of experimental apparatus.

are positioned around the mandrel fixture to allow the number of mandrels in contact with the wire (n) to be varied in the experiments by selecting the appropriate length of SMA wire and input fixture position (Figure 4.3). The total cumulative wrap angle is $\Theta_{w,n} = \frac{1}{2}\pi \cdot n$ for the quarter-wrap experiments and $\Theta_{w,n} = \pi \cdot n$ for the half-wrap experiments. The actuator's linear range of motion was measured by a laser displacement probe. Loads were applied via a Kevlar string attached to the output slider at one end and wrapped over a pulley that allows known weights to be hung off the apparatus to apply the external load.

To reduce variation in the constitutive properties of the SMA wire throughout the experiments, the linear wire (not spooled) was thermally cycled between martensite and austenite while under 45 N of applied tension and under a 6.5% maximum strain constraint. Thermal cycling continued until the motion in each phase stabilized according

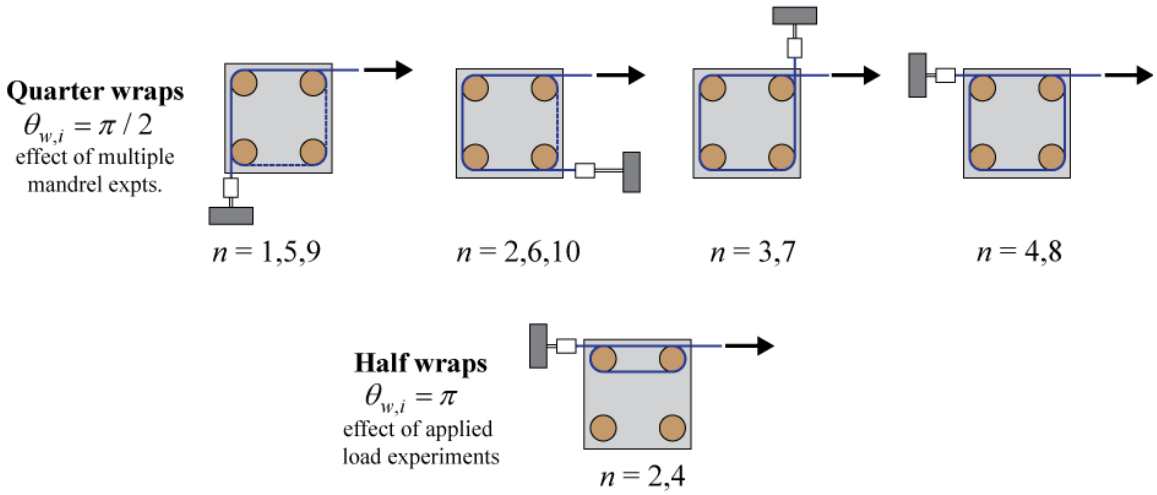

Figure 4.3. Multiple mandrel experimental configurations for spool-packaged SMA wire actuators. By varying the length of the SMA wire and the positioning of the input fixture, the number of mandrels (n) can be varied throughout the experimental validation.

to the shakedown procedures described by Sun, et al. (2008). The stress-strain behavior was measured across a range of applied stresses on the linear wire. Linear and third-order polynomial functions were fit to the data for the austenite and martensite phases, respectively, as shown in Figure 2.4. To further ensure consistent performance, the constitutive law was measured periodically throughout the set of experiments.

In a typical experiment, the SMA wire was installed in the experimental test apparatus (Figure 4.2) with the *State 0* wire length $\ell_{tot}^{(0)}$, spool configuration (input fixture position and number of mandrels n), wrap angles $\theta_{w,i}$, and applied load F_{app} set according to the particular experiment. Once the spool configuration and loads were selected, electrical current was applied to the wire (regulated and monitored by LabView software and a laptop computer equipped with data acquisition hardware) to resistively heat it to austenite (3A for about 2 seconds), and then cool it to martensite (0A for at least 3 minutes), in each case heating and cooling until a steady state deflection was reached.

4.3.2. Effect of multiple mandrels

To validate the extension of the model to the multiple mandrel case, the experiments tested different actuator configurations with a variable number of "quarter-wrap" segments (wrap angles $\theta_{w,i} = \pi/2$ for $1 \le i \le n$). While the model can accommodate any

wrap angle, quarter-wraps were selected as a typical value for wrap angle in applications in which the SMA wire is spool-packaged in a serpentine manner. Throughout testing, the input tail and *State 0* output tail lengths were maintained at $\ell_{lin,1} = 7.1$ mm and $\ell_{t,out}^{(0)} = 7.8$ mm; the intermediate linear segments were a constant $\ell_{lin,i} = 50.8$ mm $(2 \le i \le n)$ due to the set positioning of the mandrels on the fixture. Tension was applied with a 1.5 kg load, subjecting the output tail to 130 MPa of tensile stress. The experiments were performed in random order testing the range of motion of actuators with up to n = 10 wrapped segments, thermally cycling the actuator at least 5 times in each configuration.

The experimentally determined range of motion is plotted with respect to the number of wrapped segments (Figure 4.4), and is well-bounded by theory for the expected range of friction $0.1 \le \mu \le 0.15$. The data matches the model well in shape, initially increasing with n and then leveling off due to the onset of binding beyond about n = 4 quarter-wraps. Additionally, the data fits the model well in magnitude with 1.6% average error between the data and best-fit theory line (determined using the method of least squares with respect to friction, occurring at $\mu = 0.14$). The experiments demonstrate that the theory predicts the behavior of physical actuators for multiple mandrels, and accounts for the accumulation of friction and the related onset of binding. Additionally, the results

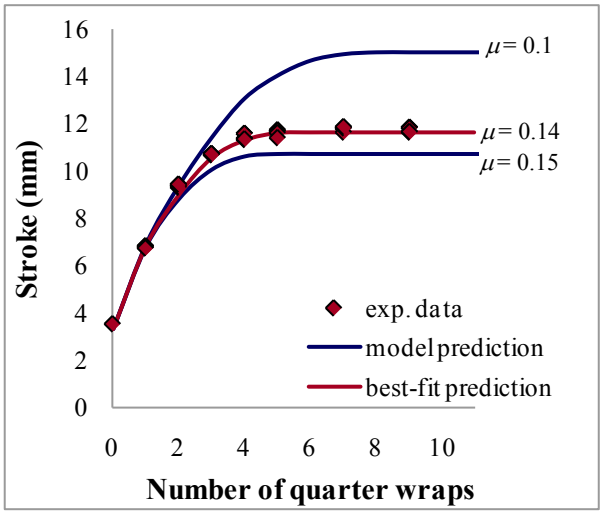

Figure 4.4. Effect of multiple wrapped segments. Motion was measured experimentally for actuators with a variable number of quarter-wraps (n) and compared to theory for the expected range of friction values.

demonstrate that there is an initial advantage with respect to range of motion for adding longer lengths of wire to the actuator without increasing the packaging footprint. Yet, as the wrap angle approaches the binding angle, the further increases in the amount of wrapping have a decreasing, and then absent, effect on the actuator's motion.

4.3.3. Effect of applied stress

To validate the model's ability to predict the motion of multiple mandrel actuators with respect to applied load, experiments were performed for two additional configurations using multiple "half-wrap" segments (wrap angles of $\theta_{w,i} = \pi$ radians) for which non-binding and binding configurations were both tested ($n = 2$ and $n = 4$, respectively). As in the first set of experiments, the input, output, and intermediate linear portions of the SMA wire remained constant ($\ell_{lin,1} = 7.1$ mm, $\ell_{t,out}^{(0)} = 7.8$ mm, and $\ell_{lin,i} = 50.8$ mm for $2 \le i \le n$).

For both the binding and non-binding cases, the data agree with the theoretical predictions in shape with the characteristic inflection in the theory reflected in the data (Figure 4.5). Due to larger deviations from the model at low applied stresses, the average error between the data and model was 23% for the n = 2 case, and 22% for the n = 4 case.

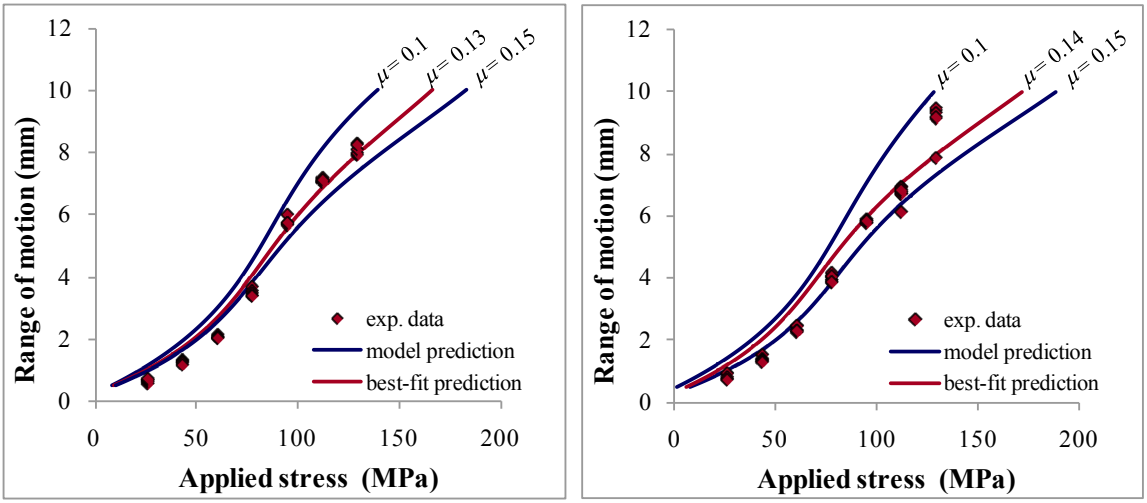

a) Two half-wraps, non-binding case *b) Four half-wraps, binding case*

Figure 4.5. Effect of applied stress on multiple mandrel spool-packaged SMA wire actuators. Two different mandrel configurations were tested for range of applied motion with respect to applied load. The best-fit curves represent the model prediction with the least-squares error with respect to the coefficient of friction. a) For the n=2 case, no binding was predicted. b) For the n=4 case, the actuator is expected to undergo frictional binding.

For ranges of motion measured at applied stresses above the martensite plateau, error was significantly reduced with average errors of 3.6% for $n = 2$ and 6.1% for $n = 4$. The distribution of error across the range of applied loads is consistent with the error from the experiments testing the effect of n since they were performed at an applied stress above the martensite plateau. The increase in error for the lower range of applied stresses results in part from the shallower slope of the martensite plateau (indicating greater compliance), which causes the strain (and the resulting motion) to be significantly more sensitive to applied stress. Thus, any inaccuracy in the constitutive law would be amplified for the low applied stresses and the portions of the wire where the martensite stress is low (closer to the input tail). Fortunately, SMA actuators are typically designed to operate at stresses above the plateau where the error is lower to take advantage of the greater strains, and thus, the range of motion.

4.4. Conclusions

Whereas single mandrel spooled SMA actuators are useful for making actuator form factors more compact, multiple mandrel architectures enable greater form customization to tight, unusually shaped packaging constraints. In this chapter, the analytical tools were developed for predicting the motion of spool-packaged SMA wire actuators with multiple mandrel topologies. A generalized architecture was defined that enables packaging of SMA wires along spooled and serpentine pathways that are highly customizable to form constraints. Expanding upon the quasi-static model for single mandrel SMA wire actuators from Chapter 2 an indexing convention was implemented for an array of variables used to describe the pathway of the wire, and an additional variable for the cumulative wrap angle was introduced to relate the impact of wrapping SMA wire around one mandrel to the neighboring segments. The multiple mandrel model is distinguished from the single mandrel model by the use of the cumulative wrap angle variables, which are important for representing frictions downstream effects on adjacent segements of SMA wire. Additionally, the compatibility formulation was expanded to the multiple mandrel architecture to ensure that the different strain functions were applied

appropriately across the entire wire throughout operation, including segments of the wire that gain and lose contact with the mandrel as the SMA wire changes phase. The model used a generalized constitutive law to describe the material behavior, considered the cumulative effect of friction resulting from wrapping SMA wire around the multiple mandrels, and adjusted for bending on wrapped segments with individually specifiable mandrel diameters. Additionally, the model prediction for the location of frictional binding was derived, and a technique for adjusting the model prediction was provided in the derivation and utilized in the experimental study. The expanded model is consistent with the single mandrel approach; the $n = 1$ case of the multiple mandrel model is equivalent to the single mandrel model with the cumulative wrap simply becoming the wrap angle.

For the model to support the design of SMA wire actuators with customizable, high performance and tailorable forms, it was developed with four features not present in the earlier models. 1) Rather than being specific to particular actuator configurations, the multiple mandrel spooling model derived in this chapter is flexible to predict for a broad range of mandrel topologies, geometries, applied loads, and material properties that can be specified by the user. 2) The model predicts friction in the wrapped segments explicitly, rather than estimating friction as an empirically determined efficiency loss or assuming that wrapped segments do not make significant contributions to motion – an assumption that breaks down for larger wrap angles. 3) The multiple-mandrel model evaluates and adjusts its prediction for the influence of bending, which is not predicted in earlier models. 4) Limitations due to binding, caused by accumulated friction, are evaluated to provide a boundary to the feasible design space or to adjust the prediction in designs where frictional binding occurs.

To verify that the mechanics of single spool actuators extend to the use of multiple mandrels, an experimental study was conducted, successfully demonstrating the expansion of the model. In experiments varying the number of discrete wrapped and linear segments and a second set varying the applied load, the model predicted the stroke

well in both form and magnitude. The results of this chapter enable the use of multiple mandrels in both the design and analysis of spool-packaged actuators, where only single spool architectures were previously modeled and understood. The expanded ability to apply spooled-packaging further broadens the ability to utilize SMA actuation in applications for lighter weight, more compact, simpler, and reduced cost actuation.

Chapter 5. Design Methodology for Spool-Packaged SMA Actuators

SMA actuators are promising candidates to fulfill needs in industry for high performance, low-cost actuation, but difficulty packaging the material within practical forms has been a significant obstacle to their use in many otherwise suitable applications. To realize the performance and cost advantages of SMA, this dissertation has developed the scientific foundations to analyze spool-packaged SMA wire actuators, thus providing a necessary basis for the synthesis of spooled actuators. Due to the large range of design possibilities, especially for multiple spool actuators, there is high potential for customization. However, this leads to complex design problems in which performance, packaging, and cost depend on an array of interrelated design parameters. Furthermore, as packaging constraints and internal obstacles are introduced, as in the design examples in Chapter 2, the design space becomes discontinuous and increasingly complex with multiple local minima and maxima. Consequently, it becomes more difficult to select high-quality designs for problems with multiple mandrels and different variations in packaging without making unnecessary sacrifices to performance and cost. To manage the competing design tradeoffs and meet unusual packaging constraints, a systematic approach to synthesizing spool-packaged actuators is vital.

This chapter develops a methodology for the synthesis of spool-packaged actuators, which iterates through an extensive range of actuator designs, evaluates their quality (using objective functions) and feasibility (using constraints), and selects designs through optimization. Three case studies, distinguished by varying form constraints and allowable topologies, demonstrate the design methodology and expose different strategies for managing design tradeoffs. These results provide a glimpse into the potential for

customizing SMA actuators to meet difficult form constraints, thus enabling their use in many otherwise suitable applications.

5.1. Design methodology overview

The design methodology developed for customizable spool-packaged SMA actuators builds on the generalized architecture and predictive models for multiple mandrel actuators. Although the design methodology distinguishes between a variety of design problem objectives and constraints, the different categories of problems rely on three common steps within an iterative design process:

1. Selecting actuator design variables to define the actuator geometry,
2. Determining the SMA wire pathway and evaluating packaging- and cost-related objectives and/or constraints, and
3. Solving for the actuator displacement and evaluating performance objectives and/or constraints.

The design methodology is described for a generalized *n* mandrel actuator, and is intended to be adaptable to application needs with the ability to define a variety of objective functions and constraints. The common thread among spooled-packaging problems is the need to balance performance, packaging, and cost trade-offs. Thus, performance, packaging, and cost metrics are crucial in defining objectives and constraints of the design problem. The methodology that is outlined in this chapter is intended to provided a starting point for developing spool-packaged actuators that meet particular application needs. In many cases, alternative design variables, objectives, and constraints can be selected by adapting the basic methodology, while adhering to the three common steps outlined above.

5.1.1. Selecting design variables

Since optimization-based synthesis iterates through many actuator designs, a systematic approach was needed to specify the range of designs and assess their feasibility with regard to packaging constraints. To generate and describe the geometry of a single or multiple mandrel spool-packaged SMA actuator, a nomenclature and indexing convention for multiple mandrel architectures is used, as is diagrammed for a generic *n*

mandrel spooled actuator in Figure 5.1. The actuator geometry is specified with three design variables per mandrel: mandrel diameter D_i, wrap angle $\theta_{w,i}$, and lengths of the i^{th} linear segments $\ell_{lin,i+1}$ for $i = [1{:}n]$. In addition, the location of the output end of the wire in *State 0* $(x_{out,sys}, y_{out,sys}) \equiv (x_{in}, y_{in})_{(n+1)}$ and the angular orientation of the output tail $\alpha_{out,sys} \equiv \alpha_{n+1}$ are assumed to be given. The parameters used to define the orientation of wire segments and relative locations of key points of an actuator are shown in Figure 5.2. In this approach, three design variables per mandrel are sufficient to completely describe the pathway of the SMA wire. The remaining geometric, loading, and material parameters are assumed to be specified beforehand, however, they can also be selected as design variables at the discretion of the designer.

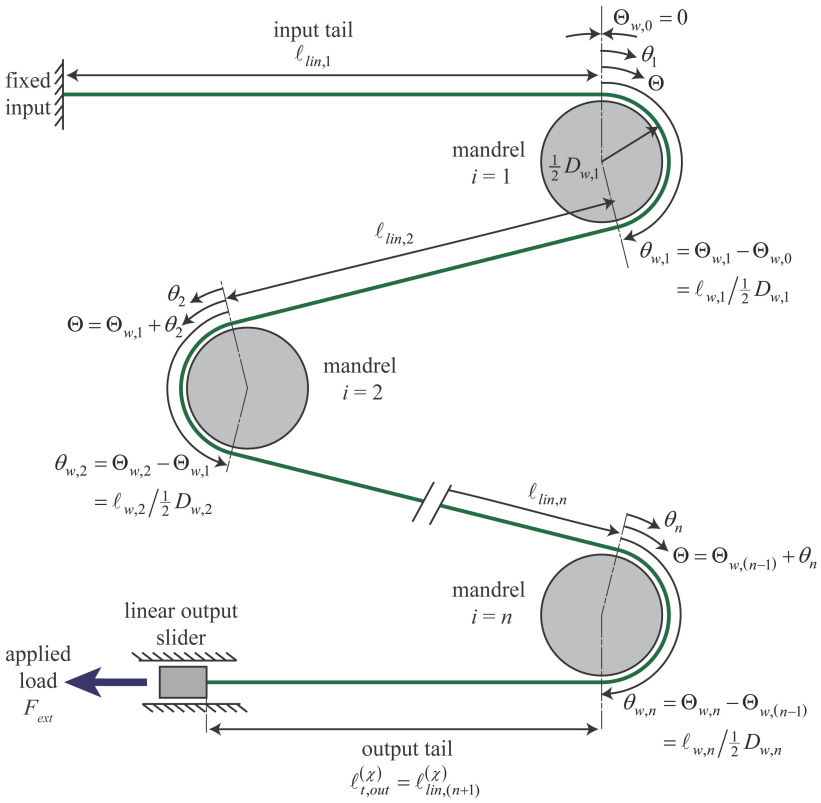

Figure 5.1. Diagram of a multiple mandrel spool-packaged SMA actuator. The generalized architecture provides a foundation for the design of a broad range of actuator geometries, which are described using the key parameters and indexing conventions shown in the figure.

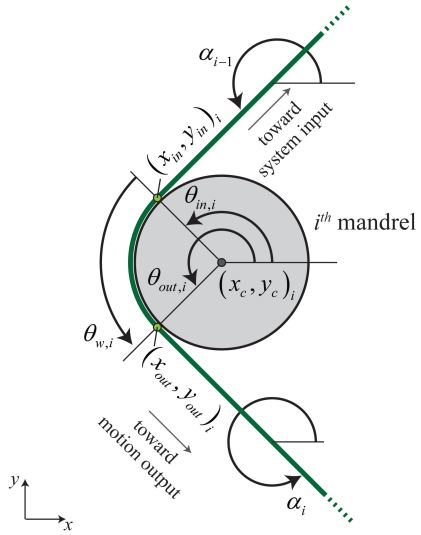

Figure 5.2. Diagram of the *ith* mandrel of an n mandrel spool packaged SMA actuator. The key parameters used to describe the pathway of a spool-packaged SMA wire through Cartesian space are indicated.

5.1.2. Evaluating actuator form and cost

To evaluate the form and cost of an actuator, the pathway of the SMA wire through Cartesian space was derived for a set of design variables. The equations for several key locations and angles that define the pathway are summarized in Table 5.1. For this analysis, a right-hand Cartesian coordinate system is used with a horizontal *x*-axis. The orientation angle of the linear segments is defined as the counterclockwise angle from the *x*-axis to the vector directed from the input to the output end of the linear segment. The geometry and key dimensions defining the SMA wire pathway around the i^{th} mandrel are shown in Figure 5.2 including the locations of the mandrel center, running-on, and running-off points; the angular positions of the running-on and running-off points with respect to the mandrel; and the linear segment angular orientations. Based on geometric relationships and the known location and orientation of the output end of the wire in *State 0*, $(x_{out,sys}, y_{out,sys}$, and $\alpha_n)$, the critical points that define the SMA wire pathway are determined recursively starting at the output end of the wire and iterating toward the input end using the equations:

$$
\begin{aligned}
x_{out,i} &= x_{in,(i+1)} - \ell_{lin,(i+1)} \cos\alpha_{(i+1)} \\
y_{out,i} &= y_{in,(i+1)} - \ell_{lin,(i+1)} \sin\alpha_{(i+1)} \\
\theta_{out,i} &= \arcsin\left(-\operatorname{sgn}\theta_{w,i}\right) + \alpha_{(i+1)} \\
\theta_{in,i} &= \theta_{out,i} - \theta_{w,i} \\
x_{c,i} &= x_{out,i} - \tfrac{1}{2} D_i \cos\theta_{out,i} \qquad \text{for } i = [n:1]. \\
y_{c,i} &= y_{out,i} - \tfrac{1}{2} D_i \sin\theta_{out,i} \\
x_{in,i} &= x_{c,i} + \tfrac{1}{2} D_i \cos\theta_{in,i} \\
y_{in,i} &= y_{c,i} + \tfrac{1}{2} D_i \sin\theta_{in,i} \\
\alpha_i &= \theta_{in,i} - \arcsin\left(\operatorname{sgn}\left(\theta_{w,i}\right)\right)
\end{aligned}
\tag{5.1}
$$

Based on the set of recursive equations for the critical point locations and angular dimensions for multiple mandrel actuators, the key points along the SMA pathway are defined except for the system input point $(x_{in,sys}, y_{in,sys})$. If the length of the input tail $\ell_{sys,in} = \ell_{lin,1}$ is known, the system input location is determined from the known length, the location of the wire running onto the first mandrel $(x_{in,1}, y_{in,1})$, and the angular orientation of the input segment α_1:

$$
\begin{aligned}
x_{in,sys} &= x_{in,1} - \ell_{lin,1} \cos\alpha_1 \\
y_{in,sys} &= y_{in,1} - \ell_{lin,1} \sin\alpha_1
\end{aligned}
\tag{5.2}
$$

For actuators in which the system input is required to be located on the perimeter of the packaging envelope, the *MATLAB* function "polyxpoly.m" is used to find the intersection between the polygonal packaging envelope (typically rectangular) and a line segment extending from $(x_{in,1}, y_{in,1})$ according to the orientation angle α_1. Alternatively, the intersection between a wrapped segment and the packaging envelope could be

Table 5.1. Nomenclature for specifying pathway of spool-packaged SMA wire.

Dimension	Variable
Mandrel center	$(x_c, y_c)_i$
Location of i^{th} running-on point	$(x_{in}, y_{in})_i$
Location of i^{th} running-off point location	$(x_{out}, y_{out})_i$
Angular position of i^{th} running-on	$\theta_{in,i}$
Angular position of i^{th} running-off	$\theta_{off,i}$
Angular orientation of i^{th} linear segment	α_i
Location of fixed end of SMA wire	$(x_{in,sys}, y_{in,sys})$
Location of sliding output end of SMA wire (*State 0*)	$(x_{out,sys}, y_{out,sys})$

determined to provide the location of the SMA wire input.

A representation of cost is beneficial in the design problem to guide actuator designs to practical solutions. While cost can refer to material use, energy use, or direct monetary cost of the actuator, each of these costs is related to the SMA wire length. Thus, in this approach, cost is included by constraining or minimizing the length of the SMA wire. Once the pathway of the SMA wire is generated, its total *State 0* is determined by summing the length of each linear and wrapped segment according to the equation:

$$\ell_{tot}^{(0)} = \sum_{i=1}^{n} \left(\tfrac{1}{2} D_{w,i} \cdot \theta_{w,i} + \ell_{lin,i+1} \right) + \ell_{lin,1} \tag{5.3}$$

where the input tail length is determined according to the procedure defined earlier in this section and the remaining terms are defined by the design variables.

5.1.3. Evaluating actuator performance

To evaluate performance objectives and constraints for a specified actuator geometry, the range of motion is solved using the spooling model developed in Chapter 4. For the case studies in this chapter, the parameters for wire diameter, friction coefficient, material stress-strain curves, and applied load were selected using a standard set of values (Table 5.2). However, when designing a spool-packaged SMA actuator for a particular application, decisions regarding the wire geometry and applied load need not be made beforehand if a designer appoints them as design variables to be determined through optimization.

The spooling model is used to predict the change in SMA wire length between the martensite and austenite states, which are differenced to provide the range of motion

Table 5.2. Standard parameter values used throughout design case studies.

Parameter	Value
SMA wire diameter	$d_{SMA} = 0.381\text{mm}$
Applied load (stress)	$F_{SMA} = 20\text{N}$ ($\sigma_{SMA} = 175\text{MPa}$)
Martensite stress-strain function	$\sigma^{(M)} = 4.1\times10^{6}\varepsilon^{3} - 2.7\times10^{5}\varepsilon^{2} + 6.7\times10^{3}\varepsilon$ [MPa]
Austenite stress-strain function	$\sigma^{(A)} = 45.1\times10^{3}\varepsilon$ [MPa]
Friction coefficient	$\mu = 0.1$

according to the expression

$$\delta\ell = \ell_{tot}^{(M)} - \ell_{tot}^{(A)} = \ell_{t,out}^{(M)} - \ell_{t,out}^{(A)}, \tag{5.4}$$

where the predictions for the martensite *State 1* output tail length $\ell_{tot}^{(M)}$ and the austenite *State 2* output tail length $\ell_{tot}^{(A)}$ account for friction and bending based on the full spooling model in Chapter 4. Relating the strains of the spool-packaged SMA wire in the austenite and martensite states to its free length using the compatibility equations, the output tail lengths $\ell_{tot}^{(M)}$ and $\ell_{tot}^{(A)}$ can be determined.

To speed up computation within the optimization algorithm by avoiding the repeated solving of the centroid strain, a functional mapping is generated that is used to quickly interpolate the centroid strain in SMA wire under bending. Using the mapping, implemented within *MATLAB*, the centroid strain is predicted as a function of tensile stress and mandrel diameter. For the case studies in this chapter, the functional mapping was generated according to the procedure described in Chapter 2 (Section 2.3.2) for stresses between 0 – 300 MPa, diameters between 1 – 100 mm, and a 100 x 100 resolution. With the actuator geometry constructed from the design variables, material parameters, and constitutive law functional mapping, the compatibility equation can be solved for the SMA lengths in each state, which are differenced to provide the actuator stroke (Equation 5.4). Since the compatibility equation is a transcendental function with the unknown variable appearing within an integrand and its limit of integration, the compatibility equations cannot be solved with closed-form solutions. Thus, compatibility is solved numerically according to the procedure described in Section 2.3.4.

To determine the length of the SMA wire that lies outside of the feasible packaging envelope, $\ell_{v,pack}$, and the length that lies inside the internal obstacle, $\ell_{v,obs}$, the path of the wire was discretized in *MATLAB* into many short segments. The function *"*inpolygon.m*"* was utilized to determine whether the midpoint of each sub-segment of the wire lies in an infeasible region. If the sub-segment was found to be infeasible, it was added to the length of SMA wire in violation of the packaging constraints, $\ell_{v,pack}$ and $\ell_{v,obs}$, as appropriate.

5.2. Design case studies for spool-packaged SMA actuators

To demonstrate the application of the spooling model to the synthesis of compact, customizable actuators, three design case studies were conducted with different types of packaging regarding form constraints and number of mandrels. Each case study shows the ability of spool-packaged SMA wire actuators to make package dimensions more compact or to redirect SMA wire within form constraints. In the first case study, there are no packaging constraints, but a compact actuator footprint is desired with minimal SMA wire length to reduce cost. In the second case study, the actuator design is subject to an external form constraint with an internal obstacle using the same specifications as in Chapter 3, Example 3. Whereas the example in Chapter 3 examines the design space to understand the relationship between the actuator's design and its performance, the case studies in this chapter demonstrate the application of the design methodology to synthesize optimal designs. The third case study considers a problem with the same objectives and constraints as in the second case study, but also employs multiple mandrel architectures to show the benefits and additional difficulties for multiple mandrel packaging strategies. The three studies demonstrate the application of the spooling model and optimization techniques to the packaging problem and provide a template for the design of compact, customizable actuators with predictable high performance.

5.2.1. Case 1: Compact packaging

While SMA wires can provide lightweight, energy dense actuation, packaging them in compact, manageable forms can be critical for their successful use in numerous applications. This case study demonstrates how the design methodology can be applied to synthesize compact actuators with mitigated costs even in the absence of specific packaging constraints.

5.2.1.1. Problem statement and mathematical model

To design a compactly packaged actuator with reasonable material and energy costs, the design methodology is applied for an example actuator required to provide 20 mm of

motion against a 20 N external dead load. The force was selected based on the guidelines by Dynalloy (2010), the manufacturer of Flexinol SMA wire. The range of motion was selected to examine a representative problem, for which a moderate motion requires a long length of wire (430 mm) that would be unwieldy for many applications (e.g., an automotive door latch). The actuator compactness is evaluated based on the sum of the length and width of the package envelope that surrounds the SMA wire and mandrel (as illustrated in Figure 5.3). The standard parameters for applied load, SMA wire diameter, and frictional and constitutive material properties are assumed as specified in Table 5.2, and the input tail length is defined to be zero millimeters. The actuator design is fully specified by three design variables: the mandrel diameter D, the wrap angle θ_w, and the *State 0* output tail length $\ell_{t,out}^{(0)}$. The motion is required to be applied at the edge of the packaging envelope to avoid obstruction or interaction between the mandrel and any attachment points at the output end of the SMA wire.

5.2.1.1.1. Objective function

To minimize SMA wire free length and the actuator's overall dimensions, the multi-objective function $F\{\mathbf{x}\}$ is

$$\text{minimize} \quad F\{\mathbf{x}\} = f_1\{\mathbf{x}\} + f_2\{\mathbf{x}\}, \quad \mathbf{x} = [D, \theta_w, \ell_{t,out}^{(0)}]^{\mathrm{T}} \tag{5.5}$$

where f_1 is the SMA free length objective, f_2 is the packaging dimensions objective, and the vector $\mathbf{x}$ contains the design variables. The SMA length objective f_1 is defined by the equation

$$f_1\{\mathbf{x}\} = \frac{w_1}{s_1}\ell_{tot}^{(0)} = \frac{w_1}{s_1}\left(\tfrac{1}{2}D\cdot\theta_w + \ell_{t,out}^{(0)}\right) \tag{5.6}$$

where w_1 is the weighting on the SMA wire length objective such that $0 \le w_1 \le 1$, and s_1 is the scaling constant. The packaging dimension objective f_2 is defined by the equation

$$f_2\{\mathbf{x}\} = \frac{(1-w_1)}{s_2}\left(L_{pack} + W_{pack}\right),$$
$$\text{where} \quad L_{pack} = \ell_{t,out}^{(0)} + \tfrac{1}{2}D \tag{5.7}$$
$$W_{pack} = D.$$

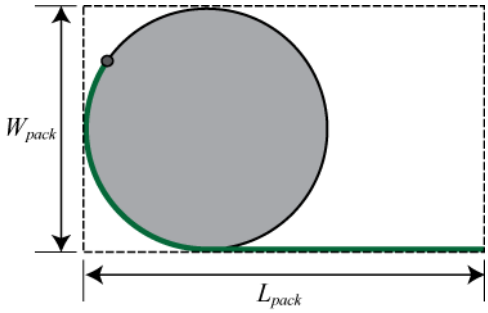

Figure 5.3. Dimensions of packaging envelope. The *State 0* SMA wire length is used to evaluate packaging.

In the equation for f_2, (1-w_1) is the weighting on the objective f_2 and s_2 is the scaling constant. The scaling constants s_1 and s_2 are determined by minimizing the objective function (Equation 5.5) with respect to one objective at a time by setting $w_1 = 0$ or 1, and solving the single objective functions (Equations 5.6 and 5.7) for the scaling constants such that $f_1\{\mathbf{x}\} = 1$ for $w_1 = 1$ and $f_2\{\mathbf{x}\} = 1$ for $w_1 = 0$.

5.2.1.1.2. Constraints

Feasibility is achieved by meeting the range of motion requirement and an additional practical constraint requiring the output motion to act at the external perimeter of the actuator envelope. The range of motion constraint, g_1, is satisfied for the inequality

$$g_1 : \delta_{spec} - \delta\{\mathbf{x}\} \leq 0 \tag{5.8}$$

where δ_{spec} = 20 mm for the particular requirements of the case study. To evaluate the constraint, the actuator's range of motion $\delta\{\mathbf{x}\}$ is solved using the multiple mandrel spooling model derived in Chapter 4.

The second constraint ensures practical geometry: that the point of output motion is at the edge of the actuator's packaging envelope. Without a constraint on the location of the output motion, crimps or attachment points to the output end of the wire may interfere with motion by coming into contact with the mandrel. While the location of the motion output can be tailored to the needs of a specific application, such a requirement is sensible to ensure feasible operation. Since the case study requires the output motion to occur at the edge of the packaging envelope, the output tail may not be shorter than the mandrel radius. Thus, the packaging constraint with regard to output tail geometry is:

$$g_2 : \tfrac{1}{2} D - \ell_{t,out}^{(0)} \le 0. \tag{5.9}$$

Additional factors can be considered within the design problem using additional objective or constraints functions. Constraints against binding and minimum bending radius were not implemented in the approach. However, the minimization of length in the objective prevents binding from occurring since binding configurations use excess length of SMA wire with neither benefit to the objective function nor aid in satisfying constraints. For applications in which fatigue is a concern, an additional constraint on the minimum mandrel diameter or the maximum strain in the SMA wire can be implemented as described in Section 3.2.2.

Assembling the objective function, constraints, and geometric relationships, the optimization problem is summarized:

$$\begin{aligned}
\text{minimize} \quad & F\{\mathbf{x}\} = \frac{w_1}{s_1}\ell_{tot}^{(0)} + \frac{(1-w_1)}{s_2}\left(L_{pack} + W_{pack}\right), \quad \mathbf{x} = [D, \theta_w, \ell_{t,out}^{(0)}]^{\mathrm{T}} \\
\text{subject to:} \quad & g_1 : \delta_{spec} - \delta\{\mathbf{x}\} \le 0 \\
& g_2 : \tfrac{1}{2} D - \ell_{t,out}^{(0)} \le 0 \\
\text{where:} \quad & \ell_{tot}^{(0)} = \tfrac{1}{2} D \cdot \theta_w + \ell_{t,out}^{(0)} \\
& L_{pack} = \ell_{t,out}^{(0)} + \tfrac{1}{2} D \\
& W_{pack} = D \\
& D, \theta_w \ge 0
\end{aligned} \tag{5.10}$$

5.2.1.2. Optimization approach

Without the presence of packaging constraints to affect the allowable geometry, the objectives for the case study are continuous with respect to the design variables. The sequential quadratic programming (SQP) method was selected because the objective function is convex and the algorithm can handle the non-linear constraint on motion g_1, which could not modeled with closed-form equations due to the complexity of governing mechanics. The SQP optimization was implemented in *iSIGHT* software, and used a *MATLAB* module to calculate actuator motion for each design as the optimization iterated. Defining the scaling constants to be the values of s_1 and s_2 that make the objective function equal to unity for the single objective optima, the constant s_1 is equal

to the minimized SMA wire length for $w_1 = 1$ and the constant s_2 is equal to the minimized package dimensions ($L_{pack} + W_{pack}$) for $w_1 = 0$.

5.2.1.3. Results

Because the design problem has multiple objectives, a range of optimal solutions was determined by varying the weighting constant within the objective function w_1 across its range ($0 \le w_1 \le 1$). Repeating the optimization across the range of objective weightings produced a Pareto set of optimal solutions (Figure 5.4), which represents designs for which a feasible improvement to one of the objectives is possible only at the expense of the other objective. The initial values and range of the design variables that were used throughout the optimization study are shown in Table 5.3. The initial design variable values were selected to provide a feasible initial design, and the range was selected to encompass a large set of designs that includes the optimal set. To ensure that the global optimum was determined, different initial design points were selected throughout the set of optimizations to verify convergence to the same final designs.

The values for the optimal design variables as they vary with the objective weighting are shown in Table 5.4, along with the values of the constraint functions (constraint activity indicated in boldface type), and the value of the multi-objective function. The trade-off between the objectives of compact packaging and minimized SMA wire length is illustrated in Figure 5.4, in which the optimal values of the single-objective functions are plotted for varied objective weightings, forming a convex Pareto set, which bounds the attainable set of designs satisfying the feasibility constraints. The stroke constraint is active along the entire Pareto set indicating the key tradeoff between the amount of SMA motion that the actuator can provide and its compact packaging. Changes to an actuator design that either increase the SMA wire length or increase the packaging dimensions

Table 5.3. Initial values and range of design variables for Case Study 1.

	Initial	Lower bound	Upper bound	
D	0.1	10^{-3}	0.5	[m]
θ_w	10	10^{-3}	20	[radians]
$\ell_{t,out}^{(0)}$	0.8	10^{-3}	1.5	[m]

will increase the actuator's range of motion, but also increase the objectives toward the interior of the attainable set in Figure 5.4.

To illustrate the trade-off of objectives as they relate to the actuator design, the design variables of the optimal spooled actuator are plotted with respect to the objective weighting w_1 in Figure 5.5a, and the objective function values are plotted with respect to w_1 in Figure 5.5b. In each plot, the design variables and objectives are continuous with the objective weighting, but at $w_1 \approx 0.17$ there is a kink in the design variables and objective functions as activity on the packaging constraint g_2 switches. Below $w_1 = 0.17$, the packaging constraint is not active as smaller values of w_1 favor short SMA wire lengths over compact packaging. Thus to meet the stroke constraint, designs lower values of w_1 are longer in length and have less of the SMA wire spooled around the mandrel. As w_1 approaches zero, the objective function only seeks to minimize the SMA wire length and the design converges to the straight wire case where wrap angle is $\theta_w = 0$. Above $w_1 = 0.17$, the packaging constraint on the location of output motion becomes active and the optimal design has a square form factor indicating that entire wire, except for the

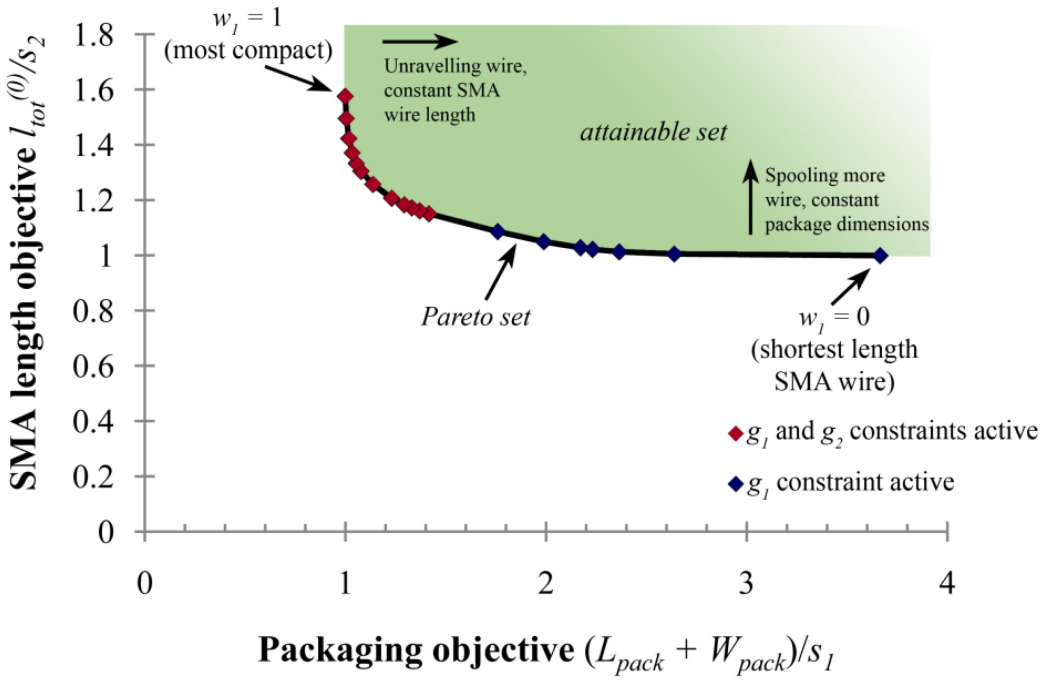

Figure 5.4. Pareto optimal set of designs for Case Study 1 optimization. The objectives values are plotted for the range of optimal designs as the relative objective weighting w_1 is varied, which defines the boundary between the infeasible and feasible design spaces where the objective is minimized given a relative objective weighting.

minimum required length on the output tail, is spooled. Increasing the weighting on the objective to minimize packaging, further reductions in the package length dimensions occur as more wire is wrapped around the mandrel. This causes an increase in the wrap angle and a decrease in the mandrel diameter, which results in increasing friction and bending losses, and thus a need for a longer length of SMA wire. As w_1 approaches 1, the objective seeks to minimize only the packaging dimensions without regard to the SMA wire length, resulting in the binding condition occurring at $w_1 = 1$.

The two types of designs that result from the optimization depend on the relative weighting between the cost and compactness objectives. For reducing cost, rectangular form factors are favorable, which become more slender (and thus less compact) as cost becomes more critical. For designing actuators that are compact, square form factors are favored, and the cost/compactness tradeoff is modulated by varying the wrap angle and diameter of the actuator. The most compact actuator available has a square actuator envelope and wraps the SMA wire up to binding, minimizing size without regard to

Table 5.4. Numerical results for Case Study 1 (single mandrel spool-packaged actuator without external form constraints). The packaging dimensions and SMA free length are minimized across a range of relative objective weightings. Constraint activity is indicated in boldface type.

	Design variables			**Constraints**			**Objective**
Objective weighting w_1	Mandrel diameter [m] D	Output tail length [m] $l_{t,out}^{(0)}$	Wrap angle [rad] θ_w	Stroke constraint g_1	Packaging constraint [m] g_2	Binding constraint [m] g_3	Objective function $F\{\mathbf{x}\}$
0	0.200	0.435	0.00	**0.00**	-0.34	-12.68	1.00
0.025	0.096	0.385	1.09	**0.00**	-0.34	-11.59	1.05
0.05	0.060	0.383	1.91	**0.00**	-0.35	-10.77	1.08
0.075	0.058	0.360	2.92	**0.00**	-0.33	-9.77	1.11
0.1	0.050	0.361	3.50	**0.00**	-0.34	-9.18	1.14
0.125	0.067	0.298	4.75	**0.00**	-0.26	-7.94	1.17
0.15	0.090	0.218	5.68	**0.00**	-0.17	-7.00	1.19
0.175	0.142	0.071	6.06	**0.00**	**0.00**	-6.62	1.20
0.2	0.137	0.069	6.36	**0.00**	**0.00**	-6.32	1.20
0.225	0.133	0.067	6.65	**0.00**	**0.00**	-6.03	1.21
0.25	0.130	0.065	6.95	**0.00**	**0.00**	-5.73	1.21
0.3	0.123	0.062	7.52	**0.00**	**0.00**	-5.16	1.21
0.4	0.114	0.057	8.60	**0.00**	**0.00**	-4.08	1.21
0.5	0.108	0.054	9.51	**0.00**	**0.00**	-3.17	1.19
0.6	0.106	0.053	9.97	**0.00**	**0.00**	-2.71	1.17
0.7	0.104	0.052	10.51	**0.00**	**0.00**	-2.17	1.14
0.8	0.102	0.051	11.14	**0.00**	**0.00**	-1.54	1.10
0.9	0.101	0.050	11.92	**0.00**	**0.00**	-0.76	1.05
1	0.100	0.050	12.68	**0.00**	**0.00**	**0.00**	1.00

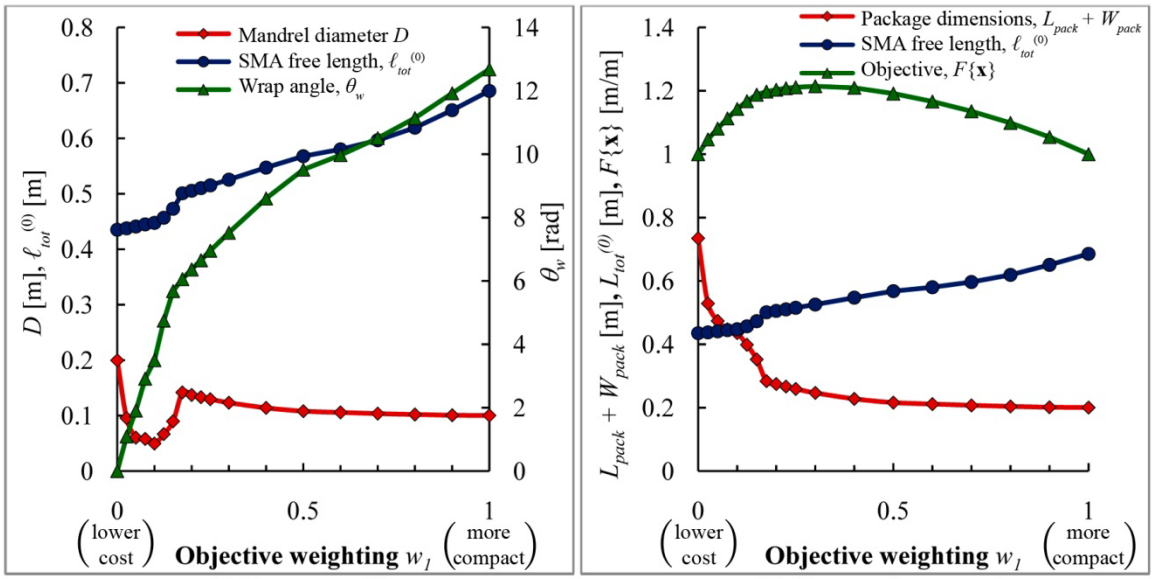

(a) Design variables *(b) Objective function values*

Figure 5.5. Design variables (a) and objective values (b) as they vary with objective weighting for Case Study 1 optimization.

friction losses and material cost.

For the example problem addressed in this case study, the design methodology provides a systematic approach that successfully defined the feasible and infeasible design spaces, and the boundary between the two where designs are optimal for a range of objective weightings. By the use of the multi-objective function, the Pareto optimal designs balance compactness and low-cost while meeting performance requirements. Adapting this approach to application specific requirements, the design methodology can be extended to a wide range of applications for which compact actuation is needed using reasonable lengths of SMA wire.

5.2.2. Case 2: Single mandrel actuator, prescribed form constraints

The first case study addressed applications in which more compact packaging is preferable, but a large class of applications can also benefit from packaging an SMA wire within an existing form constraint. For example, automotive and aerospace applications often require an actuator to be packaged within an existing structure such as an airfoil, a car door, or the engine compartment (Browne, et al., 2004; Kudva, 2004; Kumar & Lagoudas, 2009). Using spooled-packaging to redirect the wire within an existing empty space

enables the addition of actuator functionality without adding additional volume to the structure. In comparison to conventional actuators such as solenoids or hydraulics, which can be bulky and require additional space for compressors or valves, the addition of actuator functionality without high, customizable performance, low cost, and no volume penalty is possible with spool-packaged SMA wires.

5.2.2.1. Problem statement and mathematical model

To demonstrate packaging of SMA wires within a pre-existing form constraint, the methodology for spool-packaged actuators is applied to a single mandrel packaging problem with two types of form constraints – an external envelope surrounding the feasible space and an internal obstacle within the feasible envelope. While the solution of the optimization is specific to the example problem, the technique can be used to design SMA actuators with high, customizable performance and integrated packaging for a variety of applications with different types of form constraints.

The case study examines a single mandrel spool-packaged actuator with the external constraints, internal obstacle, and location and direction of the motion output shown in Figure 3.16 (reproduced in Figure 5.6 for clarity), which are the same as those in the example design space explored in Chapter 3, Section 3.4.2 (Example 3). For the example

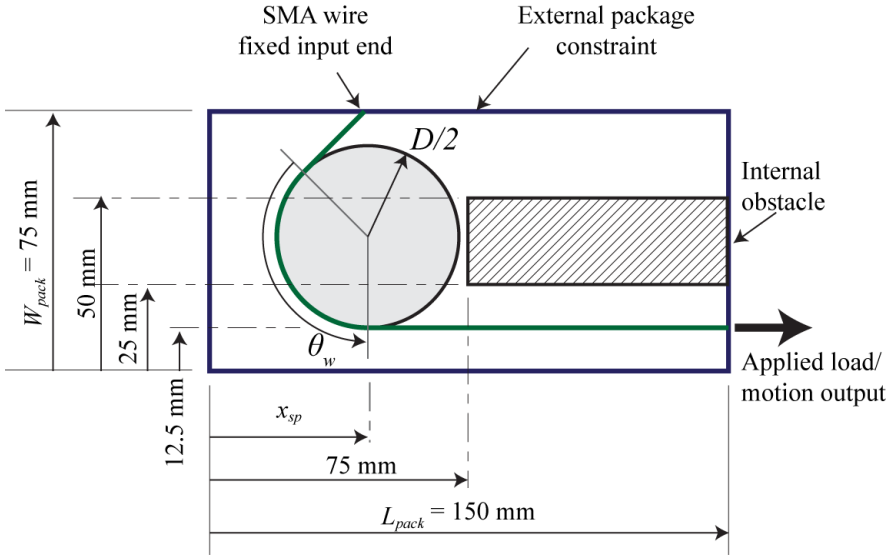

Figure 5.6. Diagram of package envelope and key dimensions for example packaging problems. The packaging problem for a spool-packaged actuator within an external package constraint considers the presence of an external obstical in example 3, while only the external package constraint is considered in example 2.

in the parameter study in Chapter 3, the dependence of a spool-packaged actuator's range of motion was explored across the entire θ_w and $\ell_{tot}^{(0)}$ design space for three different mandrel diameters, which was used to generate plots of performance as a function of a sampling of designs. The same packaging problem is addressed here, but considers the entire three dimensions of the design space with respect to the design variables $\mathbf{x} = [\theta_w, D, x_{sp}]^{\mathrm{T}}$, whereas the design space exploration in Chapter 3 looked design space cross-sections. To provide high performance at reasonable costs while adhering to packaging constraints, an actuator design is sought that balances two objectives: to maximize the range of motion and to minimize the SMA wire length. Additionally, the actuator wire is required to fit entirely within the form constraints with no portions of the SMA wire intersecting the obstacle.

5.2.2.1.1. Objective function

The objective of the design problem, to maximize range of motion and minimize SMA material use, is represented by the expression:

$$\text{minimize} \quad F\{\mathbf{x}\} = -\frac{w_1}{s_1}\delta\{\mathbf{x}\} + \frac{(1-w_1)}{s_2}\ell_{tot}^{(0)}\{\mathbf{x}\}, \qquad \mathbf{x} = [D, \theta_w, x_{sp}]^{\mathrm{T}} \tag{5.11}$$

where w_1 is the weighting on the actuator motion objective with a range of $0 \le w_1 \le 1$, $(1-w_1)$ is the weighting on the SMA wire length objective, and s_1 and s_2 are scaling constants. The actuator displacement $\delta\{\mathbf{x}\}$ is using the multiple mandrel model (Chapter 4) and the total SMA wire length is determined from the design variables (Equation 5.3).

5.2.2.1.2. Constraints

To evaluate actuator designs for feasibility, four criteria were defined with respect to the performance and packaging. While the range of motion is maximized within the objective function, strongly weighting the objective to minimize the SMA wire length can result in actuators with very small displacements. To demonstrate the range of designs where spool-packaged actuators offer benefit over non-packaged, linear SMA wire actuators, a minimum motion constraint is defined. Requiring the minimum actuator

motion to be greater than the motion of a linear SMA wire that occupies the entire length of the form constraint:

$$\delta\{\mathbf{x}\} \geq \delta_{linear} = L_{pack}\left(\varepsilon_{t,out}^{(M)} - \varepsilon_{t,out}^{(A)}\right), \tag{5.12}$$

where δ_{linear} is the motion of a linear SMA wire that occupies the length of the packaging envelope L_{pack}, and $(\varepsilon_{t,out}^{(M)} - \varepsilon_{t,out}^{(A)})$ is the strain difference in the SMA wire under load ($\sigma_{t,out}$ applied at the output) as the wire is thermally cycled between martensite and austenite. Expressing the motion inequality (Equation 5.12) in negative-null form, the minimum motion requirement is defined as

$$g_1 : L_{pack}\left(\varepsilon_{t,out}^{(M)} - \varepsilon_{t,out}^{(A)}\right) - \delta\{\mathbf{x}\} \leq 0, \tag{5.13}$$

where the range of motion $\delta\{\mathbf{x}\}$ is solved numerically.

Defining the length of SMA wire that lies outside the package envelope as $\ell_{v,pack}$ (package violation length) and the length of SMA that lies inside the obstacle as $\ell_{v,obs}$ (obstacle violation length), the packaging constraints are defined as

$$g_2 : \quad \ell_{v,pack}\{\mathbf{x}\} \leq 0, \text{ and} \tag{5.14}$$

$$g_3 : \quad \ell_{v,obs}\{\mathbf{x}\} \leq 0. \tag{5.15}$$

Lastly, to avoid designs in which frictional binding occurs, the wrap angle θ_w is required to be less than the binding angle according to the constraint

$$g_4 : \quad \theta_w - \theta_B \leq 0. \tag{5.16}$$

Assembling the objectives and constraints, the problem is formally defined in negative null form:

$$\begin{aligned}
&\text{minimize} \quad F\{\mathbf{x}\} = -\frac{w_1}{s_1}\delta\{\mathbf{x}\} + \frac{(1-w_1)}{s_2}\ell_{tot}^{(0)}\{\mathbf{x}\}, \qquad \mathbf{x} = [D, \theta_w, x_{sp}]^{\mathrm{T}} \\
&\text{subject to:} \quad g_1 : \quad L_{pack}\left(\varepsilon_{t,out}^{(M)} - \varepsilon_{t,out}^{(A)}\right) - \delta\{\mathbf{x}\} \leq 0 \\
&\qquad\qquad g_2 : \quad \ell_{v,pack}\{\mathbf{x}\} \leq 0 \\
&\qquad\qquad g_3 : \quad \ell_{v,obst}\{\mathbf{x}\} \leq 0 \\
&\qquad\qquad g_4 : \quad \theta_w - \theta_B \leq 0 \\
&\qquad\qquad \text{where} \quad 0 \leq D \leq W_{pack}, \\
&\qquad\qquad\qquad\quad 0 \leq \theta_w \leq \theta_B, \text{ and} \\
&\qquad\qquad\qquad\quad 0 \leq x_{sp} \leq L_{pack}.
\end{aligned} \tag{5.17}$$

In the problem formulation, the ranges of design variables are also defined based on practical constraints. Notably, the range of feasible wrap angles can also be defined with the upper limit equal to the binding angle, which would allow for g_4 to be omitted from the model.

5.2.2.2. Optimization approach

As demonstrated in the third design example in Chapter 3 (Section 3.4.3), the non-convexity of the feasible packaging space causes the design space to be discontinuous and the periodic characteristics of the motion with respect to wrap produce multiple local extrema. Thus, stochastic-based algorithms are suitable for finding the global optimum of spool-packaged SMA actuator designs subject to form constraints. In particular, a genetic algorithm was selected for its ability to explore the entire actuator design space with a lower likelihood of settling on local optima. While use of genetic algorithms cannot guarantee global optimality of an actuator design, they are capable of determining good designs in a reasonable length of time, even for difficult, discontinuous design spaces.

The non-dominated sorting genetic algorithm (NSGA-II, Deb, 2001) was implemented within *iSIGHT* for its ability to seek optimal designs for multi-objective problems and output a Pareto set for which one objective cannot be improved without detriment to another objective. By generating the Pareto set, the attainable set and the tradeoff between large motions and reduced SMA wire lengths can be observed.

5.2.2.3. Results

The objective function (Equation 5.17) was optimized using the NSGA-II algorithm to maximize the actuator's range of motion while minimizing the free length of the SMA wire. In Figure 5.7, the objective values of all feasible designs that were generated are shown with range of motion on the x-axis and the free length of the SMA wire on the y-axis. To compare the resulting designs to the non-packaged case, the length versus range of motion relationship between SMA wire length and range of motion is plotted. For the non-packaged case, the relationship is linear since SMA motion is proportional to wire length for straight wire actuators under constant load. The Pareto set is defined by the

final generation of designs in the genetic algorithm, which lie along the path through the points ①-⑥ in Figure 5.7. As the weighting on the range of motion objective is increased, the slope of the Pareto curve steepens due to the mounting friction losses that come with greater wrap angles needed to package longer SMA wires.

The designs that were generated throughout the optimization converged to a few main groupings, which highlight different types of designs that are optimal depending on the relative importance of each objective. To understand the design groupings and the effect of the design variables on optimality, the design variables from the final generation of the genetic algorithm are plotted with respect to the actuator's range of motion in Figure 5.8. The groupings of designs are the result of particular classes of actuator geometries that best address the objective function and meet constraints. Examples of these designs that occur at key design points along the Pareto set are shown in Figure 5.9. Examining the design variables for the optimal set as δ is varied, the wrap angle groups well, but there is more scatter in the mandrel diameter and spool position, especially for smaller ranges of motion. The scatter results from the range of motion's lower sensitivity

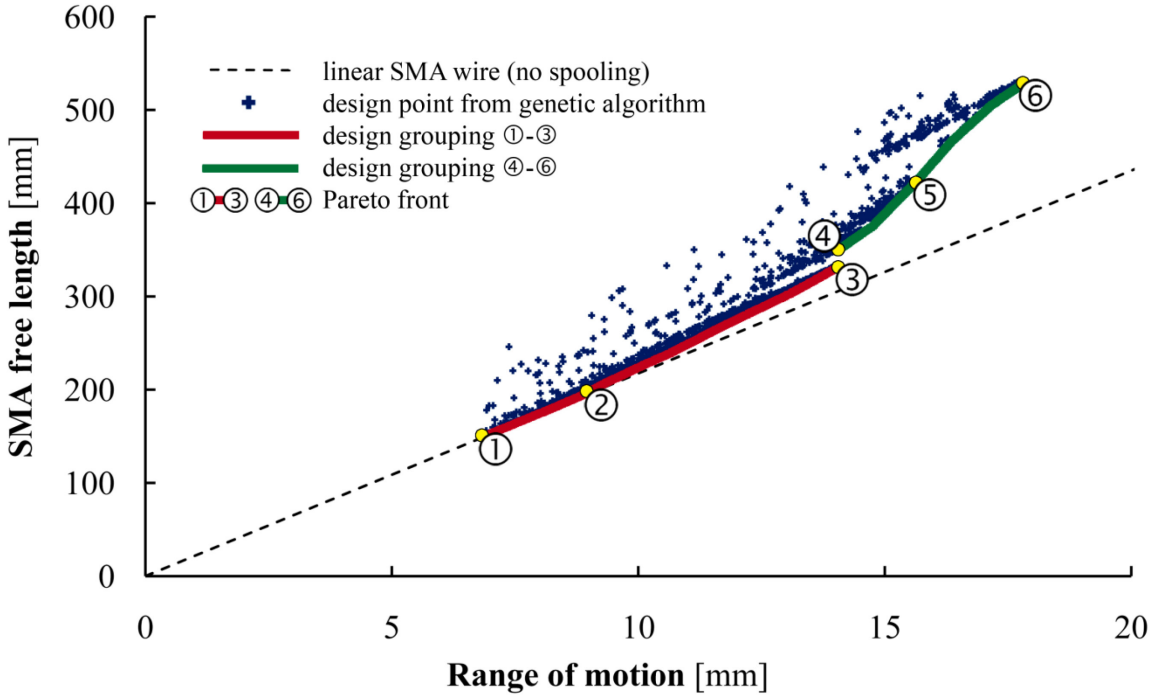

Figure 5.7. Pareto optimal designs for single mandrel spool-packaged SMA actuators within an external package constraint and with an internal obstacle (Case Study 2).

to spool position and mandrel diameter for smaller motions since the losses associated with packaging are lower.

For the single objective minimization of the SMA free length (minimizing the objective function, Equation 5.11, with the weighting $w_1 = 0$), the minimum motion constraint g_1 is active and the best design is the straight wire case (Figure 5.8, design point ①). The straight wire case is approximated by low values of the wrap angle θ_w, which results in the motion being insensitive to the size of the mandrel and the position of the mandrel within the package envelope. As the weighting on the motion objective increases, a longer free length of SMA wire is needed to accommodate larger motions.

Small variations in the weighting between the cost and motion objectives typically lead to optimal designs within a grouping of designs with similar wrap angles and varied spool position and mandrel diameter. For example, increasing the range of motion past $\delta = 9$ mm, there is a sudden increase in the wrap angle from about one quarter of a wrap ($\theta_w = \pi/2$) to a half wrap ($\theta_w = \pi$). While there is a range of feasible designs between the two wrap angles, the motion is more sensitive to changes in wrap angle in this region since small changes in wrap angle cause larger changes in the input tail length as the input sweeps across the upper wall of the packaging envelope.

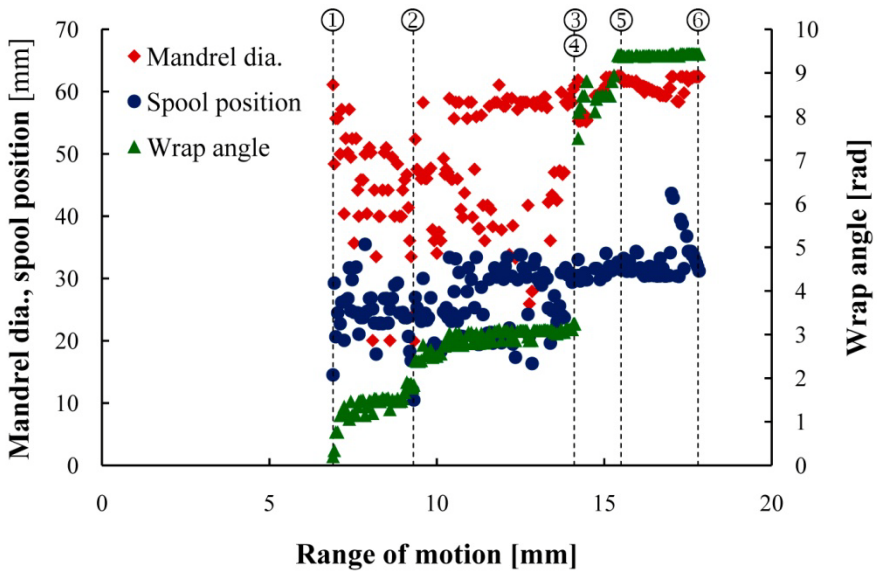

Figure 5.8. Design variables for actuators along Pareto set with respect to range of motion. Key design points that correspond with those on the Pareto front (Figure 5.7) are indicated.

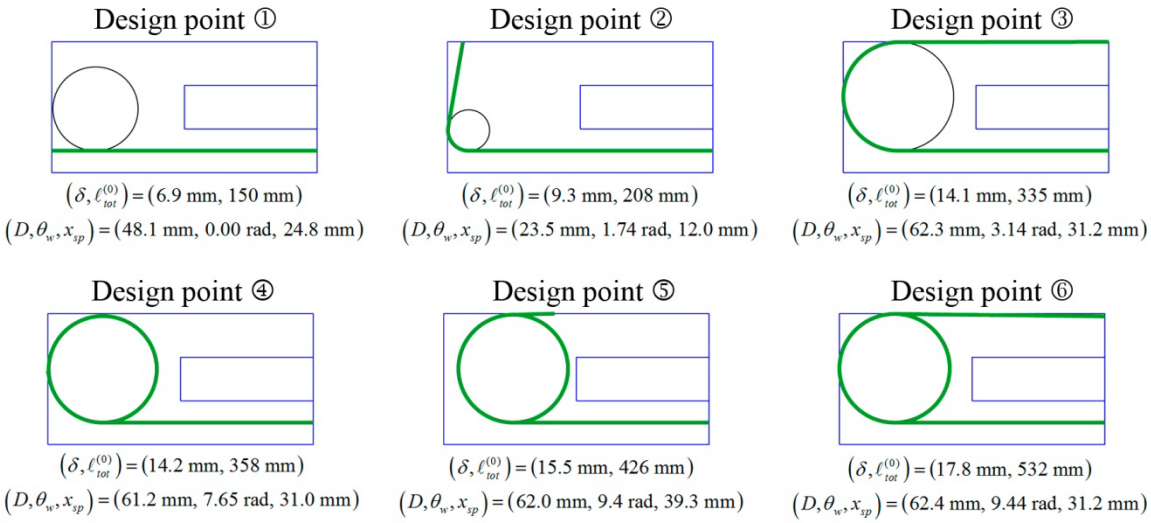

Figure 5.9. Actuator designs occurring at key design points 1-6 along Pareto set.

A discontinuity in the Pareto curve results from the non-convex design space. For motions below δ = 14.2 mm (between points ① and ③), the Pareto set comprises designs that only wrap the mandrel partially – up to about a half wrap. Beyond about a half wrap, the input tail intersects with the obstacle making the packaging constraint g_3 active, which imposes a limitation on how much motion is available from spool-packaged actuators with partial wrapping of the SMA wire for this particular problem. The Pareto front has a jump discontinuity at δ = 14.2 mm (from point ③ to ④), which corresponds to a shift between two groupings of designs. Whereas the objective is minimized with designs that are partially wrapped below δ = 14.2 mm, the partially wrapped actuators are infeasible for δ > 14.2 mm and there is a switch to the next grouping of designs, which have at least a full wrap.

Using the spooling technique with a single mandrel, the range of motion can be tailored to provide up to 17.8 mm, improving upon the 6.9 mm of motion available for a non-packaged SMA wire within the same form constraint. While binding dictates the limit to how much SMA wire can be packaged, the maximum range of motion did not result from an actuator where binding occurs. Rather, the longest non-binding length of the wire that could be packaged enabled the largest range of motion. While the result is specific to the case study, this problem demonstrates the ability to increase motion by packaging longer SMA wires with non-binding configurations.

Within the grouping of designs with at least a full wrap (④-⑥), the range of motion is increased using different combinations of the design variables until the wrap angles converge to about 3π for motions greater than 15.5 mm at design point ⑤. By adjusting the mandrel diameter and the spool position while holding the wrap angle nearly constant, there is additional flexibility in tailoring the range of motion up to its maximum (equivalent to $w_1 = 1$), which has the architecture shown in Figure 5.9, design point ⑥.

The results of the second case study demonstrate the increased range of designs that are available using spooled-packaging, and that the optimal designs span motions between 6.9 – 17.8 mm and SMA wire lengths between 150 – 530 mm depending on the relative importance between performance and cost. By implementing a spooled architecture and optimizing the performance and packaging, the potential motion within the form factor was increased by more than 150%. The increased amount of SMA wire that is needed to produce the larger motions is a design trade-off that can increase the material cost or the amount of energy needed for actuation. Despite the trade-offs, the technique optimizes the material and energy cost related to SMA wire length with respect to performance and makes larger motions available within a limited space.

5.2.3. Case 3: Multiple mandrel actuator, prescribed form constraints

The use of multiple mandrels for spool-packaged SMA actuators allows a greater ability to customize the SMA wire to difficult or unusually shaped form factors. In addition, it has the potential to increase the range of motion available within an existing set of form constraints. To demonstrate the methodology for multiple mandrel spooled-packaging and compare it to the single mandrel approach, this case study applies the methodology to the Case 2 problem (multi-objective function with external form constraint and internal obstacle) for more than one mandrel.

5.2.3.1. Problem statement

In the multiple mandrel case study, a range of optimal designs with minimized SMA free length and maximized range of motion is sought for varied relative weightings on each objective. The multiple-mandrel case study examines a problem with the same

rectangular external envelope form constraint and an internal obstacle with which the SMA wire cannot intersect as in the single mandrel case study (Case 2). The actuator design is fully specified by three design variables per mandrel where $\mathbf{x}$ is a $1\times(3\cdot n)$ vector containing the design variables according to the construction:

$$\mathbf{x}=\begin{bmatrix}\mathbf{x}_1\\ \mathbf{x}_2\\ \vdots\\ \mathbf{x}_n\end{bmatrix} \text{ where } \mathbf{x}_i=\begin{bmatrix}D_i\\ \theta_{w,i}\\ \ell_{lin,i+1}\end{bmatrix}. \tag{5.18}$$

In comparison to the single mandrel formulation, the use of the multiple mandrels enables a greater potential for customization to difficult form factors. However, each mandrel increases the dimensionality of the design space by three, which makes the problem computationally more expensive. While it becomes increasingly difficult for a genetic algorithm to converge to the global optimum for the broader design space, the trade-off between computational expense and potential for customization can be evaluated for particular application needs. In this case study attaining the globally optimal Pareto set is ideal, but cannot be guaranteed with the genetic algorithm. However, viable designs approaching optimality are sought using an algorithm that runs for a reasonable, finite length of time.

5.2.3.1.1. Objective function

As in the previous case study, the objective is to maximize the actuator's range of motion while minimizing the free length according to the expression

$$\begin{aligned}\text{minimize}\qquad & F\{\mathbf{x}\}=-\frac{w_1}{s_1}\delta\{\mathbf{x}\}+\frac{(1-w_1)}{s_2}\ell_{tot}^{(0)}\{\mathbf{x}\}\\ & \text{where } \mathbf{x}=[\mathbf{x}_1,...,\mathbf{x}_n]^{\mathrm{T}},\ \mathbf{x}_i=[D_i,\theta_{w,i},\ell_{lin,i+1}]^{\mathrm{T}},\end{aligned} \tag{5.19}$$

where w_1 is the weighting on the stroke objective, and s_1 and s_2 are scaling factors on the stroke and length objectives. The range of motion is calculated using the multiple mandrel model in Chapter 4. The total SMA wire length is determined based on the actuator design variables (Equation 5.3).

5.2.3.1.2. Constraints

The boundaries of the feasible design space are defined using the same set of four constraints as in the previous case study, which are modified to use the multiple mandrel nomenclature. Assembling the objectives and constraints, the problem statement is summarized:

$$\begin{aligned}
\text{minimize} \quad & F\{\mathbf{x}\} = -\frac{w_1}{s_1}\delta\{\mathbf{x}\} + \frac{(1-w_1)}{s_2}\ell_{tot}^{(0)}\{\mathbf{x}\}, \\
& \mathbf{x} = [\mathbf{x}_1, ..., \mathbf{x}_n]^{\mathrm{T}}, \mathbf{x}_i = [D_i, \theta_{w,i}, \ell_{lin,i+1}] \\
\text{subject to:} \quad & g_1: \quad L_{pack}\left(\varepsilon_{t,out}^{(M)} - \varepsilon_{t,out}^{(A)}\right) - \delta\{\mathbf{x}\} \le 0 \\
& g_2: \quad \ell_{v,pack}\{\mathbf{x}\} \le 0 \\
& g_3: \quad \ell_{v,obst}\{\mathbf{x}\} \le 0 \\
& g_4: \quad \sum_{i=1}^{n}\left|\theta_{w,i}\right| - \Theta_B \le 0 \\
\text{where} \quad & 0 \le D \le W_{pack}, \\
& 0 \le \theta_w \le \Theta_B, \text{ and} \\
& 0 \le x_{sp} \le L_{pack}.
\end{aligned} \tag{5.20}$$

5.2.3.2. Optimization Approach

Due to the discontinuous design space with multiple local optima, stochastic algorithms are called for to explore the design space and find good – if not globally optimal – designs within a finite amount of time. For the multiple objective problem, the non-dominated sorting genetic algorithm (NSGA-II, Deb, 2001), executed within *iSight*, was selected for its ability to generate a Pareto set of optimal designs with varied relative weightings between objectives. While the globally optimal set cannot be guaranteed, the algorithm consistently outputs a similar set of Pareto optimal designs for a given number of mandrels. The main difference between the single mandrel and multiple mandrel cases is the number of design variables used. Since there are $3 \cdot n$ design variables, the complexity of the problem grows with the number of mandrels (n).While the increased number of design variables greatly increases the range of available designs, it leads to higher computational expense within the design algorithm. For more than $n = 2$ mandrels, an initial, feasible design was specified to aid the algorithm in finding more feasible

designs more quickly. To decrease the time to evaluate infeasible designs, the range of motion was not evaluated for designs that violated the external packaging constraint. However, designs that violated the internal packaging constraint were still evaluated because they more closely resembled feasible designs and could aid the algorithm in converging to good feasible designs.

5.2.3.3. Results

To demonstrate the application of the design methodology for multiple mandrel spool-packaged SMA actuators and to gain insights into the benefit of using multiple mandrels, optimal designs were generated for actuators with between one and five mandrels. The data used to define the Pareto sets are shown in Figure 5.10 for which the set of optimal designs follows the data through design points ①-⑧.

As in the single mandrel case, there are several groupings of actuator designs along the Pareto set. For example, between design points ① and ② single mandrel designs with less than a full wrap of SMA wire are optimal. The bounding cases for the grouping are

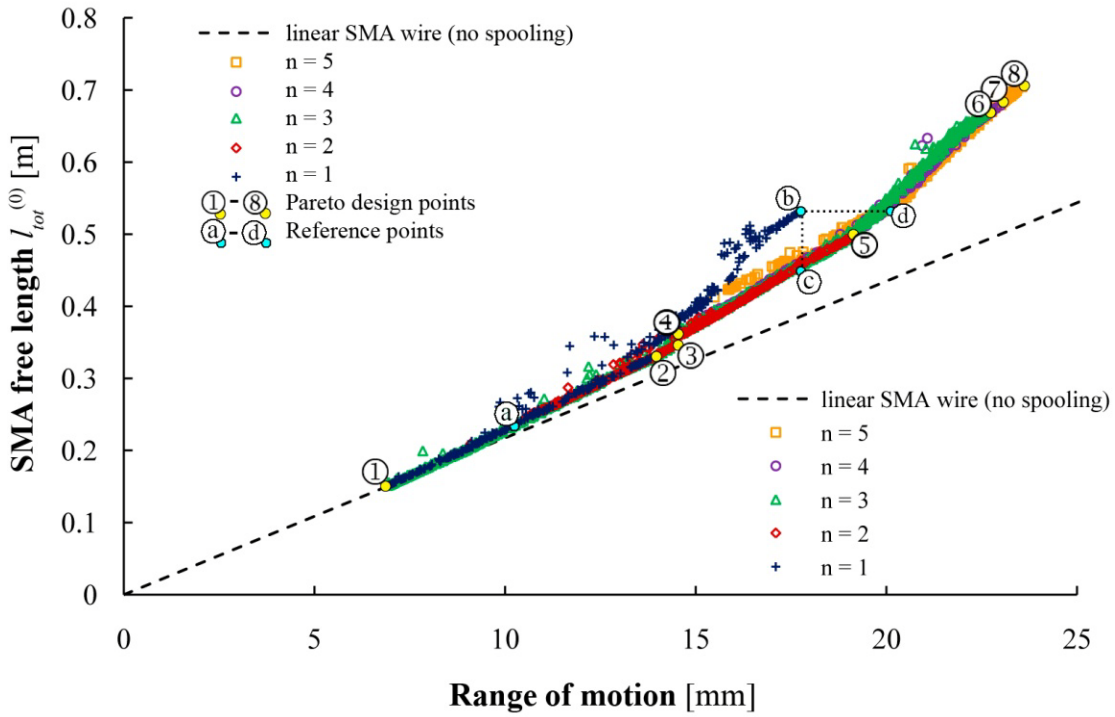

Figure 5.10. Design populations resulting from multiple mandrel optimization using genetic algorithms. The numbered design points trace the pathway along the Pareto optimal set. The lettered reference points highlight notable designs that are discussed within the text.

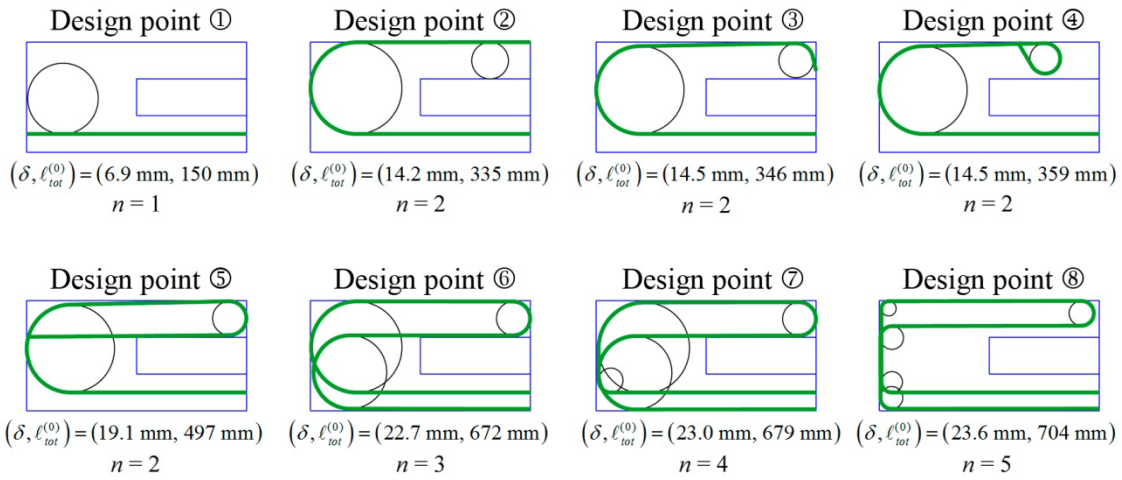

Figure 5.11. Multiple mandrel spool-packaged actuators for numbered designs along Pareto front.

shown in Figure 5.11a and b, where design point ① is for a minimally wrapped, nearly straight wire and design point ② is for an actuator with $\theta_w = \pi$ and the external packaging constraints active. Between points ② and ⑤, actuators with $n = 2$ mandrels are optimal for which the SMA wire partially wraps around both mandrels in the same direction. Moving along the Pareto set from point ② to ③ within the double mandrel design grouping (②-⑤), more motion is achievable by increasing the wrap angle on the first mandrel while a nearly constant wrap angle is maintained on the second mandrel. Increasing the wrap angle for greater motion causes the obstacle packaging constraint to become active at design point ③ (Figure 5.11c). The active constraint makes further increases to motion infeasible by simply increasing the wrap angle on the first mandrel, and the Pareto set jumps to the next best design, at design point ④ (Figure 5.11d). Jumping between designs ③ and ④ due to the activity of the obstacle constraint causes the jump discontinuity in the Pareto set.

Moving further along the Pareto set from point ④ toward higher motion designs, decreases in the wrap angle and placement of the first mandrel further toward the right side of the form factor allows greater motion by adding more SMA wire length until the external packaging constraint becomes active at design point ⑤ (Figure 5.11e). Beyond point ⑤, the actuator motion is further increased by packaging more wire within the form constraint along serpentine pathways. For the final three design groupings, serpentine-

shaped pathways are also favored for n = 3, 4, and 5 mandrels (Figure 5.11f-g). Increasing the motion by adding additional bends to the serpentine pathway, however, is limited by decreasing contributions to motion from each additional serpentine segment as additional wrapping increases friction losses and decreases the change in strain in segments further from the output tail.

Several regions along the Pareto set overlap for different numbers of mandrels. For example, between design points ① and ② there is a close overlap between the n = 1 and 2 mandrel cases. The overlap occurs because the n mandrel case is able to select designs with fewer mandrels by minimally wrapping the SMA wire such that one mandrel is nearly tangent to the SMA wire, or by selecting actuator designs with collocated mandrels. The ability of the design methodology to also predict actuator designs with fewer than n mandrels is demonstrated by considering single and double mandrel cases at reference point *a* in Figure 5.12. For the design generated at reference point *a*, the double mandrel design shown has one mandrel that is wrapped minimally; this design is equivalent to a single mandrel configuration. The design algorithm's ability to generate topologies with lower numbers of mandrels is beneficial since it is capable of exploring designs with fewer mandrels for relative objective weightings where fewer mandrels are optimal. However, the exploration of higher n configurations increases the complexity of the design space and can prevent the algorithm from finding global optima within a reasonable amount of time.

To demonstrate the potential benefit of packaging with more than one mandrel, the

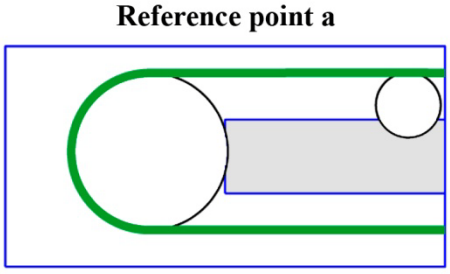

Figure 5.12. The double mandrel actuator generated at reference point *a* shows a double mandrel actuator that is equivalent to a single mandrel actuator.

single mandrel spooled SMA actuator design that produces the maximum range of motion is used as a baseline for comparison (corresponds with reference point *b* in Figure 5.10 and is diagrammed in Figure 5.13). Comparing the single mandrel actuator to other multiple mandrel actuators with the same amount of motion, the use of a second mandrel can reduce the length of SMA wire by 13.5% - and thus reduce the associated material and energy costs. The double mandrel actuator with reduced material use is represented by reference point c in Figure 5.11, and diagrammed in Figure 5.13. Next, the same single mandrel actuator is compared to multiple mandrel actuators with the same SMA free length. By using three mandrels and packaging the SMA wire along a serpentine pathway, the actuator motion can be increased by 11.2% with no additional material costs. The enhanced triple mandrel design is represented by reference point d in Figure 5.11, and is diagrammed in Figure 5.13.

The results of the multiple mandrel study demonstrate that the design methodology can be applied to problems where that packaging of an SMA wire needs to be tailored to a form factor. Relative to spooled-packaging around a single mandrel, the use of multiple spools can expand the amount of motion that is available within a form factor. The

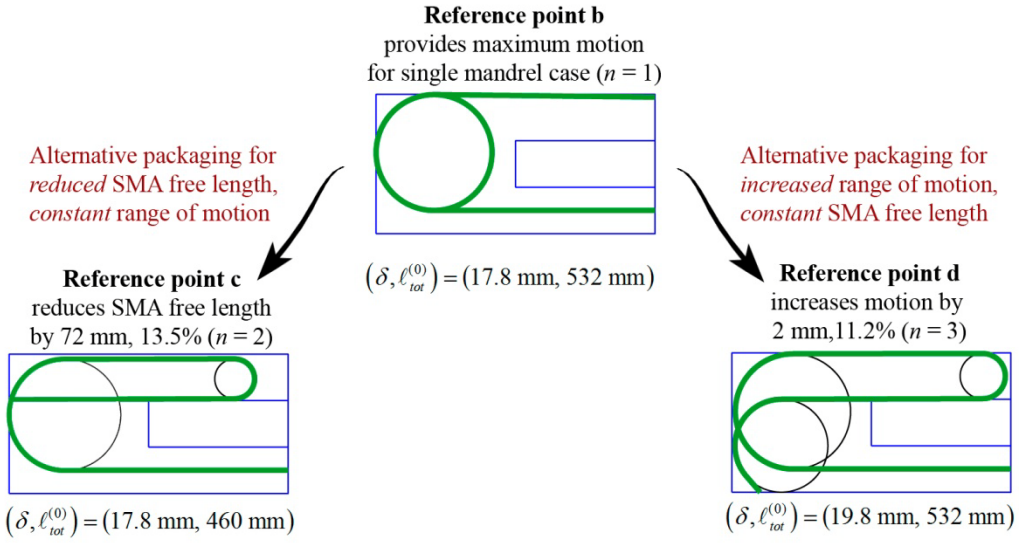

Figure 5.13. Comparison of single mandrel actuator to multiple mandrel actuators with similar motion or SMA free length. The spool-packaged actuator shown for reference point b provides the maximum motion that a single mandrel actuator is capable of producing, but with alternative multiple mandrel architectures the amount of motion can be increased and the SMA free length can be reduced.

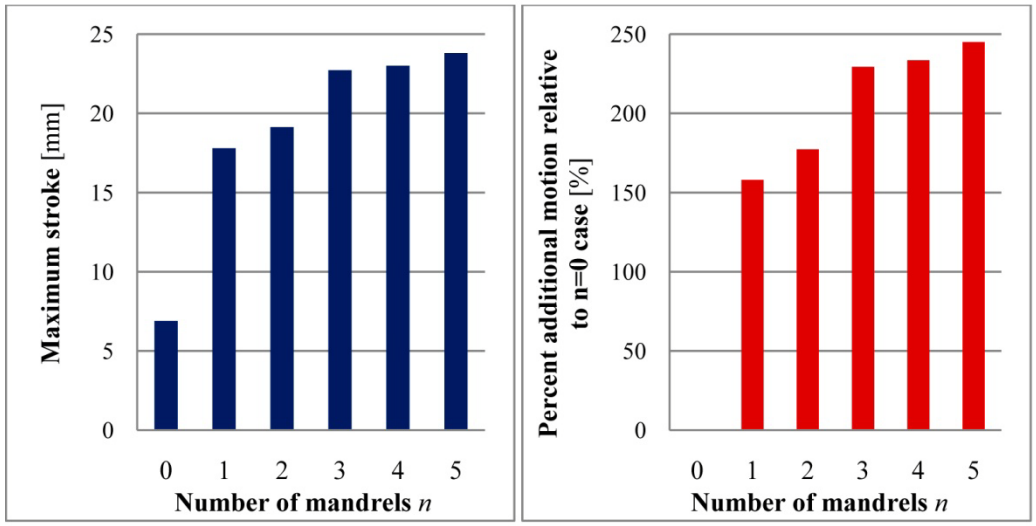

Figure 5.14. Additional motion available for multiple mandrel spool-packaged SMA actuators. The maximum motion that spool-packaged SMA actuators can provide (left) increases with the number of mandrels used to package the SMA wire. Additionally, the percentage of additional motion through the use of multiple mandrels was determined from the data (right) potential motion increases up to nearly 250% compared to a non-spooled SMA wire within the same form constraints.

increasing range of motion for use of multiple mandrels is shown in Figure 5.14a and the improvement relative to the linear, non-packaged SMA wire is shown in Figure 5.14b. Examining the maximum motion available for n = 0 through 5 mandrel actuators, the use of a single spool increases the available motion by 150%, and the level of improvement rises through the serpentine packaging of SMA within the form constraint; designs with up to 240% more motion than in the non-packaged case were generated throughout the multiple mandrel actuator design process.

5.3. Conclusions

Building upon the predictive models for spool-packaged SMA actuators, this chapter developed and demonstrated a methodology for synthesizing high performance, low cost actuators within highly customizable form factors. In Chapter 3, the potential complexity of the design problem was demonstrated for single mandrel actuators within a packaging constraint, for which simple objective functions (range of motion and SMA wire length) were discontinuous with multiple local minima and maxima across the design space. Facing an increasingly complicated problem for multiple mandrels due to the large number of design variables, the methodology described in this chapter provides a

systematic technique for actuator synthesis. While the methodology can be adapted to a variety of problems defined by their particular performance, packaging, and cost requirements, the synthesis of optimal designs is based on three steps within an iterative process: 1) selecting the actuator design variables that define its topology and geometry, 2) determining the pathway of the SMA wire through Cartesian space and evaluating package- and cost-related objectives and constraints, and 3) determining the actuator's range of motion and evaluating performance-related objectives and constraints.

The design methodology was demonstrated for three case studies with different types of form constraints and allowable topologies. The first case study was chosen to show how the design methodology can reduce packaging dimensions while mitigating costs even in the absence of specific packaging constraints. A range of optimal designs was generated by first varying the relative weighting on the cost and performance objectives, and then optimizing, which influenced the resulting designs. The resulting Pareto set was composed of two discrete design groupings, a result that helped build intuition on the selection of design strategies for managing performance and cost. For problems where compact packaging is a priority, square-shaped form factors were favored, and the cost/performance tradeoff was modulated by varying the size of the packaging envelope. For problems where cost reduction is of priority, more slender form factors are preferable with lower cost achieved as designs similar to the non-packaged case become favored.

The second case study was selected to demonstrate the design methodology's ability to tailor SMA wire to a non-convex form constraint by packaging around a single mandrel, also while maximizing performance and minimizing cost. Actuators were specified using three design variables regarding the mandrel diameter, wrap angle, and spool position within the footprint. Design optimization was performed using a genetic algorithm (NSGA-II) to generate the set of non-dominated optimal designs subject to a minimum motion constraint, two packaging constraints, and a constraint to prevent binding. Analyzing the resulting optimal set of designs, a few design groupings emerged

depending on the relative weighting of the performance and cost objectives. For example, for an actuator providing up to 14 mm of motion, partially wrapped designs with wrap angles below $\pi/2$ radians are optimal. For more motion, however, actuators with at least a full wrap of SMA wire are optimal. The different groupings are representative of strategies for trading off performance and cost, which depend on the relative weighting on each objective, or the amount of motion that a particular application requires. For moderate increases in motion relative to the non-packaged actuator (up to double the motion, in fact), designs with a partially wrapped mandrel were favored. Further increases in required motion led to a second grouping of designs where the wire is wrapped at least once. The different groupings demonstrate an evolving trade-off relationship between performance and cost that depends on the preference of objectives. Moreover, the study demonstrated that for non-convex spaces, activity of the packaging constraints leads to groupings of designs that experience more friction losses to maintain feasible packaging.

The third case study addressed a similar problem to the previous case, but also explored the ability of multiple mandrel actuators to increase the potential for form customization. The same packaging constraints and objective functions were used as in the previous case, but the algorithms for building geometry and evaluating motion and packaging constraints were augmented to accommodate up to 5 mandrels. By repeating the optimization for each number of actuators and superposing the resulting Pareto sets, a broader range of designs resulted that were capable of more motion. By designing with more mandrels, 33% more motion was available than for a single mandrel. Upwards of 240% more motion was available relative to a non-packaged linear SMA wire within the same form constraint. As in the previous case study, different groupings were optimal depending on the relative weightings on the cost and performance objectives. Tracing the optimal designs as the performance objective was weighted more strongly, different serpentine pathways were used to package the longer SMA wires. The serpentine strategy was effective in increasing motion because more SMA wire can be packaged with the addition of cumulative wrap angle – and the accompanying friction losses. Because of

these friction losses, a limit to the serpentine strategy was approached as the addition of more segments demonstrated diminishing returns.

The design methodology developed in this chapter demonstrates the potential for customization of spool-packaged SMA actuators to the performance and form requirements of an application while minimizing the SMA-related costs. Whereas SMA actuators are often limited by difficulty in packaging long lengths of wire in limited spaces, the technique and methodology for designing spool-packaged actuators enable more compact packaging and a robust capacity to integrate SMA wires within existing spaces. The methodology and case studies in this chapter are a starting point for engineers to design compact or customized actuation for particular application needs, and can be tailored with different performance, packaging, and cost requirements and problem objectives.

Chapter 6. Conclusions

Shape memory alloy actuators present an opportunity for developing high performance, low-cost actuation. However, the difficulty in packaging the material within practical form constraints has been one of the key impediments that have limited the application space of SMA actuation in products on the market. To realize the performance and cost advantages of SMA, the goal of this dissertation was to develop the scientific knowledge base for spooled packaging of low-cost SMA wire actuation that enables high, predictable performance within compact, customizable form factors. This goal was attained by achieving each of four main objectives:

1. Derive a quasi-static, analytical model for the mechanics governing a single mandrel spool-packaged SMA actuator that predicts work performance with respect to the specifiable actuator geometry, material properties within the system, and the applied loads while accounting for friction and bending,
2. Build an understanding of how actuator design parameters and packaging constraints influence performance, to facilitate the design of spool-packaged actuators through all the synthesis and analysis stages,
3. Expand the spooled-packaging technique to multiple mandrel actuator topologies by defining a parameterized architecture and developing an expanded model that enables design of actuators within customizable forms,
4. Develop and demonstrate a model-based design methodology that enables engineers to synthesize spool-packaged SMA actuators with forms and performances that can be customized to specific application requirements.

By pursuing and accomplishing these objectives, this research led to several outcomes that expand the ability to predict, understand, and design spool-packaged SMA actuators. This chapter reviews the main outcomes of the dissertation and its contributions to the field of actuation.

6.1. Research overview

Actuators provide essential mechanical functionality for technologies across society. The advancement of these technologies is often coupled to advancements in actuation, fueling a demand for high performance, low cost actuators in industry. In Chapter 1, a review of the state-of-the-art in actuation highlighted the potential for SMA to improve the cost and performance of technologies that currently rely on conventional actuators, and to enable new capabilities for products that had not been possible by conventional means. While SMA can deliver moderate to large forces and displacements using small volumes of material, they are difficult to package within practical form factors. Spooled-packaging of SMA wires has been used to overcome form factor limitations, but to date its implementation has been *ad hoc* and only successful on a case-by-case basis. Without a well-defined packaging strategy, an understanding of how the design of spool-packaged actuators affects performance, and a methodology for the systematic synthesis of spooled actuator designs, it is difficult to design actuators that behave predictably and to mitigate losses that accompany the use of this packaging technique.

6.1.1. Spooled-packaging approach

In this dissertation, spooled-packaging was developed at a level of rigor that can enable its use on a broader scale. By looking at how spooled-packaging could address a large class of problems rather than a specific application, several research issues emerged. To provide the analytical foundation for design, a model was needed to predict the range of motion of spool-packaged actuators that accounts for losses relating to the packaging technique. To implement the technique skillfully and make meaningful design choices, an understanding of how actuator design influences performance was necessary. To realize the potential for robust form customization, the technique and model needed to be applicable to a broad range of actuator topologies. Additionally, a systematic approach to spooled actuator design was necessary to meet the widely varying possibilities of form constraints and performance requirements while mitigating costs associated with the spooling technique.

Approaching the packaging technique as a solution to a class of application needs, a generalized architecture was defined based on four key components: an SMA wire, a fixed input where the SMA wire connects to mechanical ground, one or more ground-fixed cylindrical mandrels, and a rotational or linear single degree-of-freedom motion output. The generalized architecture was defined to be inclusive of a broad spectrum of designs with an array of user-specifiable parameters regarding the actuator's topology, geometry, applied loads, friction properties, and SMA material parameters. In Chapter 2, the architecture was defined for single mandrel actuators to establish the key components and design variables that needed to be represented in predictive models of performance. With the single mandrel architectures, the specification of actuators with compact packaging was possible, for which large SMA length dimensions could be reduced substantially. Expanding the spooling technique in Chapter 4, the use of multiple mandrel architectures enabled robust form customization to the most difficult form constraints. However, to expand the use of spooled-packaging beyond specific applications, the multiple mandrel architecture provided in Chapter 4 enabled the specification of any two-dimensional SMA actuator comprising a series of linear and arc-shaped segments of SMA wire. By approaching the spooled-packaging technique as a solution to a class of problems needing low-cost, high performance actuation within customizable forms, this dissertation developed a language for describing actuators with potential for broad application.

6.1.2. Analytical models

To provide a foundation for the analysis, understanding, and synthesis of spool-packaged actuators, a predictive model was derived that relates the actuator's topology, geometry, applied load, frictional parameters, and SMA constitutive behavior to its range of motion. Anticipating that the actuator design process would rely on optimization algorithms and iterative calculations of the range of motion, model simplicity was sought where possible without making undue sacrifices to rigor and accuracy.

6.1.2.1. Single mandrel spooling model

To identify and predict how packaging affects performance, the model was derived for the basic single mandrel architecture in Chapter 2. By assuming a simplified material behavior, the effects of packaging were isolated from complexities of the SMA material that result from factors such as material composition, stress-strain history (shakedown), and dynamics of phase transformation. The effect of friction between the SMA wire and mandrel was modeled based on assumptions of static Coulomb friction and unilateral motion, ensuring that the entire wire is extending or contracting in a given state. The effect of bending was also including by modeling the impact of the modified stress distribution across the SMA wire's cross-section on the centroid strain given the non-linear stress-strain behavior of SMA. Relating the centroid strain across the length of the SMA wire to the *State 0* free length, a compatibility condition was defined. The compatibility approach was necessary to ensure that all portions of the wire were accounted for when integrating strain across the length – including those portions that gain and lose contact with the mandrel during operation. Solving the compatibility equations for the total SMA wire length in *States 1* and *2*, the range of motion could be determined.

To demonstrate the model's ability to predict the range of motion of physical actuators, an experimental validation study was performed in which the range of motion was measured and compared to theory for actuators with varied geometries, loading conditions, and types of output motion (rotational or linear). In applied load experiments, the shape and form of the data was predicted well by theory, demonstrating the actuators' load-displacement characteristic curves to be deformations of the SMA stress-strain curves. Errors of the model's prediction were within a reasonable range: 3.4% average error for linear actuators and 9.0% average error for rotational actuators. The predicted bending effect was verified experimentally examining the ranges of motion of actuators with a range of wrap curvatures. Actuators with small wrap curvatures (large wrap diameters relative to the SMA wire diameter) demonstrated negligible losses from bending, and larger curvatures (for smaller wrap diameters) suffered greater losses as the

centroid strain was depressed due to increased bending. For tighter wire curvatures with the mandrel diameter less than 130 times the diameter of the SMA wire, the bending strains began to degrade performance noticeably. By including bending in the model, the experimental error was reduced from 13% to 8.3%. The complete spooling model's ability to predict motion loss with increasing bending strains is also beneficial for using the model for actuator design. Whereas the friction-only model places no penalty on the performance of very tightly spooled actuators, the complete spooling model is able to capture the tradeoff between higher performance and tighter packaging, further enhancing the model's ability to support analytical, model-based actuator design. Finally, the predicted binding behavior was demonstrated in experiments that varied the amount of packaging. The experiments demonstrated that any SMA wire wrapped beyond the binding angle did not contribute motion to the actuator, that the approximate binding angle could be identified, and suggested that binding configurations should be avoided in physical actuators to prevent unnecessary performance losses. In the particular experiment (and for the selected applied load, SMA material properties, and friction properties), binding was predicted to affect actuators with wrap angles greater than approximately 1.4 – 1.9 wraps. By selecting lower friction mandrel materials the wrap angle can be increased, thus expanding the range of available designs for application.

6.1.2.2. Multiple mandrel spooling model

To enable more customizable packaging, the spooling technique was expanded to multiple mandrel architectures in Chapter 4. The multiple mandrel model was derived by considering the same key effects of friction, bending, and binding, which were developed and demonstrated for single mandrel spooled actuators. However, the multiple mandrel model also had to predict the effect of cumulative wrapping on adjacent mandrels and to formulate the strain variation function for actuators with a variable number of wrapped and linear segments.

Expanding upon the single mandrel model, an indexing convention was implemented for an array of variables used to describe the pathway of the wire. An

additional variable for cumulative wrap angle was introduced to relate the impact of wrapping SMA wire around a mandrel to the strain variations of the neighboring segments. The compatibility formulation was expanded to the multiple mandrel architecture to ensure that the different strain functions were applied appropriately across the entire wire throughout operation, including those segments that gain and lose contact with the mandrels as the SMA wire changes phase.

To verify that the mechanics of single mandrel spool-packaged actuators extend to multiple mandrel configurations, an experimental study was conducted, successfully demonstrating the validity of the expanded model. In experiments varying the number of discrete wrapped segments with wrap angles of $\theta_{w,i} = \pi/2$ radians, the experimental data was bounded by theory for the expected range of friction ($0.1 < \mu < 0.15$). The data fit the model well in magnitude with 1.6% average error between the data and the best-fit theory line, which occurred at $\mu = 0.14$. The prediction was valid for both binding and non-binding designs. In a second set of experiments, the range of motion was tested as a function of applied load for a non-binding actuator with two half-wraps ($\theta_{w,i} = \pi$ radians) and a binding actuator with four half-wraps. The data matched theory well in form, and was most accurate for higher stresses. For applied stresses above the martensite plateau the theory demonstrated 3 – 6% average error, while for data points with martensite stresses below the plateau, the average error was about 20%. The model inaccuracy at low stresses was attributed to the strain being more highly sensitive to stress below the martensite plateau, causing any inaccuracy of the constitutive model to be amplified for low stress. Fortunately, SMA actuators are typically designed to operate at stresses above the plateau where the error is lower to take advantage of the greater strains, and thus, operate with a greater range of motion.

6.1.3. Understanding of parameter effects

To develop a deeper understanding of how the performance of spool-packaged actuators is influenced by design choices and packaging constraints, a parameter study was conducted in Chapter 3. Exploring the effects of geometry, load, and friction using

model-based simulations and select experimental studies, a knowledge base was developed that provides insights into the impacts of packaging on performance.

6.1.3.1. Geometric effects

While the spooled-packaging technique encompasses a broad range of actuator designs, the multiple dimensions of tailorability complicate the task of parameter selection. To develop an understanding of how packaging and performance are related, parameter studies of wrap angle, spool position, and mandrel diameter were conducted.

6.1.3.1.1. Wrap angle

Wrap angle plays a critical role in defining the extent to which spooled-packaging is used. Furthermore, the wrap angle impacts the amount of SMA wire needed to meet performance requirements, and modulates how compactly the SMA wire is packaged. To understand how wrap angle can be used to modulate performance within a constant form constraint, actuators with constant package lengths and variable wrap angles were explored. Experimental simulations demonstrated that significant increases to performance are available without increasing the actuator's package length, but at increasing cost. For any package length, spooling could add a set amount of motion, which is limited by the onset of binding. For short packages, the amount of extra motion was significant. Up to four fold increases in motion were demonstrated for actuators with a moderate friction coefficient (μ = 0.1) and a moderate mandrel diameter (25 mm). However, the longer wire length that could be accommodated within the package suffered substantial losses as well – up to 35% in the study. From these results, the ability to increase performance and effective package strain by increasing wrap angle was demonstrated. These increases were available up to a limit, defined by the binding condition. The most compact actuators encountered the greatest losses relative to the length of SMA wire packaged.

Considering wrap angle from an alternative perspective, constant length SMA wires with variable wrap angles were also examined. The simulations demonstrated that spooled-packaging can lead to significant improvements to packaging dimensions. The

trade-off of performance increased at a faster rate with more wrapping until the binding threshold was surpassed. Increasing the wrap angle of a constant length SMA wire beyond binding was shown to be inadvisable since further wrapping causes portions of the actuator to contribute no motion at all. In this particular case study, reductions in package length up to 70% were demonstrated with motion losses between 15-30% due to friction. For long wires, the reductions in package length were limited by the onset of binding, while in shorter wire the reductions were limited by how much wire could feasibly be wrapped around the mandrel. Both studies of wrap angle demonstrated the tradeoffs between improved package dimensions and higher performance, the increasing and intensifying friction losses that result from larger wrap angles, and the limitation on packaging due to the onset of binding.

6.1.3.1.2. Spool position

Examining the effect of spool-position within the form constraints, the design study demonstrated that higher ranges of motion are available for actuators with the mandrel placed closer to the fixed input. For the range of designs explored, the motion was linearly dependent on the position of the spool along the SMA wire. Depending on the wrap angle, a 100 mm variation in the spool position could increase the stroke by 1.5 – 3.9 mm without incurring any additional material costs. Across the range of available spool positions for the non-binding configurations of actuators, 30 – 100% increases in motion were demonstrated by moving the spool from the output end of the wire to the input end. The study lead to a guideline to place the mandrel as closely to the input as the packaging constraints allow due to the downstream effects of friction acting on portions of wire toward the actuator's input end.

6.1.3.1.3. Diameter ratio

The effect of bending was explored by examining a range of actuators with variable wrap curvatures. To isolate the effect of bending, actuators were examined with the same SMA wire diameter, variable mandrel diameters, and all other dimensions proportional to the mandrel diameter. To compare the proportionally sized actuators with variable

amounts of bending, the ranges of motion were normalized to the mandrel diameter. As a result, any variation in the normalized range of motion can be attributed to bending strains, which depress the centroid strain in the wrapped portions of the SMA wire. Bending was found to have a negligible effect for actuators with small curvatures (large mandrel diameters); deviations between the friction-only model and the full friction-and-bending spooling model were less than 2% for mandrel to SMA diameter ratios greater than 100 ($\bar{D} > 100$). For tighter wrap curvatures, the impact of bending increases with deviations between models greater than 5% for $\bar{D} > 60$, greater than 10% for $\bar{D} > 40$, and greater than 20% for $\bar{D} > 20$. However, whereas the effect of friction at a given location affects the strain variation between the given location and the input end of the wire, bending only affects the strain locally. Therefore, the impact of bending can be mitigated by decreasing the wrap angle.

6.1.3.2. Applied stress effects

To use the recoverable strain of SMA to its full potential, an understanding of how applied stress effect performance was needed. Even for applications where the external load is specified, applied stress can be targeted by based on decisions that affect the SMA's cross-sectional area (for example, through selection of wire diameter or the use of multiple SMA wires). Applied stress was explored both experimentally and in simulations, which resulted in motion versus load curves with shapes resulting from the martensite stress-strain profile. Across the range of wrap angles (0 – 20 radians) and diameter ratios (30-240), there was a steep region where the motion was more sensitive to applied load, which corresponded to the martensite plateau between about 40-60 MPa stress. Looking more closely at the relation between loss and applied stress, the distribution of strains on the martensite plateau was observed to have an important effect that impacts potential designs. Since friction has downstream effects on the strain difference in the wire as it transitions between martensite and austenite, selecting stresses and strains that are sufficiently higher than the plateau was deemed important to reduce friction losses. In general, friction losses decrease with applied load. Thus, larger loads

are desirable, but within reason: the maximum strain in the wire also needs to be evaluated based on the expected cyclic usage of an actuator.

6.1.3.3. Material effects

Friction is typically the central source of loss in spool-packaged SMA actuators. Thus, its effect on the performance and the binding limitation were explored in the parameter study. From the model, friction is known to cause increased losses for larger wrap angles and larger coefficients of friction. Using the model in the parameter study, the motion was generated for actuators with a range of friction coefficients from very low to high (μ = 0.01 – 0.5) and wrap angles up to 20 radians. Across these ranges, a relatively narrow space of actuator designs avoids binding: those with low coefficients of friction or low wrap angles. Since friction plays such a large role in performance loss, this study demonstrated the critical importance to reduce friction in the selection of mandrel materials when possible. Since other factors such as cost, strength, consistency of friction properties, temperature range, and electrical insulating properties also impact material selection, several types of materials that can be used for mandrels were discussed.

6.1.4. Design methodology

To enable the design of low-cost, high performance SMA actuators that can be customized to difficult, unusually shaped form constraints, a design methodology was developed in Chapter 5. The design space explorations in Chapter 3 provided insight into the importance of a design methodology. For three different cases with varied packaging and performance requirements, the single mandrel model was exercised across three design variables (spool position, mandrel diameter, and SMA wire length) to demonstrate how packaging can influence actuator design and performance. Even for a relatively simple case in which a single mandrel actuator was packaged within a convex rectangular form constraint (Case 2, Chapter 3), the design space was irregular with multiple local extrema and discontinuous derivatives of the range of motion with respect to the design variables. Adding internal obstacles to the packaging constraint (Case 3, Chapter 3)

created a non-convex packaging footprint, and the already irregular design space became discontinuous as well. The complexity of the design space for only one mandrel provided motivation for the need for a design methodology that could be used to explore and evaluated designs across large design spaces. As the number of design variables increases for multiple mandrel configurations, a systematic technique for design becomes even more important.

The design methodology developed in Chapter 5 provides a framework for specifying design objectives and constraints with regard to cost, performance, and packaging, and applies optimization techniques to seek desirable, if not optimal, design characteristics. The methodology was constructed to allow it to be adapted to a variety of problems defined by objectives and constraints related to performance, packaging, and cost. Once the design problem is fully defined, the design proceeds based on three main steps within an iterative process. 1) For the particular iteration, design variables are selected (three design variables per mandrel), which define the actuators topology and geometry. 2) The pathway of the SMA wire through Cartesian space is determined, and the package and cost related objectives and constraints are evaluated. 3) The actuator's range of motion is determined, and performance related objectives and constraints are evaluated. Completing the three steps within each design iteration provides information for the optimization algorithm to generate new designs and continue iterative design improvements.

In the design process, many designs need to be explored and evaluated, and the use of multiple mandrels increases the number of interacting design variables that are needed to specify actuator geometry and topology. Additionally, design optimization of spool-packaged actuators is not straightforward because the actuator motion cannot be represented with closed-form equations, and thus are computed numerically to satisfy the compatibility equations. This dissertation provides the models for solving the range of motion, but also guidelines (in Chapter 2) to aid in computation of the compatibility equations for increasing computational speed.

The design methodology was demonstrated for three cases to demonstrate application of the spooling model for synthesis and to provide a template for the design of well-packaged SMA actuators with high performance and mitigated costs. The first case study was chosen to demonstrate how the design methodology can reduce packaging dimensions while reducing costs even in the absence of specific packaging constraints. The multi-objective minimization of SMA wire length and the package perimeter was approached using a sequential quadratic programming (SQP) algorithm to generate a set of Pareto optimal designs across the range of relative weightings on each objective. The resulting designs demonstrated two potential strategies for realizing reductions in cost or size of the actuators, and the proper strategy depending on the relative weighting of the cost and performance objectives. For low cost actuators, slender rectangular actuator form factors were preferred to maximize the length of non-packaged SMA and reduce cost by avoiding friction losses. For very compact actuators, square shaped form factors were preferred, for which nearly the entire wire is wrapped around the mandrel.

The second case study was selected to demonstrate the methodology's application to non-convex form constraints for the most basic single mandrel case. Cost, represented by the SMA wire length, was minimized and performance was maximized using the non-dominated sorting genetic algorithm (NSGA-II) for a multi-objective function. The optimization resulted in a set of Pareto optimal designs that increased the available range of motion up to 17.8 mm from the 6.9 mm of motion available for a non-packaged SMA wire within the same space. Different groupings of designs emerged, which could be construed as strategies for trading off performance and cost by varying design variables within the grouping. In the example, optimal actuators providing less than 14 mm of motion had the SMA wire wrapped partially around the mandrel, while actuators providing more than 14 mm had had at least a full wrap. The design groupings demonstrated the strategy of minimizing friction losses by using smaller wrap angles, but that strategy becomes limited for larger ranges of motion.

The third case study approached the same problem, but demonstrated multiple mandrel actuator synthesis for its enhanced ability tailor the SMA's pathway within the form constraint. By also examining multiple mandrel designs, the third case study was able to demonstrate larger ranges of motion: 33% more motion than was available for single mandrel actuators, and 240% more motion than for non-packaged SMA wire. Several groupings of designs were identified in the Pareto set. For smaller ranges of motion, optimal designs relied on limited wrap angles and fewer mandrels to minimize losses. A strategy of packaging the SMA wire along serpentine pathways enabled the larger ranges of motion. However, due to the accumulation of friction as cumulative wrap angles increase, there is a limit on the maximum motion available with the use of serpentine packaging. Even so, with the design methodology the maximum potential for SMA wires can be realized within confined spaces.

6.1.5. Future work and limitations

By developing the spooled-packaging technique, this dissertation enables the design of SMA actuators that are not limited by difficult packaging. However, there is potential to expand upon this initial work to meet the needs of an even greater range of applications.

6.1.5.1. Fatigue

To use spool-packaged SMA actuators with a high level of confidence over many cycles, a study of the fatigue life is necessary. Thermal transformation fatigue for NiTi is still an active area of research, and has been studied most broadly for cyclic uniaxial loading. However, fatigue experienced under the coupled bending/tensile loading that occurs in spooled SMA wires increases the complexity of the fatigue problem. Thus, while the thermal transformation fatigue of SMA is an active area of research and a concern as the mandrel diameter decreases, it was beyond the scope of this dissertation. One strategy to avoid low-cycle fatigue failure is to limit the maximum strain in the wire, which occurs at the outer edge of the wrapped SMA wire, according to uniaxial strain guidelines for fatigue. The maximum strain is predictable using the model in Chapter 2.

By including a constraint for maximum strain in the design synthesis (augmenting the constraint sets defined in Chapter 5), longer cyclic fatigue lifetimes are possible. Dynalloy, the manufacturer of Flexinol brand NiTi, recommends maximum strains below about 4% for millions of life cycles to avoid fatigue (Dynalloy, 2010). Guidelines that are more conservative are also available, limiting strain to 2.5% to avoid fatigue (Churchill, 2009). There are additional effects that could impact the fatigue life for SMA wires under tensile and moment loading that are not present in the uniaxial case. Therefore, experimental validation is also recommended for applications using spool-packaged SMA actuators for many cycles to observe the onset of fatigue, either structural or functional.

6.1.5.2. Alternative architectures

The foundational understanding of how spool-packaged actuators are influenced by friction, bending, and binding can also be expanded to alternative architectures, enabling an even broader range of packaging possibilities. While the model and geometry building algorithms were developed for actuators within a two-dimensional plane, the same mechanics are expected to apply for SMA wires directed along three-dimensional pathways.

The model can be expanded to include non-circular mandrel surfaces as well. In the current model, the curvature of wrap is fixed for each mandrel, but constant wrap curvature term can be replaced with a function representing a wrap curvature that varies with the position on the mandrel. Using non-circular mandrels, there is yet greater potential to customize SMA pathways to the most difficult to meet form constraints. Additionally, using non-circular pathways, surfaces can be fabricated as part of the product that SMA does work on to precisely guide the wire within the available form factor. The ability to model and synthesize non-circular mandrels can be applied to cams with sliding surfaces for the SMA wire to tailor the moment arm of rotational motion actuators for desirable performance characteristics. For example, the use of cam surfaces can enable “reverse-bias” loading on the SMA wire, which can increase the strain

difference in the wire as it is cycled between martensite and austenite states, and lead to larger ranges of motion.

The analytical model was derived for fixed, non-rotating mandrels rather than rotating pulleys to develop an understanding of the key mechanics for the simpler case. In addition, fixed mandrels are typically cheaper because they lack bearings or other moving parts, which can require maintenance and are more prone to breakage. Ideally, frictionless pulleys would be desirable, but the physical implementation of pulleys with extremely low friction can lead to increased cost. The use of rotating pulleys could enable actuators with larger ranges of motion since less work would be dissipated by friction. To spool-package around rotating pulleys predictably and within a design framework, the basic mechanical understanding of spool-packaged mandrels could be extended to the alternative pulley architecture. The model would need to account for the transmission of bearing friction on the pulley and the relative motion between the SMA wire and pulley as it rotates. If successful in extending the spooling model to moveable pulleys, the updated models could expand the ability to provide even larger amounts of work with fewer losses overall.

6.1.5.3. Time dependence

The model presented in this dissertation is limited to quasi-static motions and predicts for the case of full phase transformation between austenite and martensite. However, there is potential to apply the packaging approach to time dependent applications requiring cyclic or high-speed one-way motions. To implement a model that includes time dependence, several additional research issues are expected. An appropriate constitutive model for the SMA material behavior would need to be selected and incorporated into the analytical approach. Depending on the particular application, the constitutive model may need to account for system dynamics or uneven heat transfer along the wire's length. This dissertation demonstrated the ability of a one-dimensional constitutive model to predict the behavior of spool-packaged actuators adequately for design, and other reduced-order models predicting stress and strain along a single axis

would still be appropriate for many applications. Whereas the quasi-static model assumed a constant, static coefficient of friction based on Coulomb's law, the friction is dynamic in scenarios that are rate dependent. A dynamic coefficient of friction could be estimated, or dynamic tribological models could be applied. High-speed motions would be expected to be beneficial to the range of motion since dynamic friction is typically less that static friction. While additional research issues could also be expected to arise, developing a time-dependent model to support actuator design would require simplifying assumptions where possible to enable fast computation without making unnecessary sacrifices to accuracy and rigor.

6.2. Contributions

Through the research to develop spooled-packaging for SMA wire actuators, several contributions emerged. Through these contributions, this dissertation makes strides toward enabling a new class of actuated products with high performance and low costs by pushing beyond the current limitations due to packaging.

6.2.1. Performance

Spooled-packaging of SMA actuators advances the ability to meet industry's needs for high performance products that rely on actuation. This dissertation improves upon previous attempts to implement spooled-packaging, but on a larger scale by developing a rigorous, scientific knowledge base to analyze, understand, and synthesize spool-packaged actuators that can meet application needs. Prior to this research, the predictive models for spool-packaged actuators had been developed on a case-by-case basis and could not be applied to the analysis of spool-packaged actuators in general. Building upon the models and an understanding of how spool-packaged actuators are affected by their design, the design methodology enables the customization of forms for which performance is high and costs can be mitigated. The analytical model developed in this dissertation distilled the behavior of spool-packaged actuators down to three key effects: friction, bending, and the binding limitation, and through experimental validation

determined that the model can be used to predict the performance for quasi-static actuators and a variety of single and multiple mandrel architectures.

The wealth of knowledge that was generated in the parameter study enables designers to select parameters based on a foundational understanding of the key mechanics of spool-packaged actuators. As a result, the design cycle is hastened through a greater ability to design high quality prototypes on the first attempt. Often in design, prototypes using both conventional and smart materials actuators do not behave exactly as predicted. The understanding of the key mechanical effects for spool-packaged actuators enables designers to identify why a prototype behavior differs from the modeled behavior and effectively revise designs to meet specifications. The design of SMA actuators is not always straightforward, and in many ways, a practical knowledge base that allows a user to navigate the design space artfully, is a crucial enabling contribution for SMA and spool-packaged actuator design.

The design methodology, which relies heavily upon the predictive models, makes it possible to tailor the performance of spool-packaged SMA wire actuators for particular application requirements. Prior to this research, spooled-packaging was typically an *ad hoc* approach based on approximations of behavior and application-specific models with limited applicability to other problems. In this dissertation, the design methodology builds upon the broadly applicable analytical model to provide a framework for consistently synthesizing viable actuator designs that meet performance requirements. By contrast, without the broadly applicable models and systematic design process, the *ad hoc* approach to spooled actuator design was less reliable. By enabling the design of actuators that can be tailored to specific performance requirements, prototypes are more likely to meet requirements early in the design cycle, reducing the time to market for technologies that rely on spooled actuators. By cultivating the ability to analyze, understand, and synthesize spool-packaged actuators, this dissertation takes important steps to enable spool-packaged actuation to meet a wider range of performance needs and to be a more viable packaging approach for real world problems.

6.2.2. Cost

Different types of cost play a role in the market viability of spool-packaged actuators including their financial cost, material and energy use, and performance losses. Indirect costs also arise when the actuator needs to be packaged within a product such as a car, aircraft, or spacecraft where actuator mass and volume are critical factors for an actuator's feasibility/viability. In high yield applications that call for low cost actuation, for example in cars or consumer products, cost control is often crucial for competitive advantage and success in the market.

Optimization-based design allows spool-packaged actuators to be lower in cost than if designed using the *ad hoc* approaches typical for spool-packaged actuator design prior to this research. Mitigating the costs of spool-packaged actuators is possible by representing cost in objective or constraint functions within the design problem, and in the design process laid out in the methodology the costs can be minimized or limited. Thus, the price advantage of SMA can be exploited more effectively despite the additional material use that is necessary to overcome performance losses.

This dissertation research expands the opportunities for using spool-packaged actuators based on the analytical tools, enhanced understanding of spooled-packaging, and the design methodology. By making SMA wires more practical for actuation, they can be used to replace conventional actuators to enable the same types of mechanical functionality while improving the price of the actuator. While long lengths of SMA wire cannot always replace a conventional actuator because of restricted form constraints, spooled-packaging allows for reductions in a product's weight by enabling the replacement of conventional actuators, which are often heavy and bulky, with lighter weight SMA. In aircraft and cars where reducing size and weight are critical factors for cost-control, using SMA to replace conventional actuators without making sacrifices to performance becomes possible and the advantages of using SMA can be realized.

Using spooled-packaging to create new opportunities for actuation, further improvements to product costs are possible by implementing actuators to enable cost-

saving functionality. For instance, adaptive structures on aerodynamic surfaces can improve lift and drag characteristics to result in better fuel economy for cars and aircraft, or more efficient power generation for wind turbines. Overcoming the packaging limitation makes SMA a more viable candidate for enabling cost-saving functionality. Further opportunity is available in medical technologies where implantable or handheld devices have extremely limited form factors making actuator-based mechanical functionality unattainable by conventional means, and impractical with non-packaged SMA wires. In the example of human tremor reduction, the current therapeutic approaches are commonly expensive, dangerous, or both (Pathak, 2010). Because of the difficulty in providing actuation to such small spaces, overcoming the packaging problem may be a critical step to enable medical devices that are lower cost than the currently available alternatives.

6.3. Closing

When this research began, the spooled-packaging strategy was developed as a theoretical solution to real world needs for 1) high performance and 2) low-cost actuators. SMA actuators were recognized to have potential to meet these needs, but with recoverable strain magnitudes of several percent, long unwieldy lengths of wire were often necessary to provide moderate to large displacements. This observation highlighted a third need: that to realize the high performance and low cost of SMA actuators, the form of the actuator must be practical. Spooled-packaging was approached as a potential solution to meet each of these needs regarding performance, cost, and packaging because of its unparalleled capacity for form customization. This dissertation transitions spooled-packaging from an *ad hoc* technique to a well-defined strategy for implementing high performance, low-cost actuation in a practical way. In moving from theory to practice, it became clear that performance, cost, and packaging could not be addressed separately. For spool-packaged SMA actuators, these three issues are deeply related, and there are many applications where they must be considered – not as separate needs, but – as three aspects of a larger problem that must be addressed in concert.

The goal of this dissertation was to develop the scientific knowledge base for spooled packaging of low-cost SMA wire actuators that enables high, predictable performance within compact, customizable form factors. The knowledge base that resulted from this work goes beyond developing an actuator for a particular application, but provides a strategy for developing a whole class of SMA actuators that can meet a range of needs in industry. In the end, this thesis provides a vision for the potential of spool-packaged SMA actuators to meet society's growing needs for better actuators. It is the hope of this researcher that the science and understanding developed in this thesis can enable others to overcome the packaging limitations facing SMA to improve current technologies and innovate beyond.

References

Abeyaratne, R., & Knowles, J. K. (1991). Kinetic relations and propagation of phase boundaries in solids. *Archive for Rational Mechanics and Analysis*, 144(2), pp. 119-154.

Aerfit. (2009). *Aerfit: SMA Couplings – Cryofit.* [Online] Retrieved January 2010 from http://www.aerofit.com/sma_Couplings.html.

Andreasen, G. F., & Hilleman, T. B. (1971). An evaluation of 55 cobalt substituted Nitinol wire for use in orthodontics. *Journal of the American Dental Association,* 82(6), pp. 1373-1375.

Andreasen, G. F., & Morrow, R. E. (1978). Laboratory and clinical analyses of nitinol wire. *American Journal of Orthodontics,* 73(2), pp. 142-151.

Auricchio, F., & Sacco, E. (1999). A temperature-dependent beam for shape-memory alloys: constitutive modeling, finite-element implementation and numerical simulations. *Computer Methods in Applied Mechanics and Engineering,* 174.

Barlas, T. K., & van Kuik, G. A. M. (2007). State of the art and prospective of smart rotor control for wind turbines. *Journal of Physics: Conference Series*, 75.

Barnes, B., Brei, D., Luntz, J., Browne, L., & Strom, K. (2006). Panel Deployment Using Ultrafast SMA Latches. *ASME International Mechanical Engineering Congress and Exposition, Chicago, Illinois,* IMECE2006-15206.

Bein, T., Hanselka, H., & Breitbach, E. (2000). An adaptive spoiler to control the transonic shock. *Smart Materials and Structures,* 9(2), pp. 141-148.

Berg, B. (1995a). Bending of superelastic wires, part I: experimental aspects. *Journal of Applied Mechanics*, 62.

Berg, B. (1995b). Bending of superelastic wires, part II: application to three-point bending. *Journal of Applied Mechanics,* 62.

Bertacchini, O. W., Lagoudas, D. C., Calkins, F. T., & Mabe, J. H. (2008). Thermomechanical cyclic loading and fatigue life characterization of nickel rich NiTi shape-memory alloy actuators. *Proceedings of SPIE,* 6929.

Boyd, J. G., & Lagoudas, D. C. (1994). A constitutive model for simultaneous transformation and reorientation in shape memory materials. *Mechanics of Phase Transformations and Shape Memory Alloys*, AMD 189, pp. 159–177.

Brei, D. E., Redmond, J. A., Wilmot, N. A., Browne, A. L., Johnson, N. L., & Jones, G. L. (2006). Hood latch assemblies utilizing active materials and methods of use. U.S. Patent 7,063,377 issued Jun. 20, 2006.

Brei, D., Luntz, J., Shaw, J., Johnson, N., Browne, A., Alexander, P., & Mankame, N. (2007). General Motors and the University of Michigan Smart Materials and Structures Research Laboratory. *Proceedings of SPIE,* 6527.

Brinson, L.C. (1993). One-dimensional constitutive behavior of shape memory alloys: thermomechanical derivation with non-constant material functions and redefined martensite internal variable. *Journal of Intelligent Material Systems and Structures,* 4, pp. 229–242.

Browne, A. L., Bucknor, N. K., Cheng, Y., Johnson, N. L., Lin, W. C., Namuduri, C. S., Sun, Z., & Usoro, P. B. (2004). Mechamatronics: an automotive perspective. *Proceedings of SPIE,* 5388, pp. 313-319.

Bucholz, K. (2007, April). Smart materials spur additional design possibilities. *Automotive Engineering International,* pp. 46-47.

Buehler, W. J. (1991a). Letter to Amy Hanson as reported in "The Story of Nitinol" by Kauffman and Mayo (1996).

Buehler, W. J. (1991b). Personal communication as reported in "The Story of Nitinol" by Kauffman and Mayo (1996).

Burdea, G. (1996). *Force and Touch Feedback for Virtual Reality.* New York: John Wiley & Sons.

Burkart, M. W., & Read, T. A. (1953). Diffusionless Phase Change in the Indium-thallium System. *Journal of Metals,* pp. 1516-1524.

Busch, J. D., Johnson, A. D., & Purdy, W. E. (1992). Development of a Non-Explosive Release Device for Aerospace Applications. *Proceedings of the 26th Aerospace Mechanisms Symposium,* pp. 1-16.

Calkins, F. T., Mabe, J. H., & Butler, G. W. (2006). Boeing's variable geometry chevron: morphing aerospace structures for jet noise reduction. *Proceedings of SPIE,* 6171.

Carpenter, B., Clark, C., & Weems, W. (1996). Shape memory actuated release devices. *Proceedings of SPIE,* 2721, pp. 420-426.

Chang, B., Shaw, J. A., & Iadicola, M. A. (2006). Thermodynamics of shape memory alloy wire: modeling, experiments, and application. *Continuum Mechanics and Thermodynamics*, 18(1-2), pp. 83-118.

Chang, L. C., & Read, T. A. (1951). Plastic deformation and diffusionless phase changes in metals–the gold–cadmium beta phase. *AIME Transactions,* 191, pp. 47-52.

Chen, C. W. (1957). Some characteristics of the martensite transformation in CuAlNi Alloy. *AIME Transactions,* 209, pp. 1202-1203.

Choi, S. B. (2006). Position control of a single-link mechanism activated by shape memory alloy springs: experimental results. *Smart Materials and Structures*, 15, pp. 51-58.

Chopra, I. (2002). Review of State of Art of Smart Structures and Integrated Systems. *AIAA Journal*, 40(11), pp. 2145-2187.

Churchill, C. (2009). *Experimental Techniques for Characterizing the Thermo-Electro-Mechanical Shakedown Response of SMA Wires and Tubes*. Ph. D. thesis, Department of Aerospace Engineering, University of Michigan, Ann Arbor, MI.

Churchill, C., & Shaw, J. (2008). Shakedown response of conditioned shape memory alloy wire. *Proceedings of SPIE*, 6929.

Ciferri, L. (2004, January 6). Fiat designs new door lock. *Automotive News Europe*, p. 9.

Clement, J. (2004). *Smart Attachment Mechanisms*. Ph. D. thesis, Department of Mechanical Engineering, University of Michigan, Ann Arbor, MI.

Clingman, D. J., & Ruggeri, R. T. (2004). Mechanical strain energy shuttle for aircraft morphing via wing twist or structural deformation. *Proceedings of SPIE*, 5388, pp. 288-296.

Davidson, F. M., & Liang, C. (1996). Investigation of torsional shape memory alloy actuators. *Proceedings of SPIE,* 2717, pp. 672-682.

Deb, K. (2001). Multi-Objective Optimization using Evolutionary Algorithms. Chichester, England: John Wiley & Sons, Ltd.

Dong, Y., Boming, Z., & Jun, L. (2008). A changeable aerofoil actuated by shape memory alloy springs. *Materials Science and Engineering A*, 485, pp. 243-250.

Duerig, T. W. (2002). The Use of Superelasticity in Modern Medicine. *MRS Bulletin,* 27(2).

Duerig, T. W., & Zadno, R. (1990). An Engineer's Perspective of Pseudoelasticity. In T. W. Duerig, K. N. Melton, D. Stöckel, & C. M. Wayman (Eds.), *Engineering Aspects of Shape Memory Alloys* (pp. 369-393). London: Butterworth-Heinemann Ltd.

Duerig, T., Pelton, A., & Stockel, D. (1999). An overview of nitinol medical applications. *Material Science and Engineering A,* 273-275, pp. 149-160.

Dumont, G., & Kuhl, C. (2005). Finite element simulation for design optimization of shape memory alloy spring actuators. *Engineering Computations: International Journal for Computer-Aided Engineering and Software*, 22(7), pp. 835-848.

Dunne, J. P., Hopkins, M. A., Baumann, E. W., Pitt, D. M., & White, E. V. (1999). Overview of the SAMPSON smart inlet. *Proceedings of SPIE,* 3674, pp. 380-390.

Dunne, J. P., Pitt, D. M., White, E. V., & Garcia, E. (2000). Ground demonstration of the Smart Inlet. *AIAA/ASME/ASCE/AHS/ASC Structures, Structural Dynamics, and Materials Conference and Exhibit, 41st, Atlanta, GA*.

Dynalloy, Inc. (2010). *Technical Characteristics of FLEXINOL Actuator Wires,* Version F1140RevG. [Online] Retrieved January 2010 from http://dynalloy.com/pdfs/TCF1140RevD.pdf.

Eggeler, G., Hornbogen, E., Yawny, A., Heckmann, M., & Wagner, M. (2004) Structural and functional fatigue of NiTi shape memory alloys *Material Science and Engineering A,* 368.

Epps, J. J., & Chopra, I. (2001). In-flight tracking of helicopter rotor blades using shape memory alloy actuators. *Smart Materials and Structures,* 10(1), pp. 104-111.

Erbstoeszer, B., Armstrong, B., Taya, M., & Inoue, K. (2000). Stabilization of the shape memory effect in NiTi: an experimental investigation. *Scripta Materialia,* 42(12), pp. 1145-1150.

Evans, J., Brei, D., & Luntz, J. (2006). Preliminary Experimental Study of SMA Knitted Actuation Architectures. *ASME International Mechanical Engineering Congress and Exposition, Chicago, Illinois,* IMECE2006-15409.

Firbank, T. C. (1970). Mechanics of the Belt Drive. *International Journal of Mechanical Sciences,* 12, pp. 1053-1063.

Flexon. (2006). *TiFlex by Marchon*. [Online] Retrieved October 2006 from http://www.flexon.com/HTML2001/tiflex01.html.

Fu, Y., Du, H., Huang, W., Zhang, S., & Hu, M. (2004). TiNi-based thin films in MEMS applications: a review. *Sensors and Actuators A: Physical,* 112(2-3), pp. 395–408.

Garcia, E. (2002). Smart structures and actuators: past, present, and future. *Proceedings of SPIE,* 4698.

Genevray, R. M. (1953). The martensitic transformation in muntz metal. Ph. D. thesis, Department of Metallurgy, Massachusetts Institute of Technology, Cambridge, MA.

Giurgiutiu, V., Rogers, C. A., & Zuidervaart, J. (1997). Incrementally adjustable rotor-blade tracking tab using SMA composites. *Proceedings of the 38th AIAA/ASME/ASCE/AHS/ASC Structures, Structural Dynamics, and Materials Conference, and Adaptive Structures Forum*, pp. 1387.

Goo, B.C., & Lexcellent, C. (1997). Micromechanics-based modeling of two-way shape memory effect of a single crystalline shape memory alloy. *Acta Metallurgica et Materialia*, 45(2), pp. 727-737.

Greninger, A. B. (1938). Deformation of Beta Brass. *AIME Transactions,* 128, pp. 369-377.

Greninger, A. B., & Mooradian, V. G. (1938). Strain Transformation in Metastable Beta Copper-Zinc and Beta Copper-Ti Alloys. *AIME Transactions,* 128, pp. 337-369.

Grummon, D. S., Shaw, J. A., & Foltz, J. (2006). Fabrication of cellular shape memory alloy materials by reactive eutectic brazing using niobium. *Materials Science and Engineering A,* 438-440, pp. 1113-1118.

Hartl, D., & Lagoudas, D. C. (2007). Aerospace applications of shape memory alloys. *Proceedings of Mechanical Engineers, Part G: Journal of Aerospace Engineering* 224(4), pp. 535-552.

Hesselbach, J. (2007). Shape Memory Actuators. In H. Janocha (Ed.), *Actuators in Adaptronics* (pp. 145-163). Berlin: Springer.

Howell, H. G. (1953). The general case of friction of a string round a cylinder. *The Journal of the Textile Institute*, 44(8/9), pp. t359 – t362.

Huang, M., & Brinson, L. C. (1998). Multivariant model for single crystal shape memory alloy behavior. *Journal of the Mechanics and Physics of Solids,* 46, pp. 1379-1409.

Huang, W. (1998). *Shape Memory Alloys and Their Application to Actuators for Deployable Structures.* Ph. D. thesis, Engineering Department, Cambridge University.

Huang, W. (2000). Modified Shape Memory Alloy (SMA) model for SMA wire based actuator design. *Journal of Intelligent Material Systems and Structures,* 10, pp. 221-231.

Huber, J. E., Fleck, N. A., & Ashby, M. F. (1997). The selection of mechanical actuators based on performance indices. *Proceedings of the Royal Society of London, A,* 453(1965), pp. 2185-2205.

ITW Global Appliance Group. (2009). *Door Locks.* [Online] Retrieved November 2009 from http://www.itwappliance.com/products/door_locks.htm.

Ivshin, Y., & Pence, T. J. (1994). A thermomechanical model for a one variant shape memory material. *Journal of Intelligent Material Systems and Structures,* 5(4), pp. 455-473.

Jardine, A. P., Kudva, J. N., Martin, C. A., & Appa, K. (1996). Shape memory alloy TiNi actuators for twist control of smart wing designs. *Proceedings of SPIE*, 2717, pp. 160-165.

Johnson Matthey. (2006). *Johnson Matthey, Cut Tubing*. [Online] Retrieved October 2006 from http://jmmedical.com/html/cut_tubing.html.

Johnson, B., Brei, D. E., & Patera, J. (2003). Application of SMA technology to auxiliary functions in appliances. *Proceedings of SPIE,* 4698, pp. 427-440.

Kapgan, M., & Melton, K. N. (1990). Shape Memory Alloy Tube and Pipe Couplings. T. In W. Duerig, K. N. Melton, D. Stöckel, & C. M. Wayman (Eds.), *Engineering Aspects of Shape Memory Alloys* (pp. 137-148). London: Butterworth-Heinemann Ltd.

Kauffman, G. B., & Mayo, I. (1997). The Story of Nitinol: The Serendipitous Discovery of the Memory Metal and Its Applications. *The Chemical Educator,* 2(2), pp. 1-21.

Kennedy, D. K., Straub, F. K., Schetky, L. M., Chaudhry, Z., & Roznoy, R. (2000). Development of an SMA actuator for in-flight rotor blade tracking. *Proceedings of SPIE,* 3985, pp. 62-75.

Kim, B., Lee, S., Park, J. H., & Park, J. O. (2005). Design and fabrication of a locomotive mechanism for capsule-type endoscopes using shape memory alloys (SMAs). *IEEE/ASME Transactions on Mechatronics,* 10(1), pp. 77-86.

Kornbluh, R. D., Pelrine, R., Prahlad, H., & Heydt, R. (2004). Electroactive polymers: an emerging technology for MEMS. *Proceedings of SPIE,* 5344, pp. 13-27.

Kudva, J. (2004). Overview of the DARPA smart wing project. *Journal of Intelligent Material Systems and Structures,* 15, pp. 261-267.

Kudva, J. N., Sanders, B., Pinkerton-Florance, J., & Garcia, E. (2002). The DARPA/AFRL/NASA Smart wing program - Final overview. *Proceedings of SPIE,* 4698, pp. 37-43.

Kumar, P. K., & Lagoudas, D. C. (2008). Introduction to Shape Memory Alloys. In D. C. Lagoudas (Ed.), *Shape Memory Alloys: Modeling and Engineering Applications* (Chapter 1, pp. 1-51). College Station, TX: Springer.

Kumar, P. K., & Lagoudas, D. C. (2008). Introduction to Shape Memory Alloys. In D. C. Lagoudas (Ed.), *Shape Memory Alloys: Modeling and Engineering Applications* (Chapter 1, pp. 1-51). College Station, TX: Springer.

Lagoudas, D. C., & Miller, D. A. (1999). Experiments of Thermomechanical Fatigue of SMAs. *Proceedings of SPIE,* 2675.

Lagoudas, D. C., Li, C., Miller, D. A., & Rong, L. (2000). Thermomechanical transformation fatigue of SMA actuators. *Proceedings of SPIE,* 3992.

Lagoudas, D., Entchev, P., Popov, P., Patoor, E., Brinson, L.C., & Gao, X. (2006). Shape memory alloys, Part II: Modeling of polycrystals. *Mechanics of Materials*, 38.

Liang, C., & Rogers, C.A. (1990). One-dimensional thermomechanical constitutive relations for shape memory materials. *Journal of Intelligent Material Systems and Structures,* 1, pp. 207–234.

Liang, C., Davidson, F., Schetky, L. M., & Straub, F. K. (1996). Applications of torsional shape memory alloy actuators for active rotor blade control-opportunities and limitations. *Proceedings of SPIE,* 2717, pp. 91-100.

Lucy, M., Hardy, R., & Kist, E. (1996). Report on alternative devices to pyrotechnics on spacecraft. *NASA Langley Research Center,* Hampton, VA, pp 1-22.

Luntz, J., Brei, D., Mane, P., Redmond, J., Barnes, B., Shaw, J., Johnson, N., Browne, A., Alexander, P., & Mankame, N. (2009). Automotive Research Advances in Smart Materials and Devices at the GM/UM SMS Collaborative Research Laboratory. *Proceedings of the International Conference on Adaptive Structures and Technologies, Hong Kong,* 20.

Luntz, J., Brei, D., Ypma, J., Young, J. R., & Radice, J. (2007). Feasibility study of the dual-SMART (SMA ReseTtable) lift device. *Proceedings of SPIE*, 6527.

Mabe, J. H., Cabell, R. H., & Butler, G. W. (2005). Design and control of a morphing chevron for takeoff and cruise noise reduction. *Collection of Technical Papers - 11th AIAA/CEAS Aeroacoustics Conference, Mar 23-25 2005,* pp. 1174-1188.

Machado, L. G., & Lagoudas, D. C. (2008). Thermomechanical Constitutive Modeling of SMAs. In D. C. Lagoudas (Ed.), *Shape Memory Alloys: Modeling and Engineering Applications* (Chapter 3, pp. 121-187). College Station, TX: Springer.

Magna Closures. (2008) *Magna Closures*. [Online] Retrieved November 2008 from http://www.magnaclosures.com.

Mantovani, D. (2000). Shape memory alloys: properties and biomedical applications. *The Journal of The Minerals, Metals, & Materials Society (JOM),* 52(10), pp. 36.

Mavroidis, C. (2002). Development of Advanced Actuators Using Shape Memory Alloys and Electrorheological Fluids. *Research in Nondestructive Evaluation,* 14(1), pp. 1-32.

McKnight, G., Browne, A., & Johnson, N. (2009). A reversibly deployable air dam: a bending approach based on embedded shape memory alloy actuators, Part II: technology demonstration. *Proceedings of SPIE*, 7290.

McNichols, J. L., Brookes, P. C., & Cory, J. S. (1981). NiTi Fatigue Behavior. *Journal of Applied Physics,* 52(12), pp. 7442-7444.

Melton, K. N. (1998). General applications of SMA's and smart materials. In K. Otsuka, & C. M. Wayman (Eds.), *Shape Memory Materials* (pp. 220-239). Cambridge, UK: Cambridge University Press.

Menciassi, A., Gorini, S., Moglia, A., Pernorio, G., Stefanini, C., & Dario, P. (2005). Clamping Tools of a Capsule for Monitoring the Gastrointestinal Tract Problem Analysis and Preliminary Technological Activity. *Proceedings of the 2005 IEEE International Conference on Robotics and Automation,* pp. 1309-1314.

Menciassi, A., Stefanini, C., Gorini, S., Pernorio, G., Kim, B., Park, J., & Dario, P. (2004). Locomotion of a legged capsule in the gastrointestinal tract: theoretical study and preliminary technological results. *Engineering in Medicine and Biology Society, Conference Proceedings of the 26th Annual International Conference,* 1.

Middlesex University Teaching Resources. (2006). *Smart NiTi Springs*. [Online] Retrieved October 2006 from www.mutr.co.uk/prodDetail.aspx?prodID=571.

Miyazaki, S. (1998). Medical and dental applications of shape memory alloys. In K. Otsuka, & C. M. Wayman (Eds.), *Shape Memory Materials* (pp. 267-281). Cambridge, UK: Cambridge University Press.

Morgan, N. B. (2004). Medical shape memory alloy applications - the market and its products. *European Symposium on Martensitic Transformation and Shape-Memory, 17-22 Aug. 2003,* Elsevier, Cirencester, UK, pp. 16-23.

National Research Council. (1998). *Maintaining U.S. Leadership in Aeronautics: Breakthrough Technologies to Meet Future Air and Space Transportation Needs and Goals*. Washington, D.C.: National Academy Press.

Niezrecki, C., Brei, D., Balakrishnan, S., & Moskalik, A. (2001). Piezoelectric Actuation: State of the Art. *Shock and Vibration Digest*, 33(4), pp. 269-280.

Ohkata, I., & Suzuki, Y. (1998). The design of shape memory alloy actuators and their applications. In K. Otsuka, & C. M. Wayman (Eds.), *Shape Memory Materials* (pp. 240-266). Cambridge, UK: Cambridge University Press.

Ölander, A. (1932). The Crystal Structure of AuCd. *Z. Kristal.,* 83(1/2), pp. 145-148.

O'Leary, J. P., Nicholson, J. E., & Gatturna, R. F. (1990). The Use of Ni-Ti in the Homer Mammalok. In T. W. Duerig, K. N. Melton, D. Stöckel, & C. M. Wayman (Eds.), *Engineering Aspects of Shape Memory Alloys* (pp. 477-482). London: Butterworth-Heinemann Ltd.

Osvatic, M. S. (2009). Washing machine lid lock with memory wire actuator. U.S. Patent number 7,617,703 issued November 17, 1998.

Otsuka, K. & Ren, X. (2005). Physical Metallurgy of T-Ni-based Shape Memory Alloys. *Progress in Materials Science,* 50, pp. 511-678.

Otsuka, K., & Kakeshita, T. (2002). Science and technology of shape-memory alloys: New developments. *MRS Bulletin,* 27(2), pp. 91-98.

Otsuka, K., & Ren, X. (1999). Recent developments in the research of shape memory alloys. *Intermetallics,* 7(5), pp. 511-528.

Otte, R. F., & Fischer, C. L. (1973). Cryogenic Connection Method and Means. U.S. Patent 3,740,839 issued February 13, 1979.

Pathak, A., (2010). *The Development of an Antagonistic SMA Actuation Technology for the Active Cancellation of Human Tremor*. Ph. D. thesis, Dept. of Mechanical Engineering, University of Michigan, Ann Arbor, MI.

Pathak, A., Brei, D., & Luntz, J. (2009). Design and preliminary testing of a handheld antagonistic SMA actuator for cancellation of human tremor. *Proceedings of SPIE,* 7288.

Pathak, A., Brei, D., Luntz, J., & LaVigna, C. (2007). A Dynamic Model for Generating Actuator Specifications for Small Arms Barrel Active Stabilization. *Proceedings of SPIE,* 6166.

Pathak, A., Brei, D., Luntz, J., LaVigna, C., & Kwatny, H. (2007). Design and quasi-static characterization of SMASH: SMA stabilizing handgrip. *Proceedings of SPIE,* 6523.

Patoor, E., Eberhardt, A., & Berveiller, M. (1994). Micromechanical modeling of the shape memory behavior. *Proceedings of ASME Winter Annual Meeting,* AMD189, pp. 23–37.

Pfeiffer, C., DeLaurentis, K., & Mavroidis, C. (1999). Shape memory alloy actuated robot prostheses: initial experiments. *IEEE International Conference on Robotics and Automation,*3.

Pons, J. L. (2005). Electroactive polymer actuators (EAPs). *Emerging Actuator Technologies.* West Sussex, England: John Wiley & Sons, Ltd, pp. 145-170.

Prahlad, H., & Chopra, I. (2007). Modeling and Experimental Characterization of SMA Torsional Actuators. *Journal of Intelligent Material Systems and Structures*, 18(1), pp. 29-38.

Prince, R. P., Fisher, S. M., & Clark, J. (1985). Shape Memory Metal Controls Temperature in Overwintering Structure. *1985 Winter Meeting - American Society of Agricultural Engineers.*

Purohit, P., & Bhattacharya, K. (2002). On beams made of a phase-transforming material. *International Journal of Solids and Structures,* 39.

Quackenbush, T. R., Carpenter, B. F., & Gowing, S. (2005). Design and testing of a variable geometry ducted propulsor using shape memory alloy actuation. *43rd AIAA Aerospace Sciences Meeting and Exhibit,* pp. 4105-4117.

Redmond, J. A., Brei, D., Luntz, J., Browne, A. L., Johnson, N. L., & Strom, K. (2007). Design and Experimental Validation of an Ultrafast SMART (Shape Memory Alloy ReseTtable) Latch, *ASME International Mechanical Engineering Congress and Exposition, Washington,* IMECE-43372.

Rejzner, J., Lexcellent, C., & Raniecki, B. (2002). Pseudoelastic behaviour of shape memory alloy beams under pure bending: experiments and modeling. *International Journal of Mechanical Sciences*, 44.

Rey, N., Tillman, G., Miller, R., Wynosky, T., Larkin, M., Flamm, J., & Bangert, L. (2003). Shape memory alloy actuation for a variable area fan nozzle. *Proceedings of SPIE,* 4332, pp. 371-382.

Ruggeri, R. T., Jacot, A. D., & Clingman, D. J. (2002). Shape memory actuator systems and the use of thermoelectric modules. *Smart Structures and Materials,* pp. 386-394.

Sanders, B., Crowe, R., & Garcia, E. (2004). Defense Advanced Research Projects Agency – Smart Materials and Structures Demonstration Program Overview. *Journal of Intelligent Material Systems and Structures,* 15, pp. 227-33.

Schetky, L. M. (1979). Shape-memory alloys. *Scientific American,* 241(5), pp. 68-76.

Seelecke, S., & Muller, I. (2004). Shape memory alloy actuators in smart structures: Modeling and simulation. *Applied Mechanics Reviews,* 57(1), pp. 23-46.

Shaw, J. A. (1997). *Material instabilities in a nickel-titanium shape memory alloy*. Ph. D. thesis, University of Texas, Austin, TX.

Shaw, J. A. (2002). A thermomechanical model for a 1-D shape memory alloy wire with propagating instabilities. *International Journal of Solids and Structures,* 39(5), pp. 1275-1305.

Shaw, J. A., & Kyriakides, S. (1995). Thermomechanical aspects of NiTi. *Journal of Mechanics and Physics of Solids,* 43(8), pp. 1243-1281.

Shaw, J., & Churchill, C. (2009). A reduced-order thermomechanical model and analytical solution for uniaxial shape memory alloy actuators. *Smart Materials and Structures,* 18.

Shigley, J. E., & Mischke, C. R. (2001). *Mechanical Engineering Design.* Boston: McGraw Hill, Inc.

Simon, M., Kaplow, R., Salzman, E., & Freiman, D. (1977). A vena cava filter using thermal shape memory alloy. Experimental aspects. *Radiology,* 125(1), pp. 87-94.

Singh, K., Sirohi, J., & Chopra, I. (2003). An Improved Shape Memory Alloy Actuator for Rotor Blade Tracking. *Journal of Intelligent Material Systems and Structures,* 14(12), pp. 767-786.

Siochi, E. J., Anders, J. B., Cox, D. E., Jegley, D. C., Fox, R. L., & Katzberg, S. J. (2002). Biomimetics for NASA Langley Research Center: Year 2000 Report of Findings From a Six-Month Survey. *Rep. No. NASA/TM-2002-211445,* Langley Research Center, Hampton, Virginia.

Song, G., Ma, N., & Li, H. N. (2004). Applications of shape memory alloys in civil structures. *Engineering Structures,* 28, pp. 1266-1274.

Strelec, J. K., Lagoudas, D. C., Khan, M. A., & Yen, J. (2003). Design and implementation of a shape memory alloy actuated reconfigurable airfoil. *Journal of Intelligent Material Systems and Structures,* 14(4-5), pp. 257-273.

Sun, H., Pathak, A., Luntz, J., Brei, D., Alexander, P., & Johnson, N. (2008). Stabilizing shape memory alloy actuator performance through cyclic shakedown: an empirical study. *Proceedings of SPIE,* 6930.

Sun, Q.P., & Hwang, K.C. (1993). Micromechanics modeling for the constitutive behavior of polycrystalline shape memory alloys—I. Derivation of general relations. *Journal of the Mechanics of Physics and Solids,* 41(1), pp. 1–17.

Tanaka, K. (1986). A thermomechanical sketch of shape memory effect: One-dimensional tensile behavior. *Res Mechanica,* 18, pp. 251–263.

Tanaka, Y., & Yamada, A. (1991). A rotary actuator using shape memory alloy for a robot-analysis of the response with load. *Proceedings of IEEE/RSJ International Workshop on Intelligent Robots and Systems: Intelligence for Mechanical Systems,* pp. 1163-1168.

Taub, A. (2006). Automotive Materials: Technology Trends and Challenges in the 21st Century. *MRS Bulletin,* 31, pp. 336-343.

Truskinovsky, L. (1993) Kinks versus shocks. *Journal of the Institute for Mathematics and its Applications,* 52.

Utter, B., Luntz, J., Brei, D., Teitelbaum, D., Okawada, M., & Miyasaka, E. (2009). Design and operation of a fully implantable SMA actuated implant for correcting short bowel syndrome. *Proceedings of SPIE*, 7288.

Vivet, A., & Lexcellent, C. (1998). Micromechanical modeling for tension-compression pseudoelastic behavior of AuCd single crystals. *The European Physical Journal of Applied Physics,* 4(2), pp. 125-132.

Wang, G., & Shahinpoor, M. (1998). Design of a knee and leg muscle exerciser for paraplegics using a shape memory alloy rotary joint actuator. *Proceedings of SPIE,* 3324, pp. 193-201.

Wax, S. G., & Sands, R. R. (2003). Electroactive polymer actuators and devices. *Proceedings of SPIE,* 3669, pp. 2-10.

Wayman, C. M., & Duerig, T. W. (1990). An Introduction to Martensite and Shape Memory. In T. W. Duerig, K. N. Melton, D. Stöckel, & C. M. Wayman (Eds.), *Engineering Aspects of Shape Memory Alloys* (pp. 3-20). London: Butterworth-Heinemann Ltd.

Wayman, C. M., & Harrison, J. D. (1989). Origins of the shape memory effect." *Journal of The Minerals, Metals, & Materials Society (JOM),* 41(9), pp. 26-28.

Webb, G., Wilson, L., Lagoudas, D., & Rediniotis, O. (1999). Control of SMA actuators in dynamic environments. *Proceedings of SPIE,* 3667, pp. 278-289.

Wu, M. H., & Schetky, L. M. D. (2000). Industrial Applications for Shape Memory Alloys. *SMST-2000: Proceedings of the International Conference on Shape Memory and Superelastic Technologies,* pp. 171-182.

Wu, M. H., and Ewing, W. (1994). Pilot-Operated Anti-Scald Safety Valve: Design and Actuator Considerations. *SMST-94: The First International Conference on Shape Memory and Superelastic Technologies,* pp. 311-316.

Yan, S., Liu, X., Xu, F., & Wang, J. (2007). A gripper actuated by a pair of differential SMA springs. *Journal of Intelligent Material Systems and Structures*, 0.

Yang, K., & Gu, C. L. (2008). A compact and flexible actuator based on shape memory alloy springs. *Proceedings of the Institution of Mechanical Engineers, Part C: Journal of Mechanical Engineering Science*, 222, pp. 1329-1337.

Zider, R. B., & Krumme, J. F. (1988). Eyeglass frame including shape-memory elements. U.S. Patent 4,772,112 issued Sep. 20, 1988.

Zider, R. B., & Krumme, J. F. (1990a). Eyeglass frame including shape-memory elements. U.S. Patent 4,895,438 issued Jan. 23, 1990.

Zider, R. B., & Krumme, J. F. (1990b). Eyeglass frame including shape-memory elements. U.S. Patent 4,896,955 issued Jan. 30, 1990.

3M. (2006). *3M Unitek Product Catalog*. [Online] Retrieved October 2006 from http://solutions.3m.com/wps/portal/3M/en_US/orthodontics/Unitek/products/catalog/.